

# Towards the Rational Design of Nanoparticle Catalysts

A Thesis Submitted to the College of  
Graduate Studies and Research  
In Partial Fulfillment of the Requirements  
For the Degree of Doctor of Philosophy  
In the Department of Chemistry  
University of Saskatchewan  
Saskatoon

By

Priyabrat Dash

© Copyright Priyabrat Dash, June, 2010. All rights reserved.

## **Permission to Use**

In presenting this thesis in partial fulfilment of the requirements for a Postgraduate degree from the University of Saskatchewan, I agree that the Libraries of this University may make it freely available for inspection. I further agree that permission for copying of this thesis in any manner, in whole or in part, for scholarly purposes may be granted by the professor or professors who supervised my thesis work or, in their absence, by the Head of the Department or the Dean of the College in which my thesis work was done. It is understood that any copying or publication or use of this thesis or parts thereof for financial gain shall not be allowed without my written permission. It is also understood that due recognition shall be given to me and to the University of Saskatchewan in any scholarly use which may be made of any material in my thesis.

Requests for permission to copy or to make other use of material in this thesis in whole or part should be addressed to:

Head of the Department of Chemistry

University of Saskatchewan

Saskatoon, Saskatchewan (S7N 5C9)

Canada

## ABSTRACT

This research is focused on development of routes towards the rational design of nanoparticle catalysts. Primarily, it is focused on two main projects; (1) the use of imidazolium-based ionic liquids (ILs) as greener media for the design of quasi-homogeneous nanoparticle catalysts and (2) the rational design of heterogeneous-supported nanoparticle catalysts from structured nanoparticle precursors. Each project has different studies associated with the main objective of the design of nanoparticle catalysts.

In the first project, imidazolium-based ionic liquids have been used for the synthesis of nanoparticle catalysts. In particular, studies on recyclability, reuse, mode-of-stability, and long-term stability of these ionic-liquid supported nanoparticle catalysts have been done; all of which are important factors in determining the overall “greenness” of such synthetic routes. Three papers have been published/submitted for this project. In the first publication, highly stable polymer-stabilized Au, Pd and bimetallic Au-Pd nanoparticle catalysts have been synthesized in imidazolium-based 1-butyl-3-methylimidazolium hexafluorophosphate ([BMIM]PF<sub>6</sub>) ionic liquid (*Journal of Molecular Catalysis A: Chemical*, 2008, 286, 114). The resulting nanoparticles were found to be effective and selective quasi-homogeneous catalysts towards a wide-range of hydrogenation reactions and the catalyst solution was reused for further catalytic reactions with minimal loss in activity. The synthesis of very pure and clean ILs has allowed a platform to study the effects of impurities in the imidazolium ILs on nanoparticle stability. In a later study, a new mode of stabilization was postulated where

the presence of low amounts of 1-methylimidazole has substantial effects on the resulting stability of Au and Pd-Au nanoparticles in these ILs (*Chemical Communications*, 2009, 812). In further continuation of this study, a comparative study involving four stabilization protocols for nanoparticle stabilization in BMIMPF<sub>6</sub> IL is described, and have shown that nanoparticle stability and catalytic activity of nanoparticles is dependent on the overall stability of the nanoparticles towards aggregation (*manuscript submitted*).

The second major project is focused on synthesizing structurally well-defined supported catalysts by incorporating the nanoparticle precursors (both alloy and core shell) into oxide frameworks (TiO<sub>2</sub> and Al<sub>2</sub>O<sub>3</sub>), and examining their structure-property relationships and catalytic activity. a full article has been published on this project (*Journal of Physical Chemistry C*, 2009, 113, 12719) in which a route to rationally design supported catalysts from structured nanoparticle precursors with precise control over size, composition, and internal structure of the nanoparticles has been shown. In a continuation of this methodology for the synthesis of heterogeneous catalysts, efforts were carried out to apply the same methodology in imidazolium-based ILs as a one-pot media for the synthesis of supported-nanoparticle heterogeneous catalysts via the trapping of pre-synthesized nanoparticles into porous inorganic oxide materials. Nanoparticle catalysts in highly porous titania supports were synthesized using this methodology (*manuscript to be submitted*).



## Acknowledgements

First of all, I would like to thank my supervisor Dr. Robert W. J. Scott for his thorough guidance throughout my project. He is the best supervisor I have ever seen in my life. He has provided me many opportunities throughout my graduate studies. I will always cherish that. I would like to thank other members of my advisory committee, Drs. S. R. Foley, A. Dalai, and L. D. Wilson for assisting throughout the completion of my thesis and for providing various aspects of scientific expertise. Special thanks to Dr. A.B. Scott, wife of my supervisor, for her encouragement and most importantly making those nice foods during our group get-togethers. My love to their sweet little angel, Isabel, also. Also, thanks to Dr. I. Burgess for technical guidance whenever needed.

My sincere thanks to University of Saskatchewan and Department of Chemistry for giving an opportunity to continue my PhD research. Funding for this project was provided by the Natural Sciences and Engineering Research Council of Canada (NSERC).

Also, Dr. N. Coombs, University of Toronto for doing all the STEM and EDS scans presented in this thesis. Additionally I would like to thank the Dr. N. Chan and J. Warner from Canadian Light Source (CLS) for helping me during our experiments at CLS.

My sincere thanks also go to all the past and present Scott Group members, especially N. A. Dehm, T. Bond, C. Fowler, W. Hou, M. Dasog, S. Miller, M. Klemmer, and C. Calver. Also, my thanks to my friends Vivek J. Padmanabhan, Dr. R. Gopinath,

Dr. U. Das, Dr. S. Mishra, P. Garg, and Dr. L. Meher for their constant support throughout my graduate schooling.

My sincere thanks to all my family members in India especially my parents Mr. Bhimasen Dash and Mrs. Janaki Devi and my elder sisters, brother-in-laws, younger brother, and parents-in-laws for their unlimited love, affection, support and encouragement.

Finally my whole-hearted thanks to my lady love Sukanya Panda, my wife and everything in my life; for all her love, support, help and understanding.

Most importantly, I would like to thank God, the ultimate provider for providing me enough strength throughout my life.

## **DEDICATIONS**

I would like to dedicate this thesis to my parents, my wife, and my supervisor Dr. Robert

W. J. Scott.

## TABLE OF CONTENTS

<b>PERMISSION TO USE</b>	i
<b>ABSTRACT</b>	ii
<b>ACKNOWLEDGEMENTS</b>	iv
<b>DEDICATIONS</b>	vi
<b>TABLE OF CONTENTS</b>	vii
<b>LIST OF FIGURES</b>	xii
<b>LIST OF TABLES</b>	xviii
<b>LIST OF SCHEMES</b>	xix
<b>LIST OF ABBREVIATIONS</b>	xx
<b>CHAPTER 1</b>	1
1.0 Introduction	1
1.1 Synthesis of Nanoparticle Catalysts	3
1.1.1 Monometallic Nanoparticle Catalysts	3
1.1.2 Bimetallic Nanoparticle Catalysts	8
1.1.3 Structure of Bimetallic Nanoparticle Catalysts	10
1.1.4 Synthesis of Bimetallic Nanoparticle Catalysts	13
1.1.4.1 Co-reduction	13
1.1.4.2 Successive Reduction	16
1.1.5 Au, Pd, and Bimetallic Au-Pd Nanoparticle Catalysts	17
1.2 Characterization of Nanoparticle Catalysts	20

1.2.1 UV-Visible Spectroscopy	23
1.2.2 TEM	24
1.2.3 EDS Mapping	25
1.2.4 XRD	27
1.2.5 XPS	28
1.2.6 EXAFS and XANES	30
1.2.7 CO adsorption by IR	32
1.3 Stabilizers for the Synthesis of Nanoparticle Catalysts	34
1.3.1 Polymers	34
1.3.2 Dendrimers	37
1.3.3 Ligands	39
1.3.4 Surfactants	40
1.3.5 Ionic Liquids	41
1.4 What are Ionic Liquids	41
1.4.1 Synthesis of Nanoparticle Catalysts in Ionic Liquids	46
1.4.1.1 General Synthesis	47
1.4.1.2 Use of additional Stabilizers	48
1.4.1.3 Use of Functionalized Ionic Liquids	49
1.4.2 Mode of Stabilization of Nanoparticles in Ionic Liquids	50
1.4.3 Catalytic Applications of Nanoparticles in Ionic Liquids	51
1.5 Supported Nanoparticle Catalysts	52
1.5.1 Synthetic Routes for Supported Nanoparticle Catalysts	53
1.5.2 Nature of Supports	57

1.5.3 Ionic Liquids as Media for the Synthesis of Supported Catalysts	58
1.6 Research Objectives	60
1.7 Organization and Scope	63
1.8 References	65
<b>CHAPTER 2</b>	<b>78</b>
<b>2. Bimetallic Pd-Au Nanoparticles as Hydrogenation Catalysts in Imidazolium Ionic Liquids</b>	<b>79</b>
2.1 Abstract	79
2.2 Introduction	80
2.3 Experimental	82
2.4 Results and Discussion	86
2.5 Conclusions	98
2.6 References	99
<b>CHAPTER 3</b>	<b>102</b>
<b>3. 1-Methylimidazole Stabilization of Gold Nanoparticles in Imidazolium Ionic Liquids</b>	<b>103</b>
3.1 Abstract	103
3.2 Introduction	103
3.3 Experimental	104
3.4 Results and Discussion	108
3.5 Conclusions	119
3.6 References	119

<b>CHAPTER 4</b>	122
<b>4. Stabilizing Nanoparticle Catalysts in Imidazolium-based Ionic Liquids: A Comparative Study</b>	123
4.1 Abstract	123
4.2 Introduction	124
4.3 Experimental	127
4.4 Results and Discussion	132
4.5 Conclusions	148
4.6 References	149
<b>CHAPTER 5</b>	153
<b>5. Rational Design of Supported Pd-Au Nanoparticle Catalysts from Structured Nanoparticle Precursors</b>	154
5.1 Abstract	154
5.2 Introduction	155
5.3 Experimental	160
5.4 Results and Discussion	165
5.5 Conclusions	186
5.6 References	187
<b>CHAPTER 6</b>	193
<b>6. One-pot Synthesis of Supported-Nanoparticle Materials in Ionic Liquid Solvents</b>	194
6.1 Abstract	194

6.2 Introduction	195
6.3 Experimental	198
6.4 Results and Discussion	201
6.5 Conclusions	212
6.6 References	213
<b>CHAPTER 7</b>	<b>217</b>
7.1 Summary and Conclusions	217
7.2 Outlook and Future Work	222
7.2.1 Ionic Liquid Project	222
7.2.2 Future Work	223
7.2.3 Supported Nanoparticle Catalysts Project	226
7.2.3.1 Room-temperature Plasma Cleaning	226
7.2.3.2 Synthesis of Porous Materials using Non-aqueous Routes	228
7.2.3.3 Structured Bimetallic Nanoparticles	230
7.3 References	232



## List of Figures

<b>Figure 1.1.</b>	Schematic view of the synthesis of metal nanoparticles.	4
<b>Figure 1.2.</b>	Schematic view of the electronic/ligand effect (a, b) and ensemble effect (c).	10
<b>Figure 1.3.</b>	Schematic illustration of various structures of bimetallic nanoparticles. (a) random alloy; (b) core-shell; (c) cluster-in-cluster structure; (d) intermetallics; and (e) sub-surface shells.	12
<b>Figure 1.4.</b>	Schematic view of the structures of metal nanoparticles.	21
<b>Figure 1.5.</b>	(a) STEM image of a Pt/Pd core-shell nanoparticle. (b) power spectrum data and annotated zone axis with the intensity profile represented in the inset.	25
<b>Figure 1.6.</b>	Representative EDS line scan spectra of (a) a 4.0 nm Ru/Pt core-shell nanoparticles and (b) a 4.4 nm Pt-Ru (1:1) alloy nanoparticle. The blue and red EDS lines are Ru and Pt, respectively. Ru K and Pt L lines were used for EDS line scans and a 1.5 nm probe was used to trace 10-15 nm scans across a particle.	27
<b>Figure 1.7.</b>	Schematic diagram showing the principle of XPS.	29
<b>Figure 1.8.</b>	Photoelectric effect in EXAFS spectroscopy.	30
<b>Figure 1.9.</b>	FTIR spectra of Ru/Pt core-shell and physical mixtures of Pt and Ru nanoparticles in the presence of CO(g).	33
<b>Figure 1.10.</b>	Structure of poly(vinylpyrrolidone) (PVP) polymer.	35
<b>Figure 1.11.</b>	Structure of PAMAM and PPI dendrimers.	39
<b>Figure 1.12.</b>	Structure of bis(2-ethylhexyl) sulfosuccinate (AOT) surfactant.	41
<b>Figure 1.13.</b>	Possible structures of ionic liquids.	42
<b>Figure 1.14.</b>	Schematic diagram of deposition-precipitation method.	54

<b>Figure 2.1</b>	(A) Pressure decay vs. time in Hydrogenation of Allyl Alcohol by 1:3 Au:Pd NPs in IL and (B) TON vs. time in Hydrogenation of Allyl Alcohol by 1:3 Au:Pd NPs in IL.	85
<b>Figure 2.2.</b>	UV-Vis absorption spectra of PVP-stabilized Au nanoparticles in methanol and after transfer to [BMIM]PF <sub>6</sub> IL.	88
<b>Figure 2.3.</b>	UV-Vis absorption spectra of PVP-stabilized Pd-Au nanoparticles after phase transfer to [BMIM]PF <sub>6</sub> IL.	89
<b>Figure 2.4.</b>	TEM micrographs and histograms of PVP-stabilized Au nanoparticles (A) as-synthesized in methanol and (B) after phase transfer to [BMIM]PF <sub>6</sub> IL.	90
<b>Figure 2.5.</b>	TEM micrographs and histograms of PVP-stabilized Pd-Au bimetallic nanoparticles (1:3 Au:Pd) (a) as-synthesized in methanol and (b) after phase transfer to [BMIM]PF <sub>6</sub> IL.	91
<b>Figure 2.6.</b>	TOFs for the hydrogenation of allyl alcohol as a function of the mole % Pd in PVP-stabilized Pd-Au nanoparticles in [BMIM]PF <sub>6</sub> . Conditions, [Pd+Au] = 1.1 mM, Substrate:Catalyst ratio = 670:1, Temperature = 40 °C.	93
<b>Figure 2.7.</b>	TOFs for the hydrogenation of allyl alcohol, 1,3-cyclooctadiene, trans-cinnamaldehyde, and 3-hexyn-1-ol by PVP-stabilized Pd-Au bimetallic nanoparticle series in [BMIM]PF <sub>6</sub> . Conditions, [Pd+Au] = 1.1 mM, Substrate:Catalyst ratio = 670:1, Temperature = 40 °C (allyl alcohol, 3-hexyn-1-ol, trans-cinnamaldehyde), and 35 °C (1,3-cyclooctadiene), 1.046 atm H <sub>2</sub> pressure.	94
<b>Figure 2.8.</b>	Variation in selectivity of hydrogenation reactions after 1 hour as a function of the mole % Pd loading for the hydrogenation of (A) 1, 3-cyclooctadiene, (B) trans-cinnamaldehyde, and (C) 3-hexyn-1-ol.	96-97
<b>Figure 3.1.</b>	Calibration curve obtained from Cu(II) complexation studies of the position of the absorption maxima ( $\lambda_{\text{max}}$ ) as a function of 1-methylimidazole concentration.	109

- Figure 3.2.** UV-Vis absorption spectra of Au nanoparticles (A) as-synthesized in pure [BMIM]PF<sub>6</sub> and (B) in [BMIM]PF<sub>6</sub> with 1.0 mM 1-methylimidazole added. 111
- Figure 3.3.** TEM images of Au nanoparticles as-synthesized in [BMIM]PF<sub>6</sub> IL with (A) no additives added and (B) 1.0 mM 1-methylimidazole added. 112
- Figure 3.4.** TEM images of 3:1 Pd:Au bimetallic nanoparticles as-synthesized in [BMIM]PF<sub>6</sub> IL with (A) no additive (particle size  $6.0 \pm 2.9$  nm), and (B) 1.0 mM methylimidazole additive (particle size  $3.0 \pm 0.5$  nm). 113
- Figure 3.5.** UV-Vis absorption spectra of 3:1 Pd:Au bimetallic nanoparticles in [BMIM]PF<sub>6</sub> IL. 114
- Figure 3.6.** Catalytic activity of 3:1 Pd:Au bimetallic nanoparticles in [BMIM]PF<sub>6</sub> IL for the hydrogenation of allyl alcohol (insets: the samples after 1h of hydrogenation reaction). [Pd+Au] = 1.0 mM, Substrate:Catalyst ratio = 737:1, Temperature = 40 °C, stirring rate at 1080 rpm. 115
- Figure 3.7.** TEM images of 3:1 Pd:Au bimetallic nanoparticles (A) as-synthesized in [BMIM]PF<sub>6</sub>IL (particle size  $3.4 \pm 0.5$  nm), and (B) as-synthesized in BMIMPF<sub>6</sub> IL followed by addition of 1.0 mM methylimidazole (particle size  $3.2 \pm 0.5$  nm). 116
- Figure 3.8.** Catalytic activity of smaller (3.2 – 3.4 nm) 3:1 Pd:Au bimetallic nanoparticles as-synthesized in pure [BMIM]PF<sub>6</sub> IL without additives (blue triangles) and with 1.0 mM methylimidazole added after synthesis (pink squares) for the hydrogenation of allyl alcohol. [Pd+Au] = 1.0 mM, Substrate:Catalyst ratio = 737:1, Temperature = 40 °C, stirring rate at 1080 rpm. 117
- Figure 3.9.** TEM image of 3:1 Pd:Au bimetallic nanoparticles as-synthesized in [BMIM]OTf IL without additive (particle size  $4.9 \pm 2.0$  nm). 118

- Figure 3.10.** Catalytic activity of 3:1 Pd:Au bimetallic nanoparticles in [BMIM]OTf IL for the hydrogenation of allyl alcohol (A) no additive, (B) with 100 mM methylimidazole additive (insets: the samples after 1 h hydrogenation reaction). [Pd+Au] = 1.0 mM, Substrate:Catalyst ratio = 737:1, Temperature = 40 °C, stirring rate at 1080 rpm. 118
- Figure 4.1.** UV-Vis absorption spectra of Au nanoparticles over time in (a) pure [BMIM]PF<sub>6</sub>, (b) [BMIM]PF<sub>6</sub> with 1.39 mM PVP additive, (c) [BMIM]PF<sub>6</sub> with 1 mM 1-methylimidazole additive, and (d) [BMIM]PF<sub>6</sub> with 10 mM [aemim]PF<sub>6</sub> additive. 134
- Figure 4.2.** TEM images and particle-size histograms of as-synthesized Au nanoparticles in (a) pure [BMIM]PF<sub>6</sub>, (b) [BMIM]PF<sub>6</sub> with 1.39 mM PVP additive, (c) [BMIM]PF<sub>6</sub> with 1 mM 1-methylimidazole additive, and (d) [BMIM]PF<sub>6</sub> with 10 mM [aemim]PF<sub>6</sub> additive. 137
- Figure 4.3.** TEM images of Au nanoparticles after two weeks in (a) pure [BMIM]PF<sub>6</sub>, (b) [BMIM]PF<sub>6</sub> with 1.39 mM PVP additive. 138
- Figure 4.4.** TEM images and particle-size histograms of as-synthesized 3:1 PdAu nanoparticles in (a) pure [BMIM]PF<sub>6</sub>, (b) [BMIM]PF<sub>6</sub> with 1.39 mM PVP additive, (c) [BMIM]PF<sub>6</sub> with 1 mM 1-methylimidazole additive, and (d) [BMIM]PF<sub>6</sub> with 10 mM [aemim]PF<sub>6</sub> additive. 141
- Figure 4.5.** (A) Effective Turnover Number (moles H<sub>2</sub>/moles Pd+Au) vs. time plot and (B) Plot of Surface Turnover Number (moles H<sub>2</sub>/moles surface Pd+Au) vs. time plot for hydrogenation of 1,3-cyclooctadiene in the presence of additives. Substrate:Catalyst ratio = 400:1. 143
- Figure 5.1.** TEM images of PVP-stabilized (a) Pd seeds, (b) 1:3 Pd core-Au shell nanoparticles, and (c) UV-Vis spectra of Pd seeds and 1:3 Pd core-Au shell nanoparticles. 167

<b>Figure 5.2.</b>	HRTEM images and EDS line scans of co-reduced PVP-stabilized 1:1 Pd: Au nanoparticles (a) as-synthesized in alumina, and (b) the corresponding EDS line scan; (c) in alumina calcined at 300 °C, and (d) the corresponding EDS line scan; (e) in alumina calcined at 500 °C, and (f) the corresponding EDS line scan. The blue and red EDS lines are Au and Pd, respectively.	169
<b>Figure 5.3.</b>	Thermal gravimetric analysis plots showing (a) mass loss and derivative of mass loss of PVP-stabilized 1:1 PdAu nanoparticles in alumina from 25 °C to 550 °C and (b) mass loss for same sample held at 300 °C for 5 h.	172
<b>Figure 5.4.</b>	Au- L <sub>III</sub> -edge EXAFS in <i>k</i> -space for the Pd-Au alloy nanoparticle series.	173
<b>Figure 5.5.</b>	EXAFS single shell fits for co-reduced PdAu nanoparticle series (a) as-synthesized in alumina, (b) calcined at 300 °C.	175- 176
<b>Figure 5.6.</b>	HRTEM images of core-shell PdAu nanoparticles (a) as-synthesized in alumina, (b) after calcination at 300 °C and c) EDS line scan of core-shell PdAu nanoparticles in alumina after calcination at 300 °C. The blue and red EDS lines are Au and Pd, respectively.	181
<b>Figure 5.7.</b>	EXAFS fits for core-shell PdAu nanoparticles (a,b) as-synthesized in alumina, and (c) after calcination at 300 °C.	182
<b>Figure 5.8.</b>	The Au L <sub>3</sub> -XANES spectra of as-synthesized PdAu alloy and core-shell nanoparticle series in alumina.	184
<b>Figure 6.1.</b>	Nitrogen adsorption-desorption isotherms for titania supported catalysts synthesized by hydrolysis of titanium tetrachloride in BMIMPF <sub>6</sub> ILs after washing and calcination at 550 °C.	203
<b>Figure 6.2.</b>	BJH pore-size distributions for titania supported catalysts synthesized by titanium tetrachloride hydrolysis in [BMIM]PF <sub>6</sub> followed by washing and calcined at 550 °C.	204
<b>Figure 6.3.</b>	Thermal gravimetric analysis plots showing (a) mass loss and derivative of mass loss of PVP-stabilized Au nanoparticles in	206

titania prepared after cold methanol washing and (b) after hot methanol washing.

- Figure 6.4.** TEM images PVP-stabilized Au nanoparticles (a) as-synthesized in titania, and (b) after calcination at 350 °C. 208
- Figure 6.5.** (A) Nitrogen adsorption-desorption isotherms and (B) BJH pore-size distributions for calcined Au-TiO<sub>2</sub> samples. 210
- Figure 6.6.** X-ray powder diffraction patterns of Au-TiO<sub>2</sub> systems before and after calcination. 212
- Figure 7.1.** Surface-FTIR spectra of PVP-stabilized Au nanoparticles trapped in a titania xerogel (A) before room temperature plasma treatment and (B) after room temperature plasma treatment for 20h. The sample was subjected to an oxygen plasma at 100 W within a Harrick plasma cleaner (PDC-32 G). 228
- Figure 7.2.** Schematic diagram of core-shell nanoparticles with a very thin shell. 230

## List of Tables

<b>Table 1.1.</b>	Characterization methods used for the structural determinations of metal nanoparticles.	22
<b>Table 1.2.</b>	Melting Points of some Ionic Liquids.	43
<b>Table 4.1.</b>	Hydrogenation of 3-buten-1-ol by four different stabilizers in [BMIM]PF <sub>6</sub> IL.	146
<b>Table 5.1.</b>	EXAFS fitting parameters of pure metals.	177
<b>Table 5.2.</b>	EXAFS fitting parameters of PdAu nanoparticle series.	178
<b>Table 6.1.</b>	Porosity and surface area properties of materials prepared by hydrolysis of titanium tetrachloride in [BMIM]PF <sub>6</sub> IL after calcination at 550 °C.	202
<b>Table 6.2.</b>	Porosity properties of materials prepared by hydrolysis of titanium isopropoxide in [BMIM]PF <sub>6</sub> /methanol mixture.	209

## List of Schemes

<b>Scheme 1.1.</b>	Schematic illustration of the formation of gold nanoparticles by the citrate reduction method.	6
<b>Scheme 1.2.</b>	Synthesis of transition metal nanoparticles by the radiolysis method.	7
<b>Scheme 4.1.</b>	Products detected during the hydrogenation of 3-buten-1-ol.	144



## List of Abbreviations

AOT	Bis(2-ethylhexyl) sulfosuccinate
aemim	1-(2'-aminoethyl)-3-methylimidazolium
BET	Brunauer-Emmett-Teller
BF	Bright-field
BJH	Barrett-Joyner-Halenda
BMIM	1-butyl-3-methylimidazolium
C-C	Carbon-Carbon
CLS	Canadian Light Source
CN	Co-ordination Number
COD	Cyclooctadiene
CTAB	Cetyltrimethylammonium Bromide
DAI	1,3-Dialkylimidazolium
DF	Dark-field
EDS	Energy Dispersive X-ray Spectroscopy
EMIM	1-Ethyl-3-Methylimidazolium
EXAFS	Extended X-ray Absorption Fine Structure
FTIR	Fourier Transform Infrared Spectroscopy
GC-MS	Gas Chromatography-Mass Spectrometry
HAADF	High-Angle Annular Dark Field
$^1\text{H}$ NMR	Proton Nuclear Magnetic Resonance
HRTEM	High resolution Transmission Electron Microscopy

HXMA	Hard X-ray Microprobe Analysis
Hz	Hertz
IL	Ionic Liquid
IR	Infrared
MPCs	Monolayer-Protected Clusters
M.W	Molecular Weight
OTf	triflate
PAMAM	Poly(amidoamine)
PDF	Pair Distribution Function
PEO–PPO–PEO	Polyethylene Oxide-Polypropylene Oxide- Polyethylene Oxide
PCL	Poly( $\epsilon$ -caprolactone)
PPI	Poly(propylene imine)
PVP	Poly (vinylpyrrolidone)
PVA	Poly (vinylalcohol)
SAXS	Small Angle X-ray Scattering
scCO <sub>2</sub>	Supercritical Carbon dioxide
STEM	Scanning Transmission Electron Microscopy
TEM	Transmission Electron Microscopy
TGA	Thermal Gravimetric Analysis
TOAB	Tetraoctylammonium Bromide
TOF	Turnover Frequency
TON	Turnover Number
UV-Vis	Ultraviolet Visible

XAFS	X-ray Absorption Fine Structure
XANES	X-ray Absorption Near-edge Structure
XPS	X-ray Photoelectron Spectroscopy
XRD	X-ray Diffraction

## 1.0 Introduction

More than 20 % of the gross national product of industrial countries rely on catalytic processes; thus catalysts play a major technological role in society covering a wide range of processes from biological reactions to large-scale production of bulk chemicals.<sup>1</sup> A catalyst provides an alternative reaction pathway in which the activation barriers of a reaction are lowered and the reaction rate is increased. Generally, catalysis is classified into three main categories, namely: heterogeneous, homogeneous, and enzymatic (or biocatalysts). The application of catalysts is found to be widespread in different areas including petrochemical, automotive, electrocatalysis, fuel cells, sensors, energy, and environmental applications.<sup>2,3</sup> Traditionally, a significant number of catalytic processes involve the use of transition-metal catalysts, particularly precious noble metals which are not prone to oxidation. Some of the most common metals used for catalysis are Pd, Pt, Ru, Rh, Ni, and Cu.<sup>4</sup> Thus, optimizing the usage of active (precious) materials has been a major aspect of catalyst optimization and thus many scientists have studied catalysis by nanoparticles in order to take advantage of the higher surface areas exposed to the reactants.<sup>5</sup> Another important factor is the unique physical and chemical properties associated with small nanoparticles.<sup>6</sup> As the numbers of methods to synthesize nanoparticles and characterize such particles have grown during the nanotechnology revolution, this has spurred a re-growth of the field of “nanocatalysis”.

Nanoparticles comprised of noble metals that range in size from roughly 1 to 10 nm exhibit specific physical and chemical properties that are intermediate between those of the atomic element from which they are composed relative to those of the bulk metal.<sup>6</sup>

One such property is due to the small nanoparticle dimensions is known as the “quantum size effect”.<sup>7</sup> Quantum size effects occur when the de Broglie wavelength of valence electrons ( $\lambda$ ) is of the same order of magnitude as the size of the particle ( $D$ ) itself. In this scenario, the particles behave electronically as zero dimensional particles obeying quantum mechanical rules. For particles less than 10 nm in size, these quantum size effects become valid, and thus, optical, and electronic properties change in this size range. Another special property of nanoparticles is that a high ratio of atoms is located on the surface in nanoparticles, and thus, are involved in the reaction. Also, smaller particles will have more defects, *i.e.*; more edges and kinks compared to larger particles. Stabilization of high-index crystal planes and alternative packing arrangements of atoms can also occur in small nanoparticles.<sup>8</sup> Among the chemical properties of metal nanoparticles, catalysis is of great interest and has received a lot of attention over the years.<sup>6</sup>

Catalysis by nanoparticles is one of the oldest and largest applications of nanotechnology. The very first example of nanoparticles being used in catalysis dates back to 19<sup>th</sup> century, when Ag nanoparticles were used in photography and Pt nanoparticles were used for the decomposition of hydrogen peroxide.<sup>9</sup> Pioneering catalytic applications of nanoparticles were carried out in 1940 by Nord on the reduction of nitrobenzene,<sup>10</sup> and in 1970 by Parravano on hydrogen-atom transfer between benzene and cyclohexane, and oxygen atom transfer between CO and CO<sub>2</sub> using Au nanoparticles.<sup>11</sup> A real breakthrough came with Haruta’s studies on oxide-supported Au nanoparticles which catalyzed CO oxidation by O<sub>2</sub> at low temperatures.<sup>12-14</sup> This work spurred a great deal of research interest into the reasons behind this surprising catalytic

activity, as bulk Au is typically catalytically inert and CO oxidation activity was only seen at nanoparticle sizes between 2-5 nm.<sup>15</sup> After this discovery, tremendous amounts of research activity was undertaken towards the design of nanocatalysts with the major goals of improving nanoparticle catalyst stability, activity, and selectivity and understanding the associated catalytic mechanisms.<sup>6</sup> Besides monometallic nanoparticles, bimetallic nanoparticles composed of two different metal elements are also interesting as they offer the ability to tune the catalytic activity, selectivity and stability of nanoparticle catalysts.<sup>16</sup>

The following sections of this chapter are primarily concerned with the synthesis and characterization of monometallic and bimetallic nanoparticle catalysts. The use of different stabilizers and how they affect the catalytic activity are also described, with an emphasis on the use of ionic liquids as novel media for the synthesis of nanoparticle catalysts. Towards the end of this chapter, the design of heterogeneous supported nanoparticle catalysts has been presented. Finally, the overall research objectives and the organization and scope of this thesis are documented.

## **1.1 Synthesis of Nanoparticle Catalysts**

### **1.1.1 Monometallic Nanoparticle Catalysts**

Commonly, transition metals that are not overly prone to oxidation are mostly used for catalysis; the most common metals which are used in the catalytic process include Pd, Pt, Ru, Rh, Ni, and Cu.<sup>4</sup> For better performance of nanoparticles in catalysis, it is important to have nanoparticles with controlled size, shape, and composition. These

parameters can be controlled by choosing proper synthetic methods. Metal nanoparticles can be synthesized by two main methods (Figure 1.1): (1) subdivision of metallic aggregates (a physical method) and (2) nucleation and growth of metallic nanoparticles (a chemical method).<sup>17</sup>

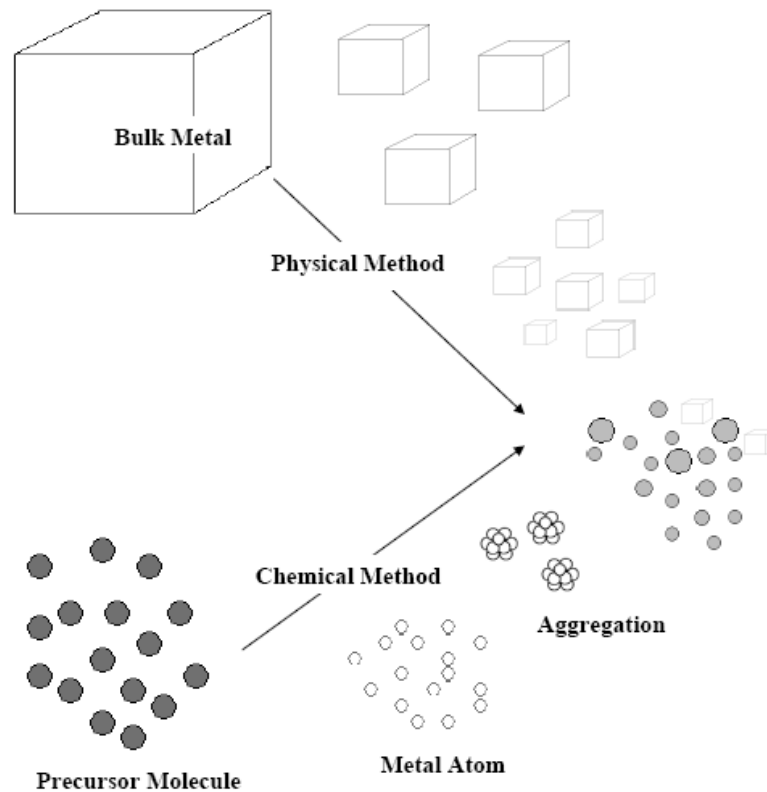


**Figure 1.1.** Schematic view of the synthesis of metal nanoparticles.<sup>16</sup> (Adapted from reference 16).

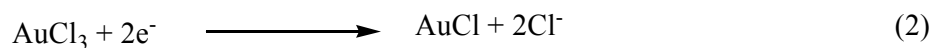
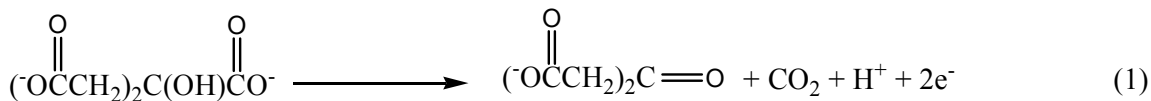
Nanoparticles synthesized by physical methods typically have broad particle size distributions (typically particle sizes greater than 10 nm with distributions greater than 20 percent) and also, are difficult to reproduce on a regular basis.<sup>18</sup> To have better control over particle sizes, chemical synthetic methods are found to be more suitable than physical methods. In chemical methods, control over the aggregation of nanoparticles is the most important step to control the overall size and composition.<sup>16</sup> In this context,

various stabilizers have been used which will be reviewed in the later part of this section. Three major routes are normally used for the chemical synthesis of transition metal nanoparticles: (1) chemical reduction of metallic salts, (2) thermal and photochemical decomposition of metal complexes, and (3) electrochemical reduction of metallic salts.

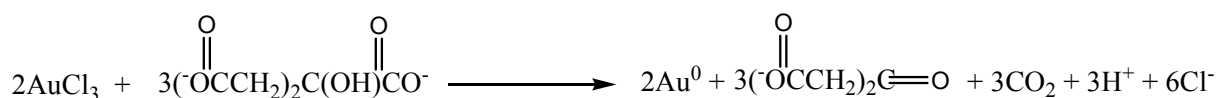
### 1.1.1.1 Chemical Reduction

This is one of the most widely used methods for the synthesis of metal nanoparticles. This method is straightforward, and involves the reduction of a metal salt with a strong reducing agent in the presence of a stabilizer. Commonly used reducing agents include hydrides such as sodium borohydride, hydrazine, gases such as molecular hydrogen or carbon monoxide, as well as other reagents such as sodium citrate and alcohol solvents. The first reported reducing agent used for Au nanoparticle synthesis was phosphorus, which was used by Faraday to reduce  $\text{AuCl}_4^-$  ions.<sup>19</sup> Sodium citrate has also been a common reducing agent used for the formation of transition metal nanoparticles.<sup>20-22</sup> Turkevitch and co-workers did many of the pioneering studies on the nucleation and growth of Au nanoparticles reduced by sodium citrate.<sup>20</sup> One advantage of this method is that the citrate anion not only acts as a reducing agent but also as a stabilizer.<sup>20</sup> This citrate reduction method involves a multiple-step process as shown in Scheme 1.1.<sup>21</sup> In the initial step, oxidation of citrate occurs forming dicarboxyacetone. The second step involves the reduction of auric salt to aurous salt, followed by the disproportionation of aurous species to gold atom in the last step. Ir and Pt nanoparticles have also been synthesized by citrate reduction methods.<sup>22,23</sup>  $\text{NaBH}_4$  or  $\text{KBH}_4$  reduction methods have been used for the synthesis of Au, Ag, Pt, Pd, and Cu nanoparticles.<sup>24-34</sup>





The final balanced equation is:



**Scheme 1.1.** Schematic illustration of the formation of gold nanoparticles by the citrate reduction method.<sup>21</sup>

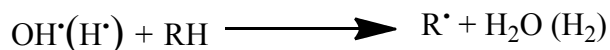
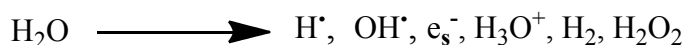
Different forms of hydrazine such as hydrazine chloride or sulfate have been used for the synthesis of Cu, Pd, and Au nanoparticles in the presence of stabilizers like polymers or surfactants.<sup>35-37</sup>

### 1.1.1.2 Thermal and Photochemical Decomposition

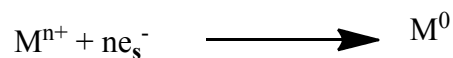
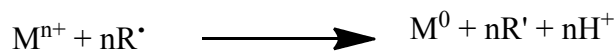
Organometallic compounds are thermally decomposed in high boiling point solvents to form their respective zerovalent species. For example, Meguro and co-workers synthesized Pd nanoparticles by this method by heating a solution of palladium acetate to 110<sup>0</sup> C.<sup>38</sup> However, broad particle size distributions are often obtained by this method if there are no secondary stabilizers present.<sup>38</sup> Photochemical methods have been found to be a promising method for the production of monodisperse transition metal nanoparticles by reduction of organometallic complexes by radiolysis. Au, Pd, Ag, Pt, Cu, and Ir nanoparticles have all been synthesized by this method.<sup>39-42</sup> The general

scheme for this method is outlined below (Scheme 1.2). During the radiolysis of an aqueous solution containing transition metal salts, solvated electrons ( $e_s^-$ ) or  $H^\bullet$  or  $OH^\bullet$  radicals are formed which react with other molecules in aqueous solutions. These solvated electrons and organic radicals ( $e_s^-$  and  $R^\bullet$ ) act as reductants and reduce the metal salts to form the nanoparticles ( $M^0$ ). The normal ionization radiation sources used are x-ray or  $\gamma$ -ray generators and UV-Visible irradiation by Hg or Xe lamps. Highly disperse Au, Ag, and Pt nanoparticles were synthesized by irradiating the corresponding transition metal salt with UV-Visible light in the presence of additional surfactants or polymers.<sup>43-45</sup>

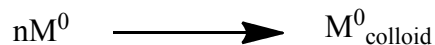
**Active species generation**



**Metal Reduction**



**Growth of Colloids**



**Scheme 1.2.** Synthesis of transition metal nanoparticles by the radiolysis method.<sup>17</sup>

In most of these photochemical methods, the irradiation time was quite long. To overcome these problems, Scaiano and co-workers have developed methods in which the irradiation time has been reduced to several minutes.<sup>46-49</sup> For example, the synthesis of

Ag nanoparticles was obtained using hydroxydiphenylmethyl as a source of radical species and the irradiation time required to reduce  $\text{Ag}^+$  cations to Ag nanoparticles was reduced to a few minutes.<sup>46</sup> They also synthesized Au nanoparticles using photochemically generated 2-hydroxy-2-propyl radicals.<sup>47,48</sup> Recently, they were able to synthesize Au-Ag alloy and core-shell nanoparticles using 2-hydroxy-2-propyl radicals generated by the photochemical cleavage of 1-[4-(2-hydroxyethoxy)phenyl]-2-hydroxy-2-methyl-1-propane-1-one.<sup>49</sup>

### 1.1.1.3 Electrochemical Reduction

Reetz *et al.* were the first group to use electrochemical methods for the synthesis of monodisperse transition metal nanoparticles.<sup>50,51</sup> In this method, a sacrificial anode is oxidized in the presence of a quaternary ammonium salt. The ions are then reduced at cathode to yield the metal nanoparticles. This process by Reetz *et al.* offers various advantages such as excellent control of particle size and simple isolation of the nanoparticles. Pd, Ni, Cu, Pt, Rh, and Ru nanoparticles were synthesized using this method.<sup>50,51</sup>

### 1.1.2 Bimetallic Nanoparticle Catalysts

Bimetallic nanoparticles consisting of two different metals have been found to improve catalyst activities and selectivities for many systems.<sup>16,52</sup> The higher activity and selectivity of bimetallic nanoparticles compared to those of monometallic nanoparticles are typically attributed to ensemble and/or ligand (electronic) effects.<sup>53,54</sup> These two effects are shown in Figure 1.2 in which metal A is the catalytically active metal, B is the

second metal, and S is the substrate. In the ligand (electronic) effect, the metal B must be present near to metal A in order to affect the electronic structure and/or electron density of metal A. As the catalytic site is located on metal A, it is not necessary that metal B should be present on the surface of the particles. However, in order to have strong effects metal B should be adjacent to metal A. There are many examples documenting this electronic effect where the addition of one metal to other metal resulted in higher activity and selectivity. For example, Baiker and co-workers have shown that mixing Pd and Au resulted in a increase in selectivity for the oxidation of benzyl alcohol to benzaldehyde with catalysts containing Au:Pd in a ratio of 1:9.<sup>55</sup> They studied the electronic effects by x-ray photoelectron spectroscopy (XPS) and x-ray absorption spectroscopy and found that that with increase in Pd content the binding energy of Au core levels was lowered and a decrease in the number of d orbital holes in the Au 5d valence band was observed from Au x-ray absorption near-edge structure (XANES) spectra.<sup>55</sup> Also, in addition to these pure electronic effects, the modifications of the interatomic distances (M-M distances) and reorganization of surfaces in bimetallic systems can also have significant effects on catalysis.<sup>53,56</sup> Normally, these types of geometric effects should also be taken into account together with the ensemble and ligand effects whenever the activity of bimetallic systems is discussed.<sup>56</sup>

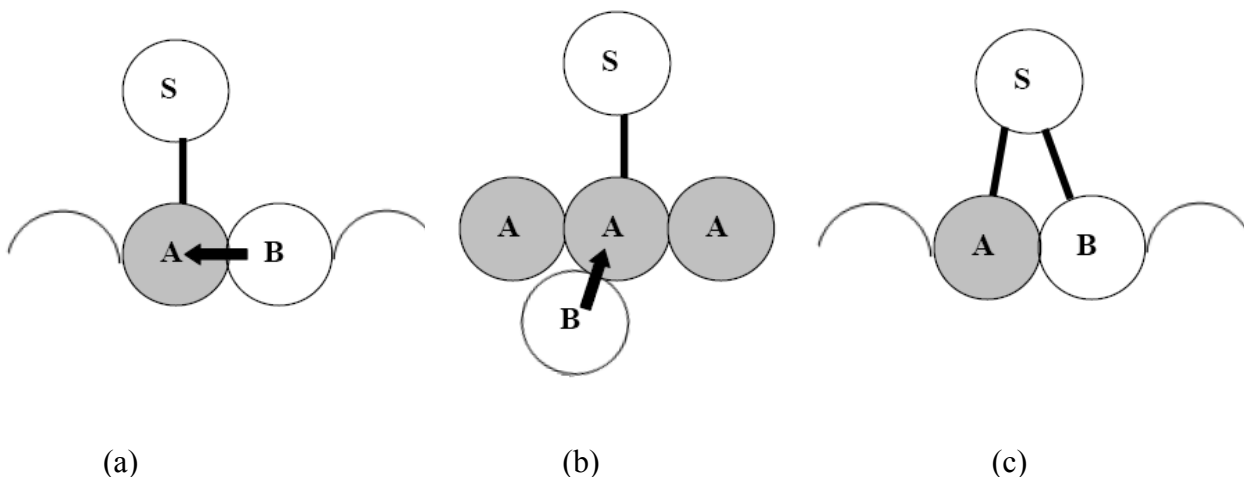


**Figure 1.2.** Schematic view of the electronic/ligand effect (a, b) and ensemble effect (c).<sup>53</sup> (Adapted from reference 53).

In the case of ensemble effects both metals must be located on the surface of the metal particles and facilitate a catalytic reaction in tandem.<sup>53</sup> For example, in the hydration of acrylonitrile by Cu-Pd nanoparticles, the presence of Pd atoms on the surface of Cu-Pd nanoparticles inhibits the oxidation of Cu atoms. In addition, the Pd atoms interact with the C=C bond of acrylonitrile, thus allowing the hydration of the CN bond of acrylonitrile to be catalyzed by adjacent Cu atoms.<sup>57</sup> Another example where the ensemble effect is prominent is the Ru-Pt bimetallic system used for fuel cell applications. In the methanol oxidation reaction, Ru provides oxygenated species at low potentials in the vicinity of Pt sites, thus promoting  $\text{CO}_{\text{ads}}$  oxidation.<sup>58</sup>

### 1.1.3 Structure of Bimetallic Nanoparticle Catalysts

When two different metals form a bimetallic particle, there can be variety of possible bimetallic structures. In many cases, the phase behavior of bimetallic mixtures is

well known in the literature; however, such phase diagrams may not be applicable for nanoscale systems.<sup>59</sup> Three specific common examples of bimetallic structures are random alloys, core-shell structures, and cluster-in-cluster nanoparticles,<sup>53,54</sup> examples of which are shown in Figure 1.3. However, it should be noted that there are many other possible structures of bimetallic nanoparticles, including intermetallic superstructures and sub-surface alloys.<sup>60,61</sup> In addition, common packing arrangements of metal atoms in the bulk may or may not be observed in nanoparticle species.<sup>59,62</sup> Finally, a number of groups have detailed the synthesis of non-spherical anisotropic particles, which will not be discussed here.<sup>63-65</sup>

A common structure formed in bimetallic nanoparticles is the random alloy structure. In the random alloy structure, the two different metals (A and B) are located completely at random, as shown in Figure 1.3(a).<sup>16</sup> However, parameters which control the formation of alloy structures such as the reduction kinetics of each metal, mole ratios and presence of external ligands can all play important roles in terms of whether or not alloy structures are realized.<sup>66</sup>

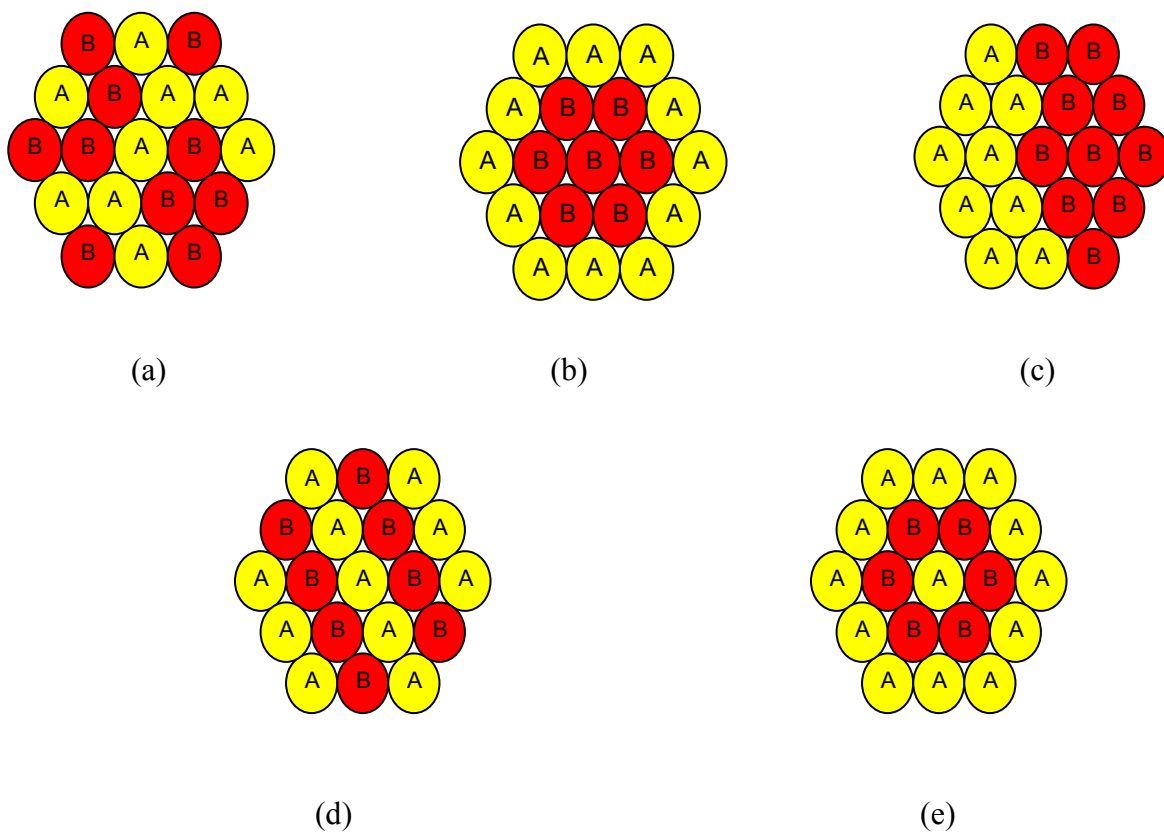


**Figure 1.3.** Schematic illustration of various structures of bimetallic nanoparticles. (a) random alloy; (b) core-shell; (c) cluster-in-cluster structure; (d) intermetallics; and (e) sub-surface shells.

Another interesting bimetallic nanoparticle structure is the core-shell structure in which one metal forms the core and the other metal surrounds the core to form a shell. Core-shell structures are often formed by co-reduction and successive reduction methods described in the next section. Design of core-shell nanoparticles is interesting because they can be used as a tool for systematic investigations of the electronic properties of catalysts and can potentially be used to minimize the amount of precious metals, such as Pd and Pt, during the synthesis of industrial bimetallic catalysts.<sup>16</sup>

Cluster-in-cluster structures often have small metal clusters which are located on/within a larger cluster, as shown in Figure 1.3(c). In this case, one element forms clusters on the surface and the other element surrounds the clusters and acts as a binder.<sup>16</sup> This type of structure may be considered as a modification of the core-shell structure which can result by coagulation and atomic rearrangement of nanoparticles, and is often seen for systems in which phase separation is problematic.<sup>16</sup>

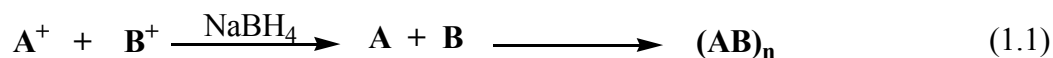
#### **1.1.4 Synthesis of Bimetallic Nanoparticle Catalysts**

For the synthesis of bimetallic nanoparticles by chemical methods, two typical procedures are normally used. The first being the co-reduction method while the second is known as the successive reduction method.<sup>16</sup> The co-reduction method is the most widely used method for the synthesis of bimetallic nanoparticles. The synthetic steps involved towards synthesizing monometallic nanoparticles are similar to that for the bimetallic nanoparticles with the only difference being that two metallic precursors are simultaneously reduced. The successive reduction method is normally used to synthesize core-shell bimetallic nanoparticles where one metal is used as the core (seed particles) while the other one is situated in the shell. In the following sections, these methods are outlined.

##### **1.1.4.1 Co-reduction**

In this method, two metallic salts are simultaneously reduced in the presence of stabilizer to form the corresponding bimetallic nanoparticles. The general scheme is outlined below in equation 1.1:





Bimetallic nanoparticles that are synthesized using this method often have an alloy structure.<sup>16,17</sup> However, it should be noted that alloy structures will be formed only if both metals are reduced at similar rates and phase separation of the two metals is not problematic, *i.e.*, the metals have similar reduction kinetics and the mixture of metal atoms is favorable thermodynamically.

Most of the synthetic methods employed for the synthesis of monometallic nanoparticles have been employed for the bimetallic nanoparticles. For example, by simultaneous reduction of metallic salts in a refluxing alcohol medium, polymer stabilized bimetallic nanoparticles have been synthesized. By using this method, Pd-Pt, Au-Pd, Pt- Rh, Pt-Ru, Pd-Ru, and Ag-Pd bimetallic nanoparticles were synthesized by Toshima and others.<sup>67-71</sup> Bonnemann's group used tetraalkylammonium hydrotriorganoborates (NR<sub>4</sub>(Bet<sub>3</sub>H)) as a reducing agent for a wide variety of bimetallic nanoparticles in organic media.<sup>72-74</sup> Also, tetraoctylammonium triethylhydroborate has been used as a reducing agent for the synthesis of Pt-Ru and Pt-Rh bimetallic nanoparticles.<sup>73,75</sup>

Another way for the synthesis of bimetallic nanoparticles involves the reduction of organometallic complexes. Chaudret *et al.* synthesized poly(vinylpyrrolidone) (PVP)-stabilized Pt-Ru nanoparticles by hydrogen reduction of Pt(dba)<sub>2</sub> and Ru(COD)(COT) organometallic complexes.<sup>76</sup> A similar procedure was used for the synthesis of Ag-Pd and Ag-Pt nanoparticles.<sup>77</sup> Thermal decomposition of two organometallic complexes in a high boiling point solvent in the presence of polymer stabilizer can also lead to the

synthesis of bimetallic nanoparticles. For example, Bradley *et al.* synthesized PVP-stabilized Pd-Cu nanoparticles by thermal decomposition of palladium acetate and copper acetate in an ethoxyethan-2-ol solvent.<sup>78</sup>

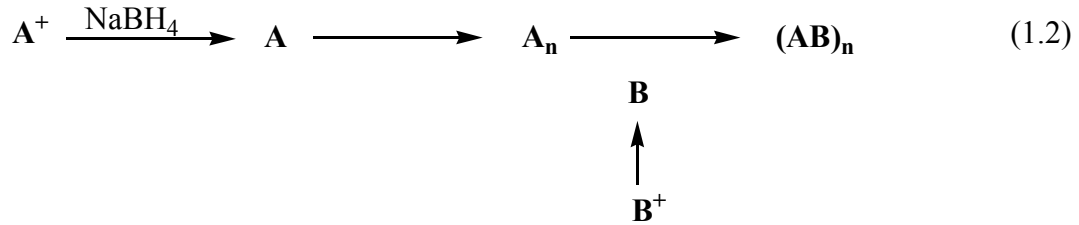
Gamma irradiation (or the radiolysis method) has also been applied for the synthesis of bimetallic nanoparticles. Remita *et al.* synthesized poly(vinyl alcohol) (PVA)-stabilized Ag-Pt nanoparticles by gamma irradiation (with the formation of reductants like solvated electrons and organic radicals) of an aqueous mixture of  $\text{Ag}_2\text{SO}_4$  and  $\text{K}_2\text{PtCl}_4$ .<sup>79</sup> Au-Pt and other bimetallic nanoparticles have also been synthesized by this gamma irradiation method.<sup>80,81</sup> Finally, Reetz *et al.* synthesized a variety of bimetallic nanoparticles by an electrochemical approach.<sup>82</sup> In this case, two different sacrificial metallic anodes and a Pt cathode were used and immersed in an electrolyte in the presence of a tetraalkylammonium salt which acts as a stabilizer. Bimetallic nanoparticles were formed after the reduction of metallic ions at the cathode.

It is important to note that co-reduction does not necessarily lead to the formation of nanoparticles with alloy structures. Core-shell nanoparticles can also be prepared by co-reduction method. In the co-reduction method, two factors have been shown to be important towards the formation of core-shell structures. The first factor is the redox potential and kinetics of reduction; the metal most easily (or quickly) reduced will often form the core.<sup>16</sup> The other important factor is the coordination ability of the polymer ligands upon the metal. Strong interactions between the ligands and one of the two types of metals in bimetallic nanoparticles can lead to surface enrichment of that species to give core-shell particles.<sup>16</sup> Toshima and co-workers synthesized Pd-Pt bimetallic nanoparticles

with a core-shell structure by simultaneous reduction of PdCl<sub>2</sub> and H<sub>2</sub>PtCl<sub>6</sub> in refluxing ethanol/water in the presence of PVP.<sup>67,83</sup> They postulated that Pd particles formed first due to the faster reduction kinetics of the PdCl<sub>2</sub> precursor, followed by hydrogen adsorption (generated from the alcohol) on the Pd surface. The Pd-H species then acted as a reducing agent for the reduction of Pt ions onto the preformed Pd nanoparticles.

#### 1.1.4.2 Successive Reduction

For the reproducible synthesis of core-shell nanoparticles, the successive reduction method has been found to be the most suitable procedure that ensures batch to batch homogeneity. In this method, a second metal is grown on the surface of pre-formed metal nanoparticle seeds. The general strategy is shown below in equation 1.2:



However, care must be taken to completely separate the nucleation and growth of the particles to minimize secondary nucleation to form new particles of the second metal *i.e.*, B<sub>n</sub>. In addition, spontaneous galvanic exchange reactions can be problematic when using such strategies.<sup>84,85</sup> This can be particularly challenging in the case of Pd/Au core-shell nanoparticle synthesis due to the different redox potentials of Pd and Au ions (Au<sup>3+</sup>/Au = 1.498 V, Pd<sup>2+</sup>/Pd = 0.951 V vs. SHE).<sup>84</sup> After the synthesis of Pd seeds, Au<sup>3+</sup> ions are added to the solution and Pd<sup>0</sup> atoms on the nanoparticles are oxidized upon the reduction of Au<sup>3+</sup> ions to Au<sup>0</sup> atoms. After the reduction of Au<sup>3+</sup> ions, the oxidized Pd

ions can then be reduced again by the reducing agent. However, galvanic reactions of  $\text{Au}^{3+}$  salts with the  $\text{Pd}^0$  nanoparticles can be avoided by pre-reducing the  $\text{AuCl}_4^-$  salt with ascorbic acid to form  $\text{Au}^+$  salts prior to addition of the Au salts to the Pd nanoparticle seeds.<sup>85</sup> This strategy was first reported by the Murphy group for the growth of larger Au nanoparticles and nanorods from Au nanoparticle seeds,<sup>86</sup> and has been adapted by a number of other groups for the growth of Au on Pd.<sup>84,87</sup> Crooks and co-workers used ascorbic acid as a mild reducing agent for the shell reduction during the synthesis of dendrimer-stabilized Au/Pd and Pd/Au core-shell nanoparticles.<sup>84</sup> Similarly, Schmid and co-workers prepared 20-35 nm Au/Pd and Pd/Au ligand-stabilized core-shell nanoparticles using hydroxylamine hydrochloride as a mild reducing agent for the shell reduction.<sup>87</sup>

Finally, it should be noted that it cannot be assumed that successive reduction methods always leads to the formation of core-shell nanoparticles. Several groups have noted that such strategies can also lead to the formation of alloy structures or physical mixtures of the two metals, particularly if care is not taken during the shell growth step.<sup>16,88</sup> To confirm the formation of core-shell structure, complete characterization of the resulting nanoparticles has to be carried out to verify their final structures.

### **1.1.5 Au, Pd, and Bimetallic Au-Pd Nanoparticle Catalysts**

Due to its resistance to oxidation, Au has historically been primarily used for monetary exchange and jewelry fabrication.<sup>89</sup> However, Haruta *et al.* in the late 1980s discovered that Au nanoparticles smaller than 5 nm supported on  $\alpha\text{-Fe}_2\text{O}_3$  were very active for CO oxidation, a reaction of key technological importance.<sup>12</sup> This is a

particularly important reaction for applications in different areas like fuel cells and the automotive industry, which typically use Pt catalysts which can suffer from CO poisoning.<sup>4</sup> Since this discovery, the applications of Au nanoparticles in catalysis have attracted great attention and have been extensively studied.<sup>9,89,90</sup> To date, most gold nanoparticle catalyst systems are heterogeneous systems in which gold nanoparticles are supported on a metal oxide support, such as Al<sub>2</sub>O<sub>3</sub>, TiO<sub>2</sub>, Fe<sub>2</sub>O<sub>3</sub>, Co<sub>2</sub>O<sub>3</sub> and La<sub>2</sub>O<sub>3</sub>.<sup>4</sup> Many factors contribute to the higher activity and selectivity for the CO oxidation reaction by small gold nanoparticles. One dominant effect as postulated by Mavrikakis and co-workers is that small gold nanoparticles possess very potent under-coordinated sites with the optimal binding environments for CO and O substrates.<sup>89</sup> Also, metal-support interactions are thought to be important for the catalytic activity and selectivity of Au nanoparticles.<sup>4</sup> Despite this intense activity, several of the key questions pertaining to Au nanoparticle catalysis are still under intense debate.<sup>88,91,92</sup> In recent years, several solution phase Au nanoparticle catalyst systems have been reported, although such examples are much fewer in number than those of heterogeneous catalyst systems involving Au nanoparticles.<sup>93-95</sup> One of the possible reasons for their infrequent use in solution phase catalysis may be of the fact that monometallic Au nanoparticles still do not have satisfactory activity and selectivity for many reactions.

One way to enhance the activity and selectivity of Au-containing nanoparticles is the design of bimetallic nanoparticle catalysts.<sup>16</sup> Bimetallic catalysts have long been of subject of interest for investigating the electronic factors in catalysis by metals.<sup>96</sup> Transition metals, especially the platinum-group metals (Ni, Pd, Pt) are the active catalysts for many reactions. In terms of the electron-band theory, a Pt-group metal such

as Pd is characterized as having an incompletely filled d-orbital, whereas Au has a filled d-orbital. In the case of a Pd-Au alloy, there can be electronic interactions between the Au and Pd, and thus by varying the composition of the alloy, one can alter the degree of filling of the d band with electrons and observe the resulting effect on catalytic activity.<sup>96</sup> Also, ensemble effects have been shown to have profound effects in the enhancement of catalytic activity and selectivity for Pd-Au systems.<sup>97</sup> Recently Goodman and co-workers studied the synthesis of vinyl acetate from acetoxylation of ethylene over Pd-Au alloys.<sup>97</sup> They documented that upon alloying Au with Pd, preferential surface enrichment of Au was observed, and that the role of the Au was to isolate surface Pd monomers upon annealing. These Pd monomers were found to be the active species in the formation of vinyl acetate.

Over the years, Pd-Au nanoparticles as a bimetallic catalyst system have been widely explored. Toshima and co-workers showed that PVP-stabilized Au-Pd bimetallic nanoparticles had higher catalytic activity than pure Au or Pd monometallic nanoparticles for the selective partial hydrogenation of 1,3-cyclooctadiene at 30<sup>0</sup> C under 1 atm of hydrogen, with a maximum catalytic activity achieved at a Au:Pd ratio of 1:4.<sup>68</sup> There are many recent examples involving the synthesis of highly active Au-Pd bimetallic nanoparticles.<sup>55,84</sup> For example, Hutchings *et al.* have shown that Pd-Au catalysts have a 25-fold increase in activity for the oxidation of alcohols to aldehydes as compared to pure Au or Pd catalysts.<sup>98</sup> Besides higher activity, the selectivity towards the formation of aldehyde products (for example,  $\geq 96$  % to benzaldehyde in the case of benzyl alcohol oxidation) was also improved upon introduction of Au to Pd.<sup>98</sup> They documented that Au acts as an electronic promoter for Pd and the active catalyst has a surface which is

enriched in Pd. Hutchings and coworkers and others have also shown that bimetallic Pd-Au nanoparticles have also shown excellent catalytic performance for the direct synthesis of H<sub>2</sub>O<sub>2</sub> from H<sub>2</sub> and O<sub>2</sub>,<sup>99-102</sup> glycerol oxidation,<sup>103</sup> the hydrochlorination of acetylene,<sup>104</sup> and many other reactions.<sup>97,105-108</sup> In the case of H<sub>2</sub>O<sub>2</sub> formation, Pd-Au nanoparticles with 1:1 Pd:Au ratios resulted in dramatic increases in activity and selectivity compared to pure Au nanoparticles.<sup>99</sup> Similarly, carbon-supported Pd-Au catalysts showed higher selectivity for glycerol oxidation to glyceric acid compared to monometallic Au catalysts (84 % vs. 65 %).<sup>103</sup>

## 1.2 Characterization of Nanoparticle Catalysts

Once metal nanoparticles have been synthesized, it is very important to completely characterize their structures. A schematic view of the structure of metal nanoparticles is given below (Figure 1.4). Over the years, many methods have been developed for the determination of nanoparticle structures.

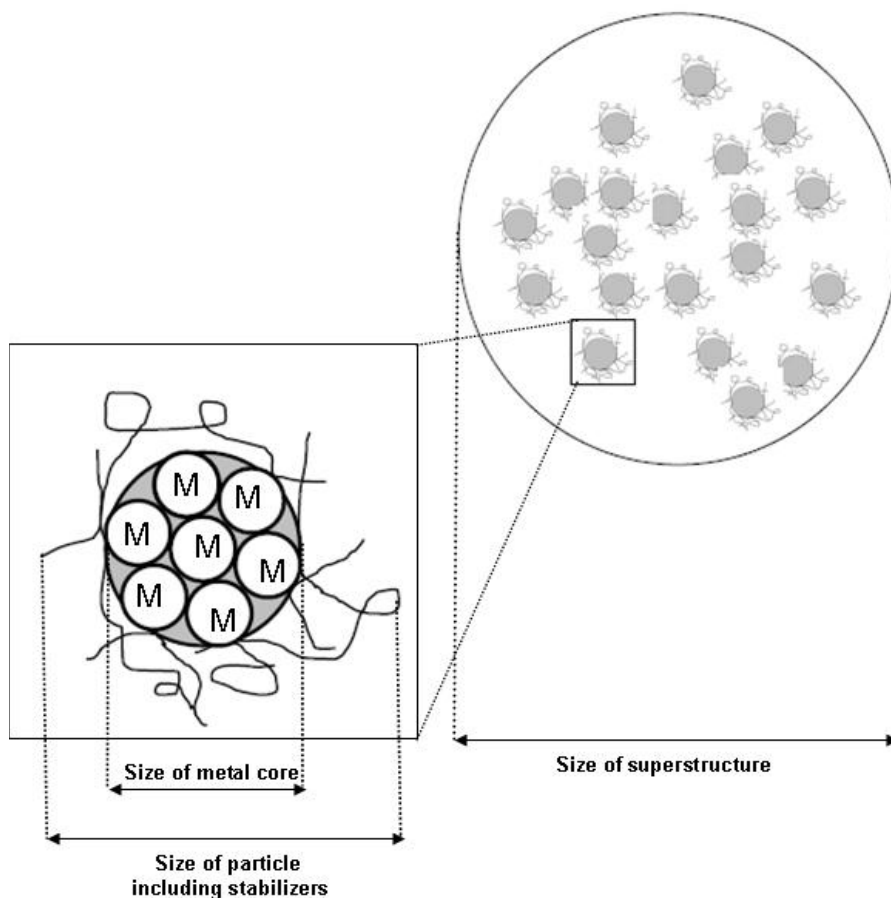


**Figure 1.4.** Schematic view of the structures of metal nanoparticles.<sup>53</sup> (Adapted from reference 53).

Some of the most commonly used characterization methods for nanoparticle catalysts are outlined below (Table 1.1). Small angle x-ray scattering (SAXS) can be used for measurement of the size of the superstructures. Light scattering methods can be used to determine the *in-situ* nanoparticle size for the whole nanoparticle including both core and stabilizer. The size of the metal nanoparticle core can be routinely measured by electron microscopy techniques. The size and coordination environments of metal clusters and nanoparticles can be measured by extended x-ray absorption fine structure spectroscopy (EXAFS) using high energy synchrotron techniques. For the determination



of bimetallic structures and compositions, EXAFS and energy dispersive x-ray spectroscopy (EDS, an x-ray fluorescence technique) are the most commonly used methods. In this section, some of the major characterization techniques used for the structural determinations of nanoparticle catalysts are outlined.

**Table 1.1.** Characterization methods used for the structural determination of metal nanoparticles.

<b>Method</b>	<b>Metal structure</b>
Light Scattering	Size (core + ligand shell)
Small angle X-ray Scattering (SAXS)	Size (core + ligand shell)
Transmission Electron Microscopy (TEM)	Size (core), Morphology, Atomic coordinates
Energy Dispersive X-ray (EDS) Spectroscopy	Elemental Distribution
X-ray diffraction (XRD)	Crystal Structure, Particle size
X-ray photoelectron Spectroscopy (XPS)	Oxidation State, Electronic Interactions
Extended X-ray Absorption Fine Structure (EXAFS) Spectroscopy	Average coordination environments, bond distances
X-ray Absorption Near-Edge Structure (XANES) Spectroscopy	Oxidation state and orbital occupancy
Ultraviolet(UV)-Visible Spectroscopy	Plasmon bands, presence of aggregates
Infrared (IR) Spectroscopy	Surface structure

### 1.2.1 UV-Visible Spectroscopy

For nanoparticles, localized surface plasmon oscillations for certain metals can give rise to intense colours for solutions containing the nanoparticles. Au, Ag, and Cu nanoparticles in particular have characteristic colors for size ranges from 1-10 nm.<sup>16</sup> This unique property has found applications since medieval times, in which artisans like the stained glass makers often used Au and Ag colloids to make red and yellow inks, respectively.<sup>109</sup> These nanoparticles exhibit strong absorption bands in the visible light regime. Thus, for these metals, the UV-Vis spectra can be a useful complementary technique for characterizing metal particles. UV-Vis spectra can also be used to qualitatively differentiate between monometallic and bimetallic nanoparticles. Monitoring UV-Vis spectral changes during successive reductions can provide important information about the formation of bimetallic nanoparticles. Comparison of UV-Vis spectra of bimetallic nanoparticles with those of physical mixtures of the respective monometallic particle dispersions can also identify secondary nucleation problems which can occur during nanoparticle synthesis. For example, Scott *et al.* used UV-Vis spectra to differentiate the formation of alloy and core-shell Pd-Au nanoparticles.<sup>84</sup> Pure Au nanoparticles show a clear plasmon band at ~ 520 nm, while UV-Vis spectra of co-reduced Pd-Au samples showed no separate Au plasmon peak at ~520 nm, confirming the likely formation of bimetallic nanoparticles. The absence of Au plasmon bands in the UV-Vis spectra in the Pd-Au sample was indicative of the fact that there is no separate formation of pure Au nanoparticles in the alloy sample. However, it is important to note that though UV-Vis spectroscopy is a useful technique to monitor the formation of

monometallic and bimetallic nanoparticles, it cannot be used decisively to determine nanoparticle structures unambiguously.

### 1.2.2 TEM

As the properties of nanoparticles depend primarily on size, measurement of both the size and size distribution is important to understanding their properties.<sup>110</sup> Among the various techniques used for the size determination of metal nanoparticles, transmission electron microscopy (TEM) is indispensable. TEM allows the direct visualization of metal nanoparticles and shows only the metal core diameter. Under a high voltage electron beam, metal nanoparticles, especially those consisting of heavy (precious) metal elements, give high contrast when the particles are dispersed on thin carbon films. Resolution of the nanoparticles at the sub-angstrom level can be obtained using TEM, thanks to the recent developments in this area.<sup>111</sup> The most common methods used for imaging in the TEM are bright-field (BF), dark-field (DF), and phase contrast imaging.<sup>111</sup> At high magnifications, it is normally referred to as high resolution TEM (HRTEM). However, it is important to know that for effective characterization, the proper selection of imaging type and magnification is required. For example, very small metal nanoparticles tend to become less stable under intense electron beams due to particle motion, structural fluctuations, coalescence, and particle destruction.<sup>111</sup> In such scenarios, scanning TEM (STEM) has proven to be advantageous. In STEM, a continuously moving rastering nanoprobe (diameter of  $\sim 0.1-10$  nm) analyzes samples, thus limits the total electron beam dose on a particular sample area.<sup>111</sup> HRTEM can also provide information on the crystal structure of the metal nanoparticles via atomic spacing measurements and

electron diffraction experiments. Also, core-shell structural information can be obtained using STEM imaging at the atomic scale. As a recent state-of-the-art example, Nuzzo and co-workers used bright-field STEM imaging as a technique for the atomic level characterization of bimetallic Pt/Pd core-shell nanoparticles, as shown in Figure 1.5.<sup>112</sup>

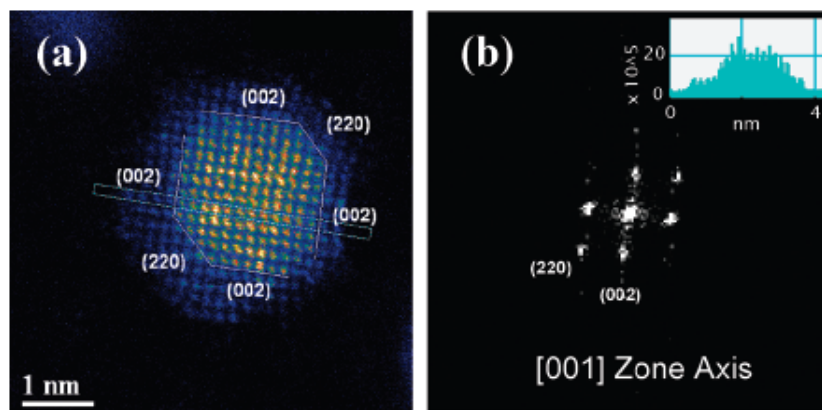


**Figure 1.5.** (a) STEM image of a Pt/Pd core-shell nanoparticle. (b) power spectrum data and annotated zone axis with the intensity profile represented in the inset.<sup>112</sup> (Published with permission from reference 112. Copyright (2009) American Chemical Society).

It was found that Pt-Pd core-shell nanoparticles have stronger scattering intensity concentrated at the center of the particle (from the Pt core) with weaker scattering atoms (Pd) around the periphery. With the improvement of new powerful techniques like aberration correction, through-focus image reconstruction, and tomography, the future of nanoparticle size characterization by TEM looks quite promising.<sup>111</sup>

### 1.2.3 EDS Mapping

Energy dispersive x-ray spectroscopy (EDS) coupled with HRTEM is one of the most revealing methods for the compositional determination of bimetallic

nanoparticles.<sup>113</sup> In this case, the electron beam is focused either on a single particle within the sample or over a wide area. The incident beam excites an electron in an inner shell, ejecting it from the shell while creating an electron hole. An electron from an outer and higher-energy shell then fills the hole and the difference in energy between the higher-energy shell and the lower energy shell is released in the form of an x-ray. The wavelength of the x-rays emitted from a specimen are characteristic of the difference in energy between the two shells and thus of the atomic structure of the element from which they were emitted, which allows the elemental composition of the specimen to be probed. This method provides analytical data which can not provided from other x-ray methods. For example, typically HRTEM images of alloy and core-shell nanoparticles look similar. However, by using an EDS probe in STEM mode, the local composition and architecture (alloy vs. core-shell) can be distinguished. Chupas *et al.* used this technique for the compositional and architectural evaluation of Ru/Pt core-shell and alloy nanoparticles.<sup>114</sup> Multiple single-particle EDS analyses of both core-shell and alloy nanoparticles confirmed the formation of bimetallic particles with no formation of secondary monometallic nanoparticles. In the case of core-shell nanoparticles, the EDS line scans showed maximum Pt distributions at the edge (*i.e.*, the shell) whereas the Ru EDS line scan shows maximum Ru concentration at the center of the particle, as seen in Figure 1.6a.<sup>114</sup> However, in the case of PtRu alloy nanoparticles, Gaussian distributions of x-rays were detected across the particle for both elements which were due to the random arrangement of atoms on the surface and in the bulk of the particle (Figure 1.6b).

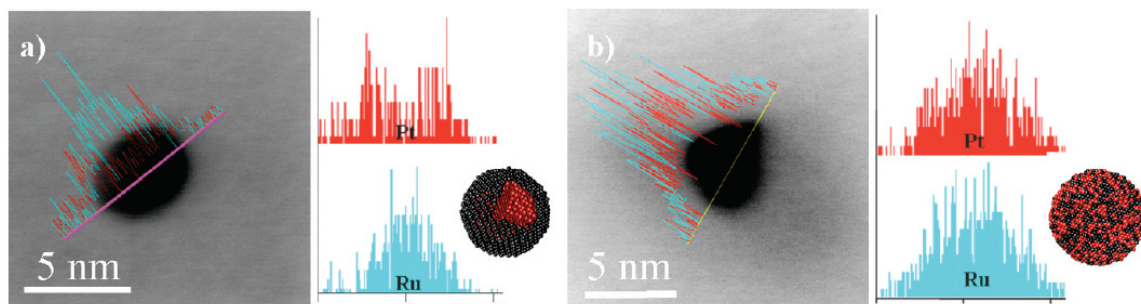


**Figure 1.6.** Representative EDS line scan spectra of (a) a 4.0 nm Ru/Pt core-shell nanoparticles and (b) a 4.4 nm Pt-Ru (1:1) alloy nanoparticle. The blue and red EDS lines are Ru and Pt, respectively. Ru K and Pt L lines were used for EDS line scans and a 1.5 nm probe was used.<sup>114</sup> (Published with permission from reference 114. Copyright (2009) American Chemical Society)

#### 1.2.4 XRD

Powder x-ray diffraction (XRD) is one of the most common non-destructive structural analysis methods used for the determination of the solid structure of metal nanoparticles. Using powder XRD, phase and particle size changes can be investigated in the case of monometallic nanoparticles.<sup>114</sup> XRD can be used for the determination of the presence of bimetallic nanoparticle alloys, as compared with a mixture of monometallic particles. The diffraction pattern of physical mixtures consists of overlapping lines of the two individual monometallic nanoparticles which is clearly distinct from that of the bimetallic nanoparticles. For example, powder x-ray diffraction profiles of Pt-Ru (1:1) alloy nanoparticles indicated the presence of an fcc structure which is intermediate between bulk fcc Pt and the fcc equivalent of metallic hcp Ru.<sup>114</sup> However, in the case of Ru/Pt core-shell nanoparticles, the XRD spectrum was found to be a superimposition of

the two components; a poorly crystalline hexagonal closed-packing (hcp) Ru core and a distorted but relatively crystalline Pt shell.

Another way of evaluating diffraction data is the atomic pair distribution function (PDF) analysis. Atomic PDF analysis has been used for probing the structures of small metal nanoparticles.<sup>115</sup> In this case, the diffraction data is evaluated in terms of the total reduced structure factor,  $F(Q)$ , and its Fourier transformed equivalent  $G(r)$ . For example, Pt-Ru alloy nanoparticles showed a long-range order whereas in Ru/Pt core-shell nanoparticles the same long range order was observed but with M-M separations different than those of the alloy nanoparticles.<sup>114</sup>

### 1.2.5 XPS

For the elucidation of oxidation states of metal nanoparticles, quantitative x-ray photoelectron spectroscopy (XPS) analysis is a powerful technique. The XPS technique is highly surface specific due to the short distance range of the photoelectrons that are excited from the surface.<sup>16</sup> Figure 1.7 shows a representation of the underlying interactions underlying XPS.<sup>116</sup> In the XPS method, a photon is absorbed by the atom in a molecule, followed by the ionization and ejection of a core or inner shell photoelectron. The kinetic energy of the photoelectrons leaving the surface gives a spectrum with a series of photoelectron peaks in which the binding energy of the peaks is unique for each element.

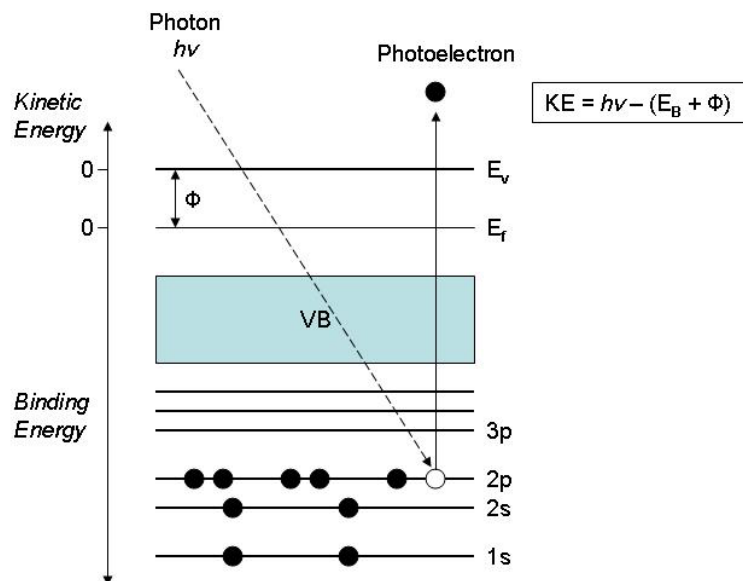


**Figure 1.7.** Schematic diagram showing the principle of XPS.<sup>116</sup> (Adapted from reference 116).

In the case of bimetallic nanoparticles, quantitative analysis of XPS spectra can, in principal, allow one to determine which elements are present in the surface region of the nanoparticles. For example, van Veggel and co-workers have recently shown that XPS with tunable synchrotron radiation can be used for the structural evaluation of NaYF<sub>4</sub>/NaGdF<sub>4</sub> core/shell nanoparticles.<sup>117</sup> In this study, photoelectron spectra of Y<sup>3+</sup> 3d (core) and Gd<sup>3+</sup> 4d (shell) were recorded at increasing excitation photon energies. At higher kinetic energies, the intensity ratio of Y<sup>3+</sup> 3d to Gd<sup>3+</sup> 4d core levels was increased, thus confirming the presence of Gd<sup>3+</sup> atoms on the surface of the particles; if alloy nanoparticles had been formed the peak ratio would have been constant.



### 1.2.6 EXAFS and XANES

In general, HRTEM and EDS mapping techniques can help follow the average particle size and atomic composition; however they do not give much information about surface vs. bulk atomic distributions. X-ray absorption fine structure spectroscopy (XAFS) comprising both x-ray absorption near-edge structure spectroscopy (XANES) and extended x-ray absorption fine structure spectroscopy (EXAFS) has been a valuable tool for the examination of metallic and bimetallic nanoparticle structures by the catalyst community.<sup>96,118,119</sup> Much of the initial pioneering work on bimetallic systems was carried out by Sinfelt and co-workers who studied a series of bimetallic nanoparticles using EXAFS techniques.<sup>54,96,119</sup> EXAFS spectroscopy uses the x-ray photoelectric effect and the wave nature of the electron to determine local structures around selected metal atoms. Figure 1.8 shows the photoelectric effect as it applies to EXAFS spectroscopy.<sup>120</sup>

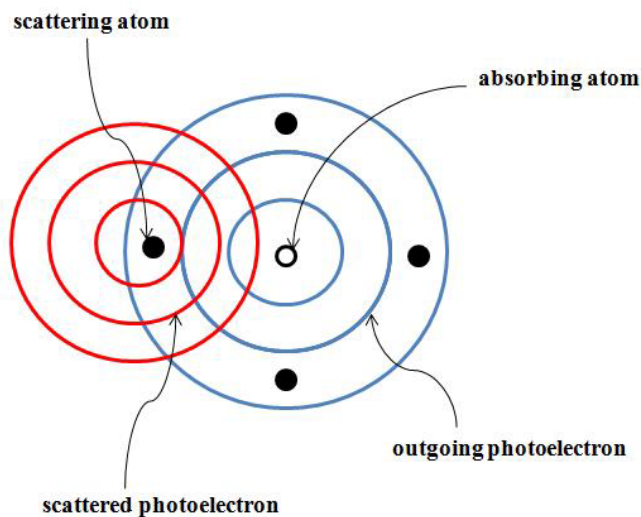


**Figure 1.8.** Photoelectric effect in EXAFS spectroscopy.<sup>120</sup> (Adapted from reference 120).

Upon absorption of a photon, excitation of the core electrons to an unoccupied continuum state occurs, resulting in the formation of photoelectrons. The interaction of incoming and outgoing photoelectrons results in an interference signal. The EXAFS technique involves the analysis of this interference signal which contains information about the average atomic environment around the absorbing atom.<sup>111</sup> The specific x-ray absorption spectrum of each metal element contains information such as the electron density and number of metal elements (i.e. the coordination number) surrounding the x-ray absorbing metal, and the interatomic distances involved in the various coordination shells. While XANES can reveal the oxidation state and d-occupancy of a specific atom,<sup>121,122</sup> EXAFS provides a valuable tool for the analysis of local atomic structure, giving information about the average local atomic coordination environment.<sup>111,123</sup> When combined with adequate models of the nanoparticle structure and composition, EXAFS measurements can be used to shed light on possible structures of such nanoparticles. For example, Toshima and co-workers structurally characterized Pt/Pd core-shell nanoparticles synthesized by the co-reduction method using EXAFS spectroscopy and demonstrated that a Pt core structure was formed in which on average 42 Pd atoms were on the surface and 13 Pt atoms were in the core.<sup>67</sup> However, in the case of Pd-Pt (1:1) bimetallic nanoparticles, a cluster-in-cluster structure was formed in which on average 28 Pt atoms were located both in the core and on the surface, while the 27 Pd atoms formed islands on the surface of bimetallic nanoparticles. Similarly, Crooks and co-workers used this methodology to determine the structure of Pd-Au dendrimer-encapsulated nanoparticles.<sup>124</sup> For a perfect Au core surrounded by a Pd shell, the total coordination surrounding the Au atom ( $N_{\text{Au-M}}$ ) should be 12, similar to bulk fcc gold whereas for the

Pd shell, the total coordination numbers ( $N_{\text{Pd-M}}$ ) should be smaller than that of the Au core. In the case of dendrimer-stabilized Au/Pd core-shell nanoparticles, the  $N_{\text{Au-M}}$  was found to be  $12.5 \pm 3.0$ , which was much higher than the  $N_{\text{Pd-M}}$  which clearly suggested the formation of an Au core and Pd shell.<sup>124</sup>

XANES can be used to gather information on the oxidation state of a specific atom. Chupas and co-workers used XANES to characterize Ru-Pt alloy nanoparticles. They found that Pt and Ru were primarily in the metallic zerovalent state in Pt-Ru alloy nanoparticles.<sup>114</sup> However, Ru was slightly oxidized, which was further confirmed from surface IR measurements using CO as a probe (see next section). Also, XANES can be used to investigate the density of unfilled states above the Fermi level in bimetallic systems. Baiker and co-workers recently used XANES to describe the electronic configuration of Au and Pd in bimetallic Pd-Au nanoparticles.<sup>55</sup> They found a clear shift to lower binding energies of Au core levels with increasing Pd content, which was an indication of a change in electronic configurations of Pd and Au. Upon examination of Au XANES spectra, a decrease in the number of d holes of the Au 5d valence band was observed with increasing Pd content.

### **1.2.7 CO adsorption by IR**

For the investigation of the surface composition of metal nanoparticles, infrared (IR) spectroscopy is one of the most widely used techniques. For this purpose, carbon monoxide which can be easily adsorbed on metal surfaces is frequently studied. Depending on the variation of the surface structure, the adsorbed CO can be adsorbed on different sites of the nanoparticle surface.<sup>16</sup> The wavenumber of adsorbed CO changes

dramatically with the binding atom, oxidation state, and coordination environment.<sup>125,126</sup>

This method can be used to determine the surface structure of bimetallic nanoparticles by comparing IR spectra of CO on a series of bimetallic nanoparticles of different metal compositions. For example, Eichhorn and co-workers used this technique to find out the surface composition of Ru/Pt core-shell nanoparticles and to confirm that only core-shell nanoparticles were formed and not physical mixtures of Ru and Pt metals (Figure 1.9).<sup>59</sup>

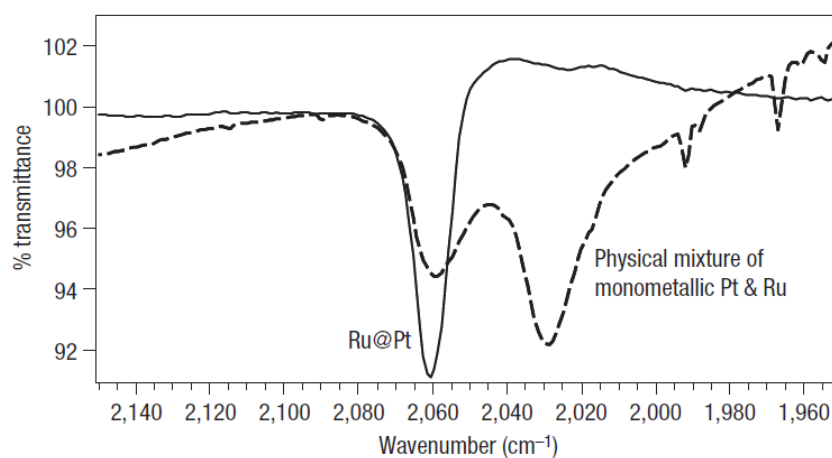


**Figure 1.9.** FTIR spectra of Ru/Pt core-shell and physical mixtures of Pt and Ru nanoparticles in the presence of CO(g).<sup>59</sup> (Published with permission from reference 59. Copyright (2008) Nature Publishing Group)

Distinct Ru–CO (2,029 cm<sup>-1</sup>) and Pt–CO (2,059 cm<sup>-1</sup>) peaks were obtained for the physical mixtures of Pt and Ru nanoparticles. In contrast, the infrared spectrum of Ru/Pt core-shell nanoparticles showed a single peak at 2,061 cm<sup>-1</sup>, thus indicating the presence of only Pt atoms on the surface.

### 1.3 Stabilizers for the Synthesis of Nanoparticle Catalysts

Generally, nanoparticle surfaces are quite unstable and tend to aggregate and even precipitate out of solution and thus lose their catalytic activities. The best way to avoid this problem is the use of stabilizers like polymers, block copolymers, dendrimers, surfactants, or organic ligands which stabilize the metal nanoparticles. Catalysis by nanoparticles in solution is commonly referred as “quasi-homogeneous catalysis” because the nanoparticles are uniformly dispersed in the solvent medium and mixed with reactants and products in a way similar to a homogeneous catalytic system.<sup>9</sup> In this section, the use of different stabilizers and their effect on catalytic activity are described.

#### 1.3.1 Polymers

One general way to prevent the aggregation of nanoparticles is the use of polymers. Polymers provide steric stabilization for metal nanoparticles through the steric bulk of their framework.<sup>9</sup> Also, they can bind weakly to the nanoparticle surface via functional groups and thus play the role of ligands. Hirai *et al.* developed a method for measuring the protecting power of polymers called their “*protective value*” which was defined by the weight (in grams) of gold in a red gold sol which is protected by 1 g of the protecting polymer against flocculation by 1 wt % sodium chloride.<sup>127</sup> The protective values of different polymers like poly(*n*-vinylpyrrolidone) (PVP), poly(vinyl alcohol), poly(acrylamide), poly(acrylic acid) and poly(ethyleneimine) are 50.0, 5.0, 1.3, 0.07 and 0.04, respectively. One excellent polymer which fulfills both steric and ligand requirements and has extremely higher protective value is poly(vinylpyrrolidone) (PVP), which is shown below (Figure 1.10).<sup>127</sup> PVP is one of the most used polymers for

nanoparticle stabilization and catalysis and the reason are twofold; 1) due to the relatively low cost of PVP and (2) it allows synthesis of stabilized nanoparticles with accessible surface areas in polar solvents such as water, even at temperatures approaching the boiling point of water.<sup>16,128</sup> In addition, many groups have shown that PVP polymers do not completely passivate the nanoparticle surface.<sup>128</sup> Hirai and co-workers speculated that one part of the PVP chain adsorbs on the nanoparticle surface while the other part suspends freely in the solution forming a protective layer.<sup>127</sup> Tsukuda and co-workers postulated that in the case of PVP-stabilized Au nanoparticles, the particles are weakly stabilized through multiple coordination of the >N-C=O groups.<sup>93</sup> Though there are major advantages for using PVP as a stabilizer, there are some disadvantages also such as the problematic separation of the catalytic nanoparticles from the polymer and unused reactants at the end of the reaction.<sup>129,130</sup>

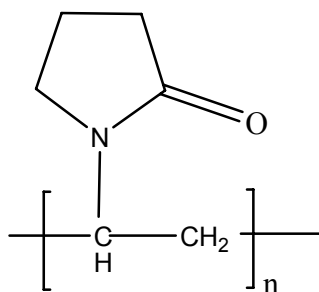


**Figure 1.10.** Structure of poly(vinylpyrrolidone) (PVP) polymer.

Over the years, PVP-stabilized nanoparticles have been used as catalysts for a variety of reactions. El-Sayed and co-workers showed that PVP-stabilized Pd nanoparticles are efficient catalysts for Suzuki C-C coupling reactions in an aqueous medium.<sup>129</sup> Tsukuda and co-workers showed that PVP-stabilized gold nanoparticles are

active for the aerobic oxidation of benzylic alcohols in an aqueous solution at ambient temperatures.<sup>93</sup> It is important to note that the PVP/metal ratio and molecular weight of PVP plays an important role in the nanoparticle catalytic activity. For example, El-Sayed and co-workers have shown that by varying the PVP/metal ratio, nanoparticles of varying sizes can be synthesized which has profound effects on their activity for Suzuki reactions.<sup>128</sup> Gniewek *et al.* have shown that during the synthesis of PVP-stabilized Pd nanoparticles, the molecular weight of PVP play a decisive role in the resulting catalytic activity of the particles towards the methoxycarbonylation of iodobenzene.<sup>131</sup> Besides monometallic nanoparticles, PVP-stabilized bimetallic nanoparticles have also been synthesized. Toshima's group synthesized both alloy and core-shell metal nanoparticles stabilized by PVP polymers.<sup>16,68,83</sup> Recently, our group synthesized PVP-stabilized Au, Pd, and bimetallic Pd-Au nanoparticles in water and these nanoparticle catalysts were found to be catalytically active and selective for aerobic oxidation of aliphatic, allylic, phenylic alcohols and diols under mild conditions.<sup>95</sup> PVP-stabilized nanoparticle catalysts have been used as standard catalysts for studying the effect of parameters such as particle size and stability during the catalytic process.<sup>129,132</sup> For example, El-Sayed and co-workers have shown that decreasing the Pd nanoparticle size down to 3 nm in the Suzuki reaction improved the catalytic activity and they postulated that low-coordination-number vertex and edge atoms on the particle surface are the active catalytic sites.<sup>129,132</sup> In some cases, PVP-stabilized nanoparticles were combined with chiral modifiers and used as enantioselective catalysts. For example, Bartok and co-workers used a combination of PVP-stabilized Pt nanoparticles with cinchonidine modifiers and the resulting catalyst gave >95% *ee* in the hydrogenation of  $\alpha$ -ketoesters.<sup>133</sup>

Besides PVP, other polymers have also been used for the synthesis of nanoparticle catalysts. For example, Sablong *et al.* have synthesized Pd nanoparticles stabilized by highly branched amphiphilic polyglycerol and the resulting system was found to be a highly active and recyclable catalyst for cyclohexene hydrogenation.<sup>134</sup> Liu *et al.* synthesized poly(N,N-dialkylcarbodiimide-stabilized Pd nanoparticles and the resulting nanoparticle catalysts were active for Suzuki C-C coupling reactions.<sup>135</sup> Sakurai and co-workers had shown that vinyl ether star polymer-stabilized Au nanoparticles were highly active and recyclable catalysts for aerobic oxidation of phenylic alcohols.<sup>136</sup> Block copolymers have also been used as stabilizers. For example, the Pluronic<sup>TM</sup> triblock copolymer polyethylene oxide-polypropylene oxide type (PEO-PPO-PEO) was used for the synthesis of Au nanoparticles.<sup>137</sup> Schubert and co-workers used 5-arm star-shaped block copolymers with a poly(ethylene oxide) (PEO) core and a poly( $\epsilon$ -caprolactone) (PLC) corona for the synthesis of Pd nanoparticles and the resulting nanoparticles were found to be highly active catalyst for Heck cross-coupling reactions.<sup>138</sup> It was found that the stability of the Pd nanoparticles was strongly dependent on the length of the PLC chains. Beletskaya *et al.* synthesized Pd nanoparticles stabilized in polystyrene-co-poly(ethylene oxide) and the catalysts were shown to be an effective catalyst for reactions involving C-C and C-heteroatom bond formation.<sup>139</sup>

### 1.3.2 Dendrimers

Dendrimers are well-defined macromolecules which originate from a central core with repetitive branching units. They have a polydispersity, which is a measure of the distribution of molecular masses in a given polymer sample, of nearly 1.0.<sup>9</sup> Over the



years, dendrimers have been found to be attractive hosts for catalytically active metal nanoparticles. Mostly, two families of dendrimers have been extensively used to stabilize metal nanoparticles as shown in Figure 1.11. One is the poly(amidoamine) (PAMAM) dendrimer family while the other one is poly(propyleneimine) (PPI) dendrimers.<sup>9,33</sup> The Crooks and Tomalia research groups described the formation of nanoparticles stabilized by dendrimers for catalysis in 1998.<sup>24-27</sup> For example, Crooks and co-workers described the synthesis of Cu, Au, Pt, Pd, Fe, and Ru nanoparticles using poly(amidoamine) (PAMAM) dendrimers.<sup>25-27</sup> Dendrimers with a higher steric bulk play a crucial role in the resulting catalytic activity of dendrimer-stabilized nanoparticles. For example, El Sayed and co-workers have shown that third and fourth generations of PAMAM dendrimers act as good stabilizers and result in higher activity in the Suzuki coupling reaction compared to that of the second generation PAMAM dendrimers.<sup>140</sup>

This dendrimer encapsulated nanoparticle strategy has also been used for the synthesis of bimetallic nanoparticles.<sup>84</sup> Three main approaches have been used for the synthesis of bimetallic nanoparticles stabilized by dendrimers: co-reduction, successive reduction, and partial (galvanic) displacement routes. One of the major advantages of dendrimer-stabilized bimetallic catalysts is that such catalysts facilitate compositional and structural control greater than compared to traditionally prepared bimetallic catalysts. Crooks and co-workers synthesized water-soluble and nearly monodisperse bimetallic alloys consisting of Pd and Pt prepared via the coreduction route using hydroxyl terminated PAMAM dendrimers.<sup>141</sup> Both alloy and core-shell nanoparticles were synthesized using dendrimers as stabilizers. For example, Crooks and co-workers synthesized Au/Pd core-shell nanoparticles in quaternary-ammonium terminated

dendrimers.<sup>84</sup> Single particle EDS data indicated that all of the Au/Pd core-shell nanoparticles were bimetallic, with the compositions similar to the molar ratio of the respective transition metal elements used during the synthesis.

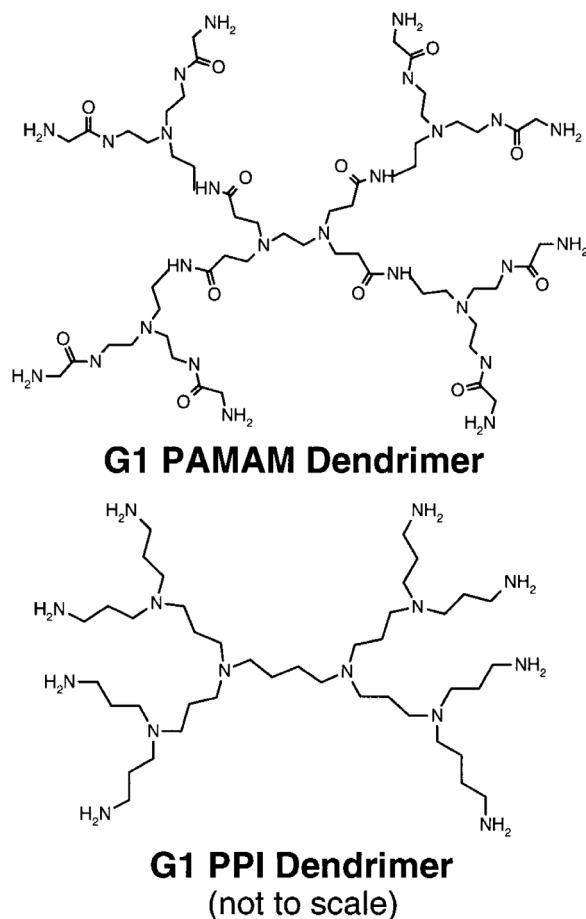


**Figure 1.11.** Structure of PAMAM and PPI dendrimers.<sup>33</sup> (Published with permission from reference 33. Copyright (2001) American Chemical Society).

### 1.3.3 Ligands

Another way to stabilize nanoparticles is the use of organic ligands with groups that have an affinity with the metal surface such as amines, phosphines, and thiols.<sup>9</sup> The stabilization occurs by the coordination of the nanoparticles with the ligand molecules. Schmid and coworkers synthesized Pt, Pd, and Ni nanoparticles stabilized by

triphenylphosphine ligands.<sup>142,143</sup> Bimetallic Ni/Pd core-shell nanoparticles have also been prepared using trioctylphosphine as stabilizer by Son *et al.*<sup>144</sup> Au nanoparticles have also been synthesized using alkanethiols and functionalized thiols as strong stabilizers, and are often referred to as monolayer-protected clusters (MPCs).<sup>145,146</sup> MPCs have a monolayer of thiols with strong coordination to the metal surface. However, they are often catalytically inactive due to complete passivation of the nanoparticle surface. However, some exceptions have been noted in which MPCs have catalytic activity; Astruc and coworkers synthesized Pd nanoparticles using dodecanethiolate ligands as stabilizers and the resulting catalysts are stable and recyclable catalysts for the Suzuki-Miyaura reaction of aryl halides under ambient conditions.<sup>147</sup>

In some cases, polymers, dendrimers, and ligands can be combined for the stabilization of metal nanoparticles. For example, Pd nanoparticles were synthesized using a phosphine terminated dendrimer and were found to be highly effective for Suzuki coupling reactions with excellent reusability.<sup>148</sup>

#### **1.3.4 Surfactants**

Tetraoctylammonium bromide (TOAB), cetyltrimethylammonium bromide (CTAB), and sodium bis(2-ethylhexyl) sulfosuccinate (AOT) surfactants are the most commonly used surfactants for the stabilization of metal nanoparticles.<sup>9,130</sup> The structure of AOT surfactant is shown in Figure 1.12. Surfactants can stabilize the nanoparticles by both electrostatic and steric stabilization; for example, CTAB acts as a stabilizer via the bromide anions adsorbing onto the metal surface, followed by electrostatic interactions with the negatively charged surfaces and the long chain cations.<sup>149</sup> However, one problem

with surfactant stabilizers is the long term stability of nanoparticles stabilized by surfactants. In some cases, stability can be improved by the addition of alternative anions. For example, Isaacs *et al.* have shown that the use of thiosulfate anions instead of bromide anions can greatly improve both the chemical and thermal stability of TOAB-stabilized Au nanoparticles.<sup>150</sup>

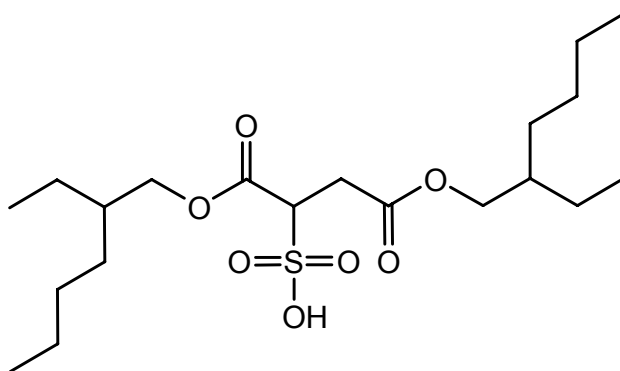


**Figure 1.12.** Structure of bis(2-ethylhexyl) sulfosuccinate (AOT) surfactant.

### 1.3.5 Ionic Liquids

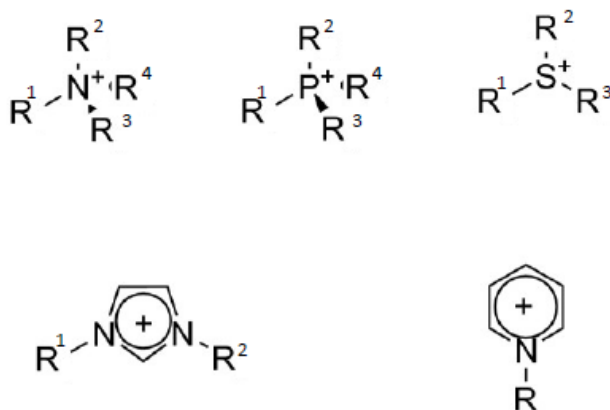
Ionic liquids (ILs), because of their unique properties, such as high polarity, negligible vapor pressure, high ionic conductivity, and thermal stability, are intriguing medium for solution-phase catalysis. More detailed discussions on ILs are outlined below.

## 1.4 What are Ionic Liquids

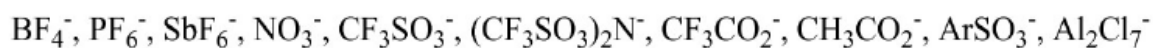
ILs are liquids which are entirely composed of ions and are in the liquid state at near ambient temperatures, typically below 100 °C.<sup>151</sup> ILs differ from molten salts in that molten salts describe high temperature, corrosive, and viscous media whereas ionic

liquids are less viscous and easier to handle at near ambient temperatures and pressures. Aqueous solutions of salts are not considered ionic liquids as they do not exclusively contain ions. For example, an aqueous solution of sodium chloride is not an ionic liquid, but an ionic solution.<sup>151</sup> Since, the late 1990s, ILs have attracted a great deal of attention as unique solvent media for organic catalysis. Room temperature ILs are generally salts of organic cations, *e.g.* tetraalkylammonium, tetraalkylphosphonium, *N*-alkylpyridinium, 1,3-dialkylimidazolium and trialkylsulfonium cations (Figure 1.13) with weakly coordinating anions.<sup>151,152</sup>

Cations:



Anions:

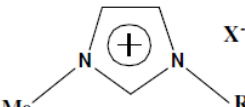


**Figure 1.13.** Possible structures of ionic liquids.<sup>151</sup> (Adapted from reference 151)

If the alkyl groups of the cation are different, then the IL will have a lower melting point, potentially below room temperature. For example, dialkylimidazolium cations with different R<sup>1</sup> and R<sup>2</sup> groups are typically room-temperature ILs.<sup>151</sup> The

melting points can also be modified by changing the cations and/or anions of the IL (Table 1.2). For example, by changing the chain lengths of the R groups from methyl to ethyl to n-butyl in methylalkylimidazolium chloride salts, the melting points can be changed from 125 to 87 to 65 °C, respectively.<sup>151</sup> Similarly, by changing the anions the melting point can be changed as shown in Table 1.2. Also, the hydrophilicity of ILs can be modified by changing the anion. For example, [BMIM]BF<sub>4</sub> is water miscible whereas [BMIM]PF<sub>6</sub> is largely immiscible with water.

**Table 1.2.** Melting Points of some Ionic Liquids.<sup>151</sup> (Adapted from reference 151)

		
<b>R</b>	<b>X<sup>-</sup></b>	<b>mp/°C</b>
Me	Cl <sup>-</sup>	125
Et	Cl <sup>-</sup>	87
N-Bu	Cl <sup>-</sup>	65
Et	NO <sub>3</sub> <sup>-</sup>	38
Et	BF <sub>4</sub> <sup>-</sup>	6
Et	CF <sub>3</sub> SO <sub>3</sub> <sup>-</sup>	-9

The development of ILs can be classified into three generations. One of the earliest generations of ILs comprised of the haloaluminate ILs.<sup>153</sup> For example, dialkylimidazolium chloroaluminates were reported by Wilkes and co-workers in 1982.<sup>154</sup> These type of ILs have been used as solvents and catalysts for Friedel-Crafts and other organic reactions. However, they react with water and thus, extreme care must be taken during handling.<sup>153</sup> The second generation of ILs involved the synthesis of non-haloaluminate ILs, and were not that popular until the late 1990s. One of the most common ionic liquids, 1-ethyl-3-methylimidazolium tetrafluoroborate ([EMIM]BF<sub>4</sub>), was

synthesized by Wilkes *et al.* in 1992.<sup>155</sup> In 1994, Haworth and co-workers reported for the first time the synthesis of the corresponding hexafluorophosphate ([EMIM]PF<sub>6</sub>) IL.<sup>156</sup> Fluoroborates and hexafluorophosphates are fairly stable in the presence of water and air and thus, attracted more interest over the years as solvents in organic chemistry.<sup>153</sup> However, recent studies have indicated the formation of toxic and corrosive hydrogen fluoride upon hydrolysis of these anions, which will be discussed below. Third generation ILs are mostly task-specific and chiral ILs which became popular after the early 2000s.<sup>153</sup>

Though there are different methods available for the synthesis of ILs, they are often made by direct alkylation or alkylation followed by anion exchange.<sup>152</sup> The alkyl cations of imidazolium, ammonium, pyridinium, and phosphonium ILs can be prepared by the alkylation of the corresponding precursor with an alkylating agent such as a haloalkane. For example, the synthesis of 1-ethyl-3-methylimidazolium chloride IL can be prepared by the reaction of 1-methylimidazole and chloroethane.<sup>157</sup> For the synthesis of tetrafluoroborate and hexafluorophosphate ILs, alkylation followed by anion exchange is normally used. First, the halide salt with the suitable cation is prepared by alkylation and then the anion is phase exchanged with the required anion.<sup>157</sup>

The room-temperature ILs have unique physical and chemical properties which make them potential candidates as media for catalysis. Some of the most important properties are outlined below:<sup>151,153</sup>

- Negligible vapor pressure – can therefore often easily remove other volatile species (such as products of a catalysis reaction).

- Higher liquidus ranges (over 300 °C) than molecular solvents (water ~ 100 °C and ethanol ~ 193 °C). They have high thermal stability and hence, high temperature experiments can be carried out without any solvent degradation.
- Designer Solvents - By suitable choice of cations and anions, polarity and hydrophilicity can be modified.
- Able to dissolve a variety of organic, inorganic, and organometallic compounds.
- Highly polar yet non-coordinating solvents in some ILs due to the presence of weakly coordinating anions like  $\text{BF}_4^-$  and  $\text{PF}_6^-$  ions.
- Widely variable solubilities of gases like  $\text{H}_2$ ,  $\text{O}_2$ ,  $\text{CO}$  and  $\text{CO}_2$  in ILs.

Due to these unique properties, ILs are often termed as green solvents for clean technology.<sup>158</sup> Besides catalysis which will be discussed in more detail later, ILs have found applications in a variety of areas like gas separations,<sup>159</sup> extraction of organic compounds,<sup>160</sup>  $\text{CO}_2$  extractions and separations,<sup>161</sup> metal ion extractions,<sup>162</sup> and membrane separations.<sup>163</sup> More recently, they have found applications in biomass conversion, carbohydrate solubility, and enzyme catalysis.<sup>153</sup> For example, the conversion of lignocellulosic biomass, a plant biomass which is the most important bio-renewable resource on earth, to biofuels and chemicals like ethanol is one of the most important research topics in the biofuels field.<sup>153</sup> Zhao and co-workers used imidazolium IL ([BMIM]Cl) for breaking down lignocellulose into glucose, xylose, and other monosaccharides by an acid-catalyzed method.<sup>164</sup> They documented that this method can provide a cost-effective method for the biomass conversion process. Zhang and co-workers showed the usefulness of imidazolium-based IL ([EMIM]Cl) as solvents for the catalytic conversion of sugars such as glucose and fructose into 5-hydroxymethylfurfural,



which could be potentially used for the synthesis of polymers and a range of chemicals.<sup>165</sup>

Though there are many advantages associated with ionic liquids for their use in a variety of applications as mentioned above, still there are many disadvantages associated for their use.<sup>153</sup> First of all, they can be quite expensive due to the lengthy processes involved in synthesizing ILs and costly starting materials. The negligible volatility of ILs also hinders the purification of ILs from leftover starting materials and other impurities as they can not simply be distilled. Though ILs have shown many green properties, they have also some non-green properties such as toxicity. For example, ILs consisting of fluorinated anions like  $\text{PF}_6^-$  and  $\text{BF}_4^-$  tend to generate toxic and corrosive decomposition products like hydrogen fluoride (HF) when heated in the presence of water.<sup>166</sup> Also, some ILs have been found to be combustible despite their low volatilities. For example, Rogers and co-workers showed that ILs with imidazolium cations and nitrate, picrate, and azolate anions were combustible when heated with a small flame torch and the rate of combustion depended on the nitrogen and oxygen content of the ILs.<sup>167</sup>

#### **1.4.1 Synthesis of Nanoparticle Catalysts in Ionic Liquids**

Since ILs are liquids composed of only bulky and diffuse cations and anions, they should be excellent media for the synthesis and stabilization of colloidal metal nanoparticles.<sup>168</sup> Ionic liquids (ILs) have recently emerged as intriguing reaction media for “quasi-homogeneous” solution-phase nanoparticle catalysis.<sup>9,168</sup> They can potentially provide electrosteric stabilization for metal nanoparticles.<sup>9</sup> In this case, the anions of the IL can offer a weak electrostatic stabilization for the electrophilic nanoparticle surface

and the long chain cations offer a steric stabilization via their bulky framework. Also, the ability to add functional groups onto the cations of many ionic liquids has led the ability to create “task-specific” ionic liquids for the stabilization of metal nanoparticles.<sup>169</sup> Deshmukh *et al.* were the first to discover the unexpected formation of Pd nanoparticles in 1,3-di-*n*-butylimidazolium tetrafluoroborate IL during Heck reactions with Pd salts.<sup>170</sup> Later on, J. Dupont’s group was the first group to understand these properties and used ILs as templates, stabilizers, and solvents for the synthesis of metal nanoparticles.<sup>171</sup> This pioneering work has stimulated many other studies towards the synthesis of nanoparticle catalysts in ILs. In the following sections, different ways of synthesizing metal nanoparticles in ILs are described.

#### 1.4.1.1 General Synthesis

As described above, J. Dupont and coworkers first discovered that stable transition metal nanoparticles could be formed in imidazolium ILs with no secondary stabilizers added.<sup>171</sup> The very first example was reported in 2002, in which they synthesized small and uniform Ir nanoparticles by treating a solution of  $[\text{IrCl}(\text{cod})]_2$  (cod=1,5-cyclooctadiene) in 1-butyl-3-methylimidazolium hexafluorophosphate ( $[\text{BMIM}]\text{PF}_6$ ) IL with  $\text{H}_2$ .<sup>171</sup> The resulting catalysts were found to be active for the hydrogenation of olefins like cyclohexene, styrene, and 1-decene. After this discovery, various other studies were carried out by J. Dupont and others in which metal nanoparticles Ir,<sup>172</sup> Rh,<sup>173</sup> Pt,<sup>174</sup> Ru,<sup>175</sup> Pd,<sup>176</sup> Ni,<sup>177</sup> Cu,<sup>178</sup> and Ag<sup>179</sup> nanoparticles were prepared directly in ILs by reducing the corresponding transition metal salts or by decomposing organometallic compounds in the IL. Also, nanoparticles have been

synthesized in ILs by thermal or photolytic decomposition; using this method, Cr, Mo, W, Fe, Ru, Os, Co, Rh, and Ir nanoparticles were generated in 1-butyl-3-methylimidazolium tetrafluoroborate ([BMIM]BF<sub>4</sub>) IL.<sup>180-182</sup> As described in these studies, very small and uniform nanoparticles were synthesized in the ILs which was attributed to the stabilization effect of the anions and the presence of low interface tensions of ILs.<sup>9,168</sup> Also, as there were no additional secondary stabilizers used during the synthesis, this could potentially lead to nearly completely unpassivated (or “naked”)<sup>9</sup> metal nanoparticle surfaces in ILs, which would be beneficial for maximizing the catalytic activity of nanoparticles.

#### **1.4.1.2 Use of Additional Stabilizers**

Though the reports described above outline the synthesis of metallic nanoparticles in pure ILs without any additional stabilizers, a number of groups also reported the aggregation of nanoparticles in pure ILs.<sup>183,184</sup> To avoid these problems various secondary stabilizers were used. Some of the common stabilizers include poly(vinylpyrrolidone) (PVP), citrate, dendrimers, and ionic-liquid co-polymers.<sup>185-187</sup> In many of these cases, the nanoparticles are synthesized in other common solvents using the stabilizers, followed by addition of the IL and removal of the initial solvent under vacuum. For example, Mu *et al.* synthesized Pt, Pd, and Rh nanoparticles in imidazolium IL by a phase transfer method.<sup>185</sup> First, the nanoparticles were synthesized by the ethanolic reduction of the corresponding metal halide salts, followed by the removal of ethanol under vacuum. The residue was then added to methanol, followed by the addition of [BMIM]PF<sub>6</sub>. Highly stable Pt, Pd, and Rh nanoparticles were suspended in the IL after

the removal of methanol under vacuum. Other groups have devised IL-containing polymers for the stabilization of nanoparticles in ILs. For example, Dyson and co-workers synthesized the block copolymer, poly[(*N*-vinyl-2-pyrrolidone)-*co*-(1-vinyl-3-butylimidazolium chloride)] and used this polymer to synthesize highly stable Rh nanoparticles in imidazolium IL.<sup>188</sup> These nanoparticles were found to be highly active catalysts for the hydrogenation of benzene and other arenes.

#### 1.4.1.3 Use of Functionalized Ionic Liquids

Another interesting way of synthesizing metal nanoparticles in ILs is the design of functionalized ILs or task-specific ILs.<sup>169,189</sup> In this case, specific functional groups (-OH, -NH<sub>2</sub>, -SH, *etc.*) are attached to the imidazolium cations of the IL moiety. One driving force towards the design of a task-specific IL is that these functional groups may bond onto metal surfaces and thus stabilize the nanoparticles more effectively. For example, Kim *et al.* used thiol-functionalized ILs for the synthesis of gold and platinum nanoparticles.<sup>190</sup> These thiol functionalized ILs bind to the nanoparticle surface and act as stabilizers. Choi *et al.* used 1-(2-hydroxyethyl)-3-methylimidazolium tetrafluoroborate for the synthesis of Ag nanoparticles.<sup>191</sup> Dyson and co-workers used nitrile-functionalized IL as a stabilizer to prevent agglomeration of Pd nanoparticles for the Stille coupling reaction between iodobenzene and tributylphenyltin, and found that this IL helped to prevent catalyst deactivation.<sup>192</sup> Finally, Niu and coworkers used 1-(3-aminopropyl)-3-methylimidazolium bromide for the synthesis of stable Au nanoparticles, and found that the resulting nanoparticles showed enhanced electrocatalytic activity and high stability in aqueous solutions.<sup>193</sup>

### 1.4.2 Mode of Stabilization of Nanoparticles in Ionic Liquids

One of the key advantages of using ILs for the synthesis of metal nanoparticles is that metal nanoparticles of very small and uniform size can be prepared which can be attributed to both electrosteric effects and low interface tensions within ILs.<sup>9</sup> Imidazolium ILs form an extended network of cations and anions connected to each other by weak hydrogen bonds.<sup>168</sup> Each monomer consists of one imidazolium cation surrounded by three anions and vice versa. 1,3-dialkylimidazolium ionic liquids are best described as hydrogen-bonded molecules of the type  $\{[(\text{DAI})_x(\text{X})_{x-n}]_n^+[(\text{DAI})_{x-n}(\text{X})_x]^{n-}\}_n$  in which DAI is the 1,3-dialkylimidazolium cation and X the anion.<sup>168</sup> J. Dupont and co-workers postulated that during the synthesis of metal nanoparticles in imidazolium ILs, the imidazolium cations can interact with the nanoparticle surface preferentially as aggregates of the above mentioned type.<sup>168</sup> They theorized that this aggregate can form a loosely bound protective layer around the nanoparticle surface, thus stabilizing the nanoparticles. They characterized this protective layer by SAXS measurements during the synthesis of Pt, Ni, and Ir nanoparticles in imidazolium ILs.<sup>194,195</sup> By x-ray photoelectron spectroscopy (XPS) and extended x-ray absorption fine structure (EXAFS) analysis, interactions between IL anions such as  $\text{PF}_6^-$  and  $\text{BF}_4^-$  and metal nanoparticles were also detected.<sup>194,195</sup> This type of cation and/or anion stabilization by imidazolium ILs is similar in nature to the electrosteric stabilization found in the surfactant molecules.<sup>9</sup> The size of the imidazolium cation has a major effect on the stabilization and size of metal nanoparticles in imidazolium ILs. For example, J. Dupont and co-workers found that by increasing the alkyl chain length of the imidazolium cation, a reduction in mean diameter and improved size distribution were obtained during the synthesis of Ni

nanoparticles in imidazolium ILs.<sup>175</sup> Also, the purity of ILs, in particular the water and halide amount in ILs, can play an important role in the physical properties of ILs and thus, on the stability and catalytic activity of the metal nanoparticles in ILs. For example, Seddon and co-workers showed that the melting points of [EMIM]BF<sub>4</sub> IL change due to the presence of water and halide impurities.<sup>196</sup> Also, the viscosities of ILs tend to increase dramatically when small amounts of chloride impurities are present.

### 1.4.3 Catalytic Applications of Nanoparticles in Ionic Liquids

Transition metal nanoparticles in imidazolium-based ILs have been found to be active catalysts for various catalytic reactions. Some of the most common reactions where these metal nanoparticles have found applications are hydrogenations of aromatic rings, double bonds, and carbonyl groups and C-C coupling reactions such as Heck, Suzuki and Sonogashira reactions.<sup>168</sup> In most of catalytic hydrogenations of alkenes, arenes, and ketones reported in imidazolium-based ILs using transition metal nanoparticles, the reactions are typically multiphase systems in which the nanoparticles are dispersed in the ILs forming the denser phase whereas the substrates and products remain in the upper phase.<sup>168</sup> Thus often the reaction products can be separated by simple decantation and the catalytic system can be reused for further catalytic reactions.

Yuan and co-workers synthesized highly stable Pd nanoparticles using hydroxyl-functionalized ILs.<sup>197</sup> The resulting Pd nanoparticles were found to be highly active catalysts for the conversion of styrene to ethylbenzene and the activity was maintained over twelve catalytic cycles. Mu *et al.* used IL-containing copolymers as stabilizers for the synthesis of Rh nanoparticles and the resulting nanoparticles were found to be highly

active catalysts for the hydrogenation of benzene with a total turnover number of 20,000.<sup>187</sup> Using an imidazolium-containing ionic copolymer, Dyson and co-workers synthesized stable Pd nanoparticles ( $5.0 \pm 0.2$  nm), and found that the resulting Pd nanoparticles were excellent catalysts for Suzuki, Stille, and Heck C-C coupling reactions and could be stored for many months without any degradation.<sup>198</sup> Huang *et al.* synthesized phenanthroline ( $C_{12}H_8N_2$ ) stabilized Pd nanoparticles in [BMIM]PF<sub>6</sub> IL and the particles were found to be highly active, selective, and reusable catalysts for the hydrogenation of olefins.<sup>199</sup> Dyson and co-workers synthesized hydroxyl-functionalized imidazolium IL in which PVP was used as a secondary stabilizer and the resulting IL was used for the synthesis of highly stable Rh nanoparticles for the hydrogenation of styrene.<sup>200</sup> Roucoux and co-workers used 2,2'-bipyridine as a secondary stabilizer for the synthesis of Rh nanoparticles in [BMIM]PF<sub>6</sub> IL and the catalysts were found to be active catalysts for styrene hydrogenation.<sup>201</sup> PVP-stabilized Pt, Pd and Rh nanoparticles synthesized by Mu *et al.* in [BMIM]PF<sub>6</sub> IL were found to be active catalysts for alkene and diene hydrogenation reactions.<sup>185</sup>

## 1.5 Supported Nanoparticle Catalysts

Small nanoparticles (< 10 nm size range) are not in a thermodynamically stable state due to their high surface energies and large surface areas. The problems faced when using nanoparticles for catalysis are the difficulties of stabilizing particles in this size range while retaining sufficient catalytic activity, and the problematic separation of the catalytic particles from the product and unused reactants at the end of the reaction. One possible way to address these problems is to immobilize the nanoparticles onto a

heterogeneous solid support. Such supported metal nanoparticle catalysts have attracted much attention over the years due to the potential for enhanced activity and selectivity and the inhibition of nanoparticle aggregation by immobilization/separation on a heterogeneous support. Supported metal nanoparticle catalysts have long been used as heterogeneous catalysts in a number of industrially important catalytic reactions such as hydrogenations, dehydrogenations, hydrocracking, and reduction and oxidation reactions in fuel cells.<sup>6</sup>

### **1.5.1 Synthetic Routes for Supported Nanoparticle Catalysts**

Over the years many synthetic strategies have been developed for the synthesis of supported nanoparticle catalysts. Some of the major challenges in this field are the control over particle size and distribution of the particles in the composites during the synthesis. Traditionally, for the synthesis of supported nanoparticle catalysts chemical routes are normally used.<sup>202</sup> Some of these major chemical routes are described below.

The wetness impregnation method is the most commonly used method to make supported catalysts, and involves the “wetting” of the solid support with the metal precursor solution. Initially, metal salt(s) are dissolved in a minimal amount of solvent (precisely calculated from the pore volume of the material), followed by the addition of solid support to form a thick paste.<sup>203</sup> As-synthesized supported catalysts are formed after the removal of the solvent, drying and calcination under oxidizing and reducing conditions. It has been found that the nanoparticles synthesized by this method often are polydisperse and the dispersity depends on the metal, metal loading, and support.<sup>204,205</sup>



Alternatively, simultaneous precipitation, or co-precipitation, of metallic precursor(s) and solid supports can be used to make supported catalysts.<sup>206</sup> Zaharescu and co-workers synthesized supported-Pd nanoparticle catalysts in which a Pd salt was incorporated into hexagonal mesoporous silica via a sol-gel technique.<sup>207</sup> The nanoparticles were found to be fairly well dispersed with particle sizes of 4-5 nm. Another way for making supported nanoparticle catalysts is the deposition/precipitation method.<sup>202</sup> The deposition/precipitation method involves the dissolution of the metal salt precursor in an appropriate solvent, followed by pH adjustment to achieve the complete precipitation of the metal precursor. The precipitate is subsequently deposited on the surface of the support, followed by the calcination of the final material. Haruta and co-workers developed this method to synthesize highly-dispersed gold catalysts on different supports.<sup>4</sup> The general scheme for the deposition-precipitation method is outlined below in Figure 1.14.

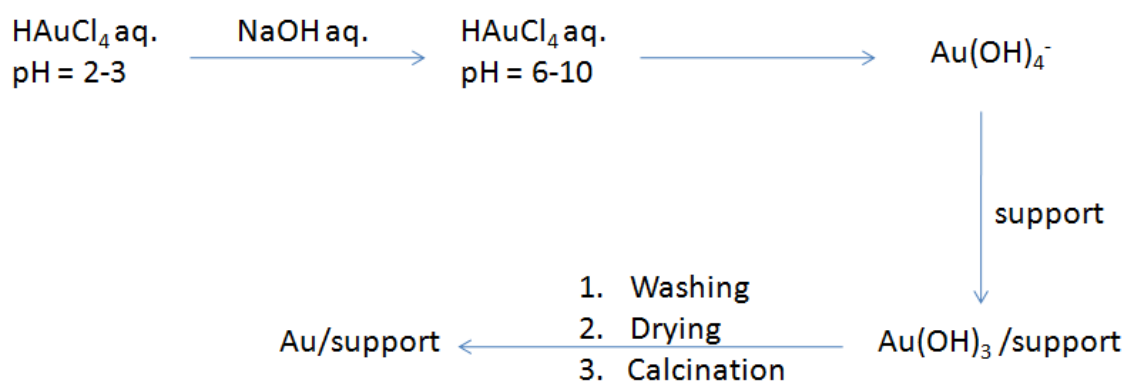


**Figure 1.14.** Schematic diagram of the deposition-precipitation method.<sup>4</sup>

Microwave irradiation exposure is another method employed for the synthesis of supported nanoparticle catalysts. Romero and co-workers synthesized mesoporous silica supported Au, Ag, and Pd nanoparticles by microwave irradiation of the metal salts.<sup>208</sup> Well dispersed nanoparticles with small sizes (Au (2 nm), Ag (3.8 nm), and Pd (11.3 nm)) were formed within the ordered mesoporous structures and these supported nanoparticle catalysts were found to be highly active in oxidation reactions. Microwave irradiation methods provide some advantages compared to that of the conventional heating methods such as shorter reaction times and formation of very small and uniform metal nanoparticles.<sup>204</sup>

One of the most efficient synthetic methods for the synthesis of supported metal nanoparticle catalysts has been the use of supercritical fluids which are substances at temperatures and pressures above their critical points. In this case, the metallic precursor is dissolved in a supercritical fluid and subsequently incorporated onto the support material, followed by the reduction of metallic precursor.<sup>204</sup> One of the most used supercritical fluids is supercritical carbon dioxide (scCO<sub>2</sub>) because it is highly abundant, inexpensive, inflammable, and non-toxic. Erkey and co-workers synthesized supported Pt and Ru nanoparticles (< 1 nm) with metal contents up to 40 wt % on various supports such as silica and alumina using scCO<sub>2</sub>.<sup>209</sup> The alumina-supported Pt nanoparticles were found to be active catalysts for hydrodesulfurization of dibenzothiophene. Using supercritical fluids, various advantages can be obtained during the synthesis of supported nanoparticle catalysts. For example, because of lower surface tensions of solid surfaces in supercritical solvents, better porosity control can be achieved.<sup>210</sup>

In all the traditional methods described above, the size distribution of nanoparticles and the degree of dispersion on the support are each highly dependent on the pH and concentration of the precursor solution, type of the oxide support, and calcination temperatures and conditions.<sup>202</sup> Also, these methods often provide limited control over the composition and structures of nanoparticles, particularly after the thermal activation steps. This is particularly challenging in the case of bimetallic nanoparticles, and often leads to significant compositional nonuniformity from particle to particle. This provides a serious challenge in understanding the size-structure-property relationships of bimetallic and multi-metallic catalysts.

Another promising way for the synthesis of supported nanoparticle catalysts is the nanoparticle encapsulation method, in which pre-synthesized nanoparticles are trapped into an inorganic matrix by sol-gel chemistry. Recent advances in synthetic methods for the preparation of nanoparticles with better size control and composition have provided new directions for this technique.<sup>108</sup> These pre-synthesized nanoparticles in which the particle size distribution, composition, and structure is very well defined are deposited onto various supports to synthesize supported-nanoparticle catalysts. Nanoparticles synthesized by dendrimers, monolayers, and polymer stabilizers have been commonly used as precursors for supported-nanoparticle catalysts.<sup>211-213</sup> For example, Crooks and co-workers utilized this methodology for the synthesis of Pd-Au/TiO<sub>2</sub> catalysts using pre-synthesized dendrimer-stabilized nanoparticles by a sol-gel route.<sup>105</sup> This approach produced a narrow distribution of PdAu nanoparticles in the oxide support after the stabilizer was removed by calcination.

### 1.5.2 Nature of Supports

A variety of solid materials have been used as supports for the synthesis of supported nanoparticle catalysts. Among the wide range of solid supports used so far, metal oxides and carbon supports are the main two families.<sup>204</sup>

Metal oxides provide many advantages as supports due to their high thermal and chemical stabilities, high surface areas and well-organized pore structures. These properties make them suitable candidates for the synthesis of supported nanoparticle catalysts. Silica, alumina, titania, and ceria are some of the most commonly used metal oxides used as supports.<sup>4,9,204</sup> For example, Haruta and co-workers pioneered the synthesis of supported Au catalysts by deposition of Au nanoparticles on various metal oxide supports like Fe<sub>2</sub>O<sub>3</sub>, Al<sub>2</sub>O<sub>3</sub>, TiO<sub>2</sub>, ZnO, and MgO and used them for various catalytic applications such as CO oxidation and propylene epoxidation.<sup>4</sup> They found that the catalytic activity and selectivity towards specific reaction products was highly dependent on the size of the Au particles, the type of supports, and the structure of the interface. For example, they found that Au nanoparticles are more active and stable for CO oxidation over reducible semiconducting metal oxides such as titania, Fe<sub>2</sub>O<sub>3</sub>, Co<sub>3</sub>O<sub>4</sub> and NiO than on insulating metal oxides such as alumina and silica. Chandler and co-workers synthesized dendrimer-stabilized Pt and bimetallic Pt–Au nanoparticles with particle sizes smaller than 3 nm and then adsorbed these nanoparticles onto a high-surface area silica support.<sup>214,215</sup> The as-synthesized catalysts were then thermally activated to remove the dendrimers and the resulting catalysts were found to be highly active catalysts for CO oxidation at room temperature.

Carbon-based supports have also found applications for many different catalytic reactions. Activated charcoal is a common carbonaceous support material which has been used for the synthesis of supported nanoparticle catalysts. Other carbon-based materials like carbon nanotubes have also been used as supports.<sup>204</sup> Carbon supports are highly thermally stable and thus are suitable candidates for high temperature catalytic applications.<sup>9,204</sup> Another advantage carbon materials offer that these materials can be modified so that adequate surface area, porosity, and pore size distribution are available.<sup>216</sup> Also, the surface of these materials can be modified via different approaches (acid or base treatment, heat treatment, doping with heteroatoms) for optimal catalyst–support interactions. For example, Kohler *et al.* synthesized Pd/C catalysts after the optimization of several parameters such as solvent, temperature, base, and metal loading.<sup>217</sup> The optimized supported Pd nanoparticle catalysts were found to be highly active catalysts for the Heck reaction of aryl bromides with olefins.

### **1.5.3 Ionic Liquids as Media For the Synthesis of Supported Catalysts**

As described earlier, ILs, owing to their unique properties, such as high polarity, negligible vapor pressure, high ionic conductivity, and thermal stability have found extensive applications as solvents in organic catalysis. Also, as described in the previous section, they are suitable media for the synthesis and stabilization of transition metal nanoparticles. More recently, ILs have attracted a lot of interest as templates for the fabrication of nanostructured inorganic porous materials due to their properties such as high thermal stability, negligible vapor pressure, and tunable solvent properties.<sup>218,219</sup> In some cases, they provide attractive alternative reaction media compared with

conventional solvents, in that they can act both as a solvent and a surfactant template/porogen. In addition, while the synthesis of crystalline anatase titania in conventional solvents like water is difficult due to the rapid hydrolysis and condensation of their alkoxide precursors, the same synthesis in ILs produce crystalline species under mild conditions.<sup>220,221</sup> In the following section, various examples of the synthesis of inorganic porous materials in ILs are outlined.

In 2000, Dai *et al.* first reported the synthesis of a silica aerogel (surface area of 720 m<sup>2</sup>/g) using 1-ethyl-3-methylimidazolium bis(trifluoromethylsulfonyl)imide ([EMIM]NTf<sub>2</sub>) IL as solvent and template.<sup>222</sup> Seddon and co-workers synthesized hexagonally-ordered mesoporous silica in imidazolium-based ILs,<sup>223</sup> while Antonietti and co-workers used a nanocasting method for the synthesis of mesoporous silica with worm like pores (pore diameter 2.5 nm, surface area 801 m<sup>2</sup>/g) in ILs.<sup>224</sup> In all these cases, the ILs acted as both the solvent and the template for porosity.

Besides silica, synthesis of mesoporous titania in ILs has also attracted a great deal of attention. In 2001, Dionysiou and co-workers synthesized anatase-containing nanostructured titania in [BMIM]PF<sub>6</sub> IL by a sol-gel method using titanium tetraisopropoxide as precursor.<sup>225</sup> High surface areas of 570 m<sup>2</sup>/g with narrow size pores were obtained by this sol-gel method. Kimizuka and co-workers later reported the synthesis of hollow titania microspheres by a single step synthesis in [BMIM]PF<sub>6</sub> IL using a water in IL microemulsion.<sup>226</sup> The size of the titania hollow spheres could be controlled by the stirring rate and temperature. They postulated that the imidazolium cations not only act as the solvent but also act as a stabilizer during the synthesis of

hollow spheres. Zhou *et al.* reported the synthesis of very fine crystalline anatase titania particles using  $\text{TiCl}_4$  as a precursor in [BMIM] $\text{BF}_4$  IL.<sup>221</sup> Well-defined and porous titania nanospheres of 70-100 nm diameter were formed. Each nanosphere was found to be composed of very small titania nanoparticles of 2-3 nm diameter.

## 1.6 Research Objectives

Two main disadvantages faced when using transition metal nanoparticles for catalysis are 1) the problematic separation of the catalytic particles from the product and unused reactants at the end of the reaction, and 2) the difficulties of stabilizing particles in this size range (<10 nm) while retaining sufficient catalytic activity. Thus, alternative solvents for the synthesis of nanoparticles are a subject of research interest. At the start of my PhD research, there were several published reports where ILs, particularly imidazolium-based ILs were found to provide “quasi-homogeneous” catalysis. However, most of the quasi-homogeneous nanoparticle catalysis in ILs reported used only monometallic nanoparticles. To the best of our knowledge, no studies investigated the catalytic activity of bimetallic nanoparticles in IL solvents. Bimetallic nanoparticles are interesting as they offer the ability to tune the catalytic activity, selectivity and stability of nanoparticle catalysts.

So, the first objective was to investigate the conditions upon which metallic Au, Pd and Pd-Au bimetallic nanoparticle catalysts could be stabilized in clean imidazolium ILs. Imidazolium based ILs, and in particular, 1-butyl-3-methylimidazolium hexafluorophosphate ([BMIM] $\text{PF}_6$ ) IL were chosen, because this was a commonly used, moderate viscosity, room-temperature IL which had been used by others for the synthesis

of nanoparticles. Clean imidazolium ILs were required because there were some reports indicating the effect of impurities on the nanoparticle stability in ILs. Another major reason for using ionic liquids for the synthesis of metal nanoparticles was to strengthen the ability to recycle/resuse the nanoparticle catalysts for many catalytic reactions. The results of these studies are documented in Chapter 2.

Continuing with the idea of quasi-homogeneous catalysis in imidazolium-based ILs, the second objective was to study the mode of stabilization of nanoparticles in ILs. Several groups had indicated that nanoparticle stabilization in ILs may be due to weak anion or cation interactions with the nanoparticle surfaces, or alternatively, that the presence of impurities such as water and halides may play a significant role on nanoparticle stability in IL solvents. For example, a number of groups have shown that Au nanoparticles are prone to aggregation in IL solvents in the absence of additional stabilizers or task-specific ILs. However, there were also reports describing the successful synthesis of unstabilized Au and bimetallic Au alloy nanoparticles in ILs. Therefore, the mode of stabilization of nanoparticles in these solvents was quite puzzling given these contradictory results. We hypothesized that another common impurity in imidazolium ILs, the 1-methylimidazole starting material, could be partially responsible for nanoparticle stability. Indeed, there were some reports which documented the binding of imidazole and 1-methylimidazole for gold and silver surfaces. Therefore, the second objective was to study the effect of 1-methylimidazole on the stability and activity of Au and Pd-Au nanoparticles in imidazolium ILs. The results of these studies are documented in Chapter 3.



The third objective came from the ideas of the previous two objectives. There have been different ways to stabilize metal nanoparticles in imidazolium-based ILs. For example, there have been reports about the synthesis of nanoparticles in pure [BMIM] ILs without any additional stabilizers. At the same time, a number of groups also reported the aggregation of nanoparticles in pure ILs. To avoid these problems various secondary stabilizers such as poly(vinylpyrrolidone) (PVP), task-specific ILs and IL-containing copolymers have also been used for the synthesis of stable metal nanoparticles in ILs. Given the numerous routes towards the synthesis of “stable” nanoparticles in ILs which exist in the literature, it was very difficult to generalize as to which method(s) can lead to the optimal formation of stable, catalytically active nanoparticles. The third research objective was to document a comparative study of nanoparticles synthesized by four different methods in imidazolium IL. The results of these studies are documented in Chapter 4.

The fourth objective was based on the idea of the rational design of heterogeneous supported nanoparticle catalysts. Supported metal nanoparticle catalysts have long been used as heterogeneous catalysts in a number of industrially important catalytic reactions such as hydrogenations, dehydrogenations, hydrocracking, and reduction and oxidation reactions in fuel cells. A major area of concern in designing supported nanoparticle catalysts from pre-synthesized nanoparticles is nanoparticle sintering, alloying/segregation, and metal oxidation upon removal of the organic stabilizers via thermal treatments. This is particularly challenging in the case of bimetallic nanoparticles where poor control over composition normally occurs after the polymer removal step. Keeping this in mind, the objective was to investigate routes towards the synthesis of

supported nanoparticle catalysts where the size, structure, and composition can be maintained in both metallic and bimetallic nanoparticle catalysts before and after the polymer removal step. The results of these studies are documented in Chapter 5.

Besides the use of ILs as a medium for the synthesis of metal nanoparticles, there have also been reports of synthesis of porous inorganic materials like titania and silica in ILs. ILs have attracted interest as templates for the fabrication of these materials due to their properties such as high thermal stability, negligible vapor pressure, and tunable solvent properties. However, the use of ionic liquids as viable solvents for the incorporation of nanoparticles into porous oxide networks has only received a small amount of study. Keeping this in mind, the fifth objective of this thesis was to develop routes which use ionic liquids as one-pot media for the synthesis of supported-nanoparticle heterogeneous catalysts via the trapping of pre-synthesized nanoparticles into porous inorganic oxide materials. The results of these studies are documented in Chapter 6.

## **1.7 Organization and Scope**

This Ph.D. thesis primarily describes the routes towards the rational design of nanoparticle catalysts. It is divided into seven chapters. Chapter 2, 3, and 5 are near-verbatim copies of articles published in different journals with minor formatting changes, Chapter 4 is a verbatim of copy of a submitted manuscript, and Chapter 6 is a manuscript to be submitted in the near future. At the beginning of each chapter, a brief summary has been provided of the chapter including (1) where the manuscript was published, submitted, or to be submitted, (2) what my contributions were to the work contained in

the chapter/manuscript, and (3) summarize the chapter and briefly indicated how it fits into the thesis as a whole.

Chapter 1 describes the brief introduction on synthesis and characterization of monometallic and bimetallic nanoparticles. The use of ionic liquids (ILs) as media for the synthesis of metal nanoparticles is documented. Additionally, routes for the synthesis of supported nanoparticle catalysts are presented. In Chapter 2, the use of Au, Pd, and bimetallic Pd-Au nanoparticles as active catalysts in imidazolium-based IL are described. Additionally, the reusability of these catalysts was studied. Chapter 3 presents a previously undocumented mode of stabilization in imidazolium-based ILs in which the presence of low amount of 1-methylimidazole has a substantial effect on the stability and activity of Au and bimetallic Pd-Au nanoparticles. The nanoparticles stabilized by 1-methylimidazole were found to be more stable and active than those synthesized in the absence of 1-methylimidazole additives. Chapter 4 presents a comparative study of the stability and catalytic activity of nanoparticles in [BMIM]PF<sub>6</sub> ionic liquid via four different stabilization methods. It was found that PVP-stabilizers are the most effective stabilizers in order to realize both nanoparticle stability and long catalyst lifetimes. Chapter 5 presents a rational methodology to synthesize supported nanoparticle catalysts. A series of PVP-stabilized metallic and bimetallic Pd-Au nanoparticles (co-reduced and core-shell) with narrow size distributions were encapsulated into alumina matrixes by sol-gel chemistry, and their chemical, structural, electronic, and catalytic behaviors were investigated. Chapter 6 documents the use of ionic liquid as a one-pot medium for the synthesis of titania supported Au nanoparticle catalysts. Finally, in Chapter 7, a final summary, outlook, and future work is presented.

## 1.8 References

- (1) Norskov, J. K. *Nature* **2001**, *414*, 405-406.
- (2) Ertl, G. *Angew. Chem., Int. Ed.* **2008**, *47*, 3524-3535.
- (3) Somorjai, G. A. *Surface Chemistry and Catalysis*; Wiley, New York, **1994**.
- (4) Haruta, M. *Cattech* **2002**, *6*, 102-115.
- (5) Dumesic, J. A.; Topsoe, H.; Khammouma, S.; Boudart, M. *J. Catal.* **1975**, *37*, 503-512.
- (6) Bell, A. T. *Science* **2003**, *299*, 1688-1691.
- (7) Mills, G.; Gordon, M. S.; Metiu, H. *J. Chem. Phys.* **2003**, *118*, 4198-4205.
- (8) Tian, N.; Zhou, Z. Y.; Sun, S. G. *J. Phys. Chem. C* **2008**, *112*, 19801-19817.
- (9) Astruc, D.; Lu, F.; Aranzaes, J. R. *Angew. Chem., Int. Ed.* **2005**, *44*, 7852-7872.
- (10) Rampino, L. D.; Nord, F. F. *J. Am. Chem. Soc.* **1941**, *63*, 2745-2749.
- (11) Cha, D. Y.; Parravan, G. *J. Catal.* **1970**, *18*, 200-211.
- (12) Haruta, M.; Kobayashi, T.; Sano, H.; Yamada, N. *Chem. Lett.* **1987**, 405-408.
- (13) Haruta, M.; Tsubota, S.; Kobayashi, T.; Kageyama, H.; Genet, M. J.; Delmon, B. *J. Catal.* **1993**, *144*, 175-192.
- (14) Haruta, M.; Yamada, N.; Kobayashi, T.; Iijima, S. *J. Catal.* **1989**, *115*, 301-309.
- (15) Valden, M.; Lai, X.; Goodman, D. W. *Science* **1998**, *281*, 1647-1650.
- (16) Toshima, N.; Yonezawa, T. *New J. Chem.* **1998**, *22*, 1179-1201.
- (17) Roucoux, A.; Schulz, J.; Patin, H. *Chem. Rev.* **2002**, *102*, 3757-3778.
- (18) Willner, I.; Mandler, D. *J. Am. Chem. Soc.* **1989**, *111*, 1330-1336.
- (19) Faraday, M. *Philos. Trans. R. Soc. London* **1857**, *147*, 145.
- (20) Turkevich, J.; Stevenson, P. C.; Hillier, J. *Discuss. Faraday Soc.* **1951**, 55-75.
- (21) Kumar, S.; Gandhi, K. S.; Kumar, R. *Ind. Eng. Chem. Res.* **2007**, *46*, 3128-3136.

- (22) Harriman, A.; Thomas, J. M.; Millward, G. R. *New J. Chem.* **1987**, *11*, 757-762.
- (23) Furlong, D. N.; Launikonis, A.; Sasse, W. H. F.; Sanders, J. V. *J. Chem. Soc., Faraday Trans.* **1984**, *80*, 571-588.
- (24) Balogh, L.; Tomalia, D. A. *J. Am. Chem. Soc.* **1998**, *120*, 7355-7356.
- (25) Zhao, M. Q.; Sun, L.; Crooks, R. M. *J. Am. Chem. Soc.* **1998**, *120*, 4877-4878.
- (26) Zhao, M. Q.; Crooks, R. M. *Angew. Chem., Int. Ed.* **1999**, *38*, 364-366.
- (27) Chechik, V.; Crooks, R. M. *J. Am. Chem. Soc.* **2000**, *122*, 1243-1244.
- (28) Mayer, A. B. R.; Mark, J. E. *Colloid Polym. Sci.* **1997**, *275*, 333-340.
- (29) Mayer, A. B. R.; Mark, J. E.; Morris, R. E. *Polym. J.* **1998**, *30*, 197-205.
- (30) Mayer, A. B. R.; Hausner, S. H.; Mark, J. E. *Polym. J.* **2000**, *32*, 15-22.
- (31) Mayer, A.; Antonietti, M. *Colloid Polym. Sci.* **1998**, *276*, 769-779.
- (32) Garcia, M. E.; Baker, L. A.; Crooks, R. M. *Anal. Chem.* **1999**, *71*, 256-258.
- (33) Crooks, R. M.; Zhao, M. Q.; Sun, L.; Chechik, V.; Yeung, L. K. *Acc. Chem. Res.* **2001**, *34*, 181-190.
- (34) Esumi, K.; Suzuki, A.; Yamahira, A.; Torigoe, K. *Langmuir* **2000**, *16*, 2604-2608.
- (35) Huang, H. H.; Yan, F. Q.; Kek, Y. M.; Chew, C. H.; Xu, G. Q.; Ji, W.; Oh, P. S.; Tang, S. H. *Langmuir* **1997**, *13*, 172-175.
- (36) Tan, C. K.; Newberry, V.; Webb, T. R.; McAuliffe, C. A. *J. Chem. Soc., Dalton Trans.* **1987**, 1299-1303.
- (37) Kiwi, J.; Gratzel, M. *J. Am. Chem. Soc.* **1979**, *101*, 7214-7217.
- (38) Tano, T.; Esumi, K.; Meguro, K. *J. Colloid Interface. Sci.* **1989**, *133*, 530-533.
- (39) Mosseri, S.; Henglein, A.; Janata, E. *J. Phys. Chem.* **1989**, *93*, 6791-6795.
- (40) Marignier, J. L.; Belloni, J.; Delcourt, M. O.; Chevalier, J. P. *Nature* **1985**, *317*, 344-345.
- (41) Ershov, B. G.; Janata, E.; Michaelis, M.; Henglein, A. *J. Phys. Chem.* **1991**, *95*, 8996-8999.

- (42) Michaelis, M.; Henglein, A. *J. Phys. Chem.* **1992**, *96*, 4719-4724.
- (43) Torigoe, K.; Esumi, K. *Langmuir* **1992**, *8*, 59-63.
- (44) Yonezawa, Y.; Sato, T.; Ohno, M.; Hada, H. *J. Chem. Soc., Faraday Trans.* **1987**, *83*, 1559-1567.
- (45) Toshima, N.; Takahashi, T.; Hirai, H. *Chem. Lett.* **1986**, 35-38.
- (46) Scaiano, J. C.; Aliaga, C.; Maguire, S.; Wang, D. *J. Phys. Chem. B* **2006**, *110*, 12856-12859.
- (47) McGilvray, K. L.; Decan, M. R.; Wang, D. S.; Scaiano, J. C. *J. Am. Chem. Soc.* **2006**, *128*, 15980-15981.
- (48) Marin, M. L.; McGilvray, K. L.; Scaiano, J. C. *J. Am. Chem. Soc.* **2008**, *130*, 16572-16584.
- (49) Gonzalez, C. M.; Liu, Y.; Scaiano, J. C. *J. Phys. Chem. C* **2009**, *113*, 11861-11867.
- (50) Reetz, M. T.; Helbig, W. *J. Am. Chem. Soc.* **1994**, *116*, 7401-7402.
- (51) Reetz, M. T.; Quaiser, S. A. *Angew. Chem., Int. Ed.* **1995**, *34*, 2240-2241.
- (52) Sinfelt, J. H. *J. Catal.* **1973**, *29*, 308-315.
- (53) Toshima, N. In *Nanoscale Materials*; Liz-Marzan, L. M., Kamat, P. V., Eds.; Kluwer Academic Pub.: Boston, **2003**, 79-96.
- (54) Sinfelt, J. H. *Bimetallic Catalysts*; Wiley, New York **1983**.
- (55) Marx, S.; Baiker, A. *J. Phys. Chem. C* **2009**, *113*, 6191-6201.
- (56) Coq, B.; Figueras, F. *J. Mol. Catal. A: Chem.* **2001**, *173*, 117-134.
- (57) Wang, Y.; Liu, H. F.; Toshima, N. *J. Phys. Chem.* **1996**, *100*, 19533-19537.
- (58) Diemant, T.; Hager, T.; Hoster, H. E.; Rauscher, H.; Behm, R. J. *Surf. Sci.* **2003**, *541*, 137-146.
- (59) Alayoglu, S.; Nilekar, A. U.; Mavrikakis, M.; Eichhorn, B. *Nature Mater.* **2008**, *7*, 333-338.
- (60) Cable, R. E.; Schaak, R. E. *Chem. Mater.* **2005**, *17*, 6835-6841.

- (61) Reichl, W.; Hayek, K. *J. Catal.* **2004**, *222*, 53-64.
- (62) Mendez-Villuendas, E.; Bowles, R. K. *Phys. Rev. Lett.* **2007**, *98*, 185503-1-185503-4.
- (63) Kim, J. W.; Larsen, R. J.; Weitz, D. A. *J. Am. Chem. Soc.* **2006**, *128*, 14374-14377.
- (64) Ge, J. P.; Hu, Y. X.; Zhang, T. R.; Yin, Y. D. *J. Am. Chem. Soc.* **2007**, *129*, 8974-8975.
- (65) Ohnuma, A.; Cho, E. C.; Camargo, P. H. C.; Au, L.; Ohtani, B.; Xia, Y. N. *J. Am. Chem. Soc.* **2009**, *131*, 1352-1353.
- (66) Christensen, A.; Ruban, A. V.; Stoltze, P.; Jacobsen, K. W.; Skriver, H. L.; Norskov, J. K.; Besenbacher, F. *Phys. Rev. B* **1997**, *56*, 5822-5834.
- (67) Toshima, N.; Harada, M.; Yonezawa, T.; Kushihashi, K.; Asakura, K. *J. Phys. Chem.* **1991**, *95*, 7448-7453.
- (68) Toshima, N.; Harada, M.; Yamazaki, Y.; Asakura, K. *J. Phys. Chem.* **1992**, *96*, 9927-9933.
- (69) Toshima, N.; Hirakawa, K. *Appl. Surf. Sci.* **1997**, *121*, 534-537.
- (70) Yu, Z. K.; Liao, S. J.; Xu, Y.; Yang, B.; Yu, D. R. *J. Mol. Catal. A: Chem.* **1997**, *120*, 247-255.
- (71) Silvert, P. Y.; Vijayakrishnan, V.; Vibert, P.; HerreraUrbina, R.; Elhsissen, K. T. *Nanostructured Mater.* **1996**, *7*, 611-618.
- (72) Bonnemann, H.; Brijoux, W.; Brinkmann, R.; Dinjus, E.; Jousen, T.; Korall, B. *Angew. Chem., Int. Ed.* **1991**, *30*, 1312-1314.
- (73) Schmidt, T. J.; Noeske, M.; Gasteiger, H. A.; Behm, R. J.; Britz, P.; Brijoux, W.; Bonnemann, H. *Langmuir* **1997**, *13*, 2591-2595.
- (74) Bonnemann, H.; Britz, P.; Vogel, W. *Langmuir* **1998**, *14*, 6654-6657.
- (75) Aleandri, L. E.; Bonnemann, H.; Jones, D. J.; Richter, J.; Roziere, J. *J. Mater. Chem.* **1995**, *5*, 749-752.
- (76) Pan, C.; Dassenoy, F.; Casanove, M. J.; Philippot, K.; Amiens, C.; Lecante, P.; Mosset, A.; Chaudret, B. *J. Phys. Chem. B* **1999**, *103*, 10098-10101.
- (77) Torigoe, K.; Esumi, K. *Langmuir* **1993**, *9*, 1664-1667.

- (78) Bradley, J. S.; Hill, E. W.; Klein, C.; Chaudret, B.; Duteil, A. *Chem. Mater.* **1993**, *5*, 254-256.
- (79) Remita, S.; Mostafavi, M.; Delcourt, M. O. *Radiat. Phys. Chem.* **1996**, *47*, 275-279.
- (80) Harriman, A. *J. Chem. Soc., Chem. Commun.* **1990**, 24-26.
- (81) Henglein, A. *J. Phys. Chem.* **1993**, *97*, 5457-5471.
- (82) Reetz, M. T.; Helbig, W.; Quaiser, S. A. *Chem. Mater.* **1995**, *7*, 2227-2228.
- (83) Toshima, N.; Kushihashi, K.; Yonezawa, T.; Hirai, H. *Chem. Lett.* **1989**, 1769-1772.
- (84) Scott, R. W. J.; Wilson, O. M.; Oh, S. K.; Kenik, E. A.; Crooks, R. M. *J. Am. Chem. Soc.* **2004**, *126*, 15583-15591.
- (85) Zhao, M. Q.; Crooks, R. M. *Chem. Mater.* **1999**, *11*, 3379-3385.
- (86) Jana, N. R.; Gearheart, L.; Murphy, C. J. *Adv. Mater.* **2001**, *13*, 1389-1393.
- (87) Schmid, G.; West, H.; Malm, J. O.; Bovin, J. O.; Grenthe, C. *Chem. -Eur. J.* **1996**, *2*, 1099-1103.
- (88) Harada, M.; Asakura, K.; Toshima, N. *J. Phys. Chem.* **1993**, *97*, 5103-5114.
- (89) Grabow, L. C.; Mavrikakis, M. *Angew. Chem., Int. Ed.* **2008**, *47*, 7390-7392.
- (90) Hashmi, A. S. K.; Hutchings, G. J. *Angew. Chem., Int. Ed.* **2006**, *45*, 7896-7936.
- (91) Campbell, C. T. *Science* **2004**, *306*, 234-235.
- (92) Chen, M. S.; Goodman, D. W. *Science* **2004**, *306*, 252-255.
- (93) Tsunoyama, H.; Sakurai, H.; Negishi, Y.; Tsukuda, T. *J. Am. Chem. Soc.* **2005**, *127*, 9374-9375.
- (94) Gopidas, K. R.; Whitesell, J. K.; Fox, M. A. *J. Am. Chem. Soc.* **2003**, *125*, 14168-14180.
- (95) Hou, W. B.; Dehm, N. A.; Scott, R. W. J. *J. Catal.* **2008**, *253*, 22-27.
- (96) Sinfelt, J. H. *Acc. Chem. Res.* **1987**, *20*, 134-139.
- (97) Chen, M. S.; Kumar, D.; Yi, C. W.; Goodman, D. W. *Science* **2005**, *310*, 291-293.



- (98) Enache, D. I.; Edwards, J. K.; Landon, P.; Solsona-Espriu, B.; Carley, A. F.; Herzing, A. A.; Watanabe, M.; Kiely, C. J.; Knight, D. W.; Hutchings, G. J. *Science* **2006**, *311*, 362-365.
- (99) Edwards, J. K.; Carley, A. F.; Herzing, A. A.; Kiely, C. J.; Hutchings, G. J. *Faraday Discuss.* **2008**, *138*, 225-239.
- (100) Landon, P.; Collier, P. J.; Papworth, A. J.; Kiely, C. J.; Hutchings, G. J. *Chem. Commun.* **2002**, 2058-2059.
- (101) Solsona, B. E.; Edwards, J. K.; Landon, P.; Carley, A. F.; Herzing, A.; Kiely, C. J.; Hutchings, G. J. *Chem. Mater.* **2006**, *18*, 2689-2695.
- (102) Han, Y. F.; Zhong, Z. Y.; Ramesh, K.; Chen, F. X.; Chen, L. W.; White, T.; Tay, Q. L.; Yaakub, S. N.; Wang, Z. *J. Phys. Chem. C* **2007**, *111*, 8410-8413.
- (103) Ketchie, W. C.; Murayama, M.; Davis, R. J. *J. Catal.* **2007**, *250*, 264-273.
- (104) Conte, M.; Carley, A. F.; Attard, G.; Herzing, A. A.; Kiely, C. J.; Hutchings, G. J. *J. Catal.* **2008**, *257*, 190-198.
- (105) Scott, R. W. J.; Sivadinarayana, C.; Wilson, O. M.; Yan, Z.; Goodman, D. W.; Crooks, R. M. *J. Am. Chem. Soc.* **2005**, *127*, 1380-1381.
- (106) Lopez-Sanchez, J. A.; Dimitratos, N.; Miedziak, P.; Ntainjua, E.; Edwards, J. K.; Morgan, D.; Carley, A. F.; Tiruvalam, R.; Kiely, C. J.; Hutchings, G. J. *Phys. Chem. Chem. Phys.* **2008**, *10*, 1921-1930.
- (107) Herzing, A. A.; Carley, A. F.; Edwards, J. K.; Hutchings, G. J.; Kiely, C. J. *Chem. Mater.* **2008**, *20*, 1492-1501.
- (108) Parvulescu, V. I.; Parvulescu, V.; Eudruschat, U.; Filoti, G.; Wagner, F. E.; Kubel, C.; Richards, R. *Chem. -Eur. J.* **2006**, *12*, 2343-2357.
- (109) Schalm, O.; Van der Linden, V.; Frederickx, P.; Luyten, S.; Van der Snickt, G.; Caen, J.; Schryvers, D.; Janssens, K.; Cornelis, E.; Van Dyck, D.; Schreiner, M. *Spectrochim. Acta Part B* **2009**, *64*, 812-820.
- (110) Bradley, J. S. In *Clusters and Colloids*; Schmid, G., Ed.; VCH, Weinheim: **1994**, 459-544.
- (111) Frenkel, A. I.; Hills, C. W.; Nuzzo, R. G. *J. Phys. Chem. B* **2001**, *105*, 12689-12703.

- (112) Sanchez, S. I.; Small, M. W.; Zuo, J. M.; Nuzzo, R. G. *J. Am. Chem. Soc.* **2009**, *131*, 8683-8689.
- (113) Schmid, G.; Lehnert, A.; Malm, J. O.; Bovin, J. O. *Angew. Chem., Int. Ed.* **1991**, *30*, 874-876.
- (114) Alayoglu, S.; Zavalij, P.; Eichhorn, B.; Wang, Q.; Frenkel, A. I.; Chupas, P. *ACS Nano* **2009**, *3*, 3127-3137.
- (115) Bedford, N.; Dablemont, C.; Viau, G.; Chupas, P.; Petkov, V. *J. Phys. Chem. C* **2007**, *111*, 18214-18219.
- (116) XPS Grad Course, University of Western Ontario, March, 20, 2010, <[http://www.uwo.ca/ssw/services//xps/xpsgradcourse/resources/xps\\_grad\\_course.pdf](http://www.uwo.ca/ssw/services//xps/xpsgradcourse/resources/xps_grad_course.pdf)>.
- (117) Abel, K. A.; Boyer, J. C.; van Veggel, F. *J. Am. Chem. Soc.* **2009**, *131*, 14644-14645.
- (118) Meitzner, G.; Via, G. H.; Lytle, F. W.; Fung, S. C.; Sinfelt, J. H. *J. Phys. Chem.* **1988**, *92*, 2925-2932.
- (119) Sinfelt, J. H.; Via, G. H.; Lytle, F. W. *Catal. Rev.: Sci. Eng.* **1984**, *26*, 81-140.
- (120) Koningsberger, D. C.; Mojet, B. L.; van Dorssen, G. E.; Ramaker, D. E. *Top. Catal.* **2000**, *10*, 143-155.
- (121) Bazin, D.; Sayers, D.; Rehr, J. J.; Mottet, C. *J. Phys. Chem. B* **1997**, *101*, 5332-5336.
- (122) Bazin, D.; Rehr, J. J. *J. Phys. Chem. B* **2003**, *107*, 12398-12402.
- (123) Hwang, B. J.; Sarma, L. S.; Chen, J. M.; Chen, C. H.; Shih, S. C.; Wang, G. R.; Liu, D. G.; Lee, J. F.; Tang, M. T. *J. Am. Chem. Soc.* **2005**, *127*, 11140-11145.
- (124) Weir, M. G.; Knecht, M. R.; Frenkel, A. I.; Crooks, R. M. *Langmuir* **2010**, *26*, 1137-1146.
- (125) Bradley, J. S.; Millar, J. M.; Hill, E. W.; Behal, S.; Chaudret, B.; Duteil, A. *Faraday Discuss.* **1991**, *92*, 255-268.
- (126) deCaro, D.; Bradley, J. S. *Langmuir* **1997**, *13*, 3067-3069.
- (127) Hirai, H.; Yakura, N. *Polym. Adv. Technol.* **2001**, *12*, 724-733.
- (128) Li, Y.; El-Sayed, M. A. *J. Phys. Chem. B* **2001**, *105*, 8938-8943.

- (129) Narayanan, R.; El-Sayed, M. A. *J. Am. Chem. Soc.* **2003**, *125*, 8340-8347.
- (130) Pachon, L. D.; Rothenberg, G. *Appl. Organometal. Chem.* **2008**, *22*, 288-299.
- (131) Gniewek, A.; Ziolkowski, J. J.; Trzeciak, A. M.; Kepinski, L. *J. Catal.* **2006**, *239*, 272-281.
- (132) Li, Y.; Boone, E.; El-Sayed, M. A. *Langmuir* **2002**, *18*, 4921-4925.
- (133) Torok, B.; Felfoldi, K.; Szakonyi, G.; Balazsik, K.; Bartok, M. *Catal. Lett.* **1998**, *52*, 81-84.
- (134) Sablong, R.; Schlotterbeck, U.; Vogt, D.; Mecking, S. *Adv. Synth. Catal.* **2003**, *345*, 333-336.
- (135) Liu, Y. B.; Khemtong, C.; Hu, J. *Chem. Commun.* **2004**, 398-399.
- (136) Kanaoka, S.; Yagi, N.; Fukuyama, Y.; Aoshima, S.; Tsunoyama, H.; Tsukuda, T.; Sakurai, H. *J. Am. Chem. Soc.* **2007**, *129*, 12060-12061.
- (137) Konya, Z.; Puentes, V. F.; Kiricsi, I.; Zhu, J.; Alivisatos, A. P.; Somorjai, G. A. *Nano Lett.* **2002**, *2*, 907-910.
- (138) Meier, M. A. R.; Filali, M.; Gohy, J. F.; Schubert, U. S. *J. Mater. Chem.* **2006**, *16*, 3001-3006.
- (139) Beletskaya, I. P.; Kashin, A. N.; Litvinov, A. E.; Tyurin, V. S.; Valetsky, P. M.; van Koten, G. *Organometallics* **2006**, *25*, 154-158.
- (140) Narayanan, R.; El-Sayed, M. A. *Top. Catal.* **2008**, *47*, 15-21.
- (141) Scott, R. W. J.; Datye, A. K.; Crooks, R. M. *J. Am. Chem. Soc.* **2003**, *125*, 3708-3709.
- (142) Duteil, A.; Schmid, G.; Meyerzaika, W. *J. Chem. Soc., Chem. Commun.* **1995**, 31-32.
- (143) Amiens, C.; Decaro, D.; Chaudret, B.; Bradley, J. S.; Mazel, R.; Roucau, C. *J. Am. Chem. Soc.* **1993**, *115*, 11638-11639.
- (144) Son, S. U.; Jang, Y.; Park, J.; Na, H. B.; Park, H. M.; Yun, H. J.; Lee, J.; Hyeon, T. *J. Am. Chem. Soc.* **2004**, *126*, 5026-5027.
- (145) Dasog, M.; Scott, R. W. J. *Langmuir* **2007**, *23*, 3381-3387.
- (146) Hou, W. B.; Dasog, M.; Scott, R. W. J. *Langmuir* **2009**, *25*, 12954-12961.

- (147) Lu, F.; Ruiz, J.; Astruc, D. *Tetrahedron Lett.* **2004**, *45*, 9443-9445.
- (148) Wu, L.; Li, B. L.; Huang, Y. Y.; Zhou, H. F.; He, Y. M.; Fan, Q. H. *Org. Lett.* **2006**, *8*, 3605-3608.
- (149) Cheng, W. L.; Dong, S. J.; Wang, E. K. *Langmuir* **2003**, *19*, 9434-9439.
- (150) Isaacs, S. R.; Cutler, E. C.; Park, J. S.; Lee, T. R.; Shon, Y. S. *Langmuir* **2005**, *21*, 5689-5692.
- (151) Sheldon, R. *Chem. Commun.* **2001**, 2399-2407.
- (152) Welton, T. *Chem. Rev.* **1999**, *99*, 2071-2083.
- (153) Freemantle, M. *An Introduction to Ionic Liquids*; RSC, Cambridge, **2010**.
- (154) Wilkes, J. S.; Levisky, J. A.; Wilson, R. A.; Hussey, C. L. *Inorg. Chem.* **1982**, *21*, 1263-1264.
- (155) Wilkes, J. S.; Zaworotko, M. J. *J. Chem. Soc., Chem. Commun.* **1992**, 965-967.
- (156) Fuller, J.; Carlin, R. T.; Delong, H. C.; Haworth, D. *J. Chem. Soc., Chem. Commun.* **1994**, 299-300.
- (157) Huddleston, J. G.; Visser, A. E.; Reichert, W. M.; Willauer, H. D.; Broker, G. A.; Rogers, R. D. *Green Chem.* **2001**, *3*, 156-164.
- (158) Welton, T. *Green Chem.* **2008**, *10*, 483-483.
- (159) Bates, E. D.; Mayton, R. D.; Ntai, I.; Davis, J. H. *J. Am. Chem. Soc.* **2002**, *124*, 926-927.
- (160) Wang, J. J.; Pei, Y. C.; Zhao, Y.; Hu, Z. G. *Green Chem.* **2005**, *7*, 196-202.
- (161) Blanchard, L. A.; Hancu, D.; Beckman, E. J.; Brennecke, J. F. *Nature* **1999**, *399*, 28-29.
- (162) Visser, A. E.; Swatloski, R. P.; Reichert, W. M.; Mayton, R.; Sheff, S.; Wierzbicki, A.; Davis, J. H.; Rogers, R. D. *Environ. Sci. Technol.* **2002**, *36*, 2523-2529.
- (163) Scovazzo, P.; Kieft, J.; Finan, D. A.; Koval, C.; DuBois, D.; Noble, R. *J. Membr. Sci.* **2004**, *238*, 57-63.
- (164) Li, C. Z.; Wang, Q.; Zhao, Z. K. *Green Chem.* **2008**, *10*, 177-182.

- (165) Zhao, H. B.; Holladay, J. E.; Brown, H.; Zhang, Z. C. *Science* **2007**, *316*, 1597-1600.
- (166) Swatloski, R. P.; Holbrey, J. D.; Rogers, R. D. *Green Chem.* **2003**, *5*, 361-363.
- (167) Smiglak, M.; Reichert, W. M.; Holbrey, J. D.; Wilkes, J. S.; Sun, L. Y.; Thrasher, J. S.; Kirichenko, K.; Singh, S.; Katritzky, A. R.; Rogers, R. D. *Chem. Commun.* **2006**, 2554-2556.
- (168) Migowski, P.; Dupont, J. *Chem. -Eur. J.* **2007**, *13*, 32-39.
- (169) Davis, J. H. *Chem. Lett.* **2004**, *33*, 1072-1077.
- (170) Deshmukh, R. R.; Rajagopal, R.; Srinivasan, K. V. *Chem. Commun.* **2001**, 1544-1545.
- (171) Dupont, J.; Fonseca, G. S.; Umpierre, A. P.; Fichtner, P. F. P.; Teixeira, S. R. *J. Am. Chem. Soc.* **2002**, *124*, 4228-4229.
- (172) Fonseca, G. S.; Umpierre, A. P.; Fichtner, P. F. P.; Teixeira, S. R.; Dupont, J. *Chem. -Eur. J.* **2003**, *9*, 3263-3269.
- (173) Bruss, A. J.; Gelesky, M. A.; Machado, G.; Dupont, J. *J. Mol. Catal. A: Chem.* **2006**, *252*, 212-218.
- (174) Scheeren, C. W.; Machado, G.; Dupont, J.; Fichtner, P. F. P.; Teixeira, S. R. *Inorg. Chem.* **2003**, *42*, 4738-4742.
- (175) Silveira, E. T.; Umpierre, A. P.; Rossi, L. M.; Machado, G.; Morais, J.; Soares, G. V.; Baumvol, I. L. R.; Teixeira, S. R.; Fichtner, P. F. P.; Dupont, J. *Chem. -Eur. J.* **2004**, *10*, 3734-3740.
- (176) Umpierre, A. P.; Machado, G.; Fecher, G. H.; Morais, J.; Dupont, J. *Adv. Synth. Catal.* **2005**, *347*, 1404-1412.
- (177) Migowski, P.; Machado, G.; Teixeira, S. R.; Alves, M. C. M.; Morais, J.; Traverse, A.; Dupont, J. *Phys. Chem. Chem. Phys.* **2007**, *9*, 4814-4821.
- (178) Singh, P.; Katyal, A.; Kalra, R.; Chandra, R. *Tetrahedron Lett.* **2008**, *49*, 727-730.
- (179) An, J.; Wang, D. S.; Luo, Q. Z.; Yuan, X. Y. *Mater. Sci. Eng. C* **2009**, *29*, 1984-1989.
- (180) Redel, E.; Thomann, R.; Janiak, C. *Chem. Commun.* **2008**, 1789-1791.

- (181) Kramer, J.; Redel, E.; Thomann, R.; Janiak, C. *Organometallics* **2008**, *27*, 1976-1978.
- (182) Redel, E.; Kramer, J.; Thomann, R.; Janiak, C. *J. Organomet. Chem.* **2009**, *694*, 1069-1075.
- (183) Wei, G. T.; Yang, Z. S.; Lee, C. Y.; Yang, H. Y.; Wang, C. R. C. *J. Am. Chem. Soc.* **2004**, *126*, 5036-5037.
- (184) Wang, Y.; Yang, H. *Chem. Commun.* **2006**, 2545-2547.
- (185) Mu, X. D.; Evans, D. G.; Kou, Y. A. *Catal. Lett.* **2004**, *97*, 151-154.
- (186) Tatumi, R.; Fujihara, H. *Chem. Commun.* **2005**, 83-85.
- (187) Mu, X. D.; Meng, J. Q.; Li, Z. C.; Kou, Y. *J. Am. Chem. Soc.* **2005**, *127*, 9694-9695.
- (188) Zhao, C.; Wang, H. Z.; Yan, N.; Xiao, C. X.; Mu, X. D.; Dyson, P. J.; Kou, Y. *J. Catal.* **2007**, *250*, 33-40.
- (189) Lee, S. G. *Chem. Commun.* **2006**, 1049-1063.
- (190) Kim, K. S.; Demberelnyamba, D.; Lee, H. *Langmuir* **2004**, *20*, 556-560.
- (191) Choi, S.; Kim, K. S.; Yeon, S. H.; Cha, J. H.; Lee, H.; Kim, C. J.; Yoo, I. D. *Korean J. Chem. Eng.* **2007**, *24*, 856-859.
- (192) Chiappe, C.; Pieraccini, D.; Zhao, D. B.; Fei, Z. F.; Dyson, P. J. *Adv. Synth. Catal.* **2006**, *348*, 68-74.
- (193) Wang, Z. J.; Zhang, Q. X.; Kuehner, D.; Ivaska, A.; Niu, L. *Green Chem.* **2008**, *10*, 907-909.
- (194) Fonseca, G. S.; Machado, G.; Teixeira, S. R.; Fecher, G. H.; Morais, J.; Alves, M. C. M.; Dupont, J. *J. Colloid Interface. Sci.* **2006**, *301*, 193-204.
- (195) Scheeren, C. W.; Machado, G.; Teixeira, S. R.; Morais, J.; Domingos, J. B.; Dupont, J. *J. Phys. Chem. B* **2006**, *110*, 13011-13020.
- (196) Seddon, K. R.; Stark, A.; Torres, M. J. *Pure Appl. Chem.* **2000**, *72*, 2275-2287.
- (197) Ou, G. N.; Xu, L.; He, B. Y.; Yuan, Y. Z. *Chem. Commun.* **2008**, 4210-4212.
- (198) Yang, X.; Fei, Z. F.; Zhao, D. B.; Ang, W. H.; Li, Y. D.; Dyson, P. J. *Inorg. Chem.* **2008**, *47*, 3292-3297.

- (199) Huang, J.; Jiang, T.; Han, B. X.; Gao, H. X.; Chang, Y. H.; Zhao, G. Y.; Wu, W. *Z. Chem. Commun.* **2003**, 1654-1655.
- (200) Yang, X.; Yan, N.; Fei, Z. F.; Crespo-Quesada, R. M.; Laurency, G.; Kiwi-Minsker, L.; Kou, Y.; Li, Y. D.; Dyson, P. J. *Inorg. Chem.* **2008**, *47*, 7444-7446.
- (201) Leger, B.; Denicourt-Nowicki, A.; Roucoux, A.; Olivier-Bourbigou, H. *Adv. Synth. Catal.* **2008**, *350*, 153-159.
- (202) Ertl, G.; Knozinger, H.; Weitkamp, J. *Handbook of Heterogeneous Catalysis*; Wiley/VCH: New York/Weinheim, **1997**.
- (203) Choi, H.; Al-Abed, S. R.; Agarwal, S.; Dionysiou, D. D. *Chem. Mater.* **2008**, *20*, 3649-3655.
- (204) White, R. J.; Luque, R.; Budarin, V. L.; Clark, J. H.; Macquarrie, D. J. *Chem. Soc. Rev.* **2009**, *38*, 481-494.
- (205) Campelo, J. M.; Lee, A. F.; Luque, R.; Luna, D.; Marinas, J. M.; Romero, A. A. *Chem. -Eur. J.* **2008**, *14*, 5988-5995.
- (206) Horvath, D.; Toth, L.; Guzzi, L. *Catal. Lett.* **2000**, *67*, 117-128.
- (207) Barau, A.; Budarin, V.; Caragheorghopol, A.; Luque, R.; Macquarrie, D. J.; Prelu, A.; Teodorescu, V. S.; Zaharescu, M. *Catal. Lett.* **2008**, *124*, 204-214.
- (208) Campelo, J. M.; Conesa, T. D.; Gracia, M. J.; Jurado, M. J.; Luque, R.; Marinas, J. M.; Romero, A. A. *Green Chem.* **2008**, *10*, 853-858.
- (209) Zhang, Y.; Erkey, C. *J. Supercrit. Fluids* **2006**, *38*, 252-267.
- (210) Zhang, Y.; Kang, D. F.; Saquing, C.; Aindow, M.; Erkey, C. *Ind. Eng. Chem. Res.* **2005**, *44*, 4161-4164.
- (211) Scott, R. W. J.; Wilson, O. M.; Crooks, R. M. *Chem. Mater.* **2004**, *16*, 5682-5688.
- (212) Zheng, N. F.; Stucky, G. D. *J. Am. Chem. Soc.* **2006**, *128*, 14278-14280.
- (213) Song, H.; Rioux, R. M.; Hoefelmeyer, J. D.; Komor, R.; Niesz, K.; Grass, M.; Yang, P. D.; Somorjai, G. A. *J. Am. Chem. Soc.* **2006**, *128*, 3027-3037.
- (214) Lang, H. F.; May, R. A.; Iversen, B. L.; Chandler, B. D. *J. Am. Chem. Soc.* **2003**, *125*, 14832-14836.

- (215) Lang, H. G.; Maldonado, S.; Stevenson, K. J.; Chandler, B. D. *J. Am. Chem. Soc.* **2004**, *126*, 12949-12956.
- (216) Tasis, D.; Tagmatarchis, N.; Bianco, A.; Prato, M. *Chem. Rev.* **2006**, *106*, 1105-1136.
- (217) Heidenreich, R. G.; Krauter, E. G. E.; Pietsch, J.; Kohler, K. *J. Mol. Catal. A: Chem.* **2002**, *182*, 499-509.
- (218) Ma, Z.; Yu, J. H.; Dai, S. *Adv. Mater.* **2010**, *22*, 261-285.
- (219) Zhou, Y. *Current Nanoscience* **2005**, *1*, 35-42.
- (220) Antonietti, M.; Kuang, D. B.; Smarsly, B.; Yong, Z. *Angew. Chem., Int. Ed.* **2004**, *43*, 4988-4992.
- (221) Zhou, Y.; Antonietti, M. *J. Am. Chem. Soc.* **2003**, *125*, 14960-14961.
- (222) Dai, S.; Ju, Y. H.; Gao, H. J.; Lin, J. S.; Pennycook, S. J.; Barnes, C. E. *Chem. Commun.* **2000**, 243-244.
- (223) Adams, C. J.; Bradley, A. E.; Seddon, K. R. *Aus. J. Chem.* **2001**, *54*, 679-681.
- (224) Zhou, Y.; Schattka, J. H.; Antonietti, M. *Nano Lett.* **2004**, *4*, 477-481.
- (225) Yoo, K.; Choi, H.; Dionysiou, D. D. *Chem. Commun.* **2004**, 2000-2001.
- (226) Nakashima, T.; Kimizuka, N. *J. Am. Chem. Soc.* **2003**, *125*, 6386-6387.



## CHAPTER 2

### 2. Bimetallic Pd-Au Nanoparticles as Hydrogenation Catalysts in Imidazolium Ionic Liquids

This work has been published in *Journal of Molecular Catalysis A: Chemical*. PVP-stabilized Pd, Au, and bimetallic Pd-Au nanoparticles have been solubilized in clean and pure imidazolium-based ILs by a simple phase transfer method with no significant change in particle size. For the first time, the catalytic behavior of IL phase bimetallic nanoparticles was explored. Bimetallic PdAu nanoparticles in the IL were shown to have decent activities for the hydrogenation of a range of substrates (allyl alcohol, 1,3-cyclooctadiene, trans-cinnamaldehyde, and 3-hexyn-1-ol), with the highest catalytic activities seen for bimetallic nanoparticles with high Pd loadings. Unreacted substrates and products were easily removed from the IL phase under reduced pressure and the catalyst solution could be reused with very little change in catalytic activity.

---

This work has been published in *J. Mol. Catal. A; Chem.*, **2008**, 286, 114-119. This paper has been co-authored by N. A. Dehm (2<sup>nd</sup> author) who did some initial studies of nanoparticle synthesis in IL. All the experimental work in this paper has been done by me along with the manuscript writing and editing. The final manuscript was submitted after thorough revisions by my supervisor Dr. Robert W. J. Scott.

# **Bimetallic PdAu Nanoparticles as Hydrogenation Catalysts in Imidazolium Ionic Liquids**

Priyabrat Dash, Nicole A. Dehm, Robert W. J. Scott\*

Department of Chemistry, University of Saskatchewan, 110 Science Place,  
Saskatoon, Saskatchewan, Canada

## **2.1 Abstract**

Metallic and bimetallic PdAu nanoparticles were solubilized in 1-butyl-3-methylimidazolium hexafluorophosphate ionic liquid (IL) by a phase transfer method using poly(vinylpyrrolidone) (PVP) as a stabilizer. Nanoparticles were characterized by UV-Vis spectroscopy and transmission electron microscopy. The bimetallic PdAu nanoparticles in the IL phase were examined as catalysts for hydrogenation reactions; both the activity and selectivity of the hydrogenation reactions could be tuned by varying the composition of the bimetallic nanoparticles, with maximum activities seen at 3:1 Pd: Au ratios. These nanoparticle/IL catalysts were recycled and then reused for further catalytic reactions with minimal loss in activity.

## 2.2 Introduction

Nanoparticles of noble metals ranging in size from 1 to 5 nm exhibit specific physical and chemical properties that are intermediate between those of the atomic element from which they are composed and those of the bulk metal.<sup>1</sup> Catalytic reactions over metallic,<sup>2-8</sup> and bimetallic,<sup>5,9,10</sup> nanoparticle surfaces are of great interest, as the nanoparticle size, composition and structure can offer the ability to tune the activity and also, in many cases, the selectivity of the catalyst.<sup>5</sup> Ionic liquids (ILs) have recently emerged as intriguing reaction media for “quasi-homogeneous” solution-phase nanoparticle catalysis due to the unique properties of ILs, such as high polarity, negligible vapor pressure, high ionic conductivity, and excellent thermal stability,<sup>11-19</sup> and the fact that the driving forces for nanoparticle aggregation have been reported to be much lower in IL solvents.<sup>20</sup> To the best of our knowledge, no studies have investigated the catalytic activity of bimetallic nanoparticles in IL solvents. Herein, we report on the stabilization of Au, Pd and bimetallic nanoparticles in room-temperature imidazolium IL, and show that they are active and reusable catalysts for hydrogenation reactions.

Two main pitfalls faced when using nanoparticles for catalysis are the difficulties of stabilizing particles in this size range while retaining sufficient catalytic activity,<sup>5</sup> and the problematic separation of the catalytic particles from the product and unused reactants at the end of the reaction.<sup>6,21</sup> One way to facilitate the separation process is to immobilize the particles on a solid support, but this may lead to a decrease in activity due to lower accessible surface area of the particles. “Quasi-homogeneous” nanoparticle solution-based routes theoretically offer much high surface areas and reactivities, but the presence

of stabilizer on the surface can significantly hinder or poison the catalytic activity,<sup>5,7</sup> while in the absence of stabilizers particle aggregation is quite problematic. J. Dupont and coworkers first discovered that stable transition metal nanoparticles could be formed in imidazolium ILs with no external stabilizers needed for stabilization of the nanoparticles, and that the subsequent IL-phase nanoparticles could be used for a range of catalytic reactions.<sup>13,14,16</sup> These IL-phase nanoparticles were efficient multiphase catalysts for the hydrogenation of alkenes and arenes under mild conditions. Given that ILs offer the ability to potentially stabilize high accessible surface areas for solution-phase nanoparticles, we wished to investigate the conditions in which metallic and bimetallic nanoparticle catalysts could be stabilized in clean imidazolium ILs.

Herein we report the phase-transfer of Pd, Au and bimetallic Pd-Au nanoparticles into 1-butyl-3-methylimidazolium ([BMIM]) hexafluorophosphate IL, and subsequent explorations of the activity of the resulting IL-phase nanoparticles for simple hydrogenation reactions. It was found to be necessary to add an external stabilizer, poly(vinylpyrrolidone), to stabilize the nanoparticles in the IL phase. Hydrogenation reactions over a bimetallic Pd-Au nanoparticle series were undergone using allyl alcohol, 1,3-cyclooctadiene, trans-cinnamaldehyde, and 3-hexyn-1-ol substrates. It was found that both the activity and selectivity of the hydrogenation reactions could be tuned by varying the compositions of the bimetallic nanoparticles, with particles with high Pd loadings showing the highest activities. In addition, we show that the resulting bimetallic nanoparticles can be reused, and retain their activities over multiple catalytic cycles.

## 2.3 Experimental

### 2.3.1 Materials

1-methylimidazole (99 %) and 1-chlorobutane (99.5 %) were purchased from Alfa and were distilled over KOH and P<sub>2</sub>O<sub>5</sub>, respectively, before use. Hexafluorophosphoric acid (*ca.* 65 % solution in water), poly(vinylpyrrolidone) (M.W. 40,000), hydrogen tetrachloroaurate hydrate (99.9%), potassium tetrachloropalladate (99.99%), allyl alcohol (99%), trans-cinnamaldehyde (98+ %), and 3-hexyn-1-ol (98 %) were purchased from Alfa and were used without further purification. 1, 3-cyclooctadiene (98 %) and sodium borohydride powder (98%) were obtained from Aldrich and were used as obtained. Deuterated solvents were purchased from Cambridge Isotope Laboratories. 18 MΩ·cm Milli-Q water (Millipore, Bedford, MA) was used throughout.

### 2.3.2 Catalyst Preparation

#### 2.3.2.1 Synthesis and purification of BMI IL

Synthesis of the 1-butyl-3-methylimidazolium ([BMIM]) hexafluorophosphate IL was carried out according to previous literature procedure with modifications.<sup>22</sup> Briefly, to a vigorously stirred solution of 1-methylimidazole (1.0 mol) in toluene (100 cm<sup>3</sup>) at 0° C, 1-chlorobutane (1.1 mol) was added. The solutions were heated to reflux at *ca.* 80° C for 72 h under a nitrogen atmosphere, yielding a two phase mixture of the IL, [BMIM]Cl, and toluene, which were then separated. White crystalline solids of [BMIM]Cl were obtained after three repeated recrystallizations with acetone, giving a final overall yield of ~ 60%. To make the [BMIM]PF<sub>6</sub> IL, 60 % HPF<sub>6</sub> was added to [BMIM]Cl in water in a

1.1:1 molar ratio and stirred for 15 h. The organic phase was repeatedly washed with small volumes of deionized water; washings were tested with  $\text{AgNO}_3$  until no  $\text{AgCl}$  precipitate was seen. The resulting [BMIM] IL was dried at  $70^\circ\text{C}$  for 8 hours under reduced pressure. The IL was kept under molecular sieves ( $3\text{ \AA}$ ) and re-dried at  $70^\circ\text{C}$  for 3 hours under reduced pressure before use. The purity of the [BMIM] $\text{PF}_6$  IL was verified by  $^1\text{H}$  NMR, UV-Vis spectroscopy, and Karl-Fischer titrations.<sup>23</sup>

### **2.3.2.2 Synthesis of metallic and bimetallic catalysts**

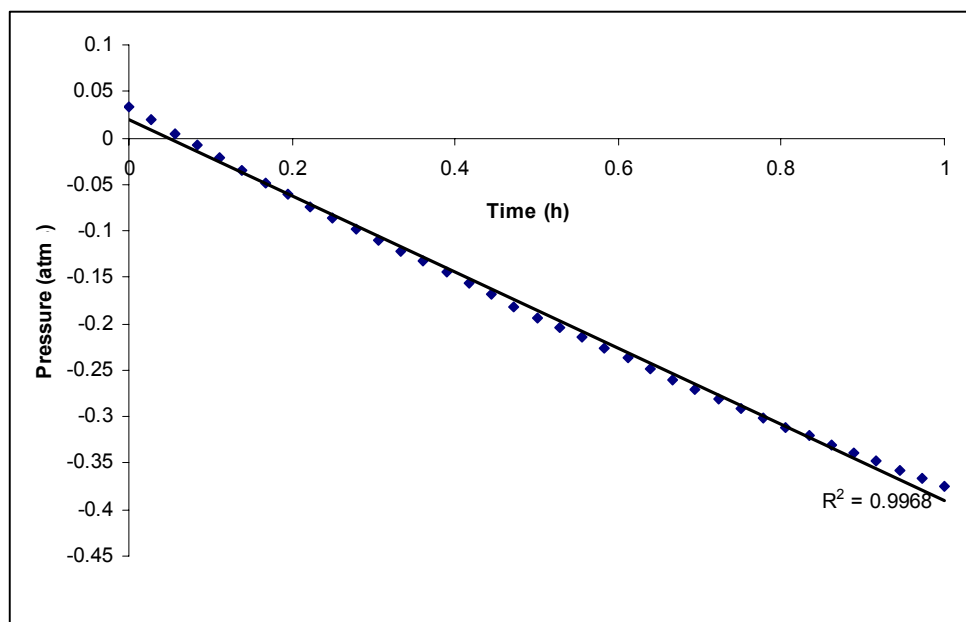
Gold nanoparticles were transferred to the [BMIM] IL according to the following procedure. First, 5.0 ml of a 1.39 mM methanol solution of PVP was added to 1.9 ml of methanol, followed by the addition of 1.1 ml of 10 mM methanol solution of  $\text{HAuCl}_4$ . The mixture was stirred for 30 min, followed by the addition of 1.0 ml of a 0.10 M  $\text{NaBH}_4$  solution in methanol prepared immediately before use. The formation of a deep red solution indicated the formation of Au nanoparticles. The excess  $\text{NaBH}_4$  was eliminated by adding 1.0 ml of 0.10 M  $\text{HCl}$  solution in methanol, followed by stirring under  $\text{N}_2$  for 10 mins. The methanol solution containing the nanoparticles was then added to 10 ml of [BMIM] IL, followed by removal of the methanol under vacuum. Pd and bimetallic Pd-Au nanoparticles were prepared and transferred to the [BMIM] IL using the same procedure above, keeping the total metal salt concentration constant.

### **2.3.3 Catalytic reactions**

Hydrogenation reactions were carried out in a three-necked round-bottom flask at  $40^\circ\text{C}$  ( $35^\circ\text{C}$  for hydrogenations of 1,3-cyclooctadiene). One end of the flask was

connected to the H<sub>2</sub> gas source, the other end with the differential pressure gauge (Model 407910, Extech Instruments Corp. with a resolution of 0.001 atm and accuracy of  $\pm 2\%$  at  $23 \pm 5$  °C) and the central neck was closed with a rubber septum. First, 10 ml of the catalyst solution was placed in the flask, followed by purging the system with H<sub>2</sub> for 10 mins. After purging, the H<sub>2</sub> source was closed and the system was stirred for 10 min to ensure equilibrium between the gas and solution phases and to confirm that there were no leaks in the system (H<sub>2</sub> was not consumed in the absence of substrate). Next, 0.5 mL of the substrate (for a substrate:catalyst ratio:  $\sim 670:1$ ) was added by syringe under vigorous stirring conditions (at 1080 rpm), followed by measurement of the H<sub>2</sub> uptake via differential pressure measurements every 10 seconds.<sup>24</sup> This, in turn allowed calculating the turnover number (TON, mol of H<sub>2</sub>/ mol metal) of the catalyst system. The turnover frequency (TOF, (mol of H<sub>2</sub>/mol metal)h<sup>-1</sup>) was then determined from the slope of linear plots of TON versus time (Figure 2.1). TOFs from NMR spectra were also determined from the slope of linear plots of turnover (mol product /mol metal) vs. time and were consistently found to be within 2% of values obtained by differential pressure measurements. Selectivities for product distributions were determined by <sup>1</sup>H NMR spectra and GC-MS. After a 1 hour interval, 1 ml of the solution was placed in a vial and then CDCl<sub>3</sub> was added. The vial was shaken to transfer the products into the CDCl<sub>3</sub> phase which was then extracted and used for NMR spectra and GC-MS analysis. All conditions (temperature, stirring speed, *etc.*) were kept constant throughout all hydrogenation reactions.

(A)



(B)

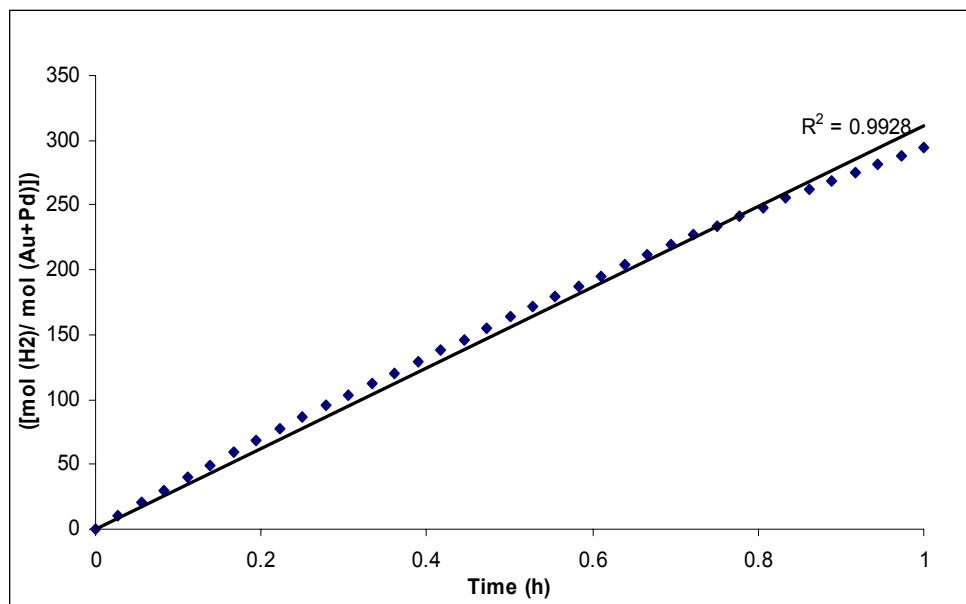


**Figure 2.1.** (A) Pressure decay vs. time in Hydrogenation of Allyl Alcohol by 1:3 Au:Pd NPs in IL and (B) TON vs. time in Hydrogenation of Allyl Alcohol by 1:3 Au:Pd NPs in IL.



### 2.3.4 Characterization

UV-Vis spectra were obtained using a Varian Cary 50 Bio UV-Vis spectrophotometer with a scan range of 300-900 nm with an optical path length of 1.0 cm. The  $^1\text{H}$ -NMR spectra were obtained using a Bruker 500 MHz Advance NMR spectrometer.  $^1\text{H}$  NMR chemical shifts were referenced to the residual protons of the deuterated solvent. TEM micrographs were obtained with a Philips 410 microscope operating at 100 keV. To prepare samples for TEM, a drop of solution containing the nanoparticles was placed on a holey-carbon coated Cu TEM grid (200 mesh). The reaction products were identified by GC-MS (GC EI+ Magnet VG 70SE) using pure standards for comparison.

### 2.4 Results and Discussion

The possible effects of impurities in imidazolium ILs upon the stabilization of metal nanoparticles in ILs have been noted by several groups.<sup>8,19</sup> Thus we worked to optimize the conditions for the synthesis of 1-butyl-3-methylimidazolium ([BMIM]) hexafluorophosphate IL in order to minimize possible halide and other impurities, as well as maximize the transparency of the IL in the visible regions such that nanoparticle formation and transfers could be followed by UV-Vis spectroscopy. It was found that several recrystallizations of the 1-butyl-3-methylimidazolium chloride precursor were necessary to yield colourless IL (with minimal absorption above 290 nm).<sup>25</sup> This was followed by copious washing steps during the ion exchange of  $\text{Cl}^-$  with  $\text{HPF}_6^-$ , until the resulting washings were neutral and showed no precipitate by  $\text{AgNO}_3$  tests (chloride content,  $< 1.8 \text{ mg L}^{-1}$ ).<sup>26</sup> The final [BMIM] $\text{PF}_6$  IL was dried over vacuum at  $70^\circ\text{C}$  for at

least 8 hours before use. The water content was measured by Karl-Fischer titration, and was found to be 211 ppm.

Initially, we attempted to synthesize Au and Pd nanoparticles directly in the [BMIM] IL with no additional external stabilizers added. An attempted synthesis of Au nanoparticles by reducing  $\text{HAuCl}_4$  directly in the [BMIM] $\text{PF}_6$  IL by  $\text{NaBH}_4$  led to Au colloids which were unstable in the IL and began to aggregate over a period of several hours.<sup>27</sup> In addition, attempts to synthesize stable Pd nanoparticles in the [BMIM] $\text{PF}_6$  IL by reducing  $\text{K}_2\text{PdCl}_4$  with  $\text{H}_2$  (1 atm) at  $80^\circ\text{C}$  for 10 mins led to similar observations.<sup>13,16</sup> Halide and/or water contents in the IL may play a large role in the stability of the resulting nanoparticles,<sup>8,19</sup> and we believe that the aggregation of Au and Pd nanoparticles is due to the extra caution taken to purify the [BMIM] $\text{PF}_6$  before nanoparticle synthesis. Upon addition of additional stabilizers such as PVP, stable Au and Pd nanoparticles could be synthesized directly in the IL, however, it was found to be difficult to control the polydispersity of the resulting particles. However, we found that PVP-stabilized Au, Pd, and bimetallic nanoparticles synthesized in methanol could be phase transferred to the [BMIM] IL,<sup>21</sup> which allowed much greater control over the final size and monodispersity of the resulting particles.

Figure 2.2 shows the UV-Vis spectra of PVP-stabilized Au nanoparticles in methanol and after transfer to the [BMIM] IL. Both spectra are quite similar in appearance, with a very small shift of the Au plasmon band shift from 525 nm to 530 nm in the absorbance of the IL layer after phase transfer.<sup>28</sup> This observation suggests that

there was little or no significant change in the size of nanoparticles before and after transfer to the IL, which was confirmed by subsequent TEM studies, shown below.

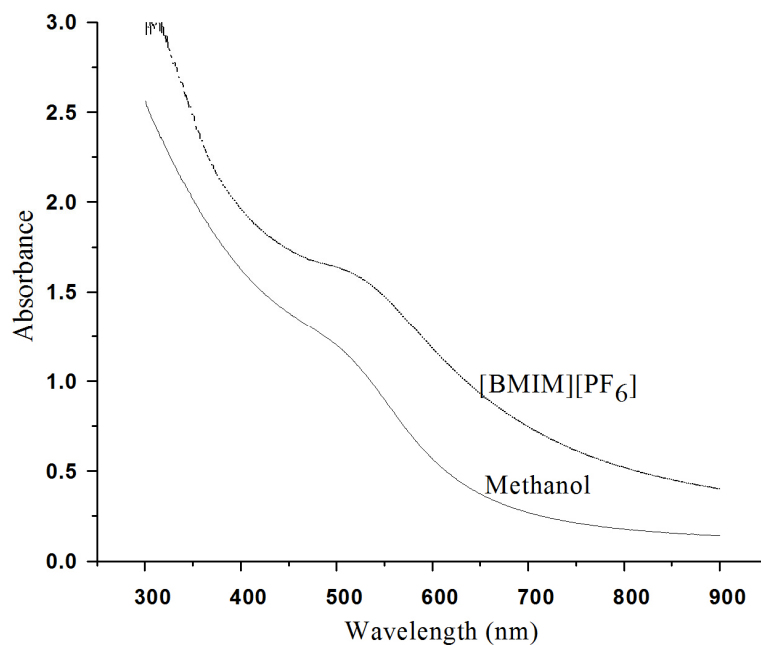


**Figure 2.2.** UV-Vis absorption spectra of PVP-stabilized Au nanoparticles in methanol and after transfer to [BMIM]PF<sub>6</sub> IL.

The UV-Vis spectra of the bimetallic PdAu series of nanoparticles after exchange to the IL phase is shown in Figure 2.3. UV-Vis spectra of the Pd-Au nanoparticles show an exponentially increasing absorbance toward higher energy; this is a consequence of interband transitions of the newly formed bimetallic Au-Pd nanoparticles.<sup>29,30</sup> The absence of Au plasmon bands in the spectra indicates that only bimetallic nanoparticles are formed, and that there is no separate formation of pure Au nanoparticles, nor any desegregation of metals upon exchange to the IL solvent.

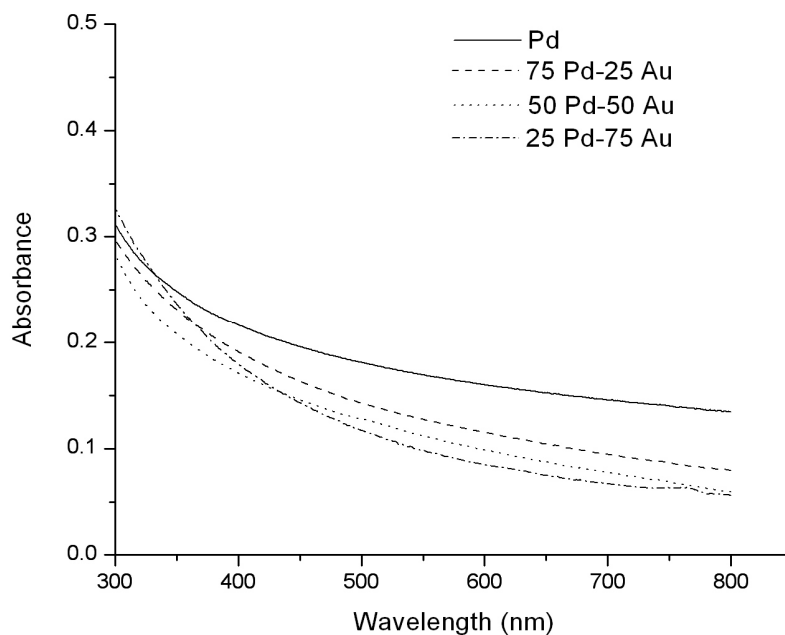


**Figure 2.3.** UV-Vis absorption spectra of PVP-stabilized Pd-Au nanoparticles after phase transfer to [BMIM]PF<sub>6</sub> IL.

Figure 2.4 shows TEM images of Au nanoparticles before and after transfer to the IL phase; the average particle size of the Au nanoparticles in the methanol phase was found to be  $2.6 \pm 0.6$  nm, while the average particle size in IL phase was  $2.9 \pm 0.9$  nm. It should be noted that the nanoparticles in the IL phase appear aggregated as the [BMIM]PF<sub>6</sub> is not volatile, and thus the IL solvent is still present under TEM conditions. We are uncertain as to the reasons behind the discrepancy in particle sizes, though it is likely due to the reduced contrast between nanoparticles and IL in the phase-transferred sample. Similarly, bimetallic PdAu nanoparticles could be transferred to the IL with little change in particle size.

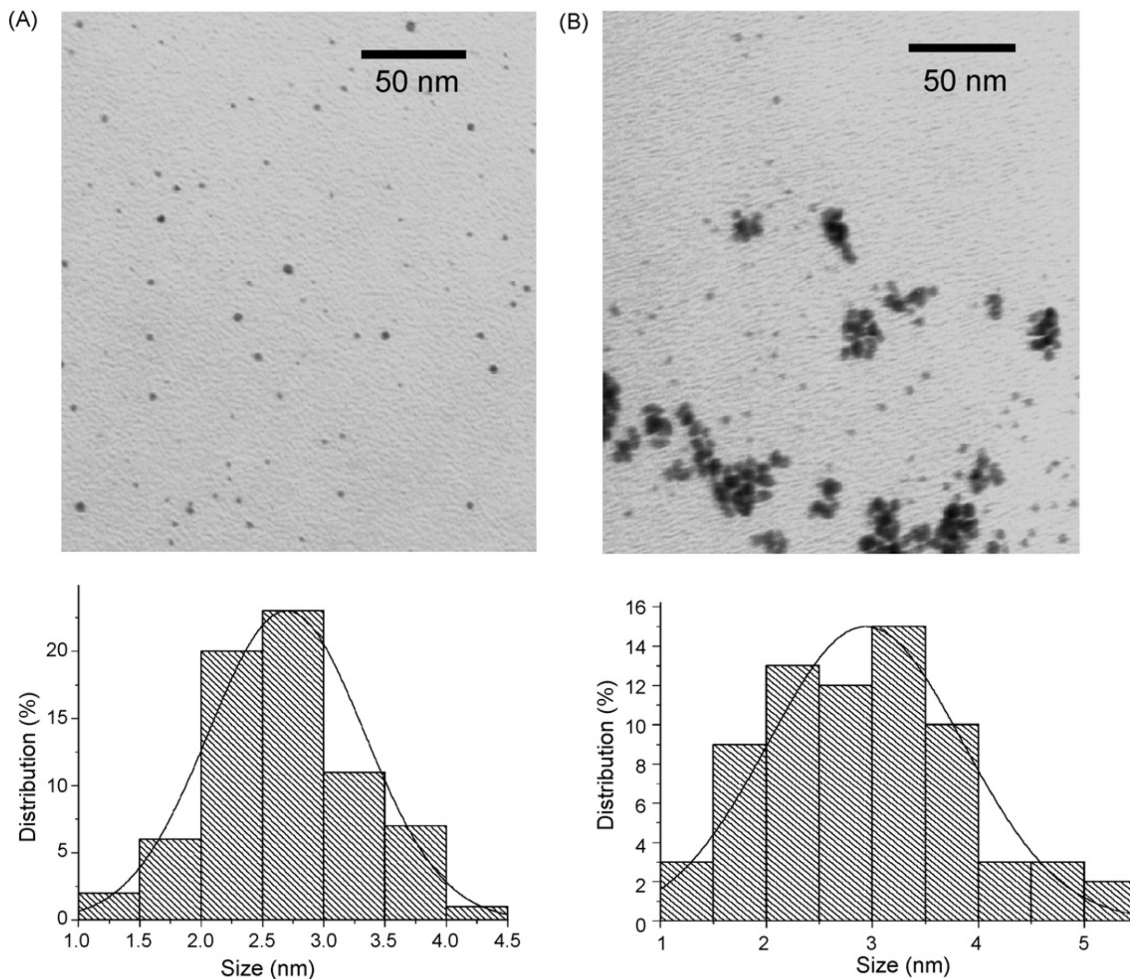


**Figure 2.4.** TEM micrographs and histograms of PVP-stabilized Au nanoparticles (A) as-synthesized in methanol and (B) after phase transfer to [BMIM]PF<sub>6</sub> IL.

TEM images of PVP-stabilized bimetallic Pd-Au before and after transfer to the IL phase are shown in Figure 2.5. The average particle size of the as-synthesized Pd-Au nanoparticles in MeOH was  $2.6 \pm 0.8$  nm, which increased to  $3.2 \pm 0.6$  nm after transfer to the IL phase. The results indicate that the Pd-Au nanoparticles predominantly retain their average size and monodispersity after transfer to the IL phase. The resulting

nanoparticles were stable in the [BMIM]PF<sub>6</sub> IL and no significant changes in the UV-Vis spectra or precipitation was observed over a period of several months. Thus, this method is an effective way of solubilizing pre-synthesized metal nanoparticles in [BMIM]PF<sub>6</sub> IL.

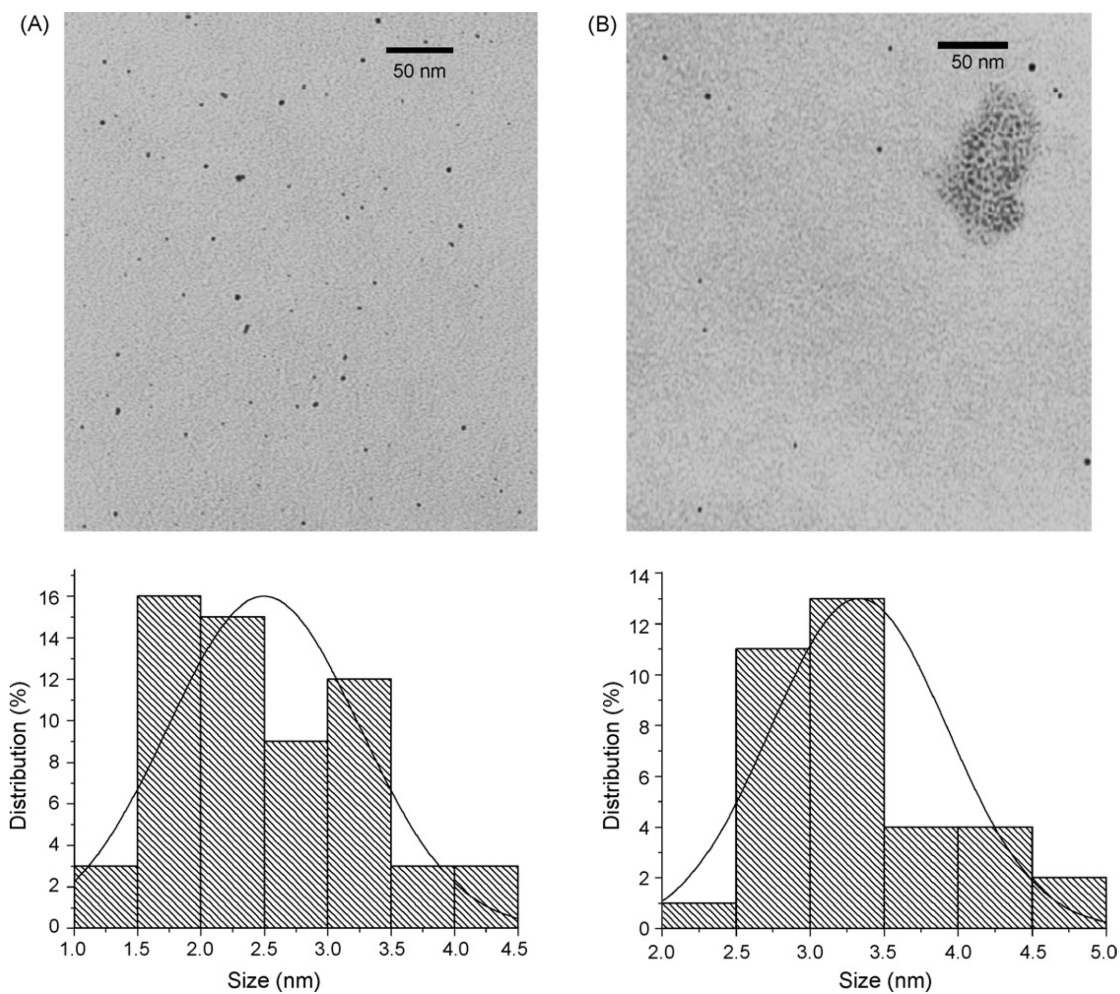


**Figure 2.5.** TEM micrographs and histograms of PVP-stabilized Pd-Au bimetallic nanoparticles (1:3 Au:Pd) (a) as-synthesized in methanol and (b) after phase transfer to [BMIM]PF<sub>6</sub> IL.

The bimetallic series of PVP-stabilized Pd-Au nanoparticles in [BMIM]PF<sub>6</sub> were examined as catalysts for the hydrogenation of allyl alcohol, 1,3-cyclooctadiene, trans-cinnamaldehyde, and 3-hexyn-1-ol. Turnover frequencies (TOFs) for these catalysts were measured by H<sub>2</sub> consumption via differential pressure measurements and substrate/product ratios determined by NMR spectroscopy (see experimental); TOFs from NMR spectra and differential pressure measurements were found to be within 2 % of each other. Several studies have shown that H<sub>2</sub> has moderate to low solubility in [BMIM] IL,<sup>31,32</sup> thus hydrogenation reactions in ILs are often mass-transfer limited. Indeed, we found that the catalyst concentrations used here (1.1 mM) give slightly mass-transfer limited conditions with respect to H<sub>2</sub>, but were selected in order to optimize both catalyst stability and overall conversion of substrates. Figure 2.6 shows the hydrogenation activities for the PdAu nanoparticle series for the hydrogenation of allyl alcohol; bimetallic nanoparticles which were rich in Pd (3:1 Pd:Au ratio) showed the highest TOFs for the hydrogenation of allyl alcohol, while pure Au nanoparticles showed no activity for this reaction. Such electronic enhancement effects in bimetallic catalysts have been previously documented in Pd-Au bimetallic catalysts, in which electronegative Au atoms withdraw electron density from Pd atoms, thereby enhancing the interaction of Pd atoms with the substrate.<sup>9,33-35</sup>

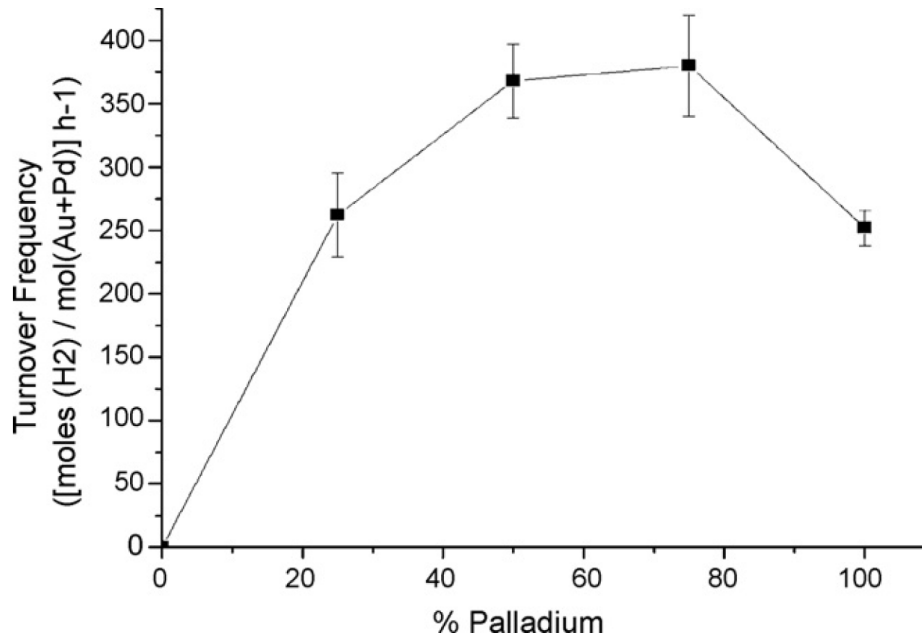


**Figure 2.6.** TOFs for the hydrogenation of allyl alcohol as a function of the mole % Pd in PVP-stabilized PdAu nanoparticles in [BMIM]PF<sub>6</sub>. Conditions, [Pd+Au] = 1.1 mM, Substrate:Catalyst ratio = 670:1, Temperature = 40 °C.

It should be noted that the reaction is zeroth order (Figure 2.1B) because of the presence of large excesses of both H<sub>2</sub> and substrate as the reaction started; at longer times the substrate concentration drops and a significant deviation from 0<sup>th</sup> order is seen. Similar synergistic effects were seen for the hydrogenation of 1, 3-cyclooctadiene, trans-cinnamaldehyde, and 3-hexyn-1-ol with the Pd-Au bimetallic nanoparticles, as shown in Figure 2.7. Pure Au nanoparticles showed no activity in all the hydrogenation reactions and hence are not included in the series of catalysts. Among the catalysts, 3:1 Pd:Au nanoparticles had the highest catalytic activity for all the substrates tested; the



lowest activities amongst the substrates were seen for the hydrogenation of trans-cinnamaldehyde.

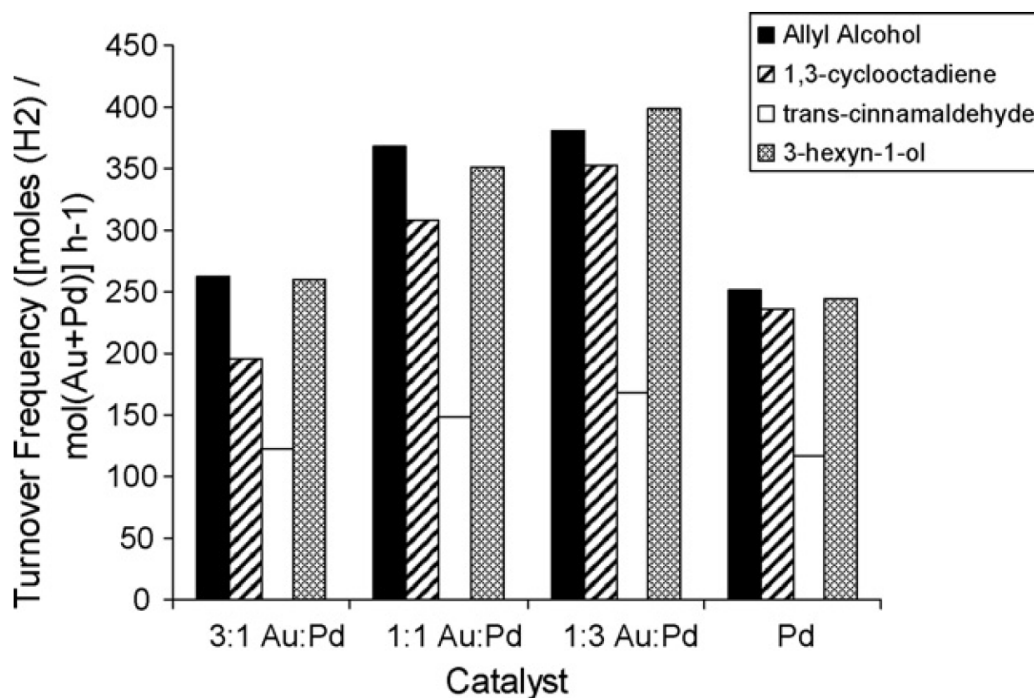


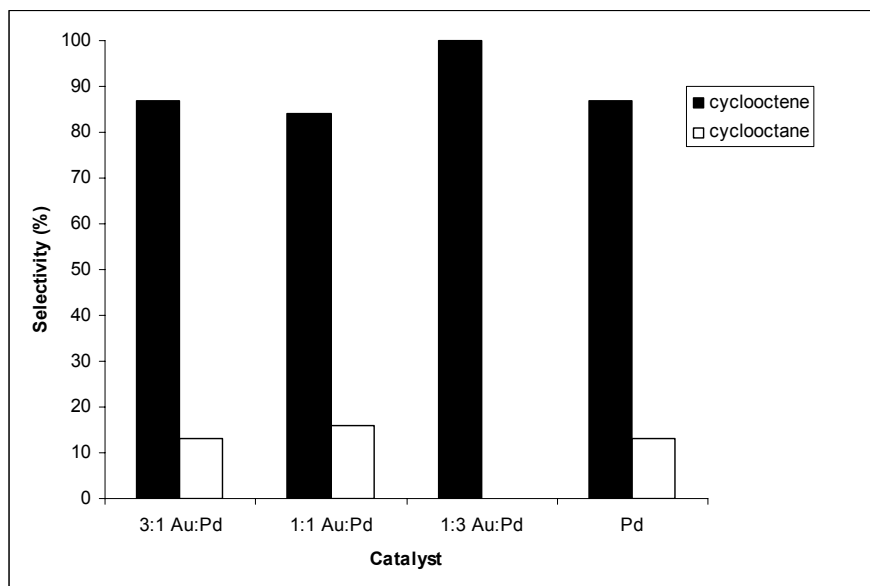
**Figure 2.7.** TOFs for the hydrogenation of allyl alcohol, 1,3-cyclooctadiene, trans-cinnamaldehyde, and 3-hexyn-1-ol by PVP-stabilized Pd-Au bimetallic nanoparticle series in [BMIM]PF<sub>6</sub>. Conditions, [Pd+Au] = 1.1 mM, Substrate:Catalyst ratio = 670:1, Temperature = 40 °C (allyl alcohol, 3-hexyn-1-ol, trans-cinnamaldehyde), and 35 °C (1,3-cyclooctadiene), 1.046 atm H<sub>2</sub> pressure.

The selectivity towards the partial hydrogenation of 1, 3-cyclooctadiene to cyclooctene (as opposed to the complete hydrogenation to cyclooctane) was also found to be highest for the 3:1 Pd:Au nanoparticles, as shown in Figure 2.8A. Figure 2.8B shows the variation of the selectivity in hydrogenation of cinnamaldehyde with different

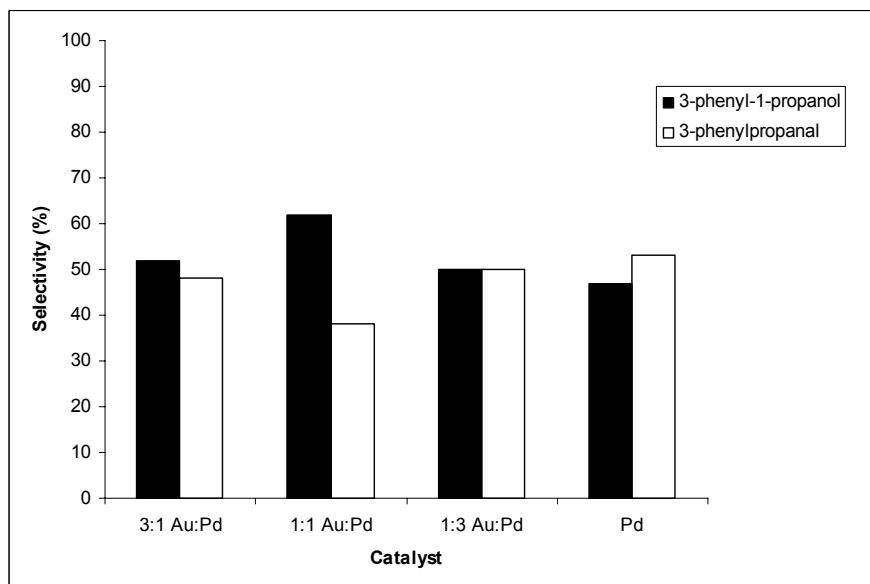
catalysts. 3-phenylpropanal and 3-phenyl-1-propanol were found to be predominant products with almost equal selectivity (*ca.* 50 %) across the bimetallic series. It should be noted that the deep hydrogenation product, cinnamyl alcohol, was not seen for any of the hydrogenation reactions. This is similar to findings by Lashdaf *et al.*, who observed that silica supported ruthenium catalysts showed good selectivity in trans-cinnamaldehyde hydrogenations producing only 3-phenylpropanal and 3-phenyl-1-propanol as reaction products.<sup>36</sup>

In the hydrogenation of 3-hexyn-1-ol, hexenols and hexanol were formed only as the reaction products (Figure 2.8C). Over the initial period of time (1 h), the kinetically favorable hydrogenation product, cis-3-hexen-1-ol, was observed as the major product, while over longer periods of time (> 2 h), the thermodynamically favorable product, trans-3-hexen-1-ol, along with the isomerization product 4-hexen-1-ol, were observed. It is important to note that the 3:1 Pd:Au catalyst exhibited the highest catalytic activity (Figure 2.7) and highest selectivity (94 %, Figure 2.8C) to cis-3-hexen-1-ol among the series of catalysts (> 90 %). This is in agreement with the work of Parvulescu *et al.*, who showed that bimetallic Pd-Au catalysts supported on silica exhibited higher catalytic activity and nearly complete cis-selectivity.<sup>37</sup>

(A)



(B)



(C)

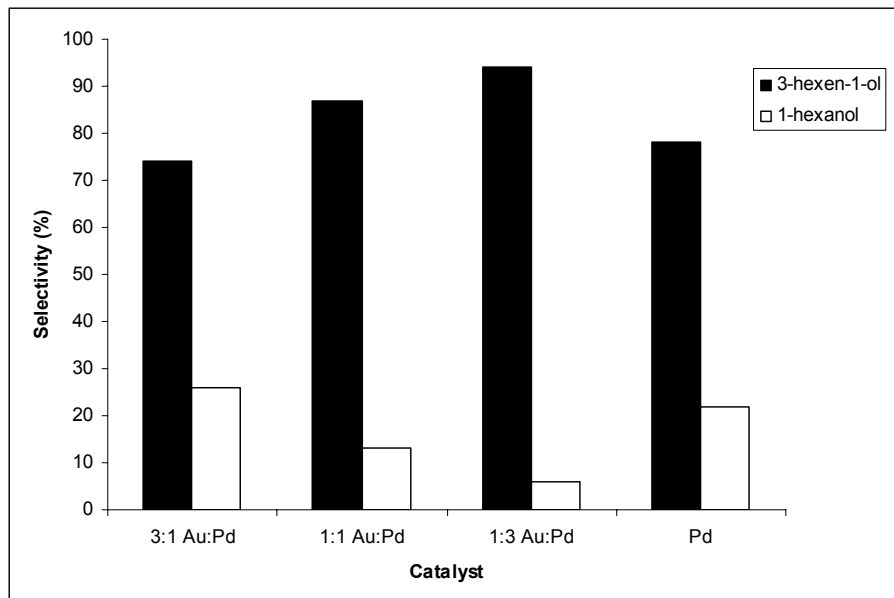


**Figure 2.8.** Variation in selectivity of hydrogenation reactions after 1 hour as a function of the mole % Pd loading for the hydrogenation of (A) 1, 3-cyclooctadiene, (B) trans-cinnamaldehyde, and (C) 3-hexyn-1-ol.

The above results show that PVP-stabilized bimetallic nanoparticles in [BMIM]PF<sub>6</sub> can be used for a wide range of hydrogenation reactions. It should be noted the activities of the catalysts in the IL-phase are not particularly higher than those in other “green” solvents, such as water. Direct comparisons of the TOF of methanol synthesized PVP-stabilized Pd nanoparticles that were transferred to [BMIM]PF<sub>6</sub> and water for hydrogenation of allyl alcohol (all conditions kept constant), indicated that the TOF of the PVP-stabilized Pd nanoparticles in water is comparable to that of the particles in the [BMIM]PF<sub>6</sub> IL (TOF was 284 h<sup>-1</sup> in water vs. 266 h<sup>-1</sup> in IL). However, the negligible volatility and high thermal stability of [BMIM]PF<sub>6</sub> IL may allow catalytic reactions in

conditions not accessible by conventional solvents.<sup>12-19</sup> In addition, it is important to note that the nanoparticle/IL catalysts can be easily separated from substrate/product mixtures and reused by removing all volatile substrates and products. We found 1:3 Au:Pd nanoparticle/IL catalysts which had been retrieved in this method showed very little loss in activity for the hydrogenation of allyl alcohol (< 4% after 2 cycles), confirming their reusability/recyclability as catalysts. Similar results were also seen for other substrates.

## **2.5 Conclusions**

In summary, we have been able to solubilize PVP-stabilized Pd, Au, and bimetallic Pd-Au nanoparticles in imidazolium-based IL by a simple phase transfer method with no significant change in particle size. For the first time, the catalytic behavior of IL phase bimetallic nanoparticles was explored. Bimetallic Pd-Au nanoparticles in the IL were shown to have good activities for the hydrogenation of a range of substrates (allyl alcohol, 1,3-cyclooctadiene, trans-cinnamaldehyde, and 3-hexyn-1-ol), with the highest catalytic activities seen for bimetallic nanoparticles with high Pd loadings. Unreacted substrates and products were easily removed from the IL phase under reduced pressure and the catalyst solution could be reused with very little change in catalytic activity.

## **Acknowledgments**

We are grateful to NSERC for financial support and Sarah Caldwell at the Western College of Veterinary Medicine, University of Saskatchewan for assistance with TEM measurements.

## 2.6 References

- (1) Bell, A. T. *Science* **2003**, *299*, 1688-1691.
- (2) Lewis, L. N. *Chem. Rev.* **1993**, *93*, 2693-2730.
- (3) Bonnemann, H.; Brijoux, W.; Brinkmann, R.; Dinjus, E.; Joussem, T.; Korall, B. *Angew. Chem., Int. Ed.* **1991**, *30*, 1312-1314.
- (4) Botha, S. S.; Brijoux, W.; Brinkmann, R.; Feyer, M.; Hofstadt, H. W.; Kelashvili, G.; Kinge, S.; Matoussevitch, N.; Nagabhushana, K. S.; Wen, F. *Appl. Organomet. Chem.* **2004**, *18*, 566-572.
- (5) Roucoux, A.; Schulz, J.; Patin, H. *Chem. Rev.* **2002**, *102*, 3757-3778.
- (6) Widegren, J. A.; Finke, R. G. *J. Mol. Catal. A: Chem.* **2003**, *191*, 187-207.
- (7) Astruc, D.; Lu, F.; Aranzaes, J. R. *Angew. Chem. Int. Ed.* **2005**, *44*, 7852-7872.
- (8) Ott, L. S.; Finke, R. G. *Coord. Chem. Rev.* **2007**, *251*, 1075-1100.
- (9) Toshima, N.; Yonezawa, T. *New J. Chem.* **1998**, *22*, 1179-1201.
- (10) Sinfelt, J. H. *Bimetallic Catalysts: Discoveries, Concepts and Applications*; Wiley: New York, **1983**.
- (11) Migowski, P.; Dupont, J. *Chem. Eur. J.* **2007**, *13*, 32-39.
- (12) Dupont, J.; de Souza, R. F.; Suarez, P. A. Z. *Chem. Rev.* **2002**, *102*, 3667-3691.
- (13) Dupont, J.; Fonseca, G. S.; Umpierre, A. P.; Fichtner, P. F. P.; Teixeira, S. R. *J. Am. Chem. Soc.* **2002**, *124*, 4228-4229.
- (14) Fonseca, G. S.; Umpierre, A. P.; Fichtner, P. F. P.; Teixeira, S. R.; Dupont, J. *Chem. Eur. J.* **2003**, *9*, 3263-3269.
- (15) Huang, J.; Jiang, T.; Han, B. X.; Gao, H. X.; Chang, Y. H.; Zhao, G. Y.; Wu, W. *Z. Chem. Commun.* **2003**, 1654-1655.
- (16) Scheeren, C. W.; Machado, G.; Dupont, J.; Fichtner, P. F. P.; Teixeira, S. R. *Inorg. Chem.* **2003**, *42*, 4738-4742.
- (17) Wasserscheid, P.; Keim, W. *Angew. Chem. Int. Ed.* **2000**, *39*, 3773-3789.
- (18) Zhao, D. B.; Wu, M.; Kou, Y.; Min, E. *Catal. Today* **2002**, *74*, 157-189.

- (19) Pârvolescu, V. I.; Hardacre, C. *Chem. Rev.* **2007**, *107*, 2615-2665.
- (20) Antonietti, M.; Kuang, D. B.; Smarsly, B.; Yong, Z. *Angew. Chem., Int. Ed.* **2004**, *43*, 4988-4992.
- (21) Mu, X. D.; Evans, D. G.; Kou, Y. A. *Catal. Lett.* **2004**, *97*, 151-154.
- (22) Huddleston, J. G.; Visser, A. E.; Reichert, W. M.; Willauer, H. D.; Broker, G. A.; Rogers, R. D. *Green Chem.* **2001**, *3*, 156-164.
- (23) Bryant, W. M. D.; Mitchell, J.; Smith, D. M.; Ashby, E. C. *J. Am. Chem. Soc.* **1941**, *63*, 2924-2927.
- (24) Wilson, O. M.; Knecht, M. R.; Garcia-Martinez, J. C.; Crooks, R. M. *J. Am. Chem. Soc.* **2006**, *128*, 4510-4511.
- (25) Billard, I.; Moutiers, G.; Labet, A.; El Azzi, A.; Gaillard, C.; Mariet, C.; Lutzenkirchen, K. *Inorg. Chem.* **2003**, *42*, 1726-1733.
- (26) Gallo, V.; Mastroilli, P.; Nobile, C. F.; Romanazzi, G.; Suranna, G. P. *J. Chem. Soc., Dalton Trans.* **2002**, 4339-4342.
- (27) Zhao, D. B.; Fei, Z. F.; Ang, W. H.; Dyson, P. J. *Small* **2006**, *2*, 879-883.
- (28) Wei, G. T.; Yang, Z. S.; Lee, C. Y.; Yang, H. Y.; Wang, C. R. C. *J. Am. Chem. Soc.* **2004**, *126*, 5036-5037.
- (29) Creighton, J. A.; Eadon, D. G. *J. Chem. Soc. Faraday Trans.* **1991**, *87*, 3881-3891.
- (30) Scott, R. W. J.; Wilson, O. M.; Oh, S.-K.; Kenik, E. A.; Crooks, R. M. *J. Am. Chem. Soc.* **2004**, *126*, 15583-15591.
- (31) Anthony, J. L.; Maginn, E. J.; Brennecke, J. F. *J. Phys. Chem. B* **2002**, *106*, 7315-7320.
- (32) Dyson, P. J.; Laurency, G.; Ohlin, C. A.; Vallance, J.; Welton, T. *Chem. Commun.* **2003**, 2418-2419.
- (33) Scott, R. W. J.; Wilson, O. M.; Crooks, R. M. *J. Phys. Chem. B* **2005**, *109*, 692-704.
- (34) Toshima, N.; Harada, M.; Yamazaki, Y.; Asakura, K. *J. Phys. Chem.* **1992**, *96*, 9927-9933.

- (35) Mizukoshi, Y.; Fujimoto, T.; Nagata, Y.; Oshima, R.; Maeda, Y. *J. Phys. Chem. B* **2000**, *104*, 6028-6032.
- (36) Lashdaf, M.; Krause, A. O. I.; Lindblad, M.; Tiitta, A.; Venalainen, T. *Appl. Catal., A* **2003**, *241*, 65-75.
- (37) Parvulescu, V. I.; Parvulescu, V.; Eudruschat, U.; Filoti, G.; Wagner, F. E.; Kubel, C.; Richards, R. *Chem. Eur. J.* **2006**, *12*, 2343-2357.



## CHAPTER 3

### 3. 1-Methylimidazole Stabilization of Gold Nanoparticles in Imidazolium Ionic Liquids

This work has been published in *Chemical Communications*, and has been adapted to improve readability by incorporating material in the supporting information of the paper directly into the thesis. A previously undocumented mode-of-stabilization of nanoparticles in imidazolium ionic liquids has been shown involving 1-methylimidazole, a common impurity from the synthesis of imidazolium-based ILs. The presence of 1.0 mM level of 1-methylimidazole has a significant effect on the stability of Au nanoparticles in [BMIM]PF<sub>6</sub> IL. In the absence of 1-methylimidazole, the nanoparticles aggregated and precipitated out in few days. In addition, such methylimidazole additives have substantial effects on the stability and retention of catalytic activity of bimetallic PdAu nanoparticles in IL. Finally, the same studies were carried out in a different anion-specific imidazolium IL, [BMIM]OTf, in order to demonstrate the generality of this mode-of-stabilization. The same observations were found in [BMIM]OTf IL as observed in [BMIM]PF<sub>6</sub> IL.

---

This work has been published in *Chem. Commun.* **2009**, 812-814. M. Klemmer did the 1-methylimidazole detection limit studies under my supervision. All the other experimental work in this paper has been done by me along with the manuscript writing and editing. The final manuscript was submitted after thorough revisions by my supervisor Dr. Robert W. J. Scott.

# 1-Methylimidazole Stabilization of Gold Nanoparticles in Imidazolium Ionic Liquids

Priyabrat Dash, Robert W. J. Scott\*

Department of Chemistry, University of Saskatchewan, 110 Science Place,  
Saskatoon, Saskatchewan, Canada

## 3.1 Abstract

Low levels of 1-methylimidazole additives have been found to have dramatic effects on the resulting stability of gold and bimetallic nanoparticles in ionic liquids .

## 3.2 Introduction

The field of quasi-homogeneous catalysis involves the use of nanoparticle catalysts which are typically solubilized in a liquid medium.<sup>1,2</sup> One of the great challenges in this area is to find routes towards the stabilization of nanoparticles while preventing passivation of the catalytic nanoparticle surface. There has been a great deal of interest in imidazolium-based room temperature ionic liquids (ILs) as the reaction media for quasi homogenous catalysts, as a number of groups have reported that nanoparticles can be solubilized in ILs in the absence of additional stabilizer(s).<sup>3-</sup><sup>13</sup> Several groups have indicated that nanoparticle stabilization in ILs may be due to weak anion or cation interactions with the nanoparticle surfaces,<sup>2,6,7,13</sup> or alternatively, that the presence of impurities such as water and halides may play a significant role on nanoparticle stability in IL solvents.<sup>14,15</sup> One particularly puzzling system is the synthesis of pure Au nanoparticles in IL solvents, as a number of groups

have shown that such nanoparticles are prone to aggregation in IL solvents in the absence of additional stabilizers<sup>13,16,17</sup> or task-specific ILs,<sup>18,19</sup> while others have successfully synthesized unstabilized gold and bimetallic gold alloy nanoparticles in ILs.<sup>10-12</sup> Herein, we show that very low levels of another common impurity often present in imidazolium ionic liquids, 1-methylimidazole, can have dramatic effects on the stability of gold nanoparticles synthesized directly in 1,3-butylmethylimidazolium hexafluorophosphate ([BMIM]PF<sub>6</sub>) IL. In addition, we show that such methylimidazole additives can have very substantial effects on the stability and retention of catalytic activity of bimetallic nanoparticles in IL solvents.

### 3.3 Experimental

#### 3.3.1 Materials

1-Methylimidazole (99 %) and 1-chlorobutane (99.5 %) were purchased from Alfa and were distilled over KOH and P<sub>2</sub>O<sub>5</sub>, respectively, before use. Hexafluorophosphoric acid (*ca.* 65 % solution. in water), poly(vinylpyrrolidone) (M.W. 40,000), hydrogen tetrachloroaurate hydrate (99.9%), potassium tetrachloropalladate (99.99%), allyl alcohol (99%) were purchased from Alfa and were used without further purification. Sodium borohydride powder (98%) was obtained from Aldrich and was used as obtained. Deuterated solvents were purchased from Cambridge Isotope Laboratories. 18 MΩ·cm Milli-Q water (Millipore, Bedford, MA) was used throughout.

### 3.3.2 Catalyst Preparation

#### 3.3.2.1 Synthesis and purification of BMI ILs

Synthesis of the 1-butyl-3-methylimidazolium ([BMIM]) hexafluorophosphate IL was carried out according to procedure described in Chapter 2. 1-butyl-3-methylimidazolium ([BMIM]) triflate (OTf) IL was made in a similar procedure to [BMIM]PF<sub>6</sub> IL, starting with the same purified [BMIM]Cl precursor. Following repeated recrystallizations of [BMIM]Cl, [BMIM]OTf IL were synthesized by ion exchange with triflic acid, followed by copious washes with deionized water.

#### 3.3.2.2 Experimental method for colorimetric titration & NMR detection limit studies

Attempts were made to measure the amount of unreacted 1-methylimidazole in the “pure” [BMIM]PF<sub>6</sub> based on the complexation of 1-methylimidazole with a copper (II) salt in methanol which forms a [Cu(mim)<sub>4</sub>]<sup>2+</sup> complex.<sup>20</sup> The concentration of 1-methylimidazole was varied between 0.1 – 1.0 mM in methanol while the Cu(II) concentration was kept constant at 1.0 mM. A calibration curve was formed from the plot of 1-methylimidazole concentration vs.  $\lambda_{\max}$  of the absorption band in UV-Vis spectra (see Figure 3.1). In a typical procedure to find out the amount of 1-methylimidazole in [BMIM]PF<sub>6</sub> IL, 30  $\mu$ L of 0.10 M methanolic Cu(II) solution was added to 3.0 ml of [BMIM]PF<sub>6</sub> IL/MeOH solution and the absorption spectra was recorded. The concentration of 1-methylimidazole in the solution (0.4 mM) was determined using the calibration curve derived from the standard solutions.

In addition, the NMR detection limits for 1-methylimidazole were investigated using  $^1\text{H}$  NMR spectra which were recorded on a Bruker 500 MHz Advance spectrometer. NMR detection limits for 1-methylimidazole using proton signals in the 6.95 – 7.10 ppm region were determined via careful spiking experiments in which scan rate, receiver gain signal, digital resolution, signal and noise areas, shimming, and wobble were kept constant. It was determined that the NMR detection limit for 1-methylimidazole in the presence of the  $[\text{BMIM}]\text{PF}_6$  was below 1.0 mM; no signal was seen for “pure”  $[\text{BMIM}]\text{PF}_6$  solutions.

### **3.3.2.3 Synthesis of Au and PdAu nanoparticles in $[\text{BMIM}]\text{PF}_6$ IL**

Au nanoparticles were synthesized in  $[\text{BMIM}]\text{PF}_6$  IL with 1-methylimidazole additives according to the following procedure. First, 8.0 ml of a 1.0 mM solution of 1-methylimidazole in  $[\text{BMIM}]\text{PF}_6$  IL was prepared. This solution was stirred for 15 min, followed by the addition of 1.0 ml of a 10 mM  $[\text{BMIM}]\text{PF}_6$  IL solution of  $\text{HAuCl}_4$ . The mixture was stirred for 15 min, followed by the addition of 1.0 ml of a 0.10 M  $\text{NaBH}_4$  solution in  $[\text{BMIM}]\text{PF}_6$  IL prepared 12 h before use. The total solution volume was 10.0 ml. The immediate formation of a deep red solution occurred upon addition of  $\text{NaBH}_4$  to the solution, indicating the formation of Au nanoparticles. Bimetallic 3:1 PdAu nanoparticles were prepared in the  $[\text{BMIM}]\text{PF}_6$  IL using the same procedure above, keeping the total metal salt concentration (Au + Pd) constant and using  $\text{K}_2\text{PdCl}_4$  as the Pd salt. The same procedure was followed for the synthesis of gold and bimetallic nanoparticles in pure  $[\text{BMIM}]\text{PF}_6$  IL except that no 1-methylimidazole was added in the initial step.

Finally, in order to make PdAu nanoparticles in the [BMIM]PF<sub>6</sub> IL of similar size in the presence and absence of the 1-methylimidazole additive, several modifications were made to the above synthesis. First, 3:1 PdAu nanoparticles were synthesized in the pure [BMIM]PF<sub>6</sub> IL in the absence of any additives, and a 0.10 M NaBH<sub>4</sub> solution in [BMIM]PF<sub>6</sub> IL was used immediately after preparation and added rapidly to the K<sub>2</sub>PdCl<sub>4</sub>/HAuCl<sub>4</sub> solution in the IL. After 15 minutes of stirring, the above solution was split into two parts and 1.0 mM methylimidazole was added to one part. TEM images show particles synthesized by this route have nearly identical particle sizes.

The same synthetic method described above was used to synthesize gold and bimetallic PdAu nanoparticles in [BMIM]OTf IL.

### **3.3.3 Hydrogenation of allyl alcohol using PdAu nanoparticles in ILs**

Hydrogenation reactions were carried out in a three-necked round-bottom flask at 40°C. A H<sub>2</sub> gas source was connected to one end of the flask while the other end with the differential pressure gauge (Model 407910, Extech Instruments Corp. with a resolution of 0.001 atm and accuracy of ± 2 % at 23 ± 5 °C) and the central opening was closed with a rubber septum. Initially, 10 ml of the nanoparticle catalyst solution in the IL was placed in the flask, followed by purging the system with H<sub>2</sub> for 10 min. The H<sub>2</sub> source was closed after purging, followed by stirring for another 10 min to ensure equilibrium between the gas and solution phases and to confirm that there were no leaks in the system (no consumption of H<sub>2</sub> in the absence of substrate). Next, 0.5 ml of the allyl alcohol substrate (substrate: catalyst ratio: ~ 737:1) was added under vigorous stirring conditions (at 1080 rpm), followed by measurement of the H<sub>2</sub> uptake via differential pressure

measurements every 10 seconds.<sup>21</sup> This, in turn, allowed calculating the turnover number (TON, mol of H<sub>2</sub>/ mol metal) of the catalyst system. The turnover frequency (TOF, (mol of H<sub>2</sub>/mol metal)h<sup>-1</sup>) was then determined from the slope of linear plots of TON versus time. All conditions (temperature, stirring speed, *etc.*) were kept constant throughout all hydrogenation reactions.

### 3.3.4 Characterization of Au and PdAu nanoparticles in [BMIM]PF<sub>6</sub>

UV–Vis spectra were obtained using a Varian Cary 50 Bio UV–Vis spectrophotometer with a scan range of 300–900 nm with an optical path length of 1.0 cm. TEM micrographs were obtained with a Philips 410 microscope operating at 100 keV. To prepare samples for TEM, a drop of solution containing the nanoparticles was placed on a holey-carbon coated Cu TEM grid (200 mesh). Due to contamination/charging effects resulting from the IL, it was not possible to examine individual PdAu nanoparticles by single-particle energy-dispersive spectroscopy (EDS). However, single-particle EDS studies of PdAu nanoparticles synthesized by similar routes (*i.e.* K<sub>2</sub>PdCl<sub>4</sub>/HAuCl<sub>4</sub> reduction with NaBH<sub>4</sub>) in other solvent systems have shown that individual particles are indeed bimetallic with metal ratios which correlate strongly with the synthetic ratios of the metal salts used.<sup>22</sup>

## 3.4 Results and Discussion

High-purity [BMIM]PF<sub>6</sub> IL was synthesized following previously documented protocols, with several small modifications.<sup>23</sup> In particular, [BMIM]Cl precursor salts were synthesized from distilled 1-methylimidazole and a slight excess of butylchloride,

followed by an average of four recrystallizations from acetone. This is particularly important as low levels methylimidazole impurities (often below NMR detection limits) can often exist in [BMIM]Cl preparations, and are very difficult to remove by vacuum due to the relatively high boiling point of the methylimidazole and its high affinity for the imidazolium chloride IL.<sup>20</sup> Following repeated recrystallizations, [BMIM]PF<sub>6</sub> IL were synthesized by ion exchange with HPF<sub>6</sub>, followed by copious washes with deionized water. 1-methylimidazole levels in the final [BMIM]PF<sub>6</sub> IL were found to be below 0.5 mM via careful NMR detection limit studies and colorimetric titrations with Cu<sup>2+</sup> salts (Figure 3.1),<sup>20</sup> while the water level was found to be 27 ppm by Karl-Fischer titrations.<sup>24</sup>

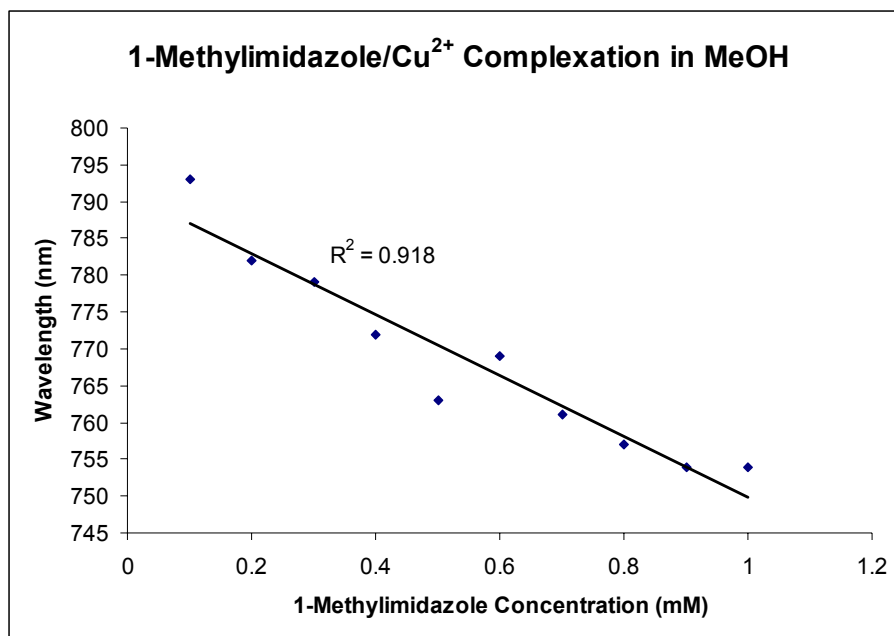


**Figure 3.1.** Calibration curve obtained from Cu(II) complexation studies of the position of the absorption maxima ( $\lambda_{\max}$ ) as a function of 1-methylimidazole concentration.



Gold nanoparticles were directly synthesized in the pure [BMIM]PF<sub>6</sub> IL via addition of HAuCl<sub>4</sub> (10 mM), followed by reduction with a ten times excess of NaBH<sub>4</sub>. Alternatively, Au nanoparticles were synthesized in [BMIM]PF<sub>6</sub> IL to which known levels of 1-methylimidazole had been added. The presence of 1-methylimidazole at levels of 1.0 mM was found to have significant effects on the stability of the final Au nanoparticles. Figure 3.2 shows UV-Vis spectra over time of Au nanoparticles synthesized in the pure IL and in the IL with 1.0 mM 1-methylimidazole added. In the absence of 1-methylimidazole, the UV-Vis spectra of Au nanoparticles in the pure [BMIM]PF<sub>6</sub> IL show a shift towards higher wavelengths over several days, while those synthesized in the presence of 1.0 mM 1-methylimidazole show no significant change in their UV-Vis spectra over similar time periods. Such UV-Vis shifts are often indicative of particle aggregation in solution,<sup>16,25</sup> and indeed, Au nanoparticle precipitates could be seen suspended in the pure [BMIM]PF<sub>6</sub> IL after 7 days.

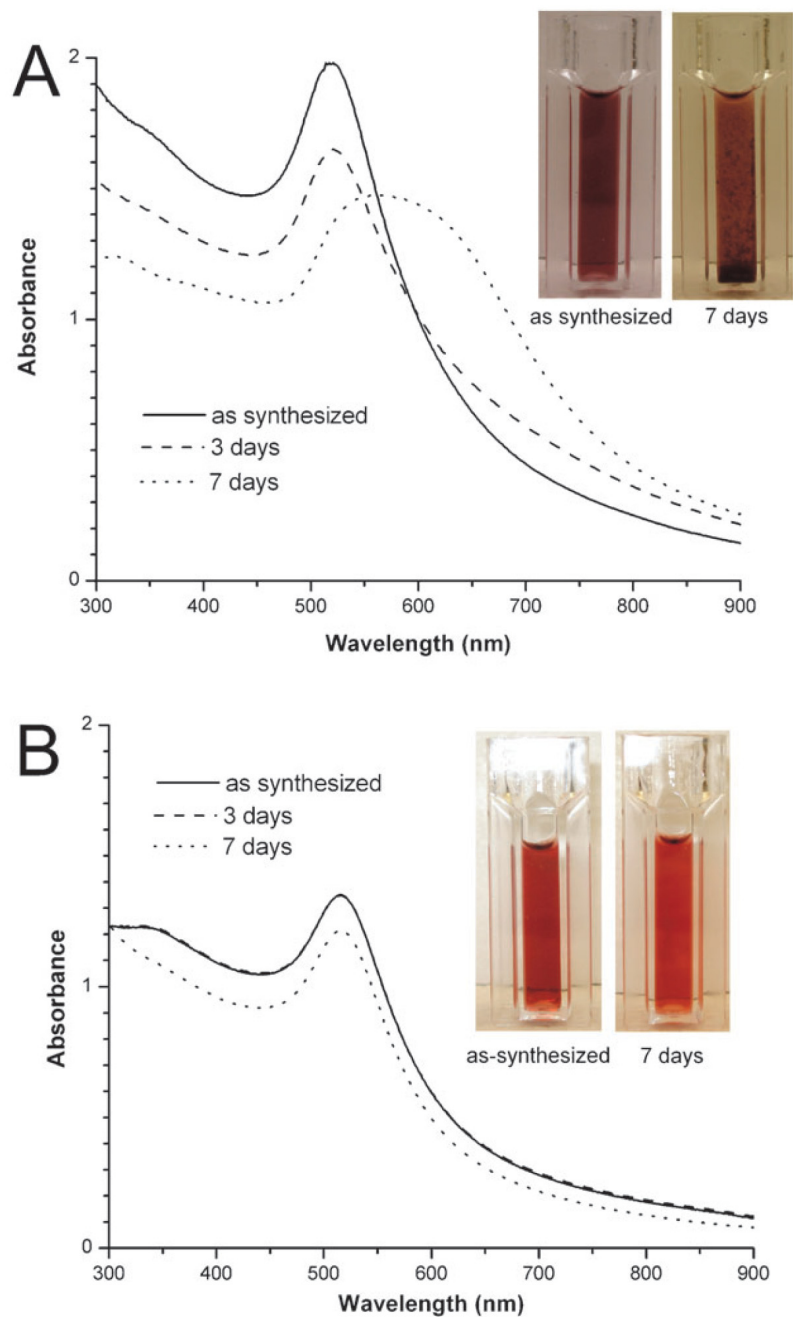


**Figure 3.2.** UV-Vis absorption spectra of Au nanoparticles (A) as-synthesized in pure [BMIM]PF<sub>6</sub> and (B) in [BMIM]PF<sub>6</sub> with 1.0 mM 1-methylimidazole added.

The nanoparticle aggregation was confirmed by HRTEM images, as shown in Figure 3.3; aggregation of Au nanoparticles was seen in the pure IL even at short time

periods, while in the presence of 1-methylimidazole, minimal aggregation was seen (it should be noted that TEM evidence alone should not be used as proof of aggregation alone, as artifacts can occur upon casting nanoparticles onto TEM grid surfaces).

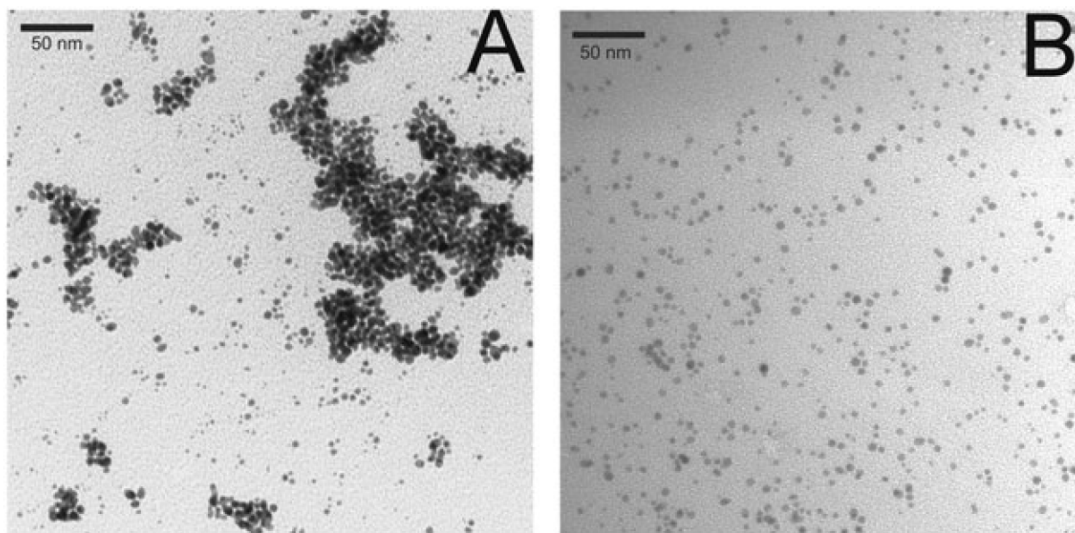


**Figure 3.3.** TEM images of Au nanoparticles as-synthesized in [BMIM]PF<sub>6</sub> IL with (A) no additives added and (B) 1.0 mM 1-methylimidazole added.

Also of note is that the monodispersity of the Au nanoparticles was much higher for particles synthesized in 1.0 mM methylimidazole ( $3.7 \pm 0.8$  nm to that of  $4.4 \pm 1.2$  nm), as the methylimidazole ligand may help slow nanoparticle growth in solution. Others have previously documented the binding of imidazole and 1-methylimidazole for gold and silver surfaces,<sup>26,27</sup> so it is not surprising that methylimidazole can behave as a stabilizer for Au nanoparticles in [BMIM]PF<sub>6</sub> IL even at such low concentrations. This concentration of 1-methylimidazole corresponds to approximately 160 1-methylimidazole ligands per Au nanoparticle. It should be noted that the Au

nanoparticles do not appear to grow in size upon aggregation, so likely anion/cation stabilization prevents the growth of the Au nanoparticles upon aggregation.

Bimetallic PdAu nanoparticles were also directly synthesized in pure [BMIM]PF<sub>6</sub> IL (particle size  $6.0 \pm 2.9$  nm) and in the presence of a 1.0 mM 1-methylimidazole additive in the [BMIM]PF<sub>6</sub> IL (particle size  $3.0 \pm 0.5$  nm) (Figure 3.4).

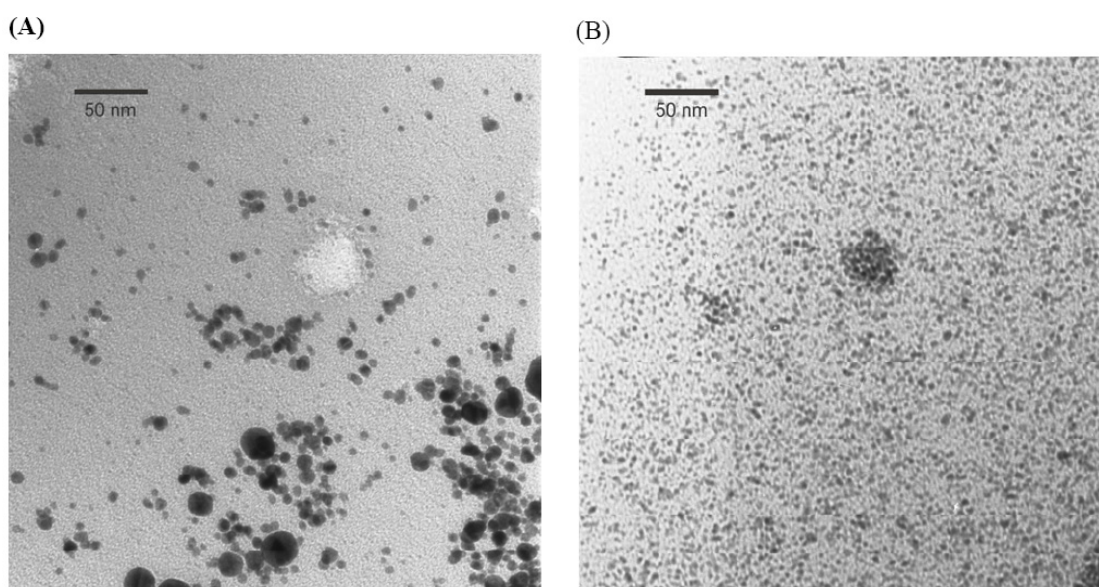


**Figure 3.4.** TEM images of 3:1 Pd:Au bimetallic nanoparticles as-synthesized in [BMIM]PF<sub>6</sub> IL with (A) no additive (particle size  $6.0 \pm 2.9$  nm), and (B) 1.0 mM methylimidazole additive (particle size  $3.0 \pm 0.5$  nm).

The absence of Au plasmon bands in the UV-Vis spectra (Figure 3.5) of both solutions is indicative that there is no separate formation of pure Au nanoparticles in either sample.<sup>28</sup> The stability of the PdAu bimetallic nanoparticles was also investigated, and the bimetallic nanoparticles were found to aggregate in the pure IL,

but are quite stable in the presence of 1.0 mM 1-methylimidazole or other stabilizers.<sup>29</sup>

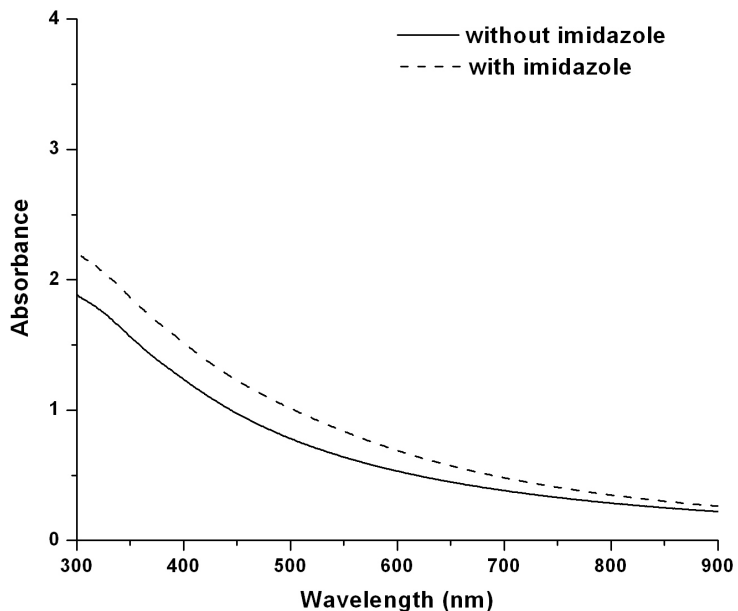


**Figure 3.5.** UV-Vis absorption spectra of 3:1 Pd:Au bimetallic nanoparticles in [BMIM]PF<sub>6</sub> IL.

Figure 3.6 shows the catalytic activity of PdAu nanoparticles synthesized with a 3:1 Pd:Au ratio in [BMIM]PF<sub>6</sub> IL for the hydrogenation of allyl alcohol. The activity of the nanoparticles synthesized directly in the pure IL began to drop dramatically within 10 minutes upon addition of the substrate, while PdAu nanoparticles synthesized in the presence of 1.0 mM 1-methylimidazole show dramatically improved retention of catalytic activity over time. After 1 h of the hydrogenation reaction, precipitation of the PdAu nanoparticles synthesized in the pure IL can be plainly seen. We note that even after aggregation, the bimetallic PdAu nanoparticles synthesized in the pure IL still retain catalytic activity, albeit at a

much lower rate, while particles synthesized in 1.0 mM 1-methylimidazole show a consistent TOFs of  $280 \text{ h}^{-1}$  over many uses. PdAu nanoparticles synthesized in higher 1-methylimidazole concentrations (up to 100 mM in the IL) also showed similar TOFs, indicating that 1-methylimidazole stabilizers do not passify the nanoparticle surface at higher concentrations.

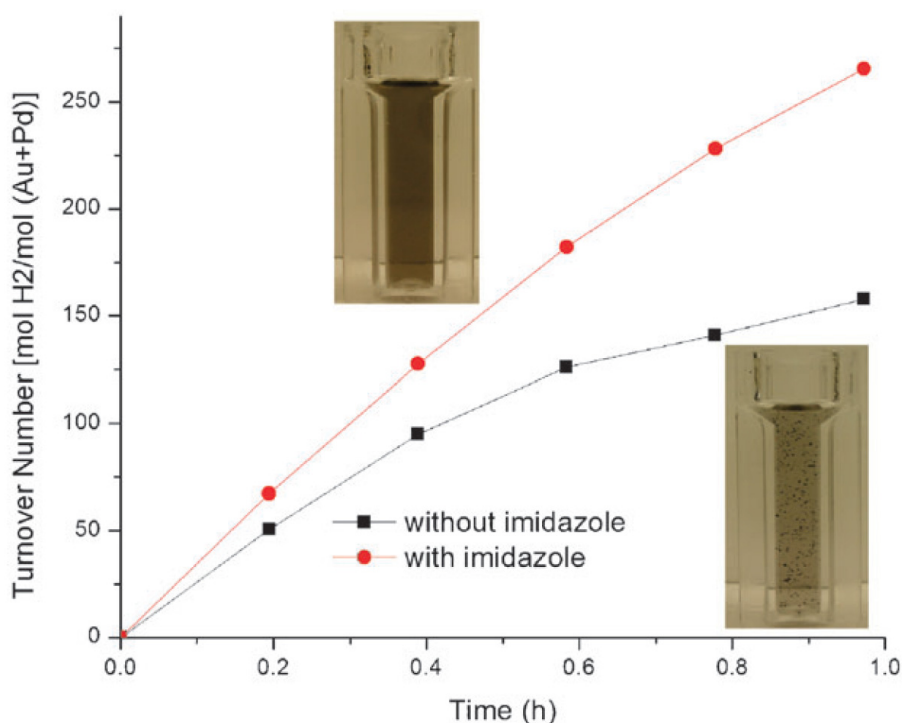


**Figure 3.6.** Catalytic activity of 3:1 Pd:Au bimetallic nanoparticles in [BMIM]PF<sub>6</sub> IL for the hydrogenation of allyl alcohol (insets: the samples after 1h of hydrogenation reaction). [Pd+Au] = 1.0 mM, substrate:catalyst ratio = 737:1, Temperature = 40 °C, stirring rate of 1080 rpm.

In order to clarify that the lower stability/activity of PdAu nanoparticles synthesized in pure [BMIM]PF<sub>6</sub> was not simply due to their larger particle sizes, smaller PdAu nanoparticles were synthesized in pure [BMIM]PF<sub>6</sub> IL, followed by separation of

this solution in two parts and addition of 1.0 mM of 1-methylimidazole to one part (Figure 3.7). TEM measurements of the particle sizes of these two solutions were found to be nearly identical, thus allowing reliable comparisons of their catalytic activity.

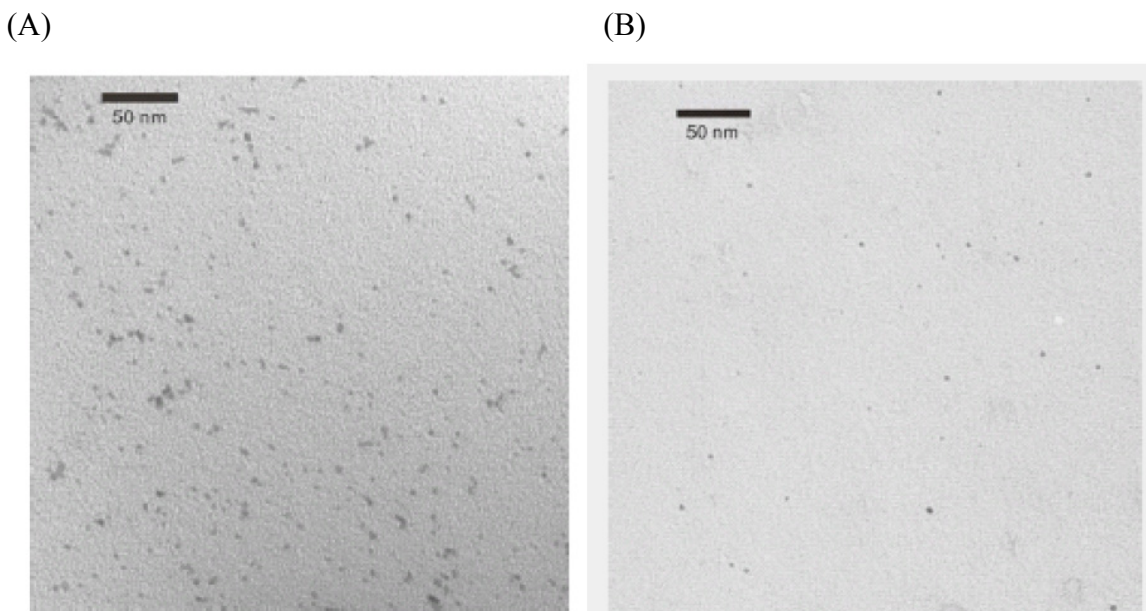


**Figure 3.7.** TEM images of 3:1 Pd:Au bimetallic nanoparticles (A) as-synthesized in [BMIM]PF<sub>6</sub> IL (particle size  $3.4 \pm 0.5$  nm), and (B) as-synthesized in [BMIM]PF<sub>6</sub> IL followed by addition of 1.0 mM methylimidazole (particle size  $3.2 \pm 0.5$  nm). Note for these particles the NaBH<sub>4</sub> solution was made immediately prior to use and added rapidly to the metal salt solution, which resulted in much smaller PdAu particle sizes than previous batches (see Section 3.3.2.3).

These two batches showed similar catalytic behaviour as in Figure 3.6 above (Figure 3.8), with the activity of the PdAu nanoparticles in the absence of the 1-

methylimidazole additive quickly decreasing with time, accompanied by precipitation of the nanoparticles.

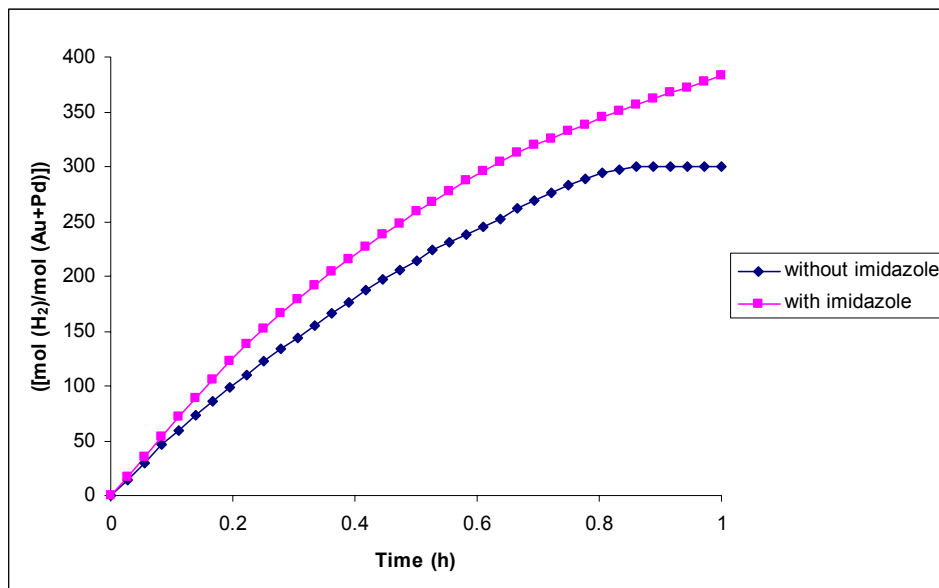


**Figure 3.8.** Catalytic activity of smaller (3.2 – 3.4 nm) 3:1 Pd:Au bimetallic nanoparticles as-synthesized in pure [BMIM]PF<sub>6</sub> IL without additives (blue triangles) and with 1.0 mM methylimidazole added after synthesis (pink squares) for the hydrogenation of allyl alcohol. [Pd+Au] = 1.0 mM, substrate:catalyst ratio = 737:1, Temperature = 40 °C, stirring rate of 1080 rpm.

Finally, PdAu nanoparticles were also synthesized in a [BMIM]OTf IL in order to demonstrate the generality of this mode of stabilization (Figure 3.9); PdAu nanoparticles in pure [BMIM]OTf solutions precipitated within 1 h in the absence of 1-methylimidazole additives during the hydrogenation reaction, whereas in the presence of 1-methylimidazole particles were stable for prolonged periods of time; however higher



concentrations of 1-methylimidazole (*ca.* 10-100 mM) were needed to stabilize the nanoparticles in [BMIM]OTf IL (Figure 3.10).

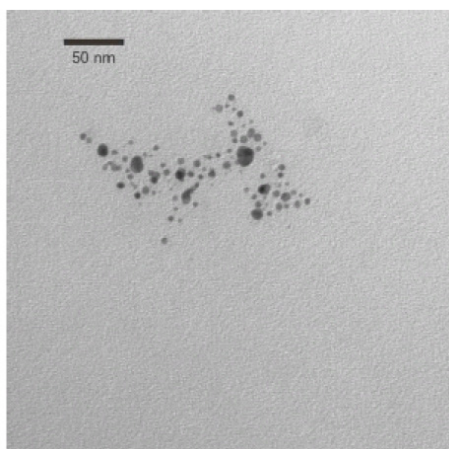


**Figure 3.9.** TEM image of 3:1 Pd:Au bimetallic nanoparticles as-synthesized in [BMIM]OTf IL without additive (particle size  $4.9 \pm 2.0$  nm).

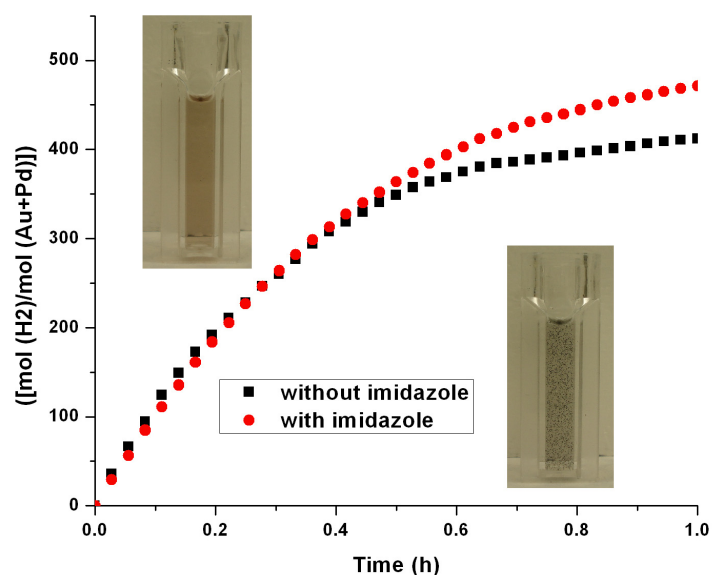


**Figure 3.10.** Catalytic activity of 3:1 Pd:Au bimetallic nanoparticles in [BMIM]OTf IL for the hydrogenation of allyl alcohol (A) no additive, (B) with 100 mM methylimidazole additive (insets: the samples after 1 h hydrogenation reaction). [Pd+Au] = 1.0 mM, substrate:catalyst ratio = 737:1, Temperature =  $40$  °C, stirring rate of 1080 rpm.

### 3.5 Conclusions

In conclusion, we have shown a previously undocumented mode-of-stabilization of nanoparticles in imidazolium ionic liquids involving 1-methylimidazole, a common impurity from the synthesis of imidazolium-based ILs. These results can begin to explain discrepancies in the literature regarding the stability of nanoparticles in ILs, and also show that the use of high-purity ILs for quasi-homogeneous reactions with nanoparticles can actually be quite detrimental; for best results, low levels of imidazole derivatives can enhance the stability and activity of nanoparticles within ILs. We are continuing to investigate the activity of Au and PdAu particles in ILs for other catalytic reactions.

### Acknowledgments

The authors would like to acknowledge financial assistance from the National Sciences and Engineering Research Council of Canada (NSERC), and M. Klemmer for assistance with 1-methylimidazole detection limit studies.

### 3.6 References

1. Roucoux, A.; Schulz, J.; Patin, H. *Chem. Rev.*, **2002**, *102*, 3757-3778.
2. Astruc, D.; Lu, F.; Aranzaes, J. R. *Angew. Chem. Int. Ed.*, **2005**, *44*, 7852-7872.
3. Dupont, J.; Fonseca, G. S.; Umpierre, A. P.; Fichtner, P. F. P.; Teixeira, S. R. *J. Am. Chem. Soc.*, **2002**, *124*, 4228-4229.
4. Fonseca, G. S.; Umpierre, A. P.; Fichtner, P. F. P.; Teixeira, S. R.; Dupont, J. *Chem. Eur. J.*, **2003**, *9*, 3263-3269.

5. Scheeren, C. W.; Machado, G.; Dupont, J.; Fichtner, P. F. P.; Teixeira, S. R. *Inorg. Chem.*, **2003**, *42*, 4738-4742.
6. Migowski, P.; Dupont, J. *Chem. Eur. J.*, **2007**, *13*, 32-39.
7. Antonietti, M.; Kuang, D. B.; Smarsly, B.; Yong, Z. *Angew. Chem., Int. Ed.*, **2004**, *43*, 4988-4992.
8. Redel, E.; Thomann, R.; Janiak, C. *Inorg. Chem.*, **2008**, *47*, 14-16.
9. Redel, E.; Thomann, R.; Janiak, C. *Chem. Commun.*, **2008**, 1789-1791.
10. Kim, K.-S.; Choi, S.; Cha, J.-H.; Yeon, S.-H.; Lee, H. *J. Mater. Chem.*, **2006**, *16*, 1315-1317.
11. Zhu, J. M.; Shen, Y. H.; Xie, A. J.; Qiu, L. G.; Zhang, Q.; Zhang, S. Y. *J. Phys. Chem. C*, **2007**, *111*, 7629-7633.
12. Okazaki, K. I.; Kiyama, T.; Hirahara, K.; Tanaka, N.; Kuwabata, S.; Torimoto, T. *Chem. Commun.*, **2008**, 691-693.
13. Schrekker, H. S.; Gelesky, M. A.; Stracke, M. P.; Schrekker, C. M. L.; Machado, G.; Teixeira, S. R.; Rubim, J. C.; Dupont, J. *J. Colloid Interface Sci.*, **2007**, *316*, 189-195.
14. Ott, L. S.; Finke, R. G. *Coord. Chem. Rev.*, **2007**, *251*, 1075-1100.
15. Pârvulescu, V. I.; Hardacre, C. *Chem. Rev.*, **2007**, *107*, 2615-2665.
16. Wei, G. T.; Yang, Z. S.; Lee, C. Y.; Yang, H. Y.; Wang, C. R. C. *J. Am. Chem. Soc.*, **2004**, *126*, 5036-5037.
17. Wang, Y.; Yang, H. *Chem. Commun.*, **2006**, 2545-2547.
18. Itoh, H.; Naka, K.; Chujo, Y.; *J. Am. Chem. Soc.*, **2004**, *126*, 3026-3027.
19. Wang, Z.; Zhang, Q.; Kuehner, D.; Ivaska, A.; Niu, L. *Green Chem.*, **2008**, *10*, 907-909.
20. Holbrey, J. D.; Seddon, K. R.; Wareing, R. *Green Chem.*, **2001**, *3*, 33-36.
21. Wilson, O. M.; Knecht, M. R.; Garcia-Martinez, J. C.; Crooks, R. M. *J. Am. Chem. Soc.*, **2006**, *128*, 4510-4511.
22. Scott, R.W.J., Wilson, O.M., Oh, S.-K., Kenik, E.A., Crooks, R.M. *J. Am. Chem. Soc.*, **2004**, *126*, 15583-15591.

23. Huddleston, J. G.; Visser, A. E.; Reichert, W. M.; Willauer, H. D.; Broker, G. A.; Rogers, R. D. *Green Chem.*, **2001**, *3*, 156-164.
24. Bryant, W. M. D.; Mitchell, J.; Smith, D. M.; Ashby, E. C. *J. Am. Chem. Soc.*, **1941**, *63*, 2924-2927.
25. Vivek, J. P.; Burgess, I. J. *J. Phys. Chem. C*, **2008**, *112*, 2872-2880.
26. Carter, D. A.; Pemberton, J. E.; Woelfel, K. J. *J. Phys. Chem. B*, **1998**, *102*, 9870-9880.
27. Souza, G. R.; Levin, C. S.; Hajitou, A.; Pasqualini, R.; Arap, W.; Miller, J. H. *Anal. Chem.*, **2006**, *78*, 6232-6237.
28. Creighton, J. A.; Eadon, D. G. *J. Chem. Soc. Faraday Trans.*, **1991**, *87*, 3881-3891.
29. Dash, P.; Dehm, N. A.; Scott, R. W. J. *J. Mol. Catal. A: Chem*, **2008**, *286*, 114-119.

## CHAPTER 4

### **4. Stabilizing Nanoparticle Catalysts in Imidazolium-based Ionic Liquids: A Comparative Study**

This work has been submitted for publication. For the first time a comparative study documenting the relative stability of nanoparticles using stabilizers in ILs and the effective activities and lifetimes of such nanoparticle/IL mixtures has been described. Four stabilization protocols for nanoparticle stabilization in [BMIM]PF<sub>6</sub> IL are documented, and we have shown that nanoparticle stability and thus catalytic activity of nanoparticles is dependent on the overall stability of the nanoparticles towards aggregation. The four different stabilization methods in [BMIM]PF<sub>6</sub> which are used include the synthesis of nanoparticles in pure ILs, and the addition of secondary PVP, 1-methylimidazole, and task-specific [aemim]PF<sub>6</sub> stabilizers. PVP-stabilized nanoparticles were found to be the most stable, catalytically active and had longer lifetimes than catalysts prepared by the other stabilization routes.

---

This manuscript has been submitted for publication to *Journal of Molecular Catalysis A: Chemical*. This paper has been co-authored by S. Miller who did the synthesis of the task-specific IL under my supervision. All the other experimental work in this paper has been done by me along with the manuscript writing and editing. The final manuscript was submitted after thorough revisions by my supervisor Dr. Robert W. J. Scott.

## 4. Stabilizing Nanoparticle Catalysts in Imidazolium-based Ionic Liquids: A Comparative Study

Priyabrat Dash, Sarah M. Miller, Robert W. J. Scott\*

Department of Chemistry, University of Saskatchewan, 110 Science Place,  
Saskatoon, Saskatchewan, Canada

### 4.1 Abstract

Room temperature imidazolium-based ionic liquids such as 1-butyl-3-methylimidazolium hexafluorophosphate ([BMIM]PF<sub>6</sub>) have been used as an effective liquid medium for the synthesis of pure Au and bimetallic PdAu nanoparticles by direct synthesis and phase-transfer methods. The mode-of-stability, long-term stability, and long lifetimes of these ionic-liquid supported nanoparticle catalysts, all of which are important factors in determining the overall “greenness” of such materials, were investigated. Four different stabilizing systems in [BMIM]PF<sub>6</sub> IL were investigated: poly(vinylpyrrolidone) (PVP), 1-methylimidazole, 1-(2'-aminoethyl)-3-methylimidazolium hexafluorophosphate, and pure [BMIM]PF<sub>6</sub> IL with the absence of a secondary stabilizer. The stability of pure Au nanoparticles synthesized by the above four stabilizers was studied using UV-Vis spectroscopy and transmission electron microscopy (TEM). It was found that PVP-stabilized nanoparticles were the most stable to aggregation. The catalytic activity of the resulting PdAu nanoparticles was examined for the hydrogenation of 1,3-cyclooctadiene and 3-buten-1-ol across all of the systems to understand which stabilizer(s) are most optimal for nanoparticle catalyst synthesis and usage; particularly which systems have high catalytic activity and selectivity as well as

long catalyst lifetimes. In agreement with Au nanoparticle stability results, PVP-stabilized PdAu nanoparticles were the most catalytically active due to improved nanoparticle stability, followed by nanoparticles stabilized by 1-methylimidazole, amine-functionalized IL, and the pure [BMIM]PF<sub>6</sub> IL.

## 4.2 Introduction

Due to their unique physiochemical properties such as high polarity, excellent thermal stability and negligible vapor pressures, room temperature ionic liquids (ILs) have provided an opportunity for chemists to studying reactions in an unique reaction medium.<sup>1-3</sup> In the past few years, ILs have also proven to be excellent solvents for the immobilization and stabilization of metal nanoparticles, thus providing an excellent medium for quasi-homogeneous catalysis.<sup>4-19</sup> In particular, 1-butyl-3-methylimidazolium-based ([BMIM]) ILs have emerged as effective media for the stabilization of nanoparticles.<sup>4-7,14,17-22</sup> Though there have been reports of the synthesis of gold and bimetallic nanoparticles in pure [BMIM] ILs without any additional stabilizers,<sup>17-19</sup> a number of groups also reported the aggregation of gold nanoparticles in pure ILs.<sup>16,23,24</sup> To avoid these problems various secondary stabilizers such as poly(vinylpyrrolidone) (PVP),<sup>25-26</sup> task-specific ILs,<sup>27-34</sup> and ionic liquid copolymers<sup>35</sup> have also been used for the synthesis of stable metal nanoparticles in ILs. In addition, our group has recently shown that low levels of 1-methylimidazole additives have dramatic effects on the stability of Au and bimetallic PdAu nanoparticles in imidazolium-based ionic liquids.<sup>36</sup> Thus, while there have been a large number of different routes to synthesize and stabilize nanoparticle catalysts in ILs, to our knowledge there have been no comparative studies

documenting the relative stability of nanoparticles using stabilizers in ILs or the effective relative activities and lifetimes of such nanoparticle/IL mixtures. This work is similar in nature to earlier pioneering work by El-Sayed and co-workers who showed that varying the type of stabilizer and the stabilizer/metal ratios had profound effects on the activity and stability of Pt nanoparticles for Suzuki reactions in aqueous conditions, with the highest activities over short time periods often associated with particles which have the poorest long-term stabilities.<sup>37-39</sup> The activation energy of the reaction increased linearly with increasing concentration of PVP.

Deshmukh *et al.* were the first to show the formation of Pd nanoparticles in 1,3-di-*n*-butylimidazolium tetrafluoroborate ILs during Heck reactions.<sup>13</sup> J. Dupont and coworkers synthesized stable transition metal nanoparticles in pure imidazolium-based ILs without any secondary stabilizer, and the resulting nanoparticle catalysts were found to be active for a range of hydrogenation reactions.<sup>4-7,14,20</sup> Gómez and co-workers synthesized stable Pd nanoparticles stabilized by pure ILs and showed that the resulting nanoparticles had higher catalytic activity for a variety of Suzuki C-C cross-coupling and sequential reactions.<sup>40-42</sup> Several groups have indicated that the stabilization of nanoparticles in ILs may be due to weak anion or cation interactions with nanoparticle surfaces,<sup>7,8,15,16</sup> while others have noted that impurities such as halides and water could also have significant effects on nanoparticle stability.<sup>11,43</sup> Recently, we have shown that millimolar levels of 1-methylimidazole, a common starting material in imidazolium-based IL syntheses, can have dramatic effects on the stability of nanoparticles in ILs, which was a previously undocumented mode of stabilization.<sup>36</sup> In addition, we previously showed that highly-stable Au, Pd and bimetallic PdAu nanoparticles can be synthesized



by a simple phase transfer method of PVP-stabilized nanoparticles from methanol to IL, and that the resulting nanoparticles were catalytically active for a range of hydrogenation reactions.<sup>26</sup>

Other groups have focused on the synthesis of task-specific ILs, which have specific functional groups attached to the imidazolium cations.<sup>30,31,44</sup> Such task-specific ILs have been shown to lead to enhanced nanoparticle stability and thus can be used to enhance the catalytic activity of nanoparticles in ILs.<sup>27-30,32-34,45</sup> For example, Kim *et al.* have documented the synthesis of gold and platinum nanoparticles using thiol-functionalized ILs which bind to the nanoparticle surface and act as stabilizers.<sup>28</sup> Similarly, nitrile-functionalized ionic liquids have been used as stabilizers to prevent agglomeration of Pd nanoparticles for the Stille coupling reaction between iodobenzene and tributylphenyltin, and were found to prevent catalyst deactivation.<sup>33</sup> Recently, Niu and coworkers synthesized stable Au nanoparticles using a functionalized IL, 1-(3-aminopropyl)-3-methylimidazolium bromide, and the resulting nanoparticles showed enhanced electrocatalytic activity and high stability.<sup>32</sup> Intrigued by this work, we chose to use a similar amine-functionalized task-specific IL as a stabilizer/surfactant dissolved in [BMIM]PF<sub>6</sub> for the synthesis of Au and bimetallic PdAu nanoparticles, and compare this stabilizer with other known methods for the stabilization of nanoparticles in ILs.

Given the numerous routes towards the synthesis of “stable” nanoparticles in ILs which exist in the literature, it can be very difficult to generalize as to which method(s) can lead to the optimal formation of stable, catalytically active nanoparticles. Thus, in order to compare a variety of stabilization methodologies, we synthesized pure Au and

bimetallic PdAu nanoparticles in 1-butyl-3-methylimidazolium hexafluorophosphate ([BMIM]PF<sub>6</sub>) IL by four different methods. Nanoparticles were synthesized in [BMIM]PF<sub>6</sub> IL by either direct synthesis or phase-transfer methods. In three different systems, PVP, 1-methylimidazole, and 1-(2'-aminoethyl)-3-methylimidazolium hexafluorophosphate ([aemim]PF<sub>6</sub>) were added as secondary stabilizers while in the fourth system nanoparticles were directly synthesized in [BMIM]PF<sub>6</sub> IL without any additional stabilizer. The long term stability of pure Au nanoparticles in each of these systems was studied by UV-Vis spectroscopy and transmission electron microscopy (TEM). Finally, in order to understand the effect that nanoparticle stability has on catalytic activity and catalyst lifetimes, bimetallic PdAu nanoparticles were synthesized by the four above mentioned methods. Hydrogenation of two substrates, 1,3-cyclooctadiene and 3-buten-1-ol, was carried out to monitor their catalytic activity, and <sup>1</sup>H NMR spectroscopy was used to measure the activity in terms of turnover number (mol product/mol catalyst).

## 4.3 Experimental

### 4.3.1 Materials

1-methylimidazole (99%) and 1-chlorobutane (99.5%) were purchased from Alfa and were distilled over KOH and P<sub>2</sub>O<sub>5</sub>, respectively, before use. Hexafluorophosphoric acid (*ca.* 65% solution. in water), poly(vinylpyrrolidone) (M.W. 40,000), hydrogen tetrachloroaurate hydrate (99.9%), potassium tetrachloropalladate (99.99%), 3-buten-1-ol (98+%), and ethylenediamine (99%), and N-(2-bromoethyl)phthalimide (98+%) were purchased from Alfa and were used without further purification. 1,3-Cyclooctadiene

(95%) and sodium borohydride powder (98%) were obtained from Aldrich and were used as obtained. Deuterated solvents were purchased from Cambridge Isotope Laboratories. 18 M $\Omega$ -cm Milli-Q de-ionized water (Millipore, Bedford, MA) was used throughout.

### 4.3.2 Catalyst Preparation

#### 4.3.2.1 Synthesis and purification of ILs

Synthesis of 1-butyl-3-methylimidazolium hexafluorophosphate ([BMIM]PF<sub>6</sub>) IL was carried out under nitrogen and purified according to previously published procedures.<sup>26</sup> The purity of the [BMIM]PF<sub>6</sub> IL was verified by <sup>1</sup>H NMR and UV-Vis spectroscopy. In the final [BMIM]PF<sub>6</sub> IL, the levels of 1-methylimidazole were below 0.5 mM through both careful NMR detection limit studies and colorimetric titrations with Cu<sup>2+</sup> salts, while the water level was below 30 ppm by Karl-Fischer titration.

Synthesis of the functionalized IL, 1-(2'-aminoethyl)-3-methylimidazolium hexafluorophosphate ([aemim]PF<sub>6</sub>) was carried out according to a previous literature procedure developed by Singer and coworkers, with minor modifications.<sup>46</sup> Briefly, N-(2-bromoethyl)phthalimide (113 mmol) was added to 100 ml freshly distilled toluene in a flask. Under N<sub>2</sub> atmosphere, freshly distilled 1-methylimidazole (125 mmol) was added to the flask, which was then heated at 70<sup>0</sup>C for 72 h with constant stirring. This resulted in a white crystalline product, 1-(2'-phthalamidoethyl)-3-methylimidazolium bromide, which was washed with 25 ml of cold toluene 3-4 times, dried after each washing step under vacuum, then stored in a desiccator under P<sub>2</sub>O<sub>5</sub> for 2-3 days, and obtained in 38% yield. 1-(2'-phthalamidoethyl)-3-methylimidazolium bromide (43 mmol) was dissolved

in 100 ml of de-ionized water. A white precipitate was formed after the addition of HPF<sub>6</sub> (54 mmol) while cooling in an ice bath. The white precipitate, 1-(2'-phthalamidoethyl)-3-methylimidazolium hexafluorophosphate, was dried under vacuum for 6 h and then stored in a desiccator for 2 days, and obtained in 70% yield. Finally, [aemim]PF<sub>6</sub> was synthesized by gradual addition of ethylenediamine (200 mmol) over 15 mins to a mixture of 1-(2'-phthalamidoethyl)-3-methylimidazolium hexafluorophosphate (25 mmol) in 200 ml of 1-butanol. The final solution was heated at 90<sup>0</sup>C for 24 h under refluxing conditions. The reaction mixture was cooled to room temperature and washed with freshly distilled cold 1-butanol (distilled over K<sub>2</sub>CO<sub>3</sub>). The white solid, [aemim]PF<sub>6</sub>, was formed after 1-butanol was removed under vacuum for 8 h, and was then stored in a desiccator overnight. The yield of the final product was 50%. The purity of the product after each step was monitored by <sup>1</sup>H NMR spectroscopy.

#### **4.3.2.2 Synthesis of metallic and bimetallic nanoparticles**

PVP, 1-methylimidazole stabilized, and “unstabilized” Au and bimetallic 3:1 PdAu nanoparticles were synthesized according to previously reported methods.<sup>26,36</sup> For all Au nanoparticle syntheses, the total gold concentration was 1.1 mM. PVP-stabilized nanoparticles were synthesized by a phase-transfer method from methanol to [BMIM]PF<sub>6</sub>. “Unstabilized” nanoparticles were directly synthesized in pure [BMIM]PF<sub>6</sub> using NaBH<sub>4</sub> as a reducing agent, while nanoparticles stabilized by 1-methylimidazole were made similarly except in the presence of 1 mM 1-methylimidazole additives.<sup>36</sup>

Au nanoparticles using [aemim]PF<sub>6</sub> as a stabilizer were synthesized by a phase transfer method. A 10 mM solution of [aemim]PF<sub>6</sub> was dissolved in 10 ml water in a

round bottomed flask. In another flask, 1.0 ml of a 10 mM of  $\text{HAuCl}_4$  in  $[\text{BMIM}]\text{PF}_6$  was added to 8.0 ml of pure  $[\text{BMIM}]\text{PF}_6$ . The mixture was stirred for 15 min, followed by the addition of 1.0 ml of a 0.10 M  $\text{NaBH}_4$  solution in  $[\text{BMIM}]\text{PF}_6$  prepared 12 h before use. The total solution volume was 10.0 ml. The immediate formation of a deep red solution occurred upon addition of  $\text{NaBH}_4$  to the solution, indicating the formation of Au nanoparticles. Then, the aqueous solution of  $[\text{aemim}]\text{PF}_6$  was added with vigorous stirring to the Au nanoparticles in  $[\text{BMIM}]\text{PF}_6$ , followed by the removal of water under vacuum. Bimetallic 3:1 Pd:Au nanoparticles were also made directly in  $[\text{BMIM}]\text{PF}_6$  using  $[\text{aemim}]\text{PF}_6$  as a stabilizer. First, 9.38 ml of a 107 mM solution of  $[\text{aemim}]\text{PF}_6$  in  $[\text{BMIM}]\text{PF}_6$  was prepared. This solution was stirred for 15 min, followed by the addition of 0.165 ml of 10 mM  $\text{K}_2\text{PdCl}_4$  in  $[\text{BMIM}]\text{PF}_6$  and 0.055 ml of 10 mM  $\text{HAuCl}_4$  in  $[\text{BMIM}]\text{PF}_6$ . The mixture was stirred for 15 min, followed by the addition of 0.40 ml of a 0.10 M  $\text{NaBH}_4$  in  $[\text{BMIM}]\text{PF}_6$  prepared 12 hrs before use. The total solution volume was 10.0 ml.

### 4.3.3 Catalytic reactions

Hydrogenation reactions were carried out in a three-necked round-bottom flask at  $40^\circ\text{C}$ . One end of the flask was connected to the  $\text{H}_2$  gas source, the other end was attached to a differential pressure gauge (Model 407910, Extech Instruments Corp.) and the central opening was closed with a rubber septum. First, 10 ml of the catalyst solution was placed in the flask, followed by purging the system with continuous  $\text{H}_2$  flow. Next, the 1,3-cyclooctadiene and/or 3-buten-1-ol substrate was added by syringe under vigorous stirring conditions (at 1080 rpm), followed by measurement of samples by  $^1\text{H}$

NMR spectroscopy. The hydrogen pressure used for all reactions was 1.0 atm, and the substrate:catalyst ratios were 400:1 for the 1,3-cyclooctadiene substrate and 15904:1 for 3-buten-1-ol. The turnover number (TON, mol of product/mol catalyst) and selectivities for product distributions were determined by  $^1\text{H}$  NMR spectroscopy. After 1 hour and 17 h intervals, 1 ml of the solution was placed in a vial and then  $\text{CDCl}_3$  was added. The vial was shaken to transfer the products into the  $\text{CDCl}_3$  phase which was then removed and used for NMR analysis. All conditions (temperature, stirring speed, *etc.*) were kept constant throughout all hydrogenation reactions. For 1,3-cyclooctadiene, the reaction was also followed by measurement of the  $\text{H}_2$  uptake through differential pressure measurements every 10 s. This, in turn, allowed calculating the moles of hydrogen consumed, which by NMR measurements was found to correlate within 3% to the moles of cyclooctene product. This allowed for real-time measurements of the effective turnover number of the catalyst system.

#### 4.3.4 Characterization

UV-Vis spectra were obtained using a Varian Cary 50 Bio UV-Vis spectrophotometer with a scan range of 300-900 nm with an optical path length of 1.0 cm. The  $^1\text{H}$ -NMR spectra were obtained using a Bruker 500 MHz Advance NMR spectrometer.  $^1\text{H}$  NMR chemical shifts were referenced to the residual protons of the deuterated solvent. TEM micrographs were obtained with a Philips 410 microscope operating at 100 kV. To prepare samples for TEM, a drop of a methanol/IL mixture containing the nanoparticles was placed on a holey-carbon coated Cu TEM grid (200

mesh) which had been pre-oxidized by air plasma treatment, followed by evaporation of the methanol.

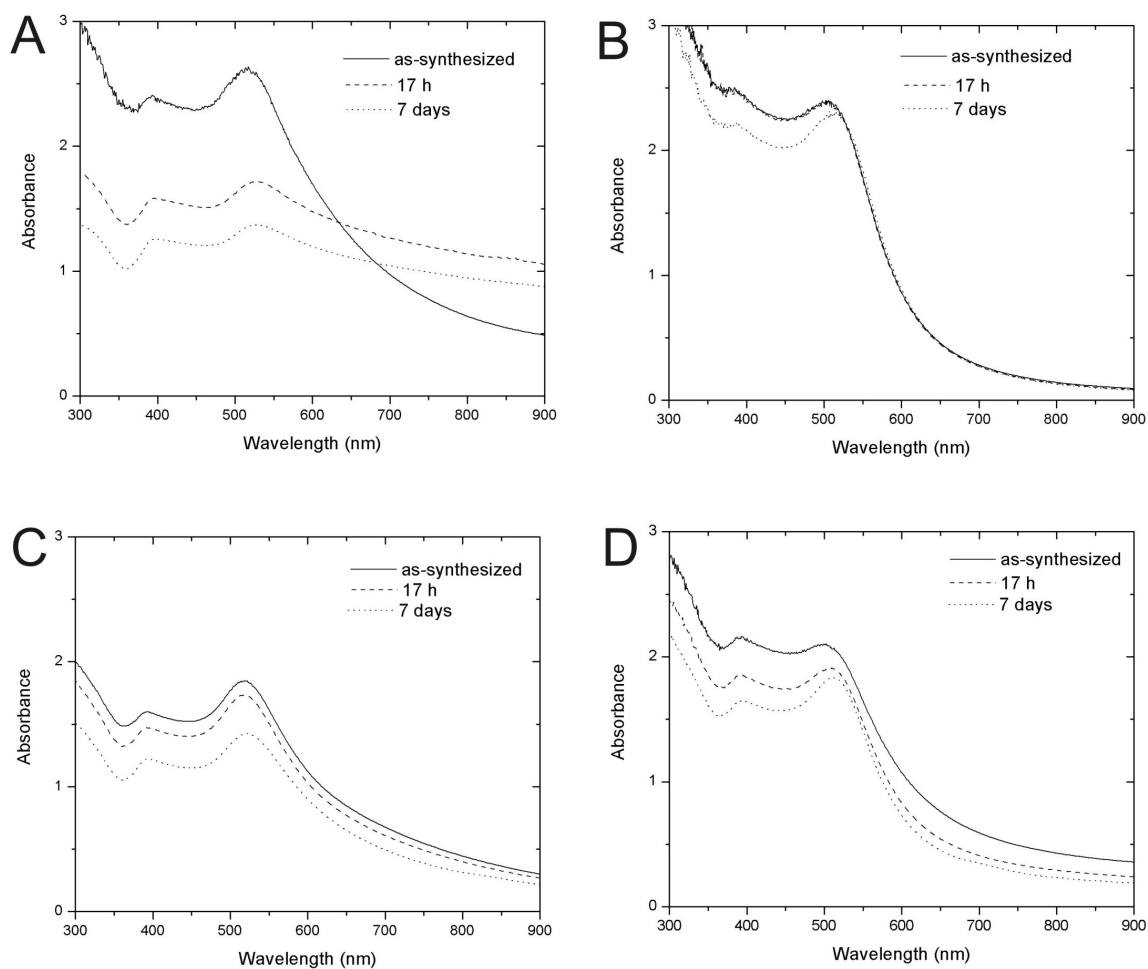
#### 4.4 Results and Discussion

Unraveling the possible modes of stabilization of nanoparticles in ionic liquids is a considerable challenge, particularly given the unique nature of the medium. In order to most effectively probe nanoparticle aggregation in solution, Au nanoparticles were chosen as the first system to investigate. The dipole-dipole interactions between plasmon bands of aggregated gold nanoparticles is manifested as a shift of the plasmon band wavelength, and thus a change in colour of the solution from red to purple, which can be easily monitored by UV-Vis spectroscopy.<sup>47</sup> The initial system studied is the formation of gold nanoparticles in pure [BMIM]PF<sub>6</sub> ionic liquids, *i.e.* “unstabilized” Au nanoparticles. As noted in the introduction, a number of groups, including ours, have shown that Au nanoparticles are prone to aggregation in ionic liquids over a time period ranging from minutes to weeks.<sup>16,23,24,36</sup> It should be noted that extremely clean ILs need to be used in order to compile reproducible results in such systems; in our case, the [BMIM]Cl precursor is recrystallized at least four times from acetone, and Cl<sup>-</sup> impurities from the final [BMIM]PF<sub>6</sub> IL are removed via multiple washes with de-ionized water until no AgCl precipitates form in the washings upon addition of AgNO<sub>3</sub>. The final [BMIM]PF<sub>6</sub> ionic liquid is then dried overnight under vacuum, resulting in water levels below 30 ppm by Karl-Fischer titrations. Finally, detailed NMR detection limit studies have shown that 1-methylimidazole impurities are below 0.5 mM in the clean IL.

Figure 4.1A shows the UV-Vis spectra over time of Au nanoparticles synthesized in pure [BMIM]PF<sub>6</sub>. A decrease in the intensity of the plasmon band at 530 nm along with a increase in the high-wavelength region of the absorption spectra over 17 hours is seen, which is indicative of particle aggregation in solution.<sup>23,48</sup> Indeed the nanoparticles precipitated out from the solution after several weeks. It should be noted that while the particles are prone to aggregation and precipitation, the particles do not grow in size as a consequence of aggregation; TEM images indicate the final precipitates are composed of particles of similar size as the originally-synthesized nanoparticles (see below). We are still unsure as to exactly what is the dominant mode of stabilization of such nanoparticles in pure [BMIM]PF<sub>6</sub> solutions, particularly compared to conventional solvents in which nanoparticle aggregation and precipitation is nearly instantaneous in the absence of external stabilizers. Others have indicated that weak anion and/or cation interactions with the nanoparticles can lead to steric stabilization of the nanoparticles,<sup>7,8,15,16</sup> but it is unlikely that this could lead to conventional double-layer stabilization given the high polarity of the IL medium. Another factor is the possibility of impurities in the IL promoting nanoparticle stabilization; control reactions have indicated that the addition of chloride and/or bromide salts do not enhance nanoparticle stability, but 1-methylimidazole additives do (see below).<sup>36</sup> Thus it is possible that 1-methylimidazole impurities below the NMR detection limit could be contributing to partial nanoparticle stability. Finally, one major factor in the slow aggregation and precipitation of the nanoparticles is the high viscosity of ILs, which are typically two orders of magnitude greater than conventional solvents ([BMIM]PF<sub>6</sub> has a viscosity of *ca.* 450 cP).<sup>3</sup> The high viscosity of [BMIM]PF<sub>6</sub> would result in a dramatically reduced number of nanoparticle-



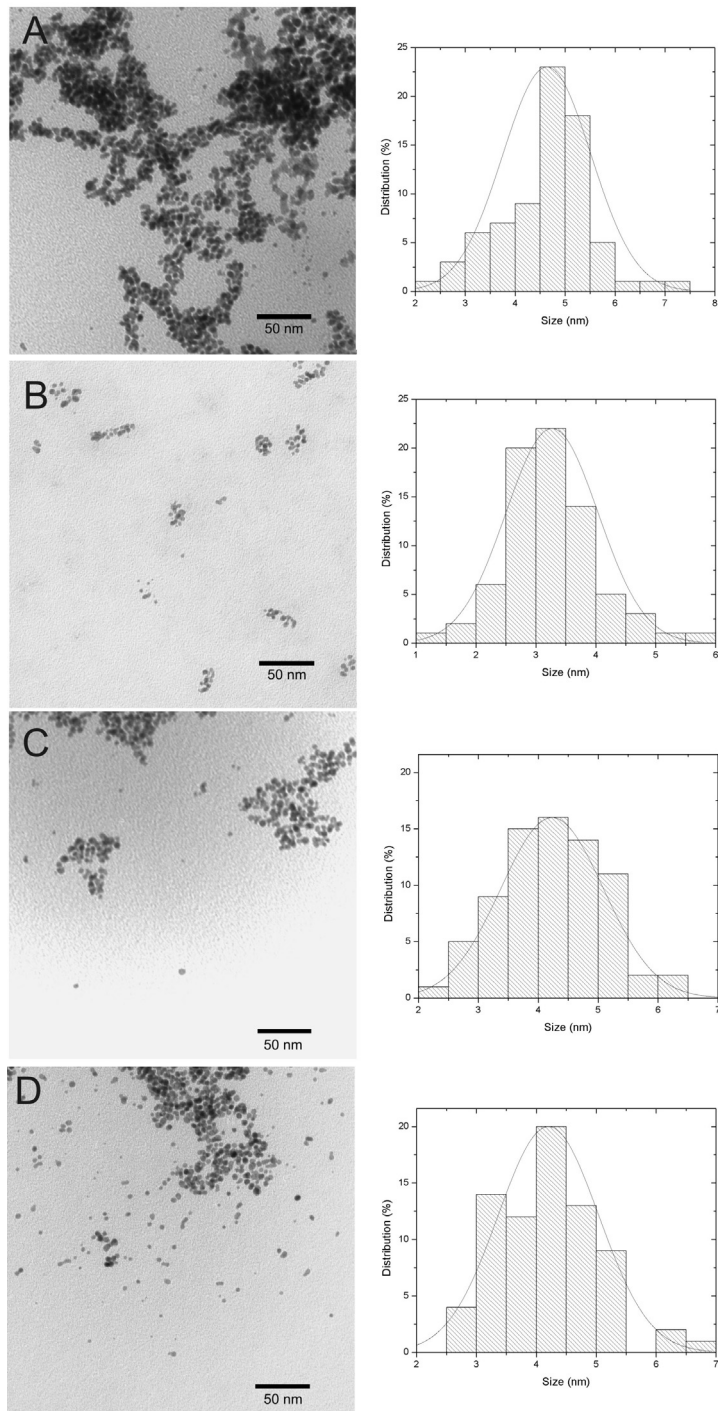
nanoparticle collisions in ILs due to Brownian motion of the particles. However, if stability were simply a consequence of the nanoparticle-nanoparticle collision frequency, then stirring Au nanoparticle/[BMIM]PF<sub>6</sub> suspensions should lead to increased rates of aggregation; however this is not observed experimentally. Instead, stirring of Au nanoparticle/[BMIM]PF<sub>6</sub> suspensions tends to break apart aggregates, suggesting the force(s) driving nanoparticle aggregation are quite weak in [BMIM]PF<sub>6</sub>.



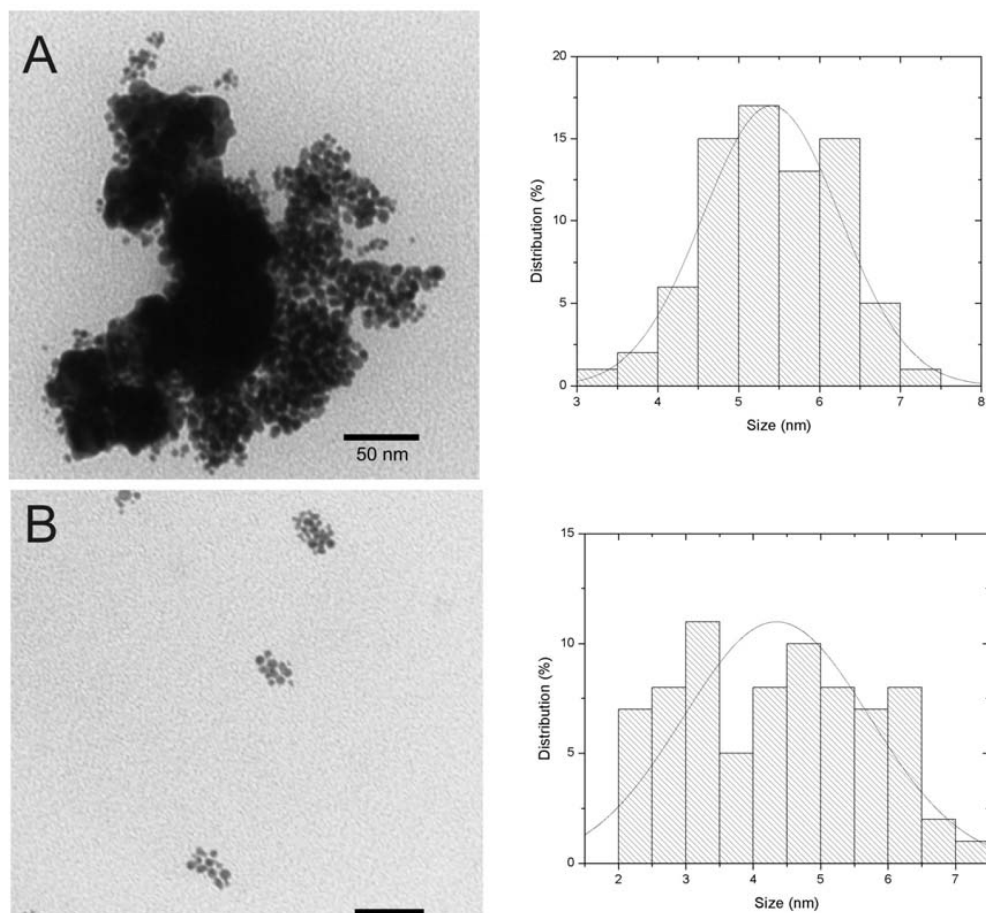
**Figure 4.1.** UV-Vis absorption spectra of Au nanoparticles over time in (a) pure [BMIM]PF<sub>6</sub>, (b) [BMIM]PF<sub>6</sub> with 1.39 mM PVP additive, (c) [BMIM]PF<sub>6</sub> with 1 mM 1-methylimidazole additive, and (d) [BMIM]PF<sub>6</sub> with 10 mM [aemim]PF<sub>6</sub> additive.

Figure 4.1B shows the UV-Vis spectra of Au nanoparticles synthesized in the presence of PVP additives. Note that in the case for PVP stabilized nanoparticles, the particles were first synthesized in MeOH and then transferred over to the [BMIM]PF<sub>6</sub> IL via removal of the methanol under vacuum, due to the difficulty in directly dissolving PVP in the IL. As can be noted in Figure 4.1B, PVP-stabilized Au nanoparticles show no significant aggregation in the UV-Vis spectra observed over a period of 1 week. Figures 4.1C and 4.1D show the representative UV-Vis spectra of 1-methylimidazole and [aemim]PF<sub>6</sub> stabilized nanoparticles. The drop in intensity of the UV-Vis spectra for these systems is due to a fraction of Au nanoparticles adhering to the sides of the glass reaction flask over time, which was not observed for the PVP system; however minimal aggregation was observed compared to the “unstabilized” Au nanoparticles, which have a rising baseline over time (Figure 4.1A). Best results for [aemim]PF<sub>6</sub>-stabilized particles were obtained for particles originally synthesized in pure [BMIM]PF<sub>6</sub> followed by addition of the [aemim]PF<sub>6</sub> stabilizer; attempts to synthesize particles directly in the presence of the stabilizer led to poorly-stabilized particles, likely due to the (surprisingly) low solubility of the [aemim]PF<sub>6</sub> in [BMIM]PF<sub>6</sub>. Also, attempts to synthesize [aemim]PF<sub>6</sub>-stabilized Au nanoparticles in water or alcohol solvents followed by phase transfer to the IL phase were unsuccessful due to the fast precipitation of the particles from the aqueous or alcohol phases. Wang *et al.* previously noted that [aemim]Br stabilized Au nanoparticles were quite stable in water; we believe that the major stabilizer in the latter case is the Br<sup>-</sup> anion,<sup>32</sup> which has been observed previously for both TOAB and CTAB stabilized Au nanoparticles.<sup>49,50</sup>

Of all the four systems, the PVP-stabilized Au nanoparticles in [BMIM]PF<sub>6</sub> are definitely the most stable, with no changes seen via UV-Vis for periods of several months. In order to fully study the nanoparticle stability, TEM images of the nanoparticles as-synthesized and after several weeks were also collected. It should be noted that TEM evidence alone should not be used as a proof of aggregation (or lack thereof) as artifacts can occur upon casting nanoparticles onto TEM grids. Typically for TEM grid preparation, solution phase nanoparticles are cast onto carbon-coated grids followed by solvent evaporation, which is untenable in the presence of pure ILs which have negligible volatility. In order to effectively make TEM samples, IL/nanoparticle mixtures were diluted in methanol and cast onto TEM grids, followed by methanol evaporation, such that the IL solvent is still present under TEM conditions. Figure 4.2 shows the TEM images of Au nanoparticles among the four stabilizing systems. In the absence of any stabilizers, aggregation of Au nanoparticles was seen even at short periods of time, with an average particle size of  $4.8 \pm 0.7$  nm. It should be noted that even after 2 weeks, only a small change in the size of the nanoparticles is seen, with the particles growing to  $5.3 \pm 0.8$  nm (see Figure 4.3A). In the presence of PVP, the average Au nanoparticle size is much smaller,  $3.3 \pm 0.6$  nm, with minimal aggregation seen for the as-synthesized samples and no further aggregation or particle size growth is seen after 2 weeks (Figures 4.2B and 4.3B). In the presence of 1-methylimidazole, minimal particle aggregation with an average particle size of  $4.2 \pm 0.7$  nm was seen, while [aemim]PF<sub>6</sub>-stabilized particles were found to be  $4.3 \pm 0.8$  nm with moderate aggregation.



**Figure 4.2.** TEM images and particle-size histograms of as-synthesized Au nanoparticles in (a) pure [BMIM]PF<sub>6</sub>, (b) [BMIM]PF<sub>6</sub> with 1.39 mM PVP additive, (c) [BMIM]PF<sub>6</sub> with 1 mM 1-methylimidazole additive, and (d) [BMIM]PF<sub>6</sub> with 10 mM [aemim]PF<sub>6</sub> additive.



**Figure 4.3.** TEM images of Au nanoparticles after two weeks in (a) pure [BMIM]PF<sub>6</sub>, (b) [BMIM]PF<sub>6</sub> with 1.39 mM PVP additive.

Finally, before moving on to discuss the catalytic activity of nanoparticles in these systems, a remark on the generality of the stability results is warranted; in particular, how changing the cation and/or anion of the IL can affect nanoparticle stability. [BMIM]PF<sub>6</sub> IL was chosen as the IL of choice due to the copious literature that exists on nanoparticle stability in [BMIM]PF<sub>6</sub>. We have not examined cation changes beyond the generation of [aemim]PF<sub>6</sub> stabilizers, however, attempts to grow Au nanoparticles in pure [BMIM]OTf IL have been attempted; in the absence of stabilizer, fast precipitation (~10-20 minutes)

of Au nanoparticles is seen for particles stabilized in pure [BMIM]OTf, and we have previously noted that much larger amounts of 1-methylimidazole (*ca.* 100 mM) are necessary for stabilization of Au nanoparticles in [BMIM]OTf.<sup>36</sup> This result suggests that weak anion interactions with Au nanoparticles may be partially responsible for the underlying stability of particles in [BMIM]PF<sub>6</sub>.

Having studied the stability of Au nanoparticles in [BMIM]PF<sub>6</sub> by the four different stabilization strategies above, we wished to further investigate whether these findings would influence the catalyst lifetime of nanoparticles in [BMIM]PF<sub>6</sub> as well. In order to do this, we chose to investigate bimetallic 3:1 PdAu nanoparticles as catalysts for the hydrogenation of 1,3-cyclooctadiene and 3-buten-1-ol. We have previously shown that PVP-stabilized PdAu bimetallic nanoparticles in [BMIM]PF<sub>6</sub> are active hydrogenation catalysts for a range of substrates, and that co-reduced 3:1 PdAu nanoparticles had the highest activity.<sup>26</sup> In addition, we later showed that bimetallic 3:1 PdAu nanoparticles stabilized by 1-methylimidazole in [BMIM]PF<sub>6</sub> were active catalysts for the hydrogenation of allyl alcohol.<sup>36</sup> However, the design of stabilized nanoparticles with long catalyst lifetimes (and therefore total turnover numbers) remains an important challenge, particularly if “greener” IL solvents are to replace conventional solvents and/or heterogeneous catalysts.

Bimetallic 3:1 PdAu nanoparticles were synthesized following similar procedures for the pure Au nanoparticles; PVP-stabilized particles were synthesized in methanol and transferred to the IL phase, while other samples were synthesized directly in neat [BMIM]PF<sub>6</sub> IL or in the IL with 1-methylimidazole or [aemim]PF<sub>6</sub> additives present. Figure 4.4 shows representative TEM images of the bimetallic nanoparticles produced by each method. TEM analysis indicates that the PVP-stabilized particles had the smallest average particle size of  $2.6 \pm 1.1$  nm, with no particle aggregation seen by TEM, as seen in Figure 4.4. Particles synthesized in the presence of 1-methylimidazole had an average particle size of  $3.2 \pm 0.6$  nm, while [aemim]PF<sub>6</sub>-stabilized nanoparticles had an average particle size of  $3.6 \pm 0.7$  nm and nanoparticles synthesized in the neat [BMIM]PF<sub>6</sub> IL had much greater average particle sizes ( $5.3 \pm 3.0$  nm) and polydispersity than any of the stabilized samples. These findings are consistent with the earlier Au nanoparticle results; in the absence of any secondary stabilizer, significantly larger particles are seen, while PVP stabilizers yield particles with the smallest average particle sizes. UV-Vis spectra for all the particles showed an exponentially decaying absorption towards higher wavelengths and the complete absence of any Au plasmon bands, which is consistent with the formation of particles with PdAu alloy structures.<sup>51</sup> Previous work in our group has shown that PVP-stabilized PdAu nanoparticles synthesized via borohydride reduction of mixtures of their salts have near-alloy structures via single-particle energy-dispersive spectroscopy (EDS) and extended x-ray absorption fine structure (EXAFS) measurements.<sup>52</sup> Unfortunately, we were not able to collect accurate single-particle EDS measurements for particles synthesized directly in the ionic liquid, due to sample “burning” effects caused by the ionic liquid present on the TEM grids.

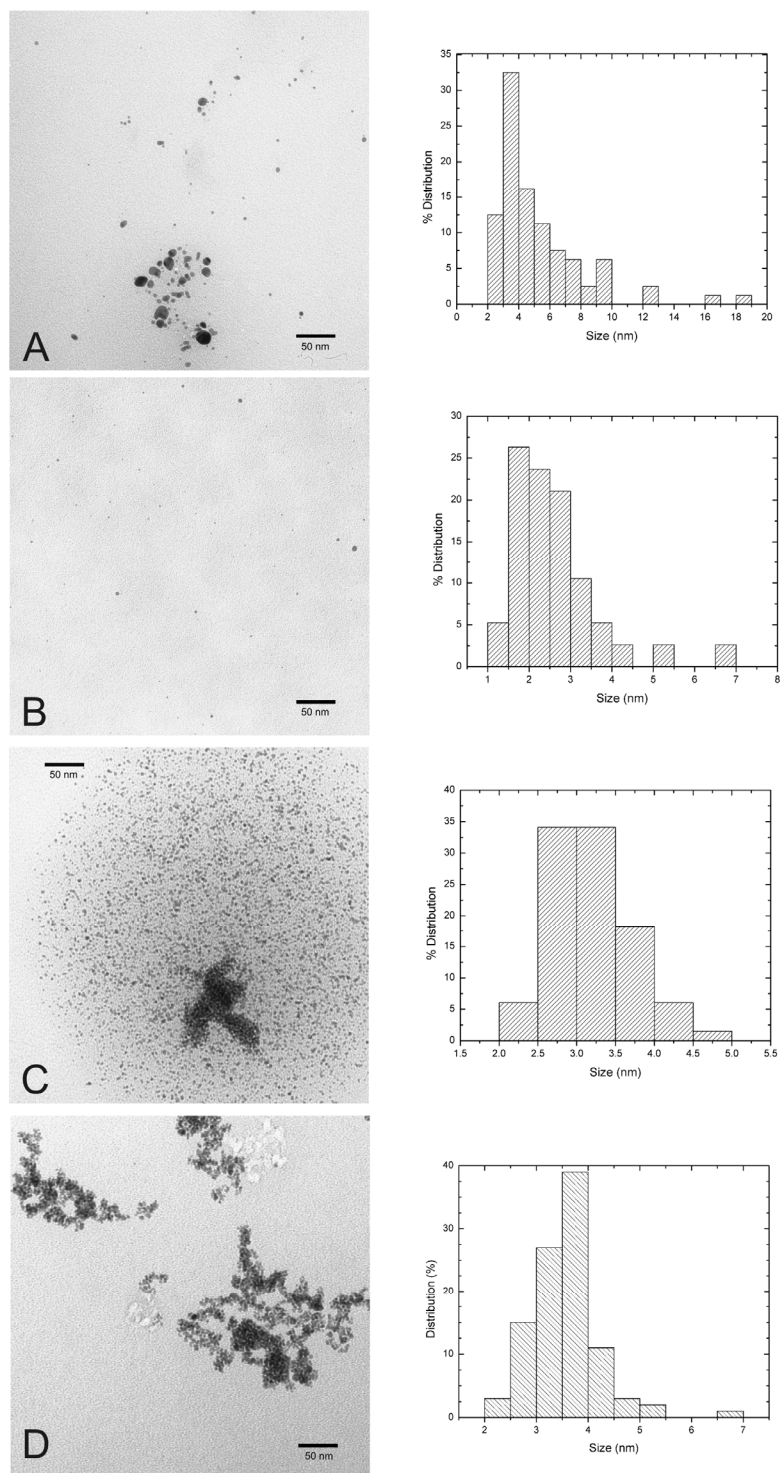
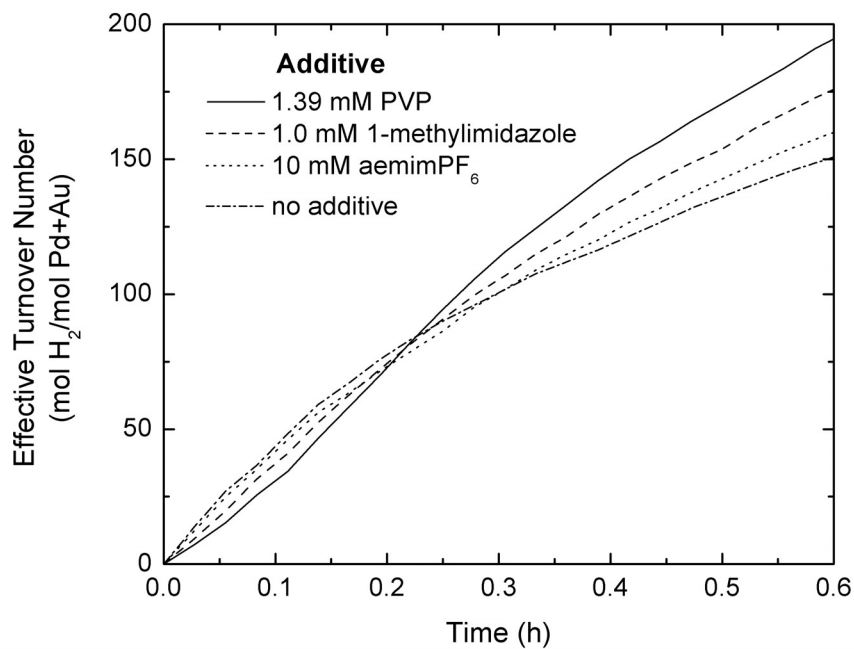


**Figure 4.4.** TEM images and particle-size histograms of as-synthesized 3:1 PdAu nanoparticles in (a) pure [BMIM]PF<sub>6</sub>, (b) [BMIM]PF<sub>6</sub> with 1.39 mM PVP additive, (c) [BMIM]PF<sub>6</sub> with 1 mM 1-methylimidazole additive, and (d) [BMIM]PF<sub>6</sub> with 10 mM [aemim]PF<sub>6</sub> additive.



We investigated the catalytic activity of 3:1 PdAu nanoparticles towards the hydrogenation of cyclooctadiene and 3-buten-1-ol using each of the four stabilizer systems as previously examined in the pure Au system. Figure 4.5A shows the plot of the effective turnover number vs. time for the partial hydrogenation of cyclooctadiene for each of the four systems. We have previously shown that 3:1 PdAu catalysts are extremely selective for the partial hydrogenation to cyclooctene,<sup>26</sup> and NMR results confirmed that the major product of this reaction was cyclooctene with 98-99% selectivities for all of the systems studied. Effective turnover numbers were collected in real-time for all samples by monitoring the decrease in partial pressure of H<sub>2</sub> during the reaction; NMR results indicated that the H<sub>2</sub> consumed correlated nearly exactly with the amount of product formed ( $\pm 3\%$ ). As can be seen in Figure 4.5A, the PVP-stabilized PdAu nanoparticles initially showed the lowest activity, but retained their activity during the course of the reaction, while the particles synthesized in the absence of any additives showed a dramatic drop off in activity in the first 10 minutes of the reaction and showed a visible precipitate after one hour. Particles stabilized by 1-methylimidazole and [aemim]PF<sub>6</sub> had intermediate activities for the hydrogenation and did not show any visible precipitation.

A



B

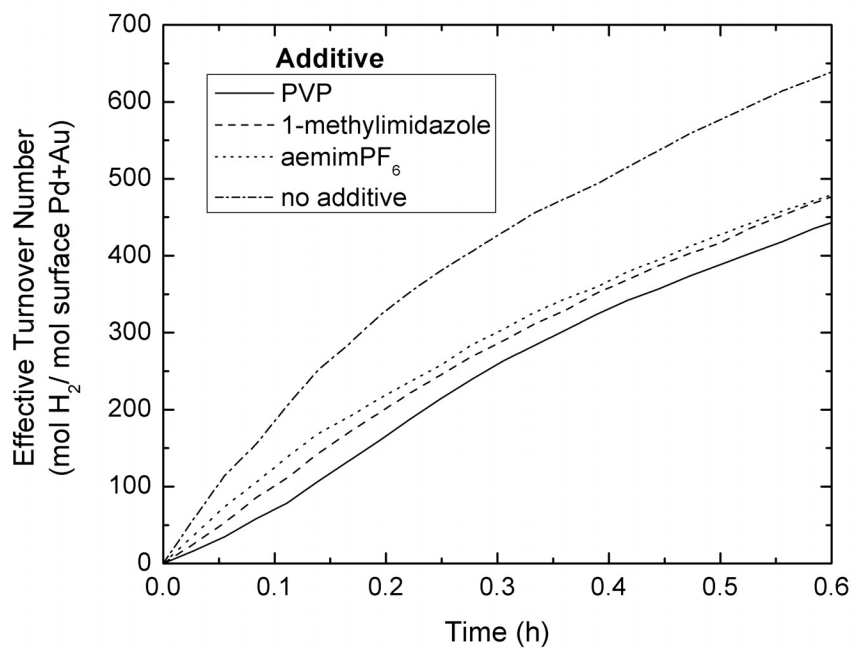
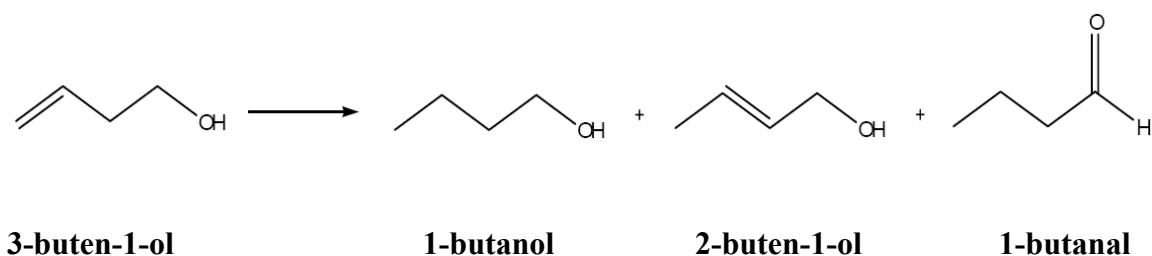


**Figure 4.5.** (A) Effective Turnover Number (moles H<sub>2</sub>/moles Pd+Au) vs. time plot and (B) Plot of Surface Turnover Number (moles H<sub>2</sub>/moles surface Pd+Au) vs. time plot for hydrogenation of 1,3-cyclooctadiene in the presence of additives. Substrate:Catalyst ratio = 400:1.

Figure 4.5B shows the similar plot in which the effective turnover number is normalized for the moles of surface metal on the particles; this was done to compensate for the dramatically different particle sizes as seen by TEM. We note that the unstabilized particles have significantly higher initial activities for this reaction; these results suggest that the PVP, 1-methylimidazole, and [aemim]PF<sub>6</sub> stabilizers do partially passivate the particle surface during the hydrogenation reaction. Attempts were made to examine the effect of PVP loading on the catalytic activity of the particles, however, it was found that at lower PVP loadings of 0.7 mM and below the particles were unstable to aggregation upon phase exchange, while at higher PVP loadings of 2.8 mM and above the IL was so viscous that negligible activity was observed due to mass transfer limitations.

3-Buten-1-ol was used as a second substrate to probe the long-term activity and stability of the PdAu nanoparticle catalysts. Allylic alcohols such as allyl alcohol and 2-buten-1-ol can also form extensive amounts of aldehyde products under hydrogenation conditions.<sup>53-55</sup> The observed reaction products for the hydrogenation and/or isomerization(s) of 3-buten-1-ol are shown in Scheme 4.1.

**Scheme 4.1.** Products detected during the hydrogenation of 3-buten-1-ol.



Initially, PVP-stabilized PdAu nanoparticles were used to optimize the catalyst conditions. While high activities could be observed at low catalyst concentrations, attempts to increase the substrate:catalyst ratio and thus the theoretical maximum turnover numbers in these reactions by lowering the amount of catalyst were unsuccessful, as extremely low yields were seen as the catalyst concentration was lowered. It was found that the optimal conditions for maximizing the turnover number of the desired product / lifetime of the catalysts was for 0.22 mM 3:1 PdAu catalysts with a substrate:catalyst ratio of approximately 16000:1; 100% substrate conversion with a 1-butanol-specific TON of over 10,000 was obtained. The selectivity towards the hydrogenation product was only 68%, as the other minor products in this reaction were the isomerization product, 2-buten-1-ol (22%), and a minor amount of 1-butanol (10%), a double isomerization/tautomerization product.<sup>54-56</sup> The PVP-stabilized PdAu nanoparticles were stable over the reaction period of time and no precipitation was observed during the reaction. We note that pure Pd nanoparticles typically show selectivities of ca. 55% for this reaction with lower activities; thus a mild enhancement of selectivity for the PdAu nanoparticles is seen for this substrate.

These optimized conditions were used to compare each of the four stabilizing systems, and the results can be found in Table 4.1. The PVP-stabilized PdAu nanoparticles had the highest catalytic activity of all the systems studied, while particles synthesized in pure [BMIM]PF<sub>6</sub> showed the lowest conversions. Indeed, “unstabilized” PdAu nanoparticles were found to precipitate out of the IL solution within a period of several hours; however, it is interesting to note that while the catalytic activity of the particles is much lower, they still remained catalytically active even after precipitation.

**Table 4.1.** Hydrogenation of 3-buten-1-ol by four different stabilizers in [BMIM]PF<sub>6</sub> IL.

Stabilizer	% Conversion	1-Butanol-TON	Selectivity	
PVP	100 %	10815	1-butanol	68 %
			2-buten-1-ol	22 %
			1-butanal	10 %
1-methylimidazole (1 mM)	83.5 %	5805	1-butanol	40 %
			2-buten-1-ol	50 %
			1-butanal	10 %
1-methylimidazole (100 mM)	32.5 %	2016	1-butanol	39 %
			2-buten-1-ol	53 %
			1-butanal	8 %
[aemim]PF <sub>6</sub> (100 mM)	60.6 %	5590	1-butanol	58 %
			2-buten-1-ol	42 %
			1-butanal	0 %
Pure [BMIM]PF <sub>6</sub>	39.5 %	1822	1-butanol	29 %
			2-buten-1-ol	62 %
			1-butanal	9 %

Conditions: 40°C, 0.22 mM [Au+Pd], Substrate:Catalyst ratio = 15904:1, time = 17h.

Because of this aggregation over time, we make no attempt to normalize activities to account for different particle sizes. Interestingly, the isomerization product 2-buten-1-ol was observed as a major impurity in all the catalytic reactions; the lower amounts of 2-buten-1-ol seen for the PVP-stabilized nanoparticles may be due to the secondary hydrogenation of this substrate to give 1-butanol, although catalytic data suggests the PdAu catalysts are less active for the hydrogenation of 2-buten-1-ol compared to the original substrate 3-buten-1-ol. Two catalytic tests were attempted with the methylimidazole stabilized PdAu nanoparticles, at 1-methylimidazole concentrations of 1 mM and 100 mM, respectively. Interestingly, much higher TONs were seen for particles in the presence of 1 mM 1-methylimidazole, suggesting that passivation of catalytic sites is occurring at higher 1-methylimidazole concentrations. Such passivation was not

previously seen at short time periods for 1-methylimidazole stabilized PdAu nanoparticles.<sup>36</sup>

Finally, the catalytic activity of the [aemim]PF<sub>6</sub>-functionalized PdAu nanoparticles is intermediate between that of PVP and the absence of stabilizer, which is in agreement with stability results using Au nanoparticles. Initially, PdAu nanoparticles were directly synthesized in [BMIM]PF<sub>6</sub> IL in the presence of 100 mM of the [aemim]PF<sub>6</sub> stabilizer. Alternatively, we tried to synthesize [aemim]PF<sub>6</sub>-stabilized PdAu nanoparticles by a phase transfer method in which PdAu nanoparticles were directly synthesized in pure [BMIM]PF<sub>6</sub> IL, followed by addition of 10 mM [aemim]PF<sub>6</sub>. The catalytic activity of these nanoparticle catalysts was found to be much lower (25% conversion at 17 h), possibly due to the lower concentration of stabilizer. Low [aemim]PF<sub>6</sub> solubility in the [BMIM]PF<sub>6</sub> IL limited attempts to increase the concentration of [aemim]PF<sub>6</sub> beyond 100 mM. One interesting factor to note in catalytic data for the [aemim]PF<sub>6</sub>-stabilized particles is the complete absence of 1-butanol formation; the possible reason(s) for this selectivity change are still unknown, but may involve the in-situ formation of 1-butanol and the primary amine group of aemimPF<sub>6</sub> to form imines..

The catalytic results show a similar trend in long-term activity as seen in the stability studies with pure Au nanoparticles; PVP-stabilized nanoparticles were the most active system, followed by 1-methylimidazole, [aemim]PF<sub>6</sub>, and “unstabilized” PdAu nanoparticles, respectively. The increased activity of the PVP-stabilized PdAu nanoparticles compared to 1-methylimidazole and [aemim]PF<sub>6</sub> stabilized particles may

be partially due to the slightly lower nanoparticle sizes of these particles compared to the other systems; similar average nanoparticle sizes were seen by TEM for both the Au and PdAu nanoparticle syntheses. PdAu nanoparticles synthesized in pure [BMIM]PF<sub>6</sub> IL had particularly low long-term catalytic activities due to their fast aggregation and precipitation; however, it should be noted that unlike other solvent systems, the aggregated PdAu nanoparticles in [BMIM]PF<sub>6</sub> still retain some catalytic activity even after precipitation. Finally, we note that PVP-stabilized nanoparticles can easily be recovered and used for subsequent catalytic reactions,<sup>26</sup> while the 1-methylimidazole and [aemim]PF<sub>6</sub> stabilized nanoparticles did not retain their activity over multiple catalytic runs.

#### 4.5 Conclusions

We have described four stabilization protocols for nanoparticle stabilization in [BMIM]PF<sub>6</sub> IL, and have shown that nanoparticle stability and thus catalytic activity of nanoparticles is dependent on the overall stability of the nanoparticles towards aggregation. The four different stabilization methods in [BMIM]PF<sub>6</sub> which were used include the synthesis of nanoparticles in pure IL, and the addition of secondary PVP, 1-methylimidazole, and [aemim]PF<sub>6</sub> stabilizers. The activity and lifetimes of 3:1 PdAu nanoparticle catalysts synthesized by these four methods were measured by hydrogenation of 1,3-cyclooctadiene and 3-buten-1-ol substrates. PVP-stabilized nanoparticles were found to be the most stable, and had the highest catalytic activity and longer lifetimes than catalysts prepared by the other stabilization routes. As there are a large number of routes towards the development of size-, shape-, and composition-

selected nanoparticle syntheses using poly(vinylpyrrolidone) polymers, the inherent stability of these particles in IL solvents suggests that a wide range of particles can be made in more conventional aqueous and alcoholic solvents, transferred to IL, and used for subsequent catalytic reactions.

## Acknowledgements

The authors would like to acknowledge financial assistance from the National Sciences and Engineering Research Council of Canada (NSERC), and Prof. Ian Burgess for helpful discussions.

## 4.6 References

- (1) Wasserscheid, P.; Keim, W. *Angew. Chem. Int. Ed.* **2000**, *39*, 3773-3789.
- (2) Welton, T. *Chem. Rev.* **1999**, *99*, 2071-2083.
- (3) Huddleston, J. G.; Visser, A. E.; Reichert, W. M.; Willauer, H. D.; Broker, G. A.; Rogers, R. D. *Green Chem.* **2001**, *3*, 156-164.
- (4) Dupont, J.; Fonseca, G. S.; Umpierre, A. P.; Fichtner, P. F. P.; Teixeira, S. R. *J. Am. Chem. Soc.* **2002**, *124*, 4228-4229.
- (5) Fonseca, G. S.; Umpierre, A. P.; Fichtner, P. F. P.; Teixeira, S. R.; Dupont, J. *Chem. Eur. J.* **2003**, *9*, 3263-3269.
- (6) Scheeren, C. W.; Machado, G.; Dupont, J.; Fichtner, P. F. P.; Teixeira, S. R. *Inorg. Chem.* **2003**, *42*, 4738-4742.
- (7) Migowski, P.; Dupont, J. *Chem. Eur. J.* **2007**, *13*, 32-39.
- (8) Antonietti, M.; Kuang, D. B.; Smarsly, B.; Yong, Z. *Angew. Chem., Int. Ed.* **2004**, *43*, 4988-4992.
- (9) Redel, E.; Thomann, R.; Janiak, C. *Inorg. Chem.* **2008**, *47*, 14-16.
- (10) Redel, E.; Thomann, R.; Janiak, C. *Chem. Commun.* **2008**, 1789-1791.



- (11) Pârvulescu, V. I.; Hardacre, C. *Chem. Rev.* **2007**, *107*, 2615-2665.
- (12) Huang, J.; Jiang, T.; Han, B. X.; Gao, H. X.; Chang, Y. H.; Zhao, G. Y.; Wu, W. *Z. Chem. Commun.* **2003**, 1654-1655.
- (13) Deshmukh, R. R.; Rajagopal, R.; Srinivasan, K. V. *Chem. Commun.* **2001**, 1544-1545.
- (14) Scheeren, C. W.; Machado, G.; Teixeira, S. R.; Morais, J.; Domingos, J. B.; Dupont, J. *J. Phys. Chem. B* **2006**, *110*, 13011-13020.
- (15) Astruc, D.; Lu, F.; Aranzaes, J. R. *Angew. Chem. Int. Ed.* **2005**, *44*, 7852-7872.
- (16) Schrekker, H. S.; Gelesky, M. A.; Stracke, M. P.; Schrekker, C. M. L.; Machado, G.; Teixeira, S. R.; Rubim, J. C.; Dupont, J. *J. Colloid Interface Sci.* **2007**, *316*, 189-195.
- (17) Kim, K.-S.; Choi, S.; Cha, J.-H.; Yeon, S.-H.; Lee, H. *J. Mater. Chem.* **2006**, *16*, 1315-1317.
- [18] Zhu, J. M.; Shen, Y. H.; Xie, A. J.; Qiu, L. G.; Zhang, Q.; Zhang, S. Y. *J. Phys. Chem. C* **2007**, *111*, 7629-7633.
- (19) Okazaki, K. I.; Kiyama, T.; Hirahara, K.; Tanaka, N.; Kuwabata, S.; Torimoto, T. *Chem. Commun.* **2008**, 691-693.
- (20) Umpierre, A. P.; Machado, G.; Fecher, G. H.; Morais, J.; Dupont, J. *Adv. Synth. Catal.*, **2005**, *347*, 1404-1412.
- (21) Silveira, E. T.; Umpierre, A. P.; Rossi, L. M.; Machado, G.; Morais, J.; Soares, G. V.; Baumvol, I. L. R.; Teixeira, S. R.; Fichtner, P. F. P.; Dupont, J. *Chem. -Eur. J.*, **2004**, *10*, 3734-3740.
- (22) Gelesky, M. A.; Umpierre, A. P.; Machado, G.; Correia, R. R. B.; Magno, W. C.; Morais, J.; Ebeling, G.; Dupont, J. *J. Am. Chem. Soc.*, **2005**, *127*, 4588-4589.
- (23) Wei, G. T.; Yang, Z. S.; Lee, C. Y.; Yang, H. Y.; Wang, C. R. C. *J. Am. Chem. Soc.* **2004**, *126*, 5036-5037.
- (24) Wang, Y.; Yang, H. *Chem. Commun.* **2006**, 2545-2547.
- (25) Mu, X. D.; Evans, D. G.; Kou, Y. A. *Catal. Lett.* **2004**, *97*, 151-154.
- (26) Dash, P.; Dehm, N. A.; Scott, R. W. J. *J. Mol. Catal. A: Chem.* **2008**, *286*, 114-119.

- (27) Tatumi, R.; Fujihara, H. *Chem. Commun.* **2005**, 83-85.
- (28) Kim, K. S.; Demberehnyamba, D.; Lee, H. *Langmuir* **2004**, *20*, 556-560.
- (29) Zhao, D. B.; Fei, Z. F.; Geldbach, T. J.; Scopelliti, R.; Dyson, P. J. *J. Am. Chem. Soc.* **2004**, *126*, 15876-15882.
- (30) Visser, A. E.; Swatloski, R. P.; Reichert, W. M.; Mayton, R.; Sheff, S.; Wierzbicki, A.; Davis, J. H.; Rogers, R. D. *Chem. Commun.* **2001**, 135-136.
- (31) Davis, J. H. *Chem. Lett.* **2004**, *33*, 1072-1077.
- (32) Wang, Z.; Zhang, Q.; Kuehner, D.; Ivaska, A.; Niu, L. *Green Chem.* **2008**, *10*, 907-909.
- (33) Chiappe, C.; Pieraccini, D.; Zhao, D. B.; Fei, Z. F.; Dyson, P. J. *Adv. Synth. Catal.* **2006**, *348*, 68-74.
- (34) Itoh, H.; Naka, K.; Chujo, Y. *J. Am. Chem. Soc.* **2004**, *126*, 3026-3027.
- (35) Mu, X. D.; Meng, J. Q.; Li, Z. C.; Kou, Y. *J. Am. Chem. Soc.* **2005**, *127*, 9694-9695.
- (36) Dash, P.; Scott, R.W.J. *Chem. Commun.* **2009**, 812-814.
- (37) Li, Y.; Boone, E.; El-Sayed, M. A. *Langmuir* **2002**, *18*, 4921-4925.
- (38) Narayanan, R.; El-Sayed, M. A. *J. Am. Chem. Soc.* **2003**, *125*, 8340-8347.
- (39) Narayanan, R.; El-Sayed, M. A. *J. Phys. Chem. B* **2005**, *109*, 12663-12676.
- (40) Durand, J.; Teuma, E.; Malbosc, F.; Kihn, Y.; Gomez, M. *Catal. Commun.* **2008**, *9*, 273-275.
- (41) Fernandez, F.; Cordero, B.; Durand, J.; Muller, G.; Malbosc, F.; Kihn, Y.; Teuma, E.; Gomez, M.; *Dalton Trans.* **2007**, 5572-5581.
- (42) S. Jansat, J. Durand, I. Favier, F. Malbosc, C. Pradel, E. Teuma, M. Gomez, *Chemcatchem.* **1** (2009) 244-246.
- (43) Ott, L.S.; Finke, R.G. *Coord. Chem. Rev.* **2007**, *251*, 1075-1100.
- (44) Lee, S.G. *Chem. Commun.* **2006**, 1049-1063.
- (45) Zhang, H.; Cui, H. *Langmuir* **2009**, *25*, 2604-2612.

- (46) Harjani, J. R.; Friscic, T.; MacGillivray, L. R.; Singer, R. D. *Inorg. Chem.* **2006**, *45*, 10025-10027.
- (47) Quinten, M.; Kreibig, U.; *Surf. Sci.* **1986**, *172*, 557-577.
- (48) Vivek, J.P.; Burgess, I.J. *J. Phys. Chem. C* **2008**, *112*, 2872-2880.
- (49) Isaacs, S.R.; Cutler, E.C.; Park, J.S.; Lee, T.R.; Shon, Y.S. *Langmuir* **2005**, *21*, 5689-5692.
- (50) Cheng, W.L.; Dong, S.J.; Wang, E.K. *Langmuir* **2003**, *19*, 9434-9439.
- (51) Creighton, J.A.; Eadon, D.G. *J. Chem. Soc. Faraday Trans.* **1991**, *87*, 3881-3891.
- (52) Dash, P.; Bond, T.; Fowler, C.; Hou, W.; Coombs, N.; Scott, R. W. J. *J. Phys. Chem. C* **2009**, *113*, 12719-12730.
- (53) Muzart, J.; *Tetrahedron* **2003**, *59*, 5789-5816.
- (54) Zharmagambetova, A. K.; Ergozhin, E. E.; Sheludyakov, Y. L.; Mukhamedzhanova, S. G.; Kurmanbayeva, I. A.; Selenova, B. A.; Utkelov, B. A. *J. Mol. Cat. A* **2001**, *177*, 165-170.
- (55) Musolino, M. G.; Maio, P. D.; Donato, A.; Pietropaolo, R. *J. Mol. Cat. A* **2004**, *208*, 219-224.
- (56) Sato, S.; Takahashi, R.; Sodesawa, T.; Yamamoto, N. *Catal. Commun.* **2004**, *5*, 397-400.

## CHAPTER 5

### 5. Rational Design of Supported PdAu Nanoparticle Catalysts from Structured Nanoparticle Precursors

This work has been published in *Journal of Physical Chemistry C*. A rational chemical method for the synthesis of heterogeneous catalysts based on co-reduced and sequentially grown PdAu nanoparticles trapped in alumina matrixes is reported. Extensive characterization (TGA, HRTEM, EDS, EXAFS, and XANES) of these supported co-reduced nanoparticle catalysts have shown that the rational design methodology is effective for the synthesis of heterogeneous catalysts in which the structural and compositional integrity of the predesigned nanoparticles has been maintained in the final heterogeneous supported nanoparticle catalysts. Supported Pd core-Au shell nanoparticles can also be synthesized by this method and the structural and geometrical integrity was maintained after the calcination step.

---

This work has been published in *J. Phys. Chem. C*, **2009**, 113, 12719-12730. This paper has been co-authored by T. Bond, C. Fowler, W. Hou, and N. Coombs. While C. Fowler synthesized the core-shell nanoparticles, T. Bond and W. Hou helped in collecting data at Canadian Light Source (CLS). Dr. N. Coombs at Univ. of Toronto did the STEM imaging. All the other experimental work in this paper has been done by me along with the manuscript writing and editing. The final manuscript was submitted after thorough revisions by my supervisor Dr. Robert W. J. Scott.

## 5. Rational Design of Supported-PdAu Nanoparticle Catalysts from Structured Nanoparticle Precursors

Priyabrat Dash,<sup>†</sup> Toby Bond,<sup>†</sup> Candace Fowler,<sup>†</sup> Wenbo Hou,<sup>†</sup> Neil Coombs,<sup>‡</sup> and

Robert W. J. Scott<sup>†,\*</sup>

<sup>†</sup> Department of Chemistry, University of Saskatchewan, 110 Science Place,  
Saskatoon, Saskatchewan, Canada

<sup>‡</sup> Department of Chemistry, University of Toronto, Toronto, Ontario, Canada

### 5.1 Abstract

A series of polyvinylpyrrolidone (PVP)-stabilized metallic and bimetallic PdAu nanoparticles (co-reduced and core-shell) with narrow size distributions were encapsulated into alumina matrices by sol-gel chemistry and their chemical, structural, electronic, and catalytic behavior were investigated. Monodisperse nanoparticles were uniformly distributed in the alumina frameworks as observed by TEM images, and single-particle energy-dispersive spectroscopy (EDS) analyses confirmed the high compositional uniformity of the bimetallic nanoparticles. A combination of TEM, EDS mapping, TGA, and XANES and EXAFS studies were used to fully characterize the alumina-supported nanoparticles before and after thermal treatments. It was observed that the size distribution of final PdAu nanoparticles was highly dependent on calcination conditions, and careful high temperature calcinations at 300 °C could be used to remove organic PVP stabilizers with minimal particle aggregation and/or structural transformations. The resulting supported-nanoparticle catalysts were found to be active as hydrogenation catalysts. EXAFS analysis of co-reduced PdAu nanoparticles indicated

they had near-alloy structures with slightly Au rich cores and Pd rich shells before and after calcination, while intentionally designed Pd-core Au-shell nanoparticles retained their structures after calcination. XANES spectra of both co-reduced and core-shell PdAu nanoparticles were also examined and showed that the PdAu co-reduced nanoparticles had fewer Au valence d-band vacancies in comparison to the monometallic nanoparticles while the PdAu core-shell nanoparticles had relatively higher Au valence d-band vacancies to that of the co-reduced PdAu nanoparticles.

## 5.2 Introduction

Supported metal nanoparticle catalysts have long been used as heterogeneous catalysts in a number of industrially-important catalytic reactions such as hydrogenations, dehydrogenations, hydrocracking, and reduction and oxidation reactions in fuel cells.<sup>1,2</sup> For many systems, bimetallic catalysts have been shown to have synergetic catalytic performances which differ from either of their individual metal components.<sup>3-5</sup> Palladium-gold is a bimetallic system which has been widely explored; for example, Hutchings *et al.* have shown that PdAu catalysts have a twenty-five fold increase in activity for the oxidation of alcohols to aldehydes as compared to pure Au or Pd catalysts.<sup>6</sup> Bimetallic PdAu nanoparticles have also shown excellent catalytic performance for the direct synthesis of H<sub>2</sub>O<sub>2</sub> from H<sub>2</sub> and O<sub>2</sub>,<sup>7-13</sup> glycerol oxidation,<sup>14,15</sup> the hydrochlorination of acetylene,<sup>16</sup> and many other reactions.<sup>17-25</sup> For many applications, it is desirable to fabricate heterogeneous supported-nanoparticle catalysts. Traditional synthetic techniques of supported-nanoparticle catalysts for industrial applications typically involve the deposition of metal precursors onto high surface area

supports, followed by various thermal activation treatments (incipient wetness method or deposition-precipitation).<sup>26</sup> The size-distribution of nanoparticles and the degree of dispersion on the support are each highly dependent on the pH and concentration of the precursor solution, type of the oxide support, and calcination temperature and procedure.<sup>26,27</sup> In addition, these methods often provide limited control over the composition and structures of bimetallic nanoparticles, which often leads to significant compositional non-uniformity from particle to particle.<sup>28</sup> Poor control over compositional homogeneity and size of bimetallic nanoparticles often provides a serious challenge in understanding the size-structure-property relationships of bimetallic and multimetallic catalysts.

In order to address these issues, we fabricated supported PdAu nanoparticle catalysts by controlling the size, structure, and composition of co-reduced and sequentially-grown PdAu nanoparticles via well-established solution synthetic routes using polyvinylpyrrolidone (PVP) stabilizers. This was followed by incorporating the pre-synthesized nanoparticles into sol-gel syntheses of alumina. This route provides an alternative method of designing industrially-relevant, supported-nanoparticle catalysts through a rational chemical approach, leading to well-dispersed PdAu nanoparticles within high-surface area alumina supports and good control over the size, composition, and internal structure of the nanoparticles. However, one of the pitfalls of this route as described above is that the PVP stabilizers must be removed without destroying the size, compositional, and structural integrity of the pre-fabricated nanoparticles in order to produce the desired supported-nanoparticle catalysts. Careful low temperature calcination temperatures were employed to remove the PVP polymer. A combination of HRTEM,

energy dispersive spectroscopy (EDS) mapping, thermal gravimetric analysis (TGA) and x-ray absorption near edge and fine structure spectroscopy (XANES and EXAFS) studies were carried out to allow for detailed characterization of the PdAu nanoparticle precursors before and after removal of the polymer stabilizers via low temperature calcinations. Finally, the activity of the catalysts was evaluated using the well-studied hydrogenation reaction a model substrate, allyl alcohol.

Among the various techniques available for the synthesis of supported-bimetallic nanoparticle catalysts, the method of entrapping pre-synthesized nanoparticles into an inorganic matrix by the sol-gel method is an interesting route which has been investigated by other groups in the past.<sup>29-31</sup> This route takes advantage of the large number of synthetic solution protocols that have been developed to carefully control metallic and bimetallic nanoparticle sizes, shapes and compositions.<sup>20</sup> Poly(N-vinyl-2-pyrrolidone) (PVP) is one of the most commonly used polymers for nanoparticle stabilization and catalysis, as it allows synthesis of stabilized nanoparticles with accessible surface areas in polar solvents such as water.<sup>5,32,33</sup> After successful synthesis and purification, the nanoparticle precursors, in which the particle size distribution, composition, and structure is well-defined, are then deposited onto various supports to synthesize highly dispersed heterogeneous bimetallic catalysts.<sup>34,35</sup> In recent years, nanoparticles synthesized by dendrimers,<sup>17,36-41</sup> monolayers,<sup>42-46</sup> and polymer stabilizers<sup>5,47,48</sup> have been used as precursors for supported nanoparticle catalysts. Entrapping pre-synthesized metal nanoparticles, including PdAu nanoparticles, into an inorganic matrix by sol-gel chemistry is an attractive route that has been used by several groups.<sup>17,30,36,43,47,49</sup> For example, Parvulescu and co-workers synthesized heterogeneous PdAu catalysts by



embedding pre-prepared tetraalkylammonium-stabilized PdAu nanoparticles in a sol-gel SiO<sub>2</sub> matrix.<sup>49</sup> More recently, Crooks and coworkers synthesized PdAu/TiO<sub>2</sub> catalysts using dendrimer-stabilized nanoparticles by a sol-gel route.<sup>17</sup> In both cases this approach produced a narrow distribution of PdAu nanoparticles in the oxide support after the stabilizer was removed by calcination. However, in neither of these cases was the structural integrity of the nanoparticle followed before and after calcination.

However, an area of major concern in designing supported nanoparticle catalysts from pre-synthesized nanoparticles is that nanoparticle sintering, alloying/segregation and metal oxidation can occur upon removal of the organic stabilizers via thermal treatments.<sup>42,50</sup> Sintering of the metal is strongly temperature-dependent and thus, coalescence of metal particles often occurs at Tammann temperature, which is half of the melting point.<sup>51</sup> For example, gold nanoparticles supported on silica support tend to form very large agglomerates above Tammann temperatures of Au.<sup>52</sup> This is a rather complicated problem in PdAu bimetallic system due to the segregation tendency of these metals.<sup>19,53,54</sup> For example, Hutchings and coworkers found that degree of segregation increases with temperature in the PdAu/Al<sub>2</sub>O<sub>3</sub> system.<sup>19</sup> After calcination, the particles began to exhibit surface enrichment of Pd, and sintering of the Pd particles on the support surface had occurred. Thus removal of the organic stabilizer(s) in order to activate supported-nanoparticle catalysts is not a trivial problem, and much care must be taken such that size, composition, and structure are retained after thermal treatments.

Though HRTEM and EDS mapping techniques can help follow the average particle size and compositions before after thermal treatment, in general they do not give

much information as to surface vs. bulk atomic distributions. X-ray absorption spectroscopy comprising both x-ray absorption near-edge spectroscopy (XANES) and extended x-ray absorption fine structure spectroscopy (EXAFS) has been used as a valuable tool for the examination of PdAu and other bimetallic nanoparticle structures by the catalyst community in the past.<sup>4,32,55-60</sup> While XANES can reveal the oxidation state and d-occupancy of a specific atom,<sup>61,62</sup> EXAFS provides a valuable tool for the analysis of local atomic structure, giving information about the average local atomic coordination environment.<sup>63,64</sup> When combined with adequate models of the nanoparticle structure and composition, EXAFS measurements of carefully-synthesized nanoparticles can be used to shed light on possible structures of such nanoparticles. Thus EXAFS has the ability to give quantitative information of the nanoparticle structure before and after thermal treatments of nanoparticles, and which can be critical in designing any industrially-relevant heterogeneous catalysts.<sup>65,66</sup>

Herein, we report a rational chemical method towards the synthesis of heterogeneous catalysts based on co-reduced and sequentially-grown PdAu nanoparticles trapped in alumina matrixes. Low temperature calcination conditions ( $\sim 300^\circ\text{C}$ ) were found to be optimal for the removal of the PVP polymer stabilizer with minimal changes in the average particle size, composition and structure. The structural, chemical and electronic properties of the supported nanoparticle catalysts were characterized by transmission electron microscopy and EDS mapping, thermal analysis (TGA), and X-ray absorption spectroscopy (EXAFS, XANES). EXAFS analysis of co-reduced PdAu nanoparticles indicated they had near-alloy structures with slightly Au rich cores and Pd rich shells before and after calcination, while intentionally designed Pd-core Au-shell

nanoparticles retained their structures after calcination. The XANES spectra of co-reduced PdAu nanoparticles showed that the PdAu co-reduced nanoparticles had fewer Au valence d-band vacancies in comparison to the monometallic nanoparticles while the PdAu core-shell nanoparticles had relatively higher Au valence d-band vacancies compared to the co-reduced PdAu nanoparticles. Extensive characterization of these supported PdAu catalysts shows that a rational design methodology is effective for the synthesis of heterogeneous catalysts in which the structural and compositional integrity of pre-designed nanoparticles is maintained in the final heterogeneous supported-nanoparticle catalysts.

## **5.3 Experimental Methods**

### **5.3.1 Materials**

Poly(vinylpyrrolidone) (M.W. 40,000), hydrogen tetrachloroaurate hydrate (99.9%), potassium tetrachloropalladate (99.99%), aluminum isopropoxide (98%), and allyl alcohol (99%) were purchased from Alfa and were used without further purification. Ascorbic acid (99.7%), isopropyl alcohol (99.8%), and nitric acid (38-40%) were purchased from EMD and were used as obtained. Sodium borohydride powder (98%) was obtained from Aldrich and was used as obtained. Deuterated solvents were purchased from Cambridge Isotope Laboratories. 18 M $\Omega$ ·cm Milli-Q water (Millipore, Bedford, MA) was used throughout. Cellulose dialysis membranes (MW cutoff 12,400 g/mol) were purchased from Aldrich.

## 5.3.2 Synthetic methods

### 5.3.2.1 Nanoparticle Synthesis

The procedure for synthesizing PVP-stabilized Au, Pd and co-reduced PdAu nanoparticles in methanol was described previously.<sup>24,67</sup> Methanol was removed from the nanoparticle solution under vacuum, followed by the addition of same volume of isopropanol to synthesize the nanoparticles in isopropanol. The procedure for synthesizing PVP-stabilized sequentially-grown 1:3 Pd:Au core-shell nanoparticles from Pd nanoparticle seeds is as follows;<sup>38</sup> PVP-stabilized Pd nanoparticle seeds were prepared by adding 10.0 mL of a 10 mM  $K_2PdCl_4$  solution and 20.0 mL of 1.39 mM PVP in 4.4 mL of water followed by stirring under nitrogen for 30 min. 2.0 mL of 0.10 M  $NaBH_4$  solution was then added, followed by stirring for 30 min. The solution was then dialyzed overnight under nitrogen. After dialysis, 3.15 mL of the Pd seed solution was added to a round bottomed flask followed by addition of 79.5  $\mu$ mol of ascorbic acid under  $N_2$ . In a separate vial, 265  $\mu$ L of a 0.10 M ascorbic acid solution was added to 2.65 mL of 0.010 M  $HAuCl_4$  and 13.2 mL of deionized water, giving a colourless solution. Core-shell 1:3 Pd:Au nanoparticles (1.75 mM) were then synthesized by rapidly adding the “ $Au^+$ ”/ascorbic acid solution to the Pd seed solution followed by stirring for 30 min.<sup>68</sup> The alumina-supported core-shell 1:3 Pd:Au core-shell nanoparticle catalysts were then prepared according to the methods described below.

### 5.3.2.2 Sol-Gel Chemistry

All sol-gel chemistry was carried out under nitrogen. PVP-stabilized Au, Pd and bimetallic PdAu nanoparticles in isopropanol were used to prepare Al<sub>2</sub>O<sub>3</sub>-supported catalysts with 2.5 wt % metal loading. Dilute aqueous nitric acid (2 mL, 5 wt %) was added dropwise to the nanoparticle solution, followed by the addition of 0.51 g of Al(O<sup>i</sup>Pr)<sub>3</sub> dissolved in 5.0 ml of freshly-dried isopropanol. Within 50-60 s, a gel was formed and was left overnight to age. The filtrate was then removed from the gel by simple decantation. In all cases the filtrate was completely colorless, confirming the trapping of all the nanoparticles in the alumina matrix. The powder was then dried in an oven at 150 °C for 3 h to give the as-synthesized xerogel-supported nanoparticles. The as-synthesized samples were then calcined in a furnace at 300 °C for 5 h in flowing air followed by reduction under H<sub>2</sub> flow at 300 °C for 1 h to remove the PVP stabilizer. The same procedure above was followed for the synthesis of Pd, 3:1, 1:1, 1:3 PdAu/TiO<sub>2</sub>-Al<sub>2</sub>O<sub>3</sub> catalysts keeping the total metal concentration constant.

### 5.3.3 Characterization

Thermogravimetric analysis (TGA) was performed using a TA instruments TGA Q5000IR under air flow. Initial samples were run from 25 °C to 600 °C with a heating rate of 10 °C/min to determine the total amount of PVP polymer present and the degradation temperature range. This was followed by running separate samples which were held for 5 h at the onset of PVP degradation temperature while monitoring the total mass loss of the sample. TEM micrographs were obtained with a Philips 410 microscope operating at 100 keV, while HRTEM investigations were performed using a Hitachi HD-

2000 microscope with a field emission cathode at 200 kV. STEM images were recorded with a high-angle annular dark field (HAADF) detector. The sample was prepared by placing a drop of the methanol solution of a well-ground catalyst powder onto a carbon-coated copper grid (200 Mesh, Electron Microscopy Sciences) followed by evaporation of the methanol. EDS line scan data were collected using an acceleration voltage of 200 kV, a collection time of 60 s, and a 0.5 nm diameter probe. Integrated intensities obtained from the  $PdL_{\alpha 1}$  and  $AuL_{\alpha 1}$  lines were used for quantification of the two metals, respectively, because they did not overlap the other X-ray emission lines. XRD measurements were carried out using a Rigaku Rotaflex RU-200 diffractometer using the  $CuK_{\alpha}$  radiation line; the sample was scanned over the  $2\theta$  range of  $5-80^{\circ}$ .

X-ray absorption spectra at the Pd K-edge and the Au  $L_{III}$ -edge were recorded at the HXMA beamline 061D-1 (energy range: 5-30 keV, resolution:  $1 \times 10^{-4} \Delta E/E$ ) at the Canadian Light Source (CLS, 2.9 GeV storage ring, 250 mA current). All samples were pressed into pellets and measured in transmission mode at room temperature. A double-crystal Si(111) monochromator was employed for energy selection at both Au  $L_{III}$ -edge (11919 eV) and Pd K-edge (24350 keV). Higher harmonics were eliminated by detuning double-crystal Si (111) by using a Rh coated 100 mm long KB mirror. The incident and transmission X-ray intensities were detected by ion chambers filled with helium-nitrogen mixtures that were installed in front of and behind the sample cell, while a third ionization chamber was present after the reference foil such that energy calibration could be performed for each scan. Energy was scanned from 200 eV below the edge to 1000 eV above the edge. Standard reference compounds, Pd foil and Au foil for the respective edges, were measured simultaneously.

Data processing was performed with the use of software package IFEFFIT.<sup>69</sup> First, the raw absorption spectrum in the pre-edge region was fitted to a straight line, and the background above the edge was fit using a cubic spline function. The EXAFS function,  $\chi$ , was obtained by subtracting the post-edge background from the overall absorption and then normalizing with respect to the edge jump step. The normalized  $\chi(E)$  was then Fourier-transformed from energy space to  $k$ -space. The  $\chi(k)$  data were  $k^3$ -weighted in order to compensate for the dampening of the EXAFS amplitude with increasing  $k$ .  $k^3$ -weighted data were Fourier transformed to  $r$ -space to separate the EXAFS contributions from different coordination shells. The EXAFS fitting was performed in  $r$ -space between 1.5-3.3 Å for Au-edge and 1.3-3.2 Å for the Pd-edge (without phase correction) using theoretical phase-shift and amplitude generated by FEFF 6.0 code.<sup>70</sup> A homogeneous PdAu alloy model for the FEFF fitting was constructed based on bulk PdAu lattice parameters reported in the literature.<sup>71</sup> The amplitude reduction factor,  $S_o^2$ , for Au and Pd were obtained by analyzing Au and Pd reference materials, respectively, and by fixing coordination numbers for the bulk fcc metals to be 12 in the IFEFFIT input file.<sup>72</sup> The  $S_o^2$  values were found to be 0.83 and 0.84 for Pd and Au respectively.

#### 5.3.4 Catalytic Test Reaction

The hydrogenation of allyl alcohol was performed in a three-necked round-bottom flask at 40°C. Initially, air trapped in the aqueous suspension of the catalysts (50 mg of catalyst in 10 ml of aqueous solution) was removed under vacuum. The procedure for the hydrogenation reaction was followed as described previously.<sup>24</sup> A H<sub>2</sub> gas source was

connected to one end of the flask while the other end was attached to a differential pressure gauge (Model 407910, Extech Instruments Corp. with a resolution of 0.001 atm and accuracy of  $\pm 2\%$  at  $23 \pm 5\text{ }^{\circ}\text{C}$ ) and the central portion was closed with a rubber septum. Initially, 10 ml of the nanoparticle catalyst aqueous solution was placed in the flask, followed by purging the system with  $\text{H}_2$  for 10 min. Next, 0.50 ml of the allyl alcohol substrate was added under vigorous stirring conditions, followed by measurement of the  $\text{H}_2$  uptake via differential pressure measurements in every 10 seconds. The turnover number (TON, mol of  $\text{H}_2$ / mol metal) of the catalyst system was calculated from the pressure decrease assuming hydrogen behaves as an ideal gas.<sup>73</sup> Correlation of hydrogen consumption and product formation (1-propanol) was found to be 100% (with an error of *ca.* 2%) via  $^1\text{H}$  NMR experiments. This allowed the turnover frequency (TOF, (mol of product/mol of metal/h<sup>-1</sup>)) to be determined from the slope of linear plots of TON versus time.

## 5.4 Results and Discussion

Co-reduced PdAu nanoparticles and sequentially-grown 1:3 Pd:Au core-shell nanoparticles were synthesized according to literature protocols.<sup>24,67</sup> The co-reduced PdAu nanoparticles (Pd:Au ratios of 3:1, 1:1, and 1:3) and pure Au and Pd nanoparticles all had average particle sizes ranging from 3.0 - 4.0 nm, and UV-Vis spectra of the PdAu samples showed no separate Au plasmon peak at  $\sim 520$  nm, confirming the formation of bimetallic random/alloy nanoparticles.<sup>38,74</sup> Pd-Au core-shell nanoparticles were synthesized by growing a successive gold shell on pre-synthesized Pd nanoparticle seeds.<sup>38</sup> Galvanic reactions of  $\text{Au}^{3+}$  salts with the  $\text{Pd}^0$  nanoparticles were avoided by pre-



reducing the  $\text{AuCl}_4^-$  salt with ascorbic acid to form  $\text{Au}^+$  salts prior to addition of the Au salts to the Pd nanoparticle seeds.<sup>75</sup> Figure 5.1 shows TEM images of the Pd seeds and sequentially grown 1:3 (molar amounts) Pd:Au core-shell nanoparticles; the initial Pd seeds had an average particle size of  $3.1 \pm 1.7$  nm, while after Au shell formation, the resulting 1:3 Pd:Au core-shell nanoparticles had an average size of  $5.2 \pm 1.8$  nm. This size increase is consistent with the respective metal loadings of the core and shell, respectively, using Equation 5.1.<sup>76</sup>

$$D = D_{\text{core}} \left( 1 + \frac{V_{\text{Au}}[\text{Au}]}{V_{\text{Pd}}[\text{Pd}]} \right)^{1/3} \quad (5.1)$$

where,  $D_{\text{core}}$  is the diameter of the experimentally measured Pd core (3.1 nm),  $V_{\text{Au}}$  and  $V_{\text{Pd}}$  and  $[\text{Au}]$  and  $[\text{Pd}]$  are the molar volumes and concentrations of Au and Pd, respectively. The molar volumes of gold and palladium used,  $V_{\text{Au}}$  and  $V_{\text{Pd}}$ , were  $10.21 \text{ cm}^3/\text{mol}$  and  $8.56 \text{ cm}^3/\text{mol}$ , respectively. Using the average measured Pd nanoparticle size of 3.1 nm, Equation 1 yields a diameter of 5.15 nm which is fairly close to the value of 5.2 nm obtained from TEM measurements. UV-Vis spectra of the Pd seeds and 1:3 Pd core -Au shell nanoparticles are shown in Figure 5.1(c). Upon growth of a gold shell on the Pd seeds, a weak plasmon band around  $\sim 520$  nm develops. The presence of a Au plasmon band is consistent with  $\sim 2$  nm Au shell growth over a Pd core; however more conclusive evidence of core-shell formation via EDS line scans and EXAFS results for these nanoparticles trapped in alumina will be presented later.

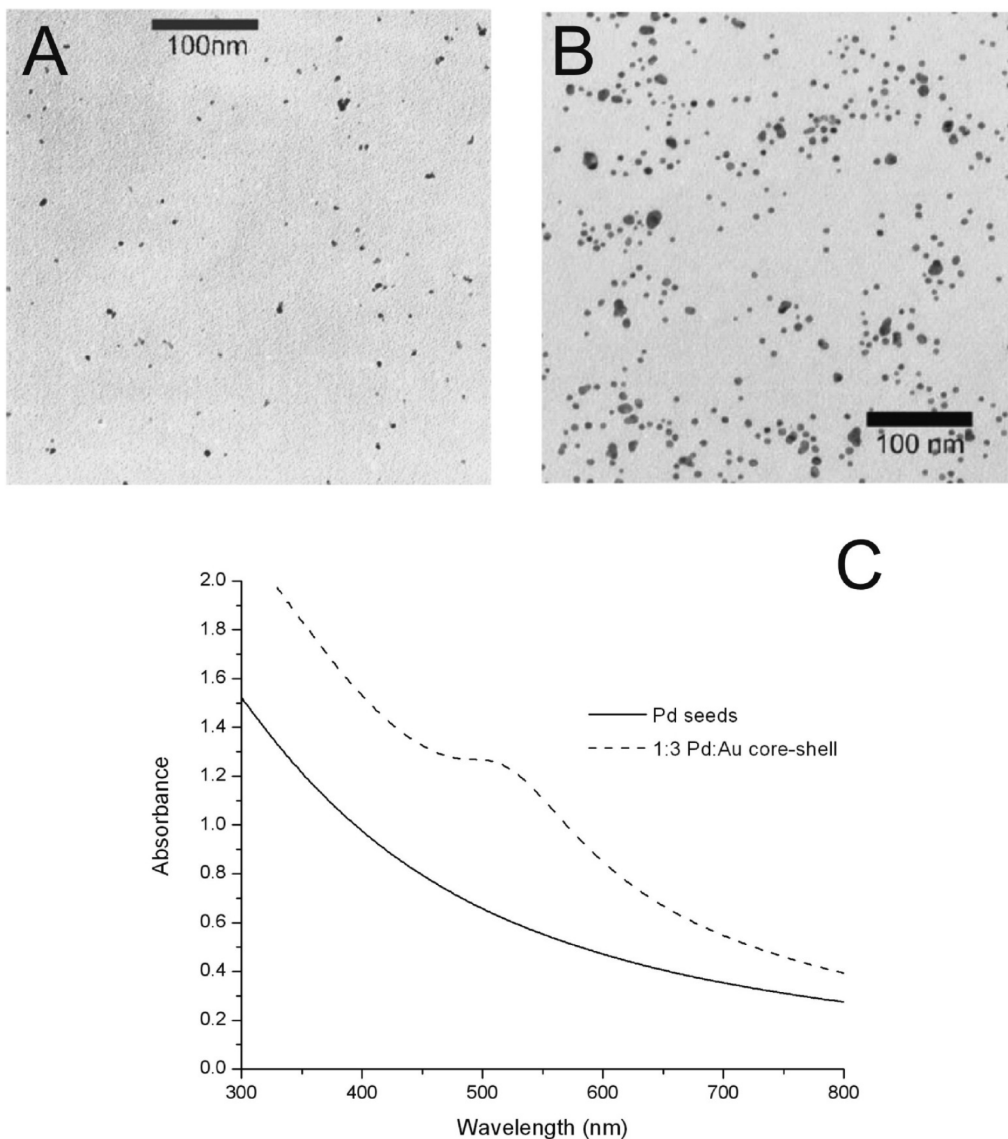


**Figure 5.1.** TEM images of PVP-stabilized (a) Pd seeds, (b) 1:3 Pd core-Au shell nanoparticles, and (c) UV-Vis spectra of Pd seeds and 1:3 Pd core-Au shell nanoparticles.

After pre-synthesizing the bimetallic PdAu nanoparticles, the particles were trapped in an alumina matrix through sol-gel chemistry. This involved the hydrolysis and condensation of an  $\text{Al}(\text{OiPr})_3$  precursor in the presence of the PVP-stabilized nanoparticles, to give 2.5% by weight metal nanoparticles in an alumina support.<sup>36</sup> After gelation of the alkoxide precursor, expulsion of clear isopropanol occurred overnight,

likely due to aging of the alumina gel (syneresis), indicating complete trapping of the PVP-stabilized particles in the gel. The mean particle sizes and size distributions of the as-synthesized nanoparticles dispersed in alumina matrixes were obtained by HRTEM images. For STEM studies, co-reduced 1:1 PdAu nanoparticles were primarily studied as representative samples as they should contain approximately equal amounts of both metals, and thus should facilitate EDS studies. Figure 5.2a shows a dark-field HRTEM image of co-reduced 1:1 PdAu nanoparticles dispersed in an amorphous alumina matrix. The particles are well dispersed within the oxide support, with an average nanoparticle size of  $4.1 \pm 0.7$  nm. This is slightly larger than the average particle size of the original synthesized particles, but is within error of the TEM technique.<sup>77</sup> Single-particle energy-dispersive spectroscopy (EDS) analyses indicate an average composition of approximately 1:1 of Pd and Au (with a standard deviation of 10%), which is in agreement to the molar percentage of respective salts during the synthesis. Figure 5.2b shows an EDS line scan which unambiguously shows the presence of both salts in individual nanoparticles. This confirms the high compositional uniformity of the bimetallic nanoparticles.

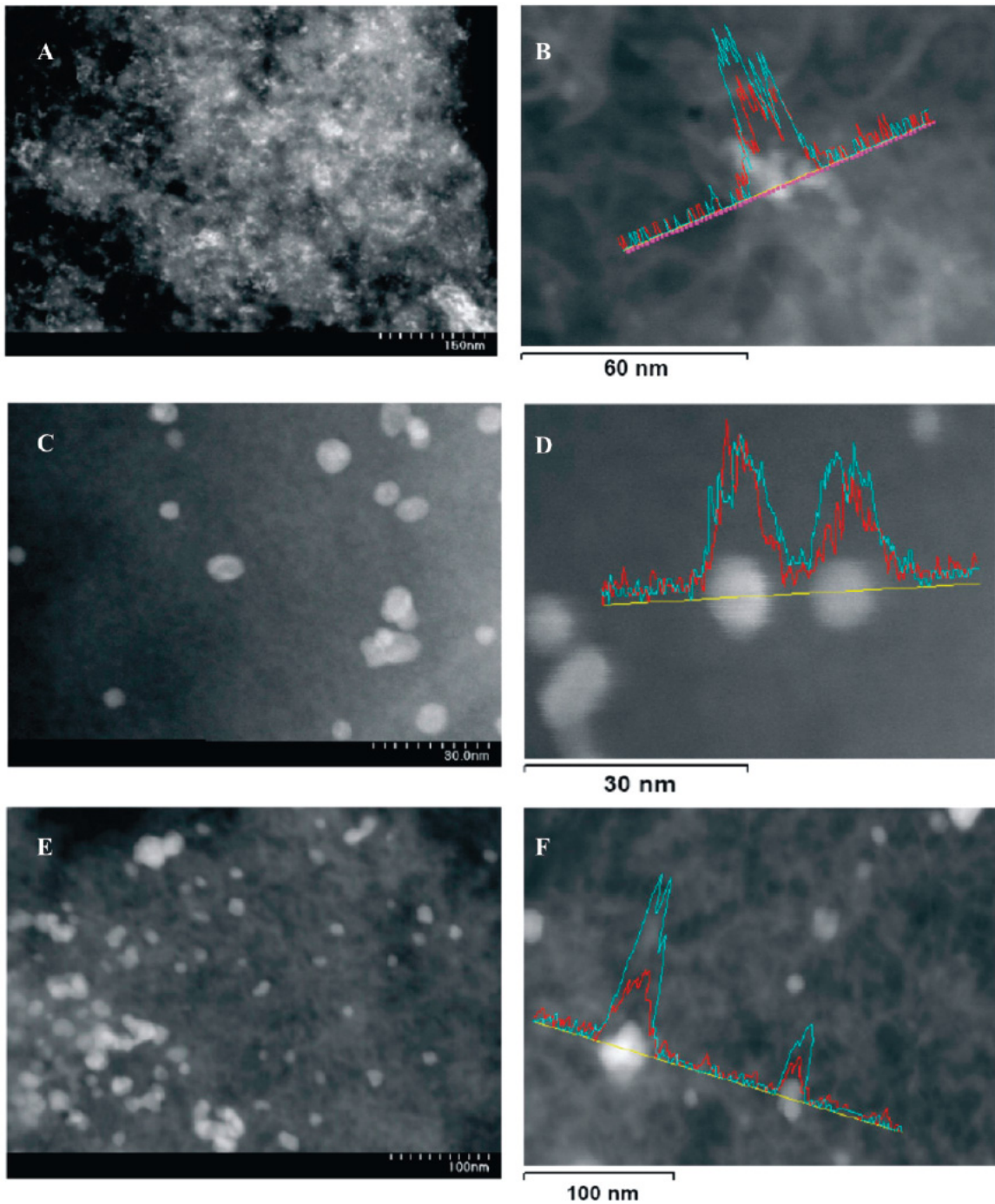


**Figure 5.2.** HRTEM images and EDS line scans of co-reduced PVP-stabilized 1:1 Pd:Au nanoparticles (a) as-synthesized in alumina, and (b) the corresponding EDS line scan; (c) in alumina calcined at 300 °C, and (d) the corresponding EDS line scan; (e) in alumina calcined at 500 °C, and (f) the corresponding EDS line scan. The blue and red EDS lines are Au and Pd, respectively.

Removal of the polymer stabilizer while maintaining the nanoparticle dispersion, composition and size represents a great challenge in utilizing pre-synthesized nanoparticles for form heterogeneous catalysts. Industrial catalysts are typically activated by thermal methods in air or inert atmospheres followed by reduction to produce a clean, reduced catalyst. We wished to identify the lowest temperature conditions which could lead to complete removal of the PVP polymer while maintaining the integrity of the nanoparticles. The as-synthesized xerogel-supported nanoparticle samples were characterized by TGA to find out the total PVP weight % and the optimal calcination temperatures. As shown in Figure 5.3a, the TGA curve of the as synthesized PdAu-alumina sample at a heating rate of 10°C/min has two distinct weight losses, with water desorbed below 100 °C (~ 10 % mass loss) and PVP decomposition at 300-500 °C (~ 41 % mass loss). Based on these observations, samples were calcined at 500<sup>0</sup> C under air for 5h and then reduced under hydrogen at 300 °C for 1h. As can be seen from Figure 5.2e, the particle sizes increased dramatically to 11.7 ± 2.9 nm for co-reduced 1:1 Pd:Au nanoparticles upon calcination at 500°C, and a great deal of particle aggregation was seen. In addition, metal segregation was problematic, as seen in the EDS line scan in Figure 5.2f. To overcome these problems, we sought to find the minimal thermal activation calcination conditions needed by running TGA experiments at a temperature just above the onset of the polymer decomposition temperature (300 °C). As shown in Figure 5.3b, by holding the temperature at 300<sup>0</sup> C for 5 h, a slightly lower mass % of polymer (~34 % mass loss) was removed at lower calcination temperatures. After calcination at 300 °C for 5 h under air, followed by the reduction under hydrogen at 300 °C for 1 h, the average particle sizes for the supported- co-reduced 1:1 Pd:Au

nanoparticles increased from  $4.1 \pm 0.7$  nm to  $5.5 \pm 1.4$  nm (Figure 5.2c). This increase is much smaller than seen at higher temperatures, and seems unavoidable to have some particle size increase due to sintering during calcination treatments. Single-particle EDS analyses of the co-reduced 1:1 Pd:Au bimetallic nanoparticles calcined at  $300\text{ }^{\circ}\text{C}$  indicates the same average compositions ( $\sim 1:1$ ) as that of the as-synthesized sample; Figure 5.2d shows a EDS line scan across several particles. These results suggest that by properly choosing thermal treatment conditions it is possible, to some extent, control the degree of sintering and hence the particle size and composition; however, some nanoparticle sintering seems unavoidable even with mild calcination conditions. In addition, the resulting particles calcined at  $300\text{ }^{\circ}\text{C}$  have been shown to be catalytically active, as will be discussed later. It should be noted that TEM and EDS measurements could not distinguish between surface and bulk compositions of the particles; EXAFS results detailed below will shed more light into the bulk vs surface distributions of the elements within the nanoparticles. Powder XRD of the calcined alumina-supported catalysts revealed peaks at  $38.0^{\circ}$ ,  $45.6^{\circ}$ , and  $67.0^{\circ}$  ( $2\theta$ ), which correspond to the  $\gamma\text{-Al}_2\text{O}_3$  phase.<sup>78</sup>

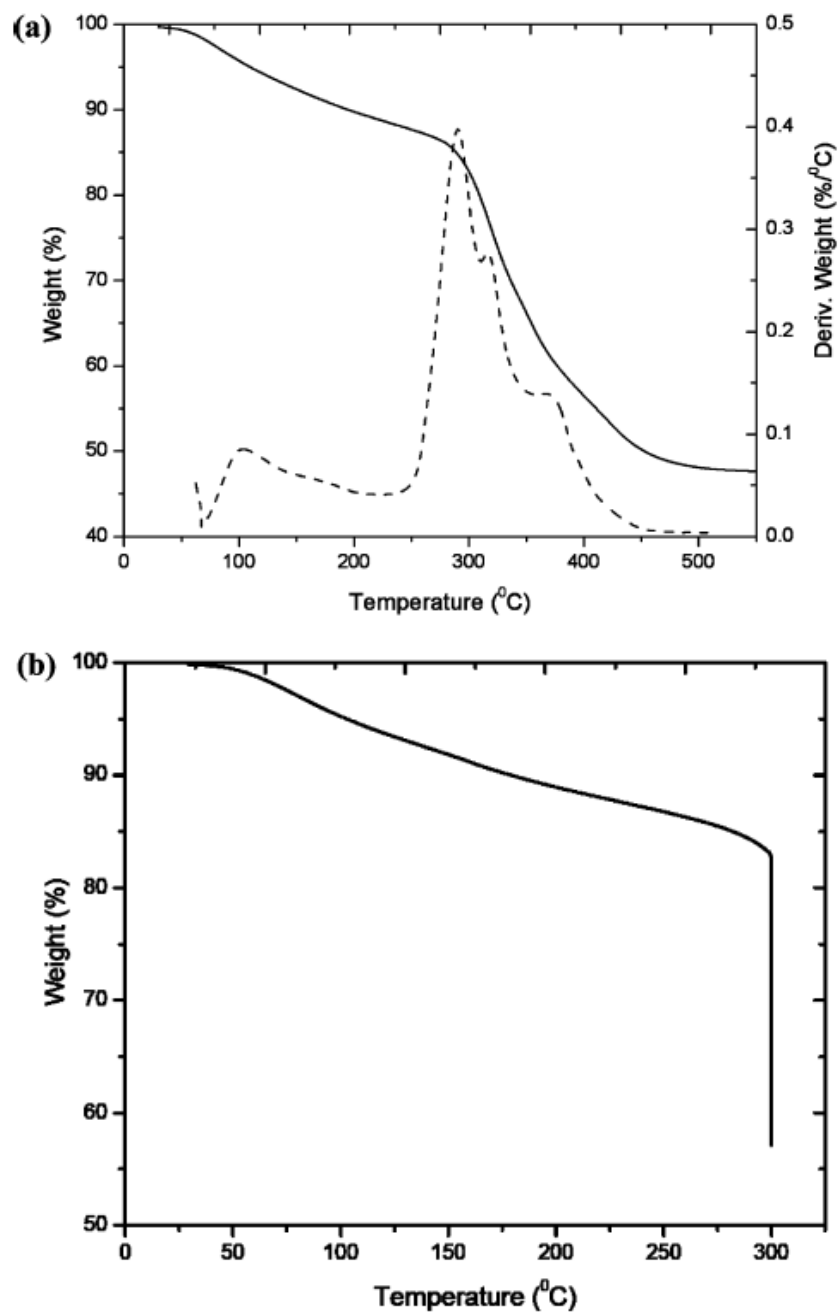


**Figure 5.3.** Thermal gravimetric analysis plots showing (a) mass loss and derivative of mass loss of PVP-stabilized 1:1 PdAu nanoparticles in alumina from 25 °C to 550 °C and (b) mass loss for same sample held at 300 °C for 5 h.

To gain further insight into the interior architecture of co-reduced PdAu nanoparticles trapped in alumina, XAS studies were carried out for both as-synthesized and calcined samples of co-reduced PdAu nanoparticles, and pure Pd and Au nanoparticles at the Au L<sub>III</sub>-edge and Pd K-edge. Initially, pure Au and Pd nanoparticles trapped in alumina were analyzed before and after calcination at 300°C. Figure 5.4 shows representative EXAFS spectra at the Au L<sub>III</sub>-edge of the co-reduced nanoparticles before calcination; high quality data was collected. It was found that the EXAFS oscillation frequencies and the features of the curves differ gradually from bulk gold to lower Au content in the bimetallic PdAu series, thus indicating some correlation between Pd and Au. This observation can be attributed to the formation of more Pd-Au bonds in the bimetallic samples.<sup>79</sup>

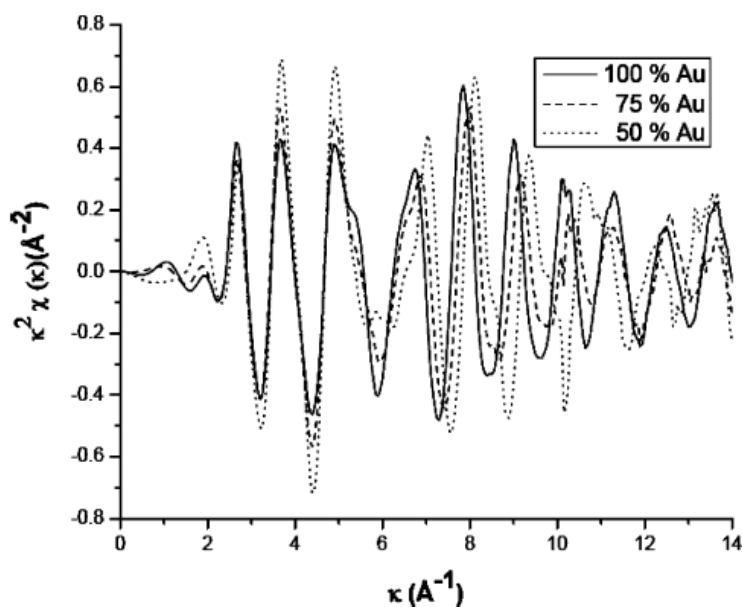


**Figure 5.4.** Au- L<sub>III</sub>-edge EXAFS in  $k$ -space for the Pd-Au alloy nanoparticle series.

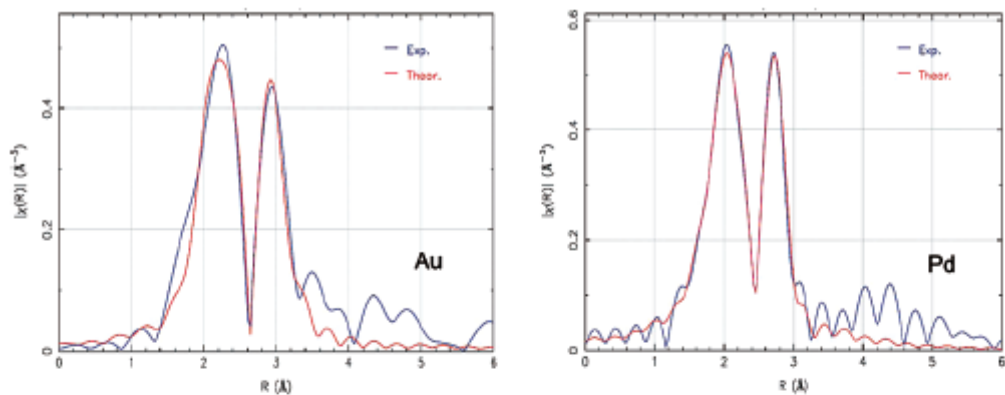


For the metallic and bimetallic nanoparticles, the Au and Pd EXAFS data of the same sample were simultaneously fit using the IFEFFIT software package.<sup>72</sup> Figure 5.5 shows the experimentally obtained Au and Pd EXAFS *r*-space for the co-reduced PdAu nanoparticles and the single shell theoretical fits; the structural parameters of the Pd:Au series generated from the EXAFS fitting parameters are presented in Tables 5.1 and 5.2. As can be seen in Figure 5.5, good fits have been obtained for all samples, confirming the high quality data of the samples. No attempt was made to fit weak shoulders at lower *r*-values in both the Au and Pd edges; these are likely due to contributions of the PVP polymer and the presence of trace levels of halide and oxide impurities bound on the surfaces.

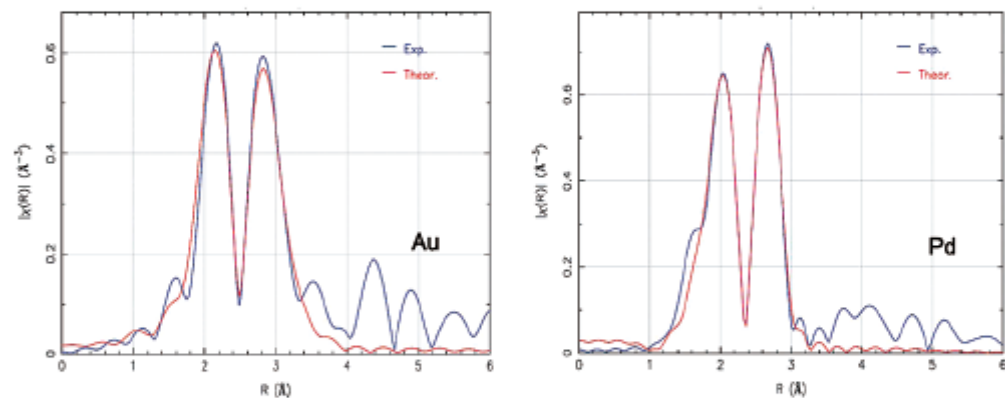
For the as-synthesized monometallic Au and Pd nanoparticles, the nearest-neighbor coordination numbers (CNs),  $N_{\text{Au-Au}}$  and  $N_{\text{Pd-Pd}}$ , are 10.8 and 8.9 respectively, both smaller than 12 (Table 5.1). This implies the presence of smaller particles and thus, relatively larger fractions of surface atoms, and that the Pd nanoparticles are significantly smaller than their Au counterparts.<sup>79,80</sup> For the gold nanoparticles the interatomic distance is 0.02 Å smaller than the bulk value of 2.86 Å. This decrease can be attributed to the increased d-d interaction in small particles due to hybridization.<sup>65,81</sup> Similarly, the Pd-Pd bond distance in Pd/Al<sub>2</sub>O<sub>3</sub> is 2.73 Å, compared to the bulk distance of 2.74 Å.<sup>82</sup> After calcination of the pure Au and Pd samples at 300 °C, slight increases in CNs were observed (Table 5.1). The Au-Au CN ( $N_{\text{Au-Au}}$ ) in the calcined Au/Al<sub>2</sub>O<sub>3</sub> system increased from 10.8 to 11.3 after calcination while in the case of Pd/Al<sub>2</sub>O<sub>3</sub> system, the  $N_{\text{Pd-Pd}}$  CN increased from 8.9 to 9.6 after calcination. This indicates that there is a moderate particle size increase due to sintering occurring in both samples.

**(a)**

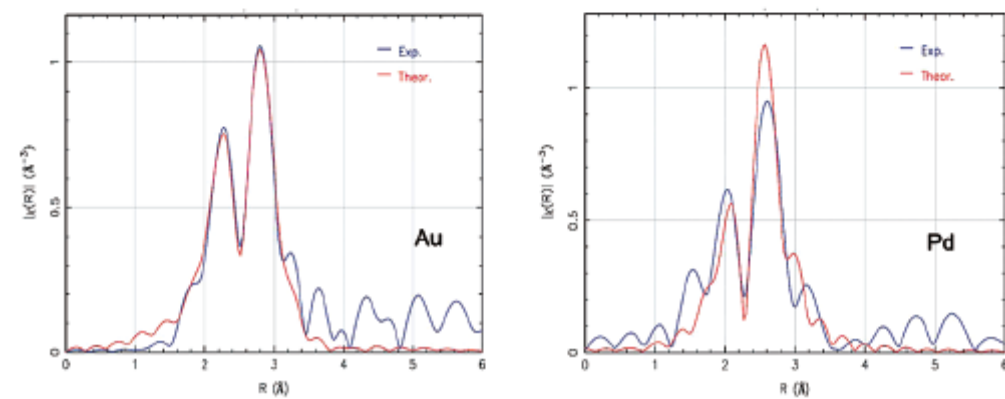
**3:1 Pd:Au NPs**



**1:1 Pd:Au NPs**



**1:3 Pd:Au NPs**



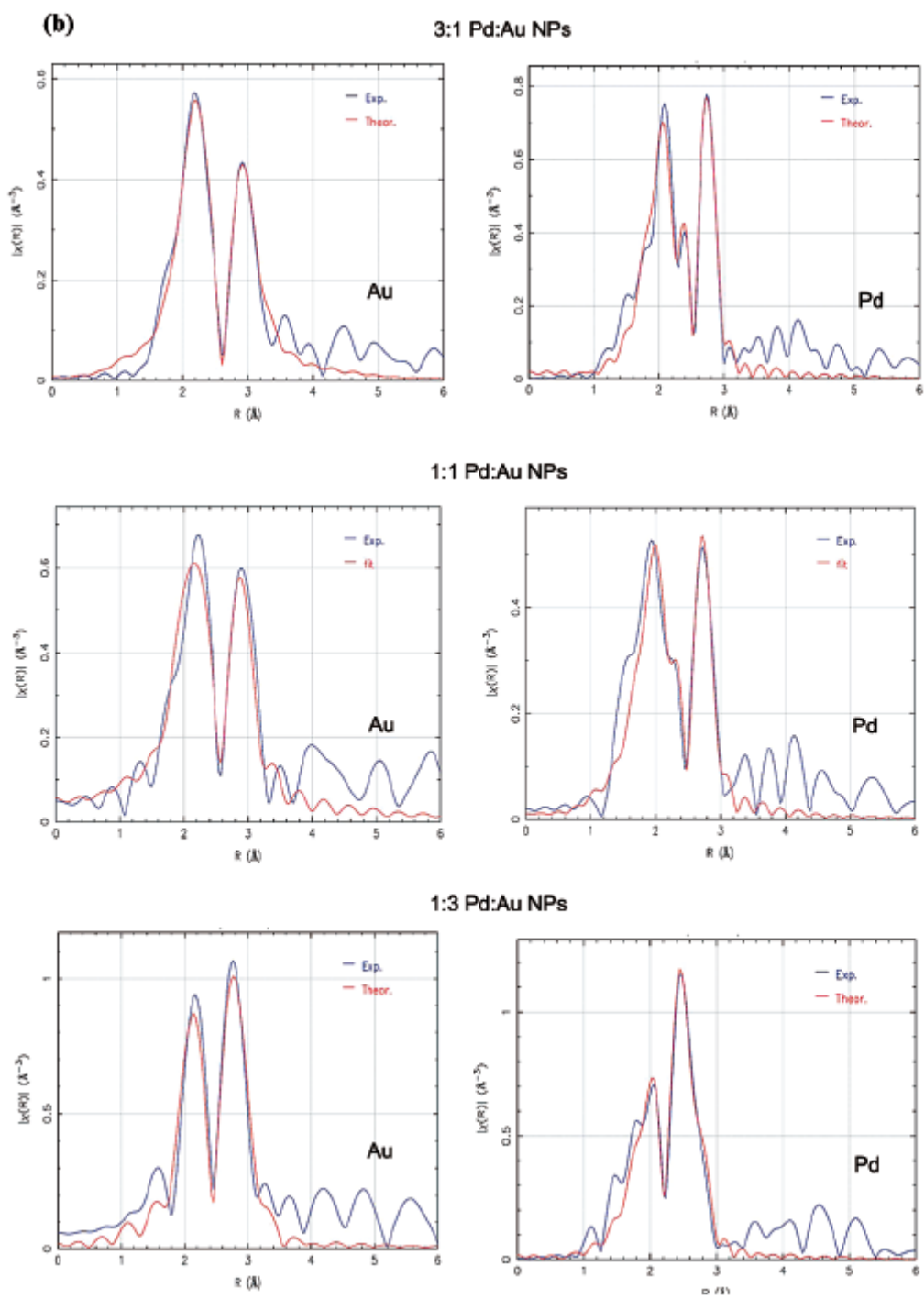


**Figure 5.5.** EXAFS single shell fits for co-reduced PdAu nanoparticle series (a) as-synthesized in alumina, (b) calcined at 300 °C.

**Table 5.1.** EXAFS fitting parameters of pure metals.

Sample	Shell	N	$R_j$ (Å)	$\Delta E_0$ (eV)	$\sigma^2$ (Å <sup>2</sup> )	R-factor
Pure Au (as-synthesized)	Au-Au	10.8 (0.5)	2.838(0.046)	4.2(0.3)	0.010(0.001)	0.006
Pure Au (calcined)	Au-Au	11.3 (0.5)	2.858(0.026)	5.5(0.2)	0.008(0.001)	0.005
Pure Pd (as-synthesized)	Pd-Pd	8.9 (0.9)	2.732(0.018)	-7.0(0.6)	0.006(0.001)	0.016
Pure Pd (calcined)	Pd-Pd	9.6(1.1)	2.731(0.019)	-5.8(0.7)	0.007(0.001)	0.005
Au foil	Au-Au	12	2.861(0.023)	5.2(0.3)	0.008(0.001)	0.008
Pd foil	Pd-Pd	12	2.743(0.007)	-5.3(0.5)	0.005(0.001)	0.004

In order to interpret the EXAFS parameters of the as-synthesized co-reduced PdAu nanoparticles, the total CNs around each metal are calculated as follows:  $N_{Au-M} = N_{Au-Au} + N_{Au-Pd}$  and  $N_{Pd-M} = N_{Pd-Pd} + N_{Pd-Au}$ . The total metal CNs,  $N_{Au-M}$  and  $N_{Pd-M}$ , for all three members of the PdAu series (before and after calcination) of catalyst are smaller than that expected for bulk fcc alloys (*i.e.* 12). This is due to the large number of under-coordinated surface atoms on the surface of the particles.<sup>79</sup> Looking at the three as-synthesized co-reduced PdAu samples in Table 5.2, it is noted that the  $N_{Pd-M}$  and  $N_{Au-M}$  CNs change linearly with Pd and Au concentration, which would be expected for ideal random alloys.<sup>83</sup> However, careful observation on the CNs indicated that  $N_{Au-M}$  CNs exceed  $N_{Pd-M}$  CNs for all of the as-synthesized bimetallic PdAu nanoparticle samples. This is indicative of the presence of slightly more Pd atoms on the surface of the particles than the bulk, thus the particles are not true alloys but have slightly Au-rich core and Pd-rich shells. In the case of 3:1 Pd:Au nanoparticles, the value of the  $N_{Au-M}$  CN is ~12 which indicates that the Au atoms nearly all reside in the core of the nanoparticle. We are uncertain as to the reasons for this deviation from alloy behavior in the as-synthesized co-reduced PdAu samples, but note that other groups have reported similar findings.<sup>32,79,83,84</sup>

**Table 5.2.** EXAFS fitting parameters of PdAu nanoparticle series.

Sample	Shell	$N$	$R_j$ ( $\text{\AA}$ )	$\Delta E_0$ (eV)	$\sigma^2$ ( $\text{\AA}^2$ )	$R$ -factor
1:3 Pd:Au (as-synthesized)	Au-Au	8.0(1.5)	2.798(0.008)	4.7(0.5)	0.010(0.002)	0.016
	Au-Pd	1.9(0.6)	2.770(0.005)		0.010(0.001)	
	Pd-Pd	0.7(0.2)	2.749(0.015)	-6.2(0.4)	0.006(0.002)	
	Pd-Au	8.9(0.6)	2.770(0.005)		0.010(0.001)	
1:3 Pd:Au (calcined)	Au-Au	9.2(1.4)	2.808(0.043)	4.6(0.5)	0.011(0.002)	0.007
	Au-Pd	1.8(0.4)	2.794(0.056)		0.008(0.001)	
	Pd-Pd	2.1(1.1)	2.739(0.112)	-6.1(0.7)	0.008(0.004)	
	Pd-Au	8.8(1.5)	2.794(0.056)		0.008(0.001)	
1:1 Pd:Au (as-synthesized)	Au-Au	7.0(2.3)	2.801(0.016)	4.7(0.6)	0.010(0.004)	0.004
	Au-Pd	4.2(0.8)	2.777(0.040)		0.010(0.001)	
	Pd-Pd	3.6(0.3)	2.776(0.040)	-5.8(0.2)	0.010(0.001)	
	Pd-Au	7.2(0.4)	2.777(0.040)		0.010(0.001)	
1:1 Pd:Au (calcined)	Au-Au	9.2(2.5)	2.782(0.035)	1.7(1.2)	0.008(0.002)	0.016
	Au-Pd	2.7(1.0)	2.770(0.047)		0.009(0.002)	
	Pd-Pd	3.0(1.6)	2.726(0.091)	-6.4(1.0)	0.012(0.005)	
	Pd-Au	6.9(1.8)	2.770(0.047)		0.009(0.002)	
3:1 Pd:Au (as-synthesized)	Au-Au	5.1(2.6)	2.834(0.030)	4.4(1.2)	0.009(0.006)	0.019
	Au-Pd	7.1(1.9)	2.866(0.020)		0.009(0.002)	
	Pd-Pd	7.2(1.5)	2.779(0.010)	1.9(0.8)	0.009(0.002)	
	Pd-Au	2.6(1.6)	2.866(0.020)		0.009(0.002)	
3:1 Pd:Au (calcined)	Au-Au	5.3(3.1)	2.777(0.026)	4.8(1.1)	0.006(0.006)	0.018
	Au-Pd	6.1(1.5)	2.772(0.014)		0.007(0.002)	
	Pd-Pd	6.4(0.9)	2.746(0.008)	-6.5(0.5)	0.007(0.001)	
	Pd-Au	4.1(1.1)	2.772(0.014)		0.007(0.002)	
Core-shell 1:3 Pd:Au (as-synthesized)	Au-Au	10.1(0.8)	2.850(0.002)	5.5(0.4)	0.008(0.000)	0.013
	Au-Pd	0.9(0.6)	2.798(0.053)		0.008(0.004)	
	Pd-Pd	8.1(2.1)	2.772(0.079)	-7.8(1.0)	0.008(0.002)	
	Pd-Au	4.0(2.4)	2.798(0.053)		0.008(0.004)	
Core-shell 1:3 Pd:Au (calcined)	Au-Au	8.8(2.4)	2.850(0.004)	6.2(1.3)	0.006(0.003)	0.013
	Au-Pd	2.3(1.3)	2.801(0.044)		0.006(0.004)	

Several possible explanations include the presence of slightly faster kinetics for Au reduction vs. Pd reduction upon synthesis of the nanoparticles with  $\text{NaBH}_4$ , or surface segregation of the Pd to the surface due to oxidation, or preferential binding of the PVP stabilizer thus pulling Pd to the surface of the nanoparticles. However, it should be noted that all as-synthesized samples were kept under nitrogen during synthesis and prior to

EXAFS analysis. The coordination numbers obtained from EXAFS analysis can be a strong function of the particle size if the particle size is small (3-5 nm) and the particle size distribution is narrow.<sup>82</sup> This behavior has been used by others in EXAFS analysis to estimate average particle sizes.<sup>64,66</sup> The average of the first shell  $N_{\text{Au-M}}$  and  $N_{\text{Pd-M}}$  CNs of the 1:1 Pd: Au system is found to be 11.0, indicating an average particle size from EXAFS of approximately 4.6 nm which is close to the value of 4.1 nm obtained from HRTEM measurement.<sup>66</sup>

The calcined (300°C) co-reduced PdAu materials also show higher total Au CNs than Pd CNs ( $N_{\text{Au-M}} > N_{\text{Pd-M}}$ ) as was observed in the particles prior to calcination, which indicates that structures were fairly well preserved after the thermal treatment method (Figure 5.5b, Table 5.2). Others have previously noted PdAu alloy to Au core-Pd shell transitions upon calcination and/ or ligand extractions, presumably due to Pd metal oxidation and re-reduction during the synthesis,<sup>19,83</sup> however, no increase in Pd surface segregation occurred for the calcined samples, likely due to the low calcination temperatures employed in this work. It should be noted that due to fairly high CN errors in EXAFS analysis (~15-20%) it is extremely difficult to monitor small changes in Pd and Au bulk-vs-surface speciation by EXAFS. In the calcined samples the Au-Au bond distance decreases with increasing Pd content, from 2.81 Å in 1:3 Pd: Au sample to 2.79 Å in the 1:1 Pd: Au sample to 2.78 Å in 3:1 Pd: Au sample. This decrease in distance has been attributed by others to the increased d-d interaction in small particles due to hybridization.<sup>65</sup> In addition, the Debye-Waller EXAFS terms ( $\sigma^2$ ) for the Au-Au and Pd-Pd in the as-synthesized nanoparticle systems are all slightly higher than seen after calcination. This can be attributed to contributions from the slightly large number of

surface atoms in as-synthesized system, which would have larger  $\sigma^2$  values.<sup>80</sup> These findings also support to the HRTEM measurement where small particle size change was observed after calcination.

In order to further test whether the rational catalyst design strategy is effective, alumina-supported 1:3 Pd:Au core-shell nanoparticles were also synthesized. Core-shell nanoparticles are interesting because they can be used as a tool for systematic investigations of the electronic properties of catalysts, and can minimize the amount of precious metals, such as Pd and Pt during the synthesis of industrial catalysts.<sup>35,85</sup> HRTEM images of the supported 1:3 Pd:Au core-shell catalysts indicate the presence of particles with particle size of  $5.0 \pm 1.3$  nm (Figure 5.6a). A small particle size change from  $5.0 \pm 1.3$  nm to  $5.5 \pm 1.9$  nm has been observed after calcination at 300°C to remove the PVP stabilizer (Figure 5.6b). Large-area and single-particle energy-dispersive spectroscopy (EDS) analyses of the calcined core-shell nanoparticles indicated an average composition of approximately 33:67 of Pd:Au, which is in agreement to their molar percentage of respective salts during the synthesis. More importantly, the EDS line scan shown in Figure 5.6c strongly supports core-shell formation, with the FWHM of the two Au EDS signals (from left to right) of 6.0 nm and 7.0 nm, respectively, compared to 4.0 nm and 3.0 nm for the two Pd EDS signals. This strongly supports the fact that Pd-core-Au-shell compositional fidelity was maintained during the synthesis of the supported catalyst.

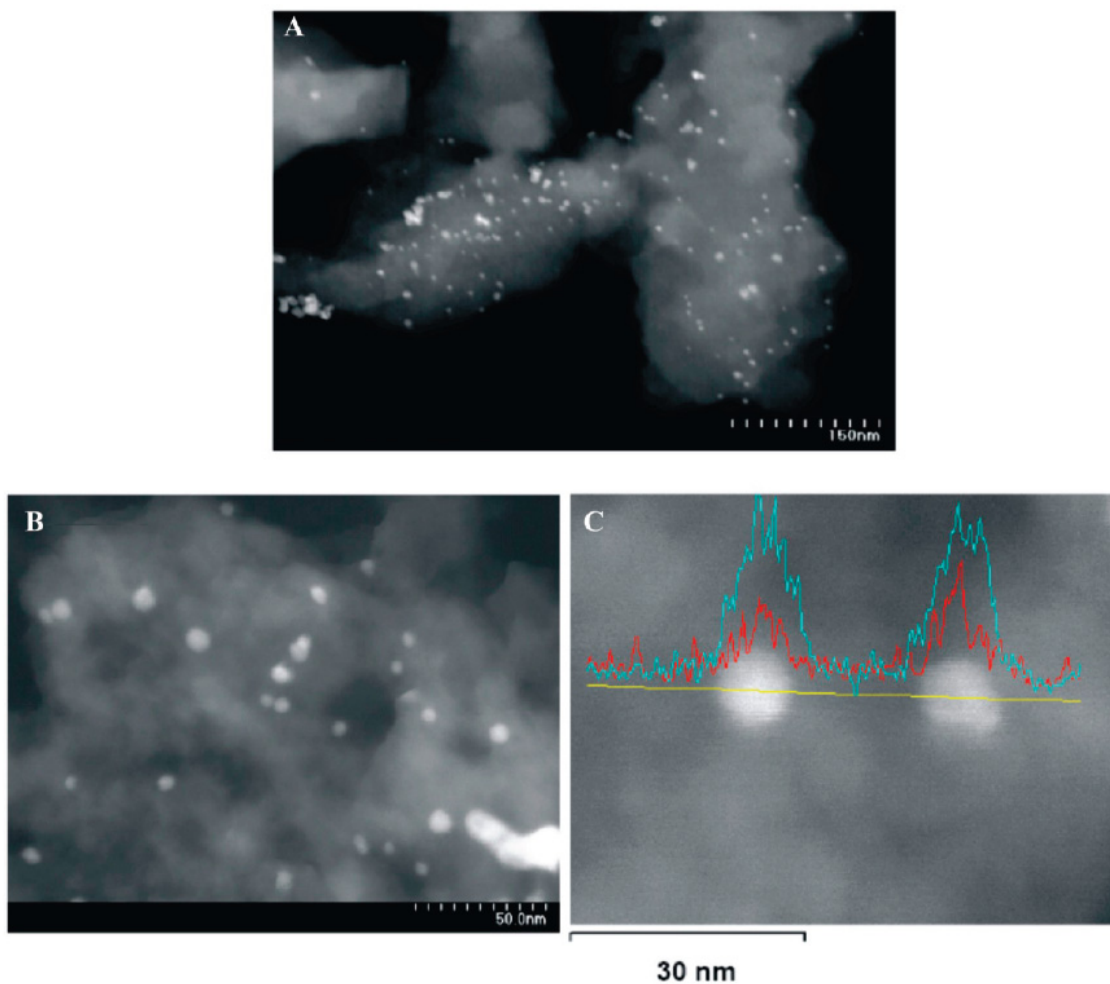


**Figure 5.6.** HRTEM images of core-shell PdAu nanoparticles (a) as-synthesized in alumina, (b) after calcination at 300 °C and c) EDS line scan of core-shell PdAu nanoparticles in alumina after calcination at 300 °C. The blue and red EDS lines are Au and Pd, respectively.

In order to further confirm that the core-shell structure was indeed fabricated in the as-synthesized alumina-supported sample and was maintained after calcination, EXAFS characterization of the core-shell Pd-Au nanoparticles was carried out. Single shell fits are shown in Figure 5.7, and the fitting results are shown in the Table 5.2.



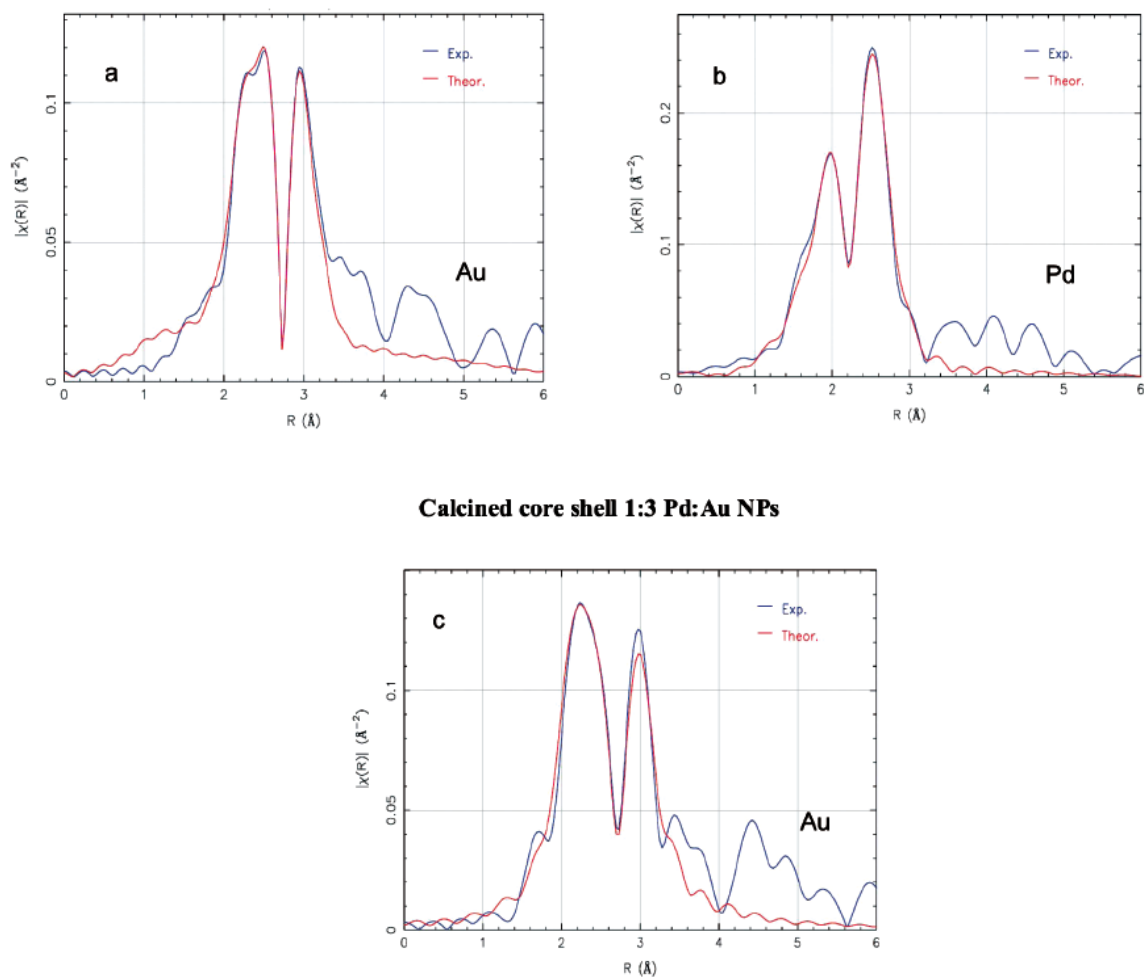


**Figure 5.7.** EXAFS fits for core-shell PdAu nanoparticles (a,b) as-synthesized in alumina, and (c) after calcination at 300 °C.

The formation of a Pd:Au core-shell structure can be confirmed from the CNs obtained from the EXAFS fitting of the as-synthesized sample; the  $N_{\text{Pd-M}}$  CN is approximately 12, and is much higher than the  $N_{\text{Au-M}}$  CN (11.0), thus confirming the presence of a Pd-rich core and Au-rich shell. In addition, the first shell Au-Au distance is much higher than that seen for co-reduced PdAu samples and is fairly similar to that seen for pure Au clusters. Unfortunately, due to instrumental availability only the Au  $L_{\text{III}}$ -edge data was collected on the calcined sample, however, the resulting  $N_{\text{Au-M}}$  coordination

number of  $\sim 11.1$  suggests that Au atoms are still primarily on the surface of the nanoparticle, but the higher  $N_{\text{Au-Pd}}$  suggests some alloying at the Au-Pd interface has occurred.

Finally, the XANES spectra of the Au  $L_{\text{III}}$  edge of the series of as-synthesized co-reduced PdAu nanoparticles and bulk Au foil are shown in Figure 5.8. The white line, the first feature after the edge jump, can be clearly seen for the Au foil and also for the pure Au nanoparticle catalysts at 11925 eV.<sup>56</sup> The Au  $L_{\text{III}}$ -edge probes the transition of 2p electrons to unoccupied 5d states or empty density of states that have mainly d-character. Hence, the intensity of the white line depends on number of d-holes in the Au atoms. For bulk gold the electronic configuration would be expected to be  $5d^{10} 6s^1$ ; however due to the presence of large number of atoms, the overlap of bands becomes significant which leads to more pronounced s-p-d hybridization. Due to this s-p-d hybridization a small amount of 5d electrons are transferred to s-p states, thus resulting in an electronic configuration of  $5d^{10-x} 6s^{1+x}$  for bulk gold.<sup>86,87</sup> The weak white line in the Au-foil XANES spectra can be attributed to this depletion of the d-band. While going from the bulk to nanosized particles the number of atoms forming the lattice decreases and hence the width of bands also decreases, which leads to less overlap of bands and thus, less s-p-d hybridization. Consequently, the white line intensity of small Au nanoparticles should be less intense than that of the bulk, and indeed this has been documented by a number of other groups.<sup>79,87,88</sup>

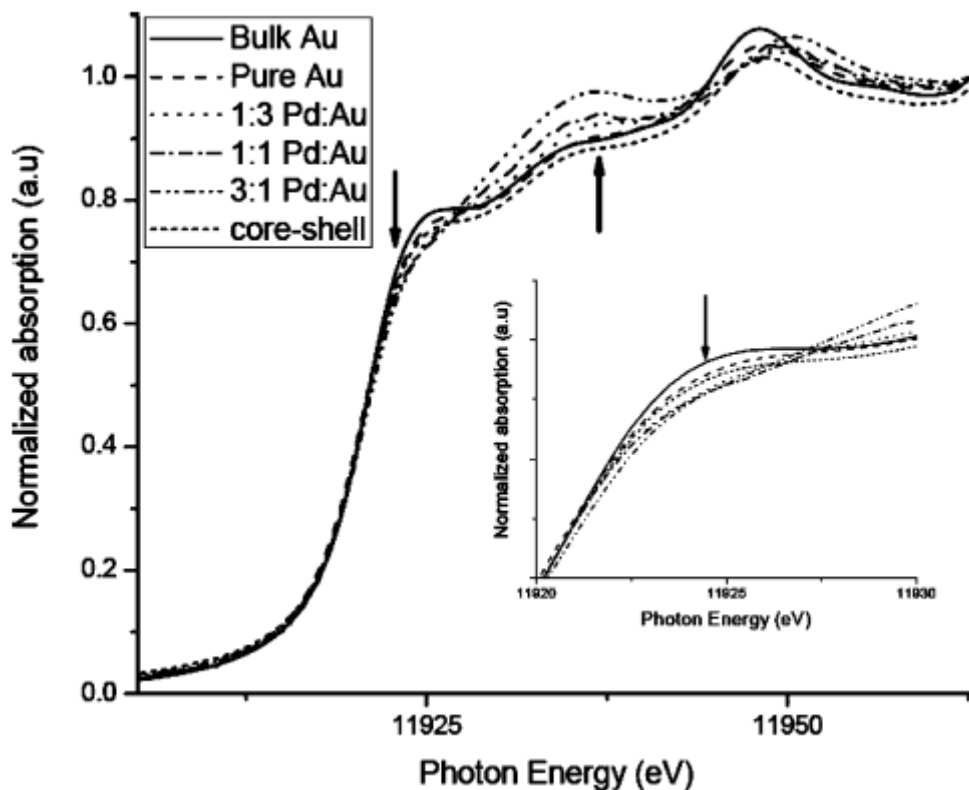


**Figure 5.8.** The Au L<sub>3</sub>-XANES spectra of as-synthesized PdAu alloy and core-shell nanoparticle series in alumina.

Upon examination of the XANES data in Figure 5.8, it is noted that the intensity of the white line diminishes with increasing Pd content and is completely absent for 3:1 Pd:Au nanoparticles. The same trend has also been observed for the calcined samples, which confirms that no major electronic changes have occurred after calcination. Zhang *et al.*<sup>79</sup> also found that increasing Pd content in PdAu alloys has a pronounced effect in the enhanced filling of the Au d-band (an increase of the d-electron density), leading to a decrease in the white line. A possible reason for the enhanced filling of the Au d-band in the PdAu alloys is via charge transfer from the Pd s-band (and perhaps p-band) to the Au d-band.<sup>89</sup> A second feature in the XANES spectra in Figure 5.8 that merits attention is the

increase in the intensity of the second band after the edge (11935 eV) with increased Pd loading. Others have attributed changes in this second feature to distance effects in which intra-atomic redistribution of charge occurs when atoms come closer together or further apart.<sup>90</sup> Finally, the XANES spectra of the Au-L<sub>III</sub> edge for the Pd-core-Au-shell nanoparticles is also included in Figure 5.8, and a white line feature can be seen. This further supports the presence of a Pd shell-Au core structure, particularly as the white line feature is much more intense for the 1:3 Pd:Au core-shell sample than it is for the 1:3 Pd:Au co-reduced sample.

To test the catalytic activity of these catalysts, the catalytic hydrogenation of allyl alcohol was chosen as a suitable test reaction. This reaction has been extensively studied on both Au and Pd metals and is therefore excellently suited to find out the catalytic activity of these nanoparticle catalysts synthesized by our methods.<sup>24,37</sup> The pure Pd catalyst is found to be catalytic active towards the hydrogenation of allyl alcohol with a turnover frequency (TOF) of 203 h<sup>-1</sup>. For the 3:1 Pd:Au co-reduced catalysts, there is a slight increase in the TOF to 210 h<sup>-1</sup>. Others, including ourselves, have previously shown much higher synergetic interactions between Pd and Au,<sup>24,25,37</sup> the small synergetic effect here may possibly be attributed to the fact that the hydrogenation reaction was performed in water where mass-transfer limitation problems (*i.e.* H<sub>2</sub> to the catalyst surface) are a major factor.<sup>25</sup> However, these results confirm that the catalysts are catalytically active. The catalytic activity of calcined core-shell Pd-Au nanoparticle catalysts showed much lower catalytic activity (TOF of 60 h<sup>-1</sup>) compared to that of the alloy PdAu catalysts. This lower activity can be attributed to the presence of large number of surface Au atoms, which typically show no activity towards the hydrogenation of allyl alcohol, and lend

support to fairly good retention of the Pd-core, Au-shell structure after calcination of the nanoparticles.<sup>24</sup> High temperature gas-phase reactions with rationally-designed supported-PdAu nanoparticles are currently underway in our laboratories.

## 5.5. Conclusions

The field of heterogeneous catalysis has greatly been improved by the development of nanoparticle synthesis and characterization methods. We have shown that one such improvement is the ability to rationally control nanoparticle catalyst structures during synthesis, which enables the production of catalysts with specific catalytic selectivity. A series of PVP-stabilized Au, Pd and PdAu bimetallic nanoparticles were synthesized and then trapped in alumina matrix by sol-gel chemistry. Careful high-temperature calcinations were carried out to remove the organic PVP stabilizer and generate structurally and compositionally well-defined nanoparticles. The change in composition and internal architecture was investigated before and after calcination by TGA, HRTEM, EDS, EXAFS, and XANES. The structural investigations suggest that co-reduced PdAu nanoparticles have slightly Au rich cores and Pd-rich shells. The Au L<sub>III</sub> XANES spectra reveal an increase in the d-holes of the Au 5d valence band as Au content rises in the co-reduced PdAu bimetallic nanoparticle catalysts. We further showed that supported- Pd core-Au shell nanoparticles can be synthesized by such methods, and that the structural and geometrical integrity was maintained after the calcinations step. Finally, the co-reduced PdAu catalysts are found to be catalytically active towards the hydrogenation of allyl alcohol and should be active for many other catalytic reactions.<sup>20,24</sup>

## Acknowledgements

The authors would like to acknowledge financial assistance from the National Sciences and Engineering Research Council of Canada (NSERC), and thank Ning Chen and Jeff Warner at the Canadian Light Source for assistance with XAS measurements. The XAS measurements described in this paper were performed at the Canadian Light Source, which is supported by NSERC, NRC, CIHR, and the University of Saskatchewan.

## 5.6. References

- (1) Bond, G. C. *Chem. Rev.* **1991**, *20*, 441-475.
- (2) Sinfelt, J. H. *Science* **1977**, *195*, 641-646.
- (3) Sinfelt, J. H. *Acc. Chem. Res.* **1977**, *10*, 15-20.
- (4) Sinfelt, J. H. *Acc. Chem. Res.* **1987**, *20*, 134-139.
- (5) Toshima, N.; Yonezawa, T. *New J. Chem.* **1998**, *22*, 1179-1201.
- (6) Enache, D. I.; Edwards, J. K.; Landon, P.; Solsona-Espriu, B.; Carley, A. F.; Herzing, A. A.; Watanabe, M.; Kiely, C. J.; Knight, D. W.; Hutchings, G. J. *Science* **2006**, *311*, 362-365.
- (7) Edwards, J. K.; Carley, A. F.; Herzing, A. A.; Kiely, C. J.; Hutchings, G. J. *Faraday Discuss.* **2008**, *138*, 225-239.
- (8) Landon, P.; Collier, P. J.; Papworth, A. J.; Kiely, C. J.; Hutchings, G. J. *Chem. Commun.* **2002**, 2058-2059.
- (9) Solsona, B. E.; Edwards, J. K.; Landon, P.; Carley, A. F.; Herzing, A.; Kiely, C. J.; Hutchings, G. J. *Chem. Mater.* **2006**, *18*, 2689-2695.
- (10) Edwards, J. K.; Solsona, B.; Landon, P.; Carley, A. F.; Herzing, A.; Watanabe, M.; Kiely, C. J.; Hutchings, G. J. *J. Mater. Chem.* **2005**, *15*, 4595-4600.

- (11) Edwards, J. K.; Solsona, B. E.; Landon, P.; Carley, A. F.; Herzing, A.; Kiely, C. J.; Hutchings, G. J. *J. Catal.* **2005**, *236*, 69-79.
- (12) Landon, P.; Collier, P. J.; Carley, A. F.; Chadwick, D.; Papworth, A. J.; Burrows, A.; Kiely, C. J.; Hutchings, G. J. *Phys. Chem. Chem. Phys.* **2003**, *5*, 1917-1923.
- (13) Han, Y. F.; Zhong, Z. Y.; Ramesh, K.; Chen, F. X.; Chen, L. W.; White, T.; Tay, Q. L.; Yaakub, S. N.; Wang, Z. *J. Phys. Chem. C* **2007**, *111*, 8410-8413.
- (14) Ketchie, W. C.; Murayama, M.; Davis, R. J. *J. Catal.* **2007**, *250*, 264-273.
- (15) Villa, A.; Campione, C.; Prati, L. *Catal. Lett.* **2007**, *115*, 133-136.
- (16) Conte, M.; Carley, A. F.; Attard, G.; Herzing, A. A.; Kiely, C. J.; Hutchings, G. J. *J. Catal.* **2008**, *257*, 190-198.
- (17) Scott, R. W. J.; Sivadinarayana, C.; Wilson, O. M.; Yan, Z.; Goodman, D. W.; Crooks, R. M. *J. Am. Chem. Soc.* **2005**, *127*, 1380-1381.
- (18) Lopez-Sanchez, J. A.; Dimitratos, N.; Miedziak, P.; Ntainjua, E.; Edwards, J. K.; Morgan, D.; Carley, A. F.; Tiruvalam, R.; Kiely, C. J.; Hutchings, G. J. *Phys. Chem. Chem. Phys.* **2008**, *10*, 1921-1930.
- (19) Herzing, A. A.; Carley, A. F.; Edwards, J. K.; Hutchings, G. J.; Kiely, C. J. *Chem. Mater.* **2008**, *20*, 1492-1501.
- (20) Parvulescu, V. I.; Parvulescu, V.; Eudruschat, U.; Filoti, G.; Wagner, F. E.; Kubel, C.; Richards, R. *Chem. Eur. J.* **2006**, *12*, 2343-2357.
- (21) Chen, M. S.; Kumar, D.; Yi, C. W.; Goodman, D. W. *Science* **2005**, *310*, 291-293.
- (22) Wei, T.; Wang, J.; Goodman, D. W. *J. Phys. Chem. C* **2007**, *111*, 8781-8788.
- (23) Wang, D.; Villa, A.; Porta, F.; Su, D. S.; Prati, L. *Chem. Commun.* **2006**, 1956-1958.
- (24) Dash, P.; Dehm, N. A.; Scott, R. W. J. *J. Mol. Catal. A: Chem.* **2008**, *286*, 114-119.
- (25) Hou, W. B.; Dehm, N. A.; Scott, R. W. J. *J. Catal.* **2008**, *253*, 22-27.
- (26) Ertl, G.; Knozinger, H.; Weitkamp, J. *Handbook of Heterogeneous Catalysis*; Wiley/VCH: New York/Weinheim, **1997**.
- (27) Haruta, M. *Catal. Today* **1997**, *36*, 153-166.

- (28) Hoover, N. N.; Auten, B. J.; Chandler, B. D. *J. Phys. Chem. B* **2006**, *110*, 8606-8612.
- (29) Lindner, E.; Schneller, T.; Auer, F.; Mayer, H. A. *Angew. Chem. Int. Ed.* **1999**, *38*, 2155-2174.
- (30) Schweyer, F.; Braunstein, P.; Estournes, C.; Guille, J.; Kessler, H.; Paillaud, J. L.; Rose, J. *Chem. Commun.* **2000**, 1271-1272.
- (31) Mandal, S.; Roy, D.; Chaudhari, R. V.; Sastry, M. *Chem. Mater.* **2004**, *16*, 3714-3724.
- (32) Toshima, N.; Harada, M.; Yamazaki, Y.; Asakura, K. *J. Phys. Chem.* **1992**, *96*, 9927-9933.
- (33) Du, Y. K.; Yang, P.; Mou, Z. G.; Hua, N. P.; Jiang, L. *J. Appl. Polym. Sci.* **2006**, *99*, 23-26.
- (34) Bonnemann, H.; Brijioux, W.; Brinkmann, R.; Dinjus, E.; Jousen, T.; Korall, B. *Angew. Chem. Int. Ed.* **1991**, *30*, 1312-1314.
- (35) Schmid, G.; Lehnert, A.; Malm, J. O.; Bovin, J. O. *Angew. Chem. Int. Ed.* **1991**, *30*, 874-876.
- (36) Scott, R. W. J.; Wilson, O. M.; Crooks, R. M. *Chem. Mater.* **2004**, *16*, 5682-5688.
- (37) Scott, R. W. J.; Wilson, O. M.; Crooks, R. M. *J. Phys. Chem. B* **2005**, *109*, 692-704.
- (38) Scott, R. W. J.; Wilson, O. M.; Oh, S. K.; Kenik, E. A.; Crooks, R. M. *J. Am. Chem. Soc.* **2004**, *126*, 15583-15591.
- (39) Lafaye, G.; Siani, A.; Marecot, P.; Amiridis, M. D.; Williams, C. T. *J. Phys. Chem. B* **2006**, *110*, 7725-7731.
- (40) Lang, H. F.; May, R. A.; Iversen, B. L.; Chandler, B. D. *J. Am. Chem. Soc.* **2003**, *125*, 14832-14836.
- (41) Lang, H. G.; Maldonado, S.; Stevenson, K. J.; Chandler, B. D. *J. Am. Chem. Soc.* **2004**, *126*, 12949-12956.
- (42) Zheng, N. F.; Stucky, G. D. *J. Am. Chem. Soc.* **2006**, *128*, 14278-14280.
- (43) Budroni, G.; Corma, A. *Angew. Chem. Int. Ed.* **2006**, *45*, 3328-3331.



- (44) Konya, Z.; Puentes, V. F.; Kiricsi, I.; Zhu, J.; Ager, J. W.; Ko, M. K.; Frei, H.; Alivisatos, P.; Somorjai, G. A. *Chem. Mater.* **2003**, *15*, 1242-1248.
- (45) Long, C. G.; Gilbertson, J. D.; Vijayaraghavan, G.; Stevenson, K. J.; Pursell, C. J.; Chandler, B. D. *J. Am. Chem. Soc.* **2008**, *130*, 10103-10115.
- (46) Chou, J.; McFarland, E. W. *Chem. Commun.* **2004**, 1648-1649.
- (47) Song, H.; Rioux, R. M.; Hoefelmeyer, J. D.; Komor, R.; Niesz, K.; Grass, M.; Yang, P. D.; Somorjai, G. A. *J. Am. Chem. Soc.* **2006**, *128*, 3027-3037.
- (48) Bratlie, K. M.; Lee, H.; Komvopoulos, K.; Yang, P. D.; Somorjai, G. A. *Nano Lett.* **2007**, *7*, 3097-3101.
- (49) Bonnemann, H.; Endruschat, U.; Tesche, B.; Rufinska, A.; Lehmann, C. W.; Wagner, F. E.; Filoti, G.; Parvulescu, V.; Parvulescu, V. I. *Eur. J. Inorg. Chem.* **2000**, 819-822.
- (50) Singh, A.; Chandler, B. D. *Langmuir* **2005**, *21*, 10776-10782.
- (51) Sun, J. M.; Ma, D.; Zhang, H.; Liu, X. M.; Han, X. W.; Bao, X. H.; Weinberg, G.; Pfander, N.; Su, D. S. *J. Am. Chem. Soc.* **2006**, *128*, 15756-15764.
- (52) Min, B. K.; Wallace, W. T.; Goodman, D. W. *Surf. Sci.* **2006**, *600*, L7-L11.
- (53) Bond, G. C.; Rawle, A. F. *J. Mol. Catal. A: Chem.* **1996**, *109*, 261-271.
- (54) Juszczyk, W.; Karpinski, Z.; Lomot, D.; Pielaszek, J.; Sobczak, J. W. *J. Catal.* **1995**, *151*, 67-76.
- (55) Meitzner, G.; Sinfelt, J. H. *Catal. Lett.* **1995**, *30*, 1-10.
- (56) Sinfelt, J. H.; Meitzner, G. D. *Acc. Chem. Res.* **1993**, *26*, 1-6.
- (57) Via, G. H.; Drake, K. F.; Meitzner, G.; Lytle, F. W.; Sinfelt, J. H. *Catal. Lett.* **1990**, *5*, 25-33.
- (58) Meitzner, G.; Via, G. H.; Lytle, F. W.; Sinfelt, J. H. *J. Phys. Chem.* **1992**, *96*, 4960-4964.
- (59) Meitzner, G.; Via, G. H.; Lytle, F. W.; Sinfelt, J. H. *Physica B* **1989**, *158*, 138-141.
- (60) Sinfelt, J. H.; Via, G. H.; Lytle, F. W. *Catal. Rev.-Sci. Eng.* **1984**, *26*, 81-140.

- (61) Bazin, D.; Sayers, D.; Rehr, J. J.; Mottet, C. *J. Phys. Chem. B* **1997**, *101*, 5332-5336.
- (62) Bazin, D.; Rehr, J. J. *J. Phys. Chem. B* **2003**, *107*, 12398-12402.
- (63) Hwang, B. J.; Sarma, L. S.; Chen, J. M.; Chen, C. H.; Shih, S. C.; Wang, G. R.; Liu, D. G.; Lee, J. F.; Tang, M. T. *J. Am. Chem. Soc.* **2005**, *127*, 11140-11145.
- (64) Frenkel, A. I.; Hills, C. W.; Nuzzo, R. G. *J. Phys. Chem. B* **2001**, *105*, 12689-12703.
- (65) Bus, E.; van Bokhoven, J. A. *J. Phys. Chem. C* **2007**, *111*, 9761-9768.
- (66) de Graaf, J.; van Dillen, A. J.; de Jong, K. P.; Koningsberger, D. C. *J. Catal.* **2001**, *203*, 307-321.
- (67) Dash, P.; Scott, R. W. *J. Chem. Commun.* **2009**, 812-814.
- (68) Jana, N. R.; Gearheart, L.; Murphy, C. J. *Chem. Mater.* **2001**, *13*, 2313-2322.
- (69) Stern, E. A.; Newville, M.; Ravel, B.; Yacoby, Y.; Haskel, D. *Physica B-Condens. Matt.* **1995**, *208*, 117-120.
- (70) Rehr, J. J.; Albers, R. C.; Zabinsky, S. I. *Phys. Rev. Lett.* **1992**, *69*, 3397-3400.
- (71) Maeland, A.; Flanagan, T. B. *Can. J. Phys.* **1964**, *42*, 2364-2366.
- (72) Ravel, B.; Newville, M. *J. Synchrotron Rad.* **2005**, *12*, 537-541.
- (73) Wilson, O. M.; Knecht, M. R.; Garcia-Martinez, J. C.; Crooks, R. M. *J. Am. Chem. Soc.* **2006**, *128*, 4510-4511.
- (74) Creighton, J. A.; Eadon, D. G. *J. Chem. Soc. Faraday Trans.* **1991**, *87*, 3881-3891.
- (75) Zhao, M. Q.; Crooks, R. M. *Chem. Mater.* **1999**, *11*, 3379-3385.
- (76) Hodak, J. H.; Henglein, A.; Giersig, M.; Hartland, G. V. *J. Phys. Chem. B* **2000**, *104*, 11708-11718.
- (77) Pyrz, W. D.; Buttrey, D. J. *Langmuir* **2008**, *24*, 11350-11360.
- (78) Gniewek, A.; Ziolkowski, J. J.; Trzeciak, A. M.; Zawadzki, M.; Grabowska, H.; Wrzyszczyk, J. *J. Catal.* **2008**, *254*, 121-130.
- (79) Liu, F.; Wechsler, D.; Zhang, P. *Chem. Phys. Lett.* **2008**, *461*, 254-259.

- (80) Shibata, T.; Tostmann, H.; Bunker, B.; Henglein, A.; Meisel, D.; Cheong, S.; Boyanov, M. *J. Synchrotron Rad.* **2001**, *8*, 545-547.
- (81) Delley, B.; Ellis, D. E.; Freeman, A. J.; Baerends, E. J.; Post, D. *Phys. Rev. B* **1983**, *27*, 2132-2144.
- (82) Chen, C. H.; Sarma, L. S.; Chen, J. M.; Shih, S. C.; Wang, G. R.; Liu, D. G.; Tang, M. T.; Lee, J. F.; Hwang, B. J. *ACS Nano* **2007**, *1*, 114-125.
- (83) Knecht, M. R.; Weir, M. G.; Frenkel, A. I.; Crooks, R. M. *Chem. Mater.* **2008**, *20*, 1019-1028.
- (84) Remita, H.; Etcheberry, A.; Belloni, J. *J. Phys. Chem. B* **2003**, *107*, 31-36.
- (85) Schmid, G.; West, H.; Malm, J. O.; Bovin, J. O.; Grenthe, C. *Chem. Eur. J.* **1996**, *2*, 1099-1103.
- (86) Wertheim, G. K. *Z. Phys. D-Atoms Molecules and Clusters* **1989**, *12*, 319-326.
- (87) van Bokhoven, J. A.; Miller, J. T. *J. Phys. Chem. C* **2007**, *111*, 9245-9249.
- (88) Zhang, P.; Sham, T. K. *Phys. Rev. Lett.* **2003**, *90*, 245502-245505.
- (89) Marx, S.; Baiker, A. *J. Phys. Chem. C* **2009**, *113*, 6191-6201.
- (90) Pedersen, M. O.; Helveg, S.; Ruban, A.; Stensgaard, I.; Laegsgaard, E.; Norskov, J. K.; Besenbacher, F. *Surf. Sci.* **1999**, *426*, 395-409.

## CHAPTER 6

### **6. One-pot Synthesis of Supported-Nanoparticle Materials in Ionic Liquid Solvents**

This work is a manuscript in preparation which describes the one-pot synthesis of supported-nanoparticle catalysts in imidazolium-based ionic liquids (ILs). This is a continuation of work described in Chapter 5 where a rational methodology was described for the synthesis of supported nanoparticle catalysts. The same methodology was utilized for the synthesis of highly porous catalysts in imidazolium-based ILs. Highly porous supported nanoparticle catalysts have been synthesized by a rational method involving the encapsulation of poly(vinylpyrrolidone) (PVP)-stabilized Au nanoparticles into titania xerogels employing room temperature ionic liquids (1-butyl-3-methylimidazolium hexafluorophosphate, [BMIM]PF<sub>6</sub>) as a medium. Highly mesoporous catalyst materials with BET surface areas of 200 m<sup>2</sup>/g and average pore sizes of 3-5 nm were obtained by this method.

---

This manuscript is in preparation to be submitted soon. All the experimental work in this paper has been done by me along with the manuscript writing and editing.

# One-pot Synthesis of Supported-Nanoparticle Materials in Ionic Liquid Solvents

Priyabrat Dash, Robert W. J. Scott\*

Department of Chemistry, University of Saskatchewan, 110 Science Place,  
Saskatoon, Saskatchewan, Canada

## 6.1 Abstract

Highly porous supported nanoparticle catalysts were synthesized by a rational method involving the encapsulation of poly(vinylpyrrolidone) (PVP)-stabilized Au nanoparticles into titania xerogels employing room temperature ionic liquids (1-butyl-3-methylimidazolium hexafluorophosphate, [BMIM]PF<sub>6</sub>) as a medium followed by solvent extraction of the ionic liquid and calcination of the materials. The materials were thoroughly characterized by thermal gravimetric analysis, electron microscopy, nitrogen adsorption-desorption isotherms, and powder x-ray diffraction techniques. Two different approaches were employed for the synthesis of supported nanoparticle catalysts; the first involved the synthesis of the materials directly in [BMIM]PF<sub>6</sub> IL via the hydrolysis of titanium tetrachloride while the second method involved the sol-gel encapsulation of PVP-stabilized nanoparticles in methanol/IL mixtures. The latter method afforded the complete encapsulation of Au nanoparticles inside the titania matrix. After careful low temperature calcinations at 350 °C, the Au-titania system synthesized by the second method resulted in the formation of a highly mesoporous catalyst with BET surface areas of 200 m<sup>2</sup>/g and average pore sizes of 3-5 nm. Control experiments confirmed the major

role of the PVP polymer as a template towards the final porosity of the supported nanoparticles in [BMIM]PF<sub>6</sub> IL. The final materials were moderately thermally stable with minimal changes in pore size and pore volume upon calcination at 550 °C.

## 6.2 Introduction

Ionic liquids (ILs), consisting of entirely of diffuse, weakly-coordinated cations and anions, have attracted a great deal of attention as novel solvents owing to their unique solvent properties such as high polarity, negligible vapor pressure, and thermal stability.<sup>1,2</sup> The use of ILs as media for the syntheses of various metallic nanoparticles has been reported in recent years.<sup>2</sup> In addition, ILs have attracted a lot of interest as templates for the fabrication of nanostructured inorganic materials, as the possibility exists for the IL to act as both the solvent and porogen in such systems.<sup>3</sup> Many porous inorganic oxide materials including zeolitic materials,<sup>4,5</sup> mesoporous silica with wormlike porous and highly ordered lamellar structures,<sup>6-8</sup> mesoporous titania,<sup>9-14</sup> and titania nanoparticles have been synthesized in ILs.<sup>15</sup> As ILs can be used as novel media for the synthesis of both stable transition metal nanoparticles and porous inorganic materials, we were intrigued at the possibility of using ILs for the incorporation of nanoparticles into porous oxide materials. Among the various techniques available for the synthesis of supported-bimetallic nanoparticle catalysts, the method of entrapping pre-prepared nanoparticles into an inorganic matrix by sol-gel method is particularly attractive.<sup>16,17</sup> This method can provide a general route to synthesize supported metallic and bimetallic catalysts which are nearly monodisperse in size and composition, which can lead to a better understanding of structure-activity relationships in such catalysts.<sup>16</sup> Herein, we

report a rational methodology towards the design of porous supported-Au nanoparticle catalysts by using imidazolium-based IL as an one-pot medium via the trapping of pre-synthesized nanoparticles into titania sol-gel syntheses.

In 2000, Dai *et al.* first reported the use of IL for the synthesis of silica aerogels using 1-ethyl-3-methylimidazolium bis(trifluoromethylsulfonyl)imide ([EMIM]NTf<sub>2</sub>) IL.<sup>18</sup> They employed a non-hydrolytic sol-gel reaction in the absence of any secondary porogen in the IL, followed by removal of the EMIMNTf<sub>2</sub> IL from the final composite by solvent extraction using acetonitrile. Since this pioneering work, there have been many reports describing the syntheses of various inorganic nanostructures in ILs.<sup>3</sup> In 2004, Antonietti and co-workers used a nanocasting method for the synthesis of mesoporous silica with worm-like pores (pore diameter 2.5 nm, surface area 801 m<sup>2</sup>/g) in [BMIM]BF<sub>4</sub> IL.<sup>8</sup> The authors postulated that hydrogen bonding between ions of the IL and the silica matrix resulted in the formation of mesoporous silica. In all these cases, the IL acts both as the solvent and the template.

ILs have also been used by a large number of groups for the synthesis and stabilization of metallic nanoparticles.<sup>2</sup> J. Dupont *et al.* showed the formation of stable Ir nanoparticles in imidazolium ILs and the resulting catalysts were found to be active catalysts for hydrogenation reactions.<sup>19</sup> Though there have been many reports of the synthesis of metal nanoparticles in pure ILs without any additional stabilizers,<sup>20-27</sup> a number of groups also reported the aggregation of nanoparticles in pure ILs.<sup>28-29</sup> To avoid these problems various secondary stabilizers have also been used for the synthesis of stable metal nanoparticles in ILs. Recently, we have shown that highly-stable PVP-

stabilized Au, Pd and bimetallic PdAu nanoparticles can be synthesized in [BMIM]PF<sub>6</sub> IL by a phase transfer method and the resulting nanoparticles were catalytically active for a range of hydrogenation reactions.<sup>30</sup> Encouraged by the fact that highly porous materials can also be synthesized in imidazolium-based IL, we sought to investigate whether PVP-stabilized Au nanoparticles in [BMIM]PF<sub>6</sub> IL could be used for the synthesis of highly porous Au catalysts supported on titania.

Recently, there have been some examples involving the synthesis of supported nanoparticle catalysts in ILs, mostly involving silica supports.<sup>3</sup> For example, Anderson *et al.* synthesized Pd nanoparticles supported on porous silica using an IL route.<sup>31</sup> In this case, Pd colloids were formed by mixing Pd(OAc)<sub>2</sub>, [BMIM]NTf<sub>2</sub> IL, and triphenylphosphine. After the formation of Pd nanoparticles, a porous silica support was then synthesized by the reaction of Si(OEt)<sub>4</sub> and formic acid.<sup>31</sup> J. Dupont and co-workers synthesized silica-supported Rh nanoparticles in [BMIM]BF<sub>4</sub> IL by a sol-gel method. However, low BET surface areas of 65 m<sup>2</sup>/g were obtained in the case of Rh-SiO<sub>2</sub> materials prepared in acidic conditions.<sup>32</sup> In both of these cases, the role of the IL towards the final porosity of the materials was studied, but no additional stabilizers were present. Recently, Chen and co-workers demonstrated an IL-facilitated synthesis of Ag nanoclusters on titania supports.<sup>33,34</sup> The Ag nanoclusters were found to be highly dispersed on the titania support, however, the porosity of the final supported catalysts was not discussed.

Herein, we report rational methodology for the synthesis of highly porous supported nanoparticle catalysts involving Au nanoparticles in titania using [BMIM]PF<sub>6</sub>



IL. Two different methods were employed for the synthesis of supported catalysts in IL. In the first method, PVP-stabilized Au nanoparticles were synthesized in [BMIM]PF<sub>6</sub> IL by a phase transfer method from methanol, followed by the addition of TiCl<sub>4</sub> into the nanoparticle solution. In the second method, PVP-stabilized Au nanoparticles were encapsulated in titania by a sol-gel method in a methanol/[BMIM]PF<sub>6</sub> IL mixture, followed by the evaporation of methanol overnight. The latter method resulted in a complete incorporation of pre-synthesized Au nanoparticles into the titania matrix. Low temperature calcination conditions, at 350<sup>0</sup>C, resulted in highly porous materials (~ 200 m<sup>2</sup>/g BET surface areas and pore sizes of 3.3 nm). The combination of PVP stabilizer and [BMIM]PF<sub>6</sub> IL act as template towards the porosity of the final material, though the major contribution to porosity was from the PVP polymer.

## **6.3 Experimental**

### **6.3.1 Materials**

1-Methylimidazole (99%) and 1-chlorobutane (99.5%) were purchased from Alfa and were distilled over KOH and P<sub>2</sub>O<sub>5</sub>, respectively, before use. Hexafluorophosphoric acid (*ca.* 65% solution. in water), poly(vinylpyrrolidone) (M.W. 40,000), hydrogen tetrachloroaurate hydrate (99.9%), titanium isopropoxide (98%) were purchased from Alfa and were used without further purification. Titanium chloride (99.9%) and sodium borohydride powder (98%) were obtained from Aldrich and was used as obtained. 18 MΩ·cm Milli-Q de-ionized water (Millipore, Bedford, MA) was used throughout.

### 6.3.2 Catalyst Preparation

Synthesis of the 1-butyl-3-methylimidazolium hexafluorophosphate ([BMIM]PF<sub>6</sub>) IL was carried out under nitrogen and purified according to previously published procedures.<sup>30</sup> The purity of the [BMIM]PF<sub>6</sub> IL was verified by <sup>1</sup>H NMR, UV-Vis spectroscopy, and Karl-Fischer titrations. PVP-stabilized Au nanoparticles were synthesized according to the following procedure. First, 6.0 ml of a 1.39 mM methanol solution of PVP was added to 1.9 ml of methanol, followed by the addition of 1.1 ml of a 10 mM methanol solution of HAuCl<sub>4</sub>. The mixture was stirred for 15 min, followed by the addition of 1.0 ml of a freshly prepared 0.10 M NaBH<sub>4</sub> solution in methanol. The formation of a deep red solution indicated the formation of Au nanoparticles. The methanol solution containing the nanoparticles was then added to 10 ml of [BMIM]PF<sub>6</sub> IL, followed by removal of the methanol under vacuum, resulting in the suspension of Au nanoparticles in the IL.

The synthesis for incorporating Au nanoparticles into titania frameworks was carried out to yield a titania powder nominally containing 1 wt % Au. In the first method, Au nanoparticles were transferred to [BMIM]PF<sub>6</sub> IL by the above phase transfer method from methanol. After the solution was stirred for few minutes, 0.25 ml of a titanium tetrachloride precursor was added dropwise to the solution, giving a turbid solution. The resulting sol solution was gelled in an open Petri dish under 100 % humidity conditions for 3 days. The titania gels were then washed with methanol and collected by filtration, followed by drying in an oven at 150 °C for 12 h. The as-synthesized samples were then calcined at 550 °C in air for 6 h, followed by reduction under H<sub>2</sub> at 300 °C for 1 h. Pure

titania samples without any incorporation of Au nanoparticles were also synthesized according to the method mentioned above. Two samples were prepared; one with PVP present, and one in pure [BMIM]PF<sub>6</sub> IL using TiCl<sub>4</sub> as the precursor. Typical yields based on the mass of titania for all the syntheses were 60-70 %.

In the second method, titania-supported catalysts were prepared according to the following procedure: 5 vol % of water was added to a PVP-stabilized Au nanoparticle solution in methanol, followed by stirring for 15 min. 2.02 ml of Ti(O<sup>i</sup>Pr)<sub>4</sub>, dissolved in 5 ml of methanol freshly dried over molecular sieves was added slowly to the Au nanoparticle solution, followed by addition of 5.0 mL of [BMIM]PF<sub>6</sub> IL. Within 15-20 s, a gel was formed, and was aged overnight. The titania gels were washed with methanol and collected by filtration, and then dried in an oven at 150 °C for 3 h. After this the powdered materials were calcined in a furnace at 350 or 550 °C for 6 h in flowing air, followed by reduction under H<sub>2</sub> at 300 °C for 1 h. Pure titania samples without any incorporation of Au nanoparticles were also synthesized according to the methodology described above. Two samples were prepared; one with PVP present and the other in the pure [BMIM]PF<sub>6</sub> IL using Ti(O<sup>i</sup>Pr)<sub>4</sub> as the precursor. Typical yields based on the mass of titania for all the syntheses were 60-70 %.

### **6.3.3 Characterization**

Thermogravimetric analysis (TGA) was performed using a TA instruments TGA Q5000IR under air flow. Initial samples were run from 25 °C to 600 °C with a heating rate of 5 °C/min to determine the total amount of PVP polymer and IL present in the samples and the degradation temperature range. This was followed by running separate samples

which were held for 6 h at the onset of PVP degradation temperature while monitoring the total mass loss of the sample. Adsorption-desorption isotherms of the final porous materials were obtained using a Micrometrics ASAP 2010 volumetric adsorption analyzer. Before the measurement, the samples were degassed at 100<sup>o</sup> C for 15 h to remove the moisture and adsorbed gases. The isotherms were analyzed using the Brunauer-Emmett-Teller (BET) model.<sup>35</sup> Pore-size distributions were calculated using the Barrett-Joyner-Halenda (BJH) method.<sup>36</sup> XRD measurements were carried out using a Rigaku Rotaflex RU-200 diffractometer using the CuK<sub>α</sub> radiation line; the sample was scanned over the 2θ range of 5-80<sup>o</sup>. TEM micrographs were obtained with a Philips 410 microscope operating at 100 keV. To prepare samples for TEM, a drop of acetone/well-ground catalyst powder mixture containing the nanoparticles was placed on a holey-carbon coated Cu TEM grid (200 mesh) which had been pre-oxidized by air plasma treatment, followed by evaporation of the acetone.

#### **6.4 Results and Discussion**

The initial purpose of performing these experiments was to observe the effect of stabilizer (PVP) and IL on porosity. A significant degree of meso- and macroporosity as well as high surface area are needed for effective heterogeneous catalyst supports.<sup>37</sup> As sol-gel reactions can be performed in IL, we anticipated that both the PVP stabilizer and the IL can act as templates to control the porosity of titania after calcinations. Keeping this in mind, we synthesized two different sets of pure titania samples (without any incorporation of Au nanoparticles) in [BMIM]PF<sub>6</sub> IL using titanium tetrachloride; one

without PVP in IL and one with PVP in IL. The samples were calcined and reduced as described in the experimental section.

Figure 6.1 shows the nitrogen adsorption-desorption isotherms for the two control titania samples (synthesized with and without PVP present) After calcination at 550 °C, the titania control sample with no added PVP showed a type III isotherm, which is typical of macroporous materials, as seen in Figure 6.1. The isotherm for the titania/PVP sample, which shows significant hysteresis at intermediate partial pressures (type IV isotherm), is typical of mesoporous materials. The pore size distribution based on desorption branch of the isotherm is relatively narrow for the PVP-titania sample with an average pore size of 3.6 nm whereas in the pure titania sample the average pore sizes is quite broad. The BET surface area was increased from 21 m<sup>2</sup>/g in the pure titania sample to 27 m<sup>2</sup>/g in the PVP-titania sample. These results suggest a weak templating effect of PVP towards the porosity of titania prepared via the hydrolysis of titanium tetrachloride.

**Table 6.1.** Porosity and surface area properties of materials prepared by hydrolysis of titanium tetrachloride in [BMIM]PF<sub>6</sub> IL after calcination at 550 °C.

<b>Material</b>	<b>Porosity (cc/g)</b>	<b>Pore size (Å<sup>0</sup>)</b>	<b>BET Surface area (m<sup>2</sup>/g)</b>
TiO <sub>2</sub>	0.05	154	21
PVP-TiO <sub>2</sub>	0.06	36	27
PVP-Au-TiO <sub>2</sub>	0.10	36	50

We then sought to investigate the synthesis of supported nanoparticle catalysts employing Au nanoparticles in [BMIM]PF<sub>6</sub> IL. The Au nanoparticles were synthesized in [BMIM]PF<sub>6</sub> by a phase transfer method from methanol,<sup>30</sup> followed by the addition of

TiCl<sub>4</sub> into the nanoparticle solution. The resulting PVP-Au-TiO<sub>2</sub> sample after calcination at 550 °C showed an isotherm which is typical of mesoporous materials, albeit with a higher BET surface area (Table 6.1, Figure 6.1). The increase in surface area of the supported porous materials was likely a consequence of the mesoporosity introduced by the PVP-Au nanoparticle templates. The role of PVP as a template towards the final materials has been observed by other groups.<sup>38,39</sup> For example, Zhang *et al.* had shown that by using PVP as template, mesoporous titania with surface areas up to 65 m<sup>2</sup>/g was obtained after calcination at 500 °C.<sup>38</sup> However, in the absence of PVP the titania samples had a lower surface area of 23.5 m<sup>2</sup>/g.

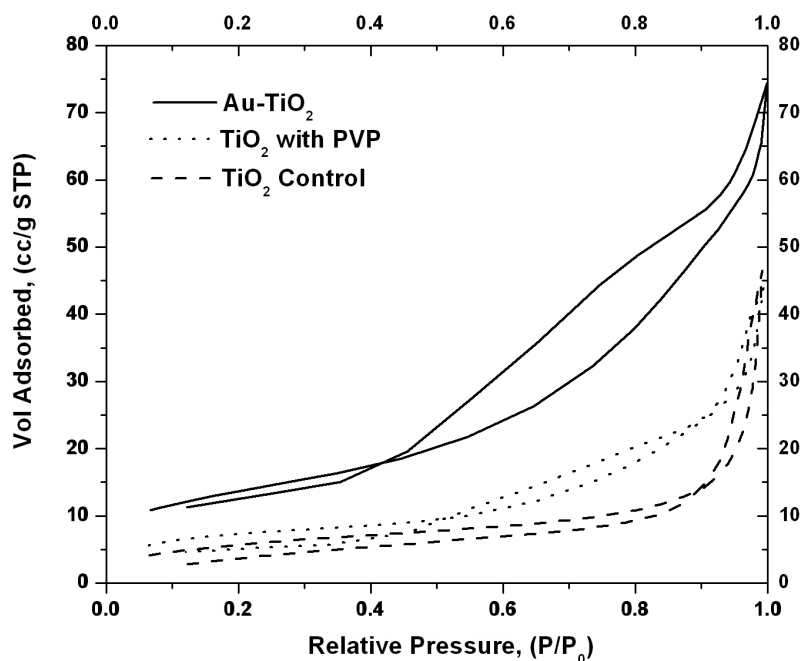


**Figure 6.1.** Nitrogen adsorption-desorption isotherms for titania supported catalysts synthesized by hydrolysis of titanium tetrachloride in [BMIM]PF<sub>6</sub> IL after washing and calcination at 550 °C.

Figure 6.2 shows the average BJH pore size distributions for each of the three samples discussed above. Sharp BJH pore size distributions are centered at 3.6 nm in the PVP-titania and PVP-Au-titania samples, but this feature is absent in the titania control sample (with no PVP added). It shows that the final material is mesoporous after the removal of PVP through calcination. Also, the total pore volume increased in the Au-TiO<sub>2</sub> sample with PVP to 0.1 cm<sup>3</sup>/g from 0.06 cm<sup>3</sup>/g in the pure TiO<sub>2</sub> sample with PVP.

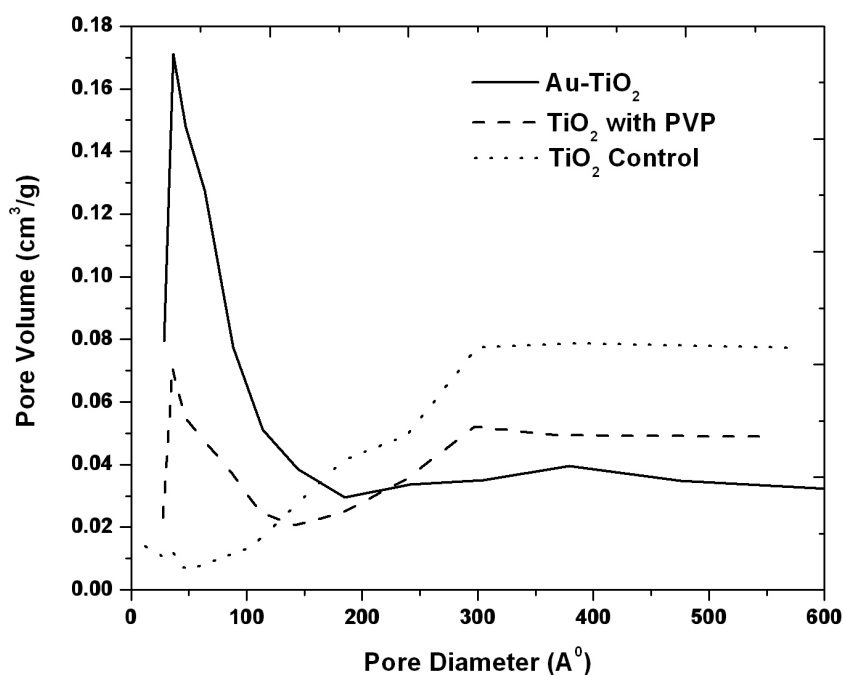


**Figure 6.2.** BJH pore-size distributions for titania supported catalysts synthesized by titanium tetrachloride hydrolysis in [BMIM]PF<sub>6</sub> followed by washing and calcination at 550°C.

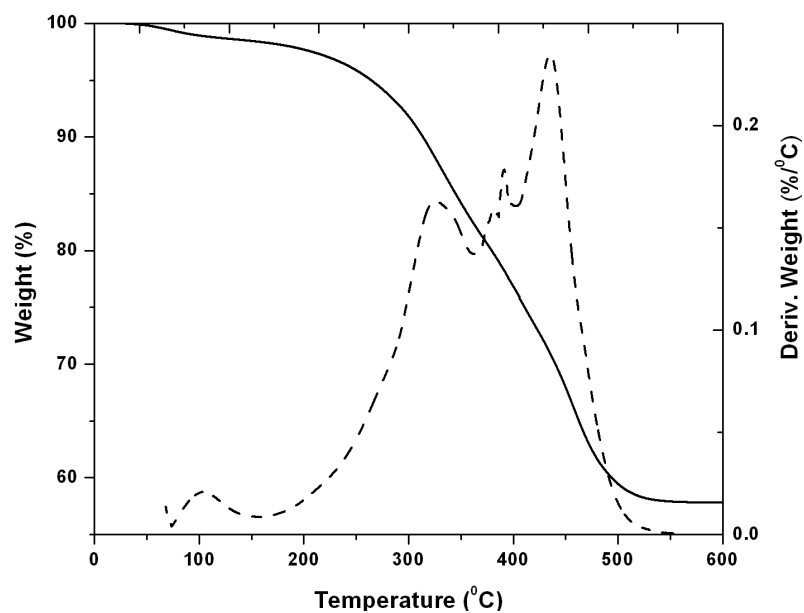
Though porous materials were synthesized by the above method, the hydrolysis of titanium chloride chemistry had some limitations. The ageing of the titania gel resulted in an inhomogeneous distribution of Au nanoparticles on the titania support. Also, the

resulting porosities were low compared to other literature on similar system.<sup>10,11,13,14</sup> Thus we examined a second method for the synthesis of supported nanoparticle catalysts. In previous work, we showed that bimetallic PdAu nanoparticles could be uniformly deposited within an alumina matrix via the encapsulation of PVP-stabilized nanoparticles into alumina sol-gel syntheses in isopropanol solvents.<sup>40</sup> We sought to use the same method for the synthesis of supported catalysts in IL. Initially, the same methodology employed directly in [BMIM]PF<sub>6</sub> IL was not successful due to solubility issues of titanium isopropoxide in the IL; however using methanol as a cosolvent allowed for this method to be adapted. The sample was aged overnight leaving a titania xerogel containing Au nanoparticles in the IL. Due to their negligible volatility, the IL can play an important role in allowing for longer aging times for the formation of stable sol-gel networks.

The as-synthesized xerogel supported nanoparticle samples washed with cold methanol were characterized by TGA to find out the total organic content of the materials and the optimal calcination temperatures. As shown in Figure 6.3A, the TGA curve of the as-synthesized Au-titania sample has three distinct weight losses, with water desorbed below 100 °C (~5 % mass loss) and IL and PVP decomposition at 300-500 °C (~37% mass loss). TGA analysis of titania control samples synthesized in [BMIM]PF<sub>6</sub> IL without any PVP showed the decomposition of IL in the range of 350-500 °C. Thus, both PVP and IL decompose in the temperature range of 300-500 °C. To examine how much of the templates could be removed without calcination, we examined hot methanol washing. Figure 6.3B shows the TGA curve after hot methanol washing, the mass loss around 300-500 °C was lowered slightly to 32 %, but could not be lowered further.



(A)



(B)

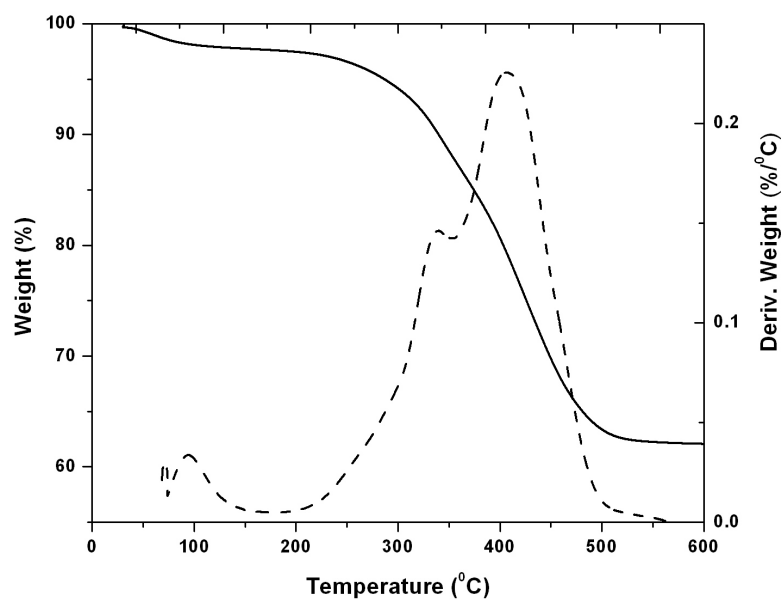


**Figure 6.3.** Thermal gravimetric analysis plots showing (a) mass loss and derivative of mass loss of PVP-stabilized Au nanoparticles in titania prepared after cold methanol washing and (b) after hot methanol washing.

We sought to find the minimal conditions needed by running TGA experiments at a temperature just above the onset of the polymer and IL decomposition temperature (350 °C). By holding the temperature at 350 °C for 5 h, a slightly lower mass % of polymer and IL (~ 24% mass loss) was removed at lower calcination temperatures. After calcination at 350 °C for 5 h under air, the samples were reduced under hydrogen at 300 °C for 1 h.

The mean particle sizes and size distributions of the as-synthesized nanoparticles dispersed in titania matrixes were obtained by TEM images. Figure 6.4a shows a TEM image of Au nanoparticles dispersed in the amorphous titania matrix. The particles are well dispersed within the oxide support, with an average nanoparticle size of  $5.5 \pm 2.3$  nm. After calcination at 350 °C for 5 h under air, followed by the reduction under hydrogen at 300 °C for 1 h, the average particle sizes for the supported- Au nanoparticles increased from  $5.5 \pm 2.3$  nm to  $8.8 \pm 2.5$  nm (Figure 6.4b). This increase seems unavoidable due to sintering during calcination treatments. This nanoparticle size is comparable to that obtained by the XRD analysis which is described in the later section.

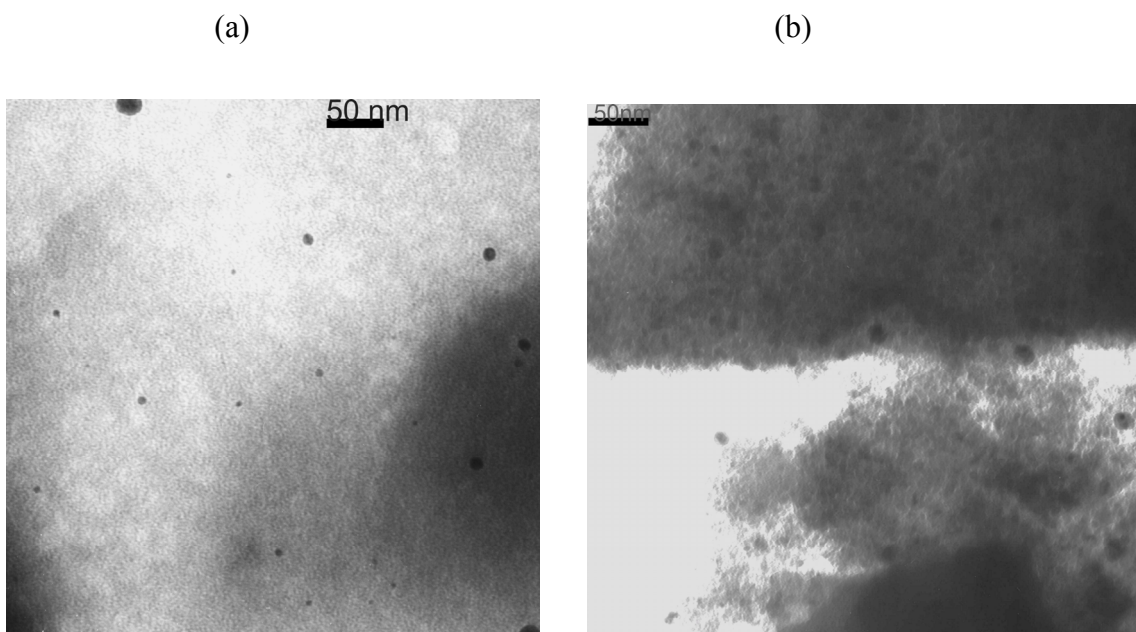


**Figure 6.4.** TEM images PVP-stabilized Au nanoparticles (a) as-synthesized in titania, and (b) after calcination at 350 °C.

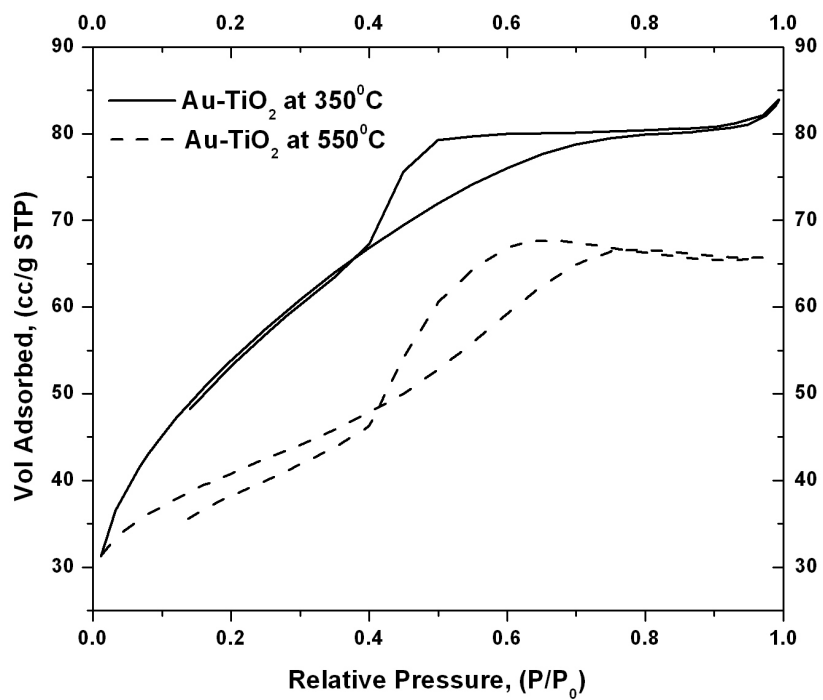
The textural properties of the Au-TiO<sub>2</sub> materials prepared by the second method after calcination at 350 and 550 °C were characterized by nitrogen adsorption-desorption isotherms. Figure 6.5 shows nitrogen adsorption-desorption isotherms and BJH pore-size distributions for the Au-TiO<sub>2</sub> samples. The as-synthesized xerogel-supported nanoparticle sample had a very low BET surface area of 2 m<sup>2</sup>/g. This low value may be attributed to the presence of large amounts of PVP polymer trapped inside the titania which cannot be removed by solvent extraction. However, upon calcination at 350 °C in air the BET surface area significantly increased to 200 m<sup>2</sup>/g; the hysteresis loop seen in Figure 6.5A is a type IV isotherm suggesting the formation of mesoporosity in the final material. The calcined sample has a pore volume of 0.69 cm<sup>3</sup>/g and average BJH pore size of 3.3 nm. Others have also documented the synthesis of mesoporous titania in IL with surface areas

ranging from 200-550 m<sup>2</sup>/g.<sup>10,11,13,14</sup> For example, Liu *et al.* documented the synthesis of mesoporous nanostructured anatase TiO<sub>2</sub> with a surface area of 312 m<sup>2</sup>/g, pore volume of 0.66 cm<sup>3</sup>/g, and BJH pore size of 7.7 nm after calcination at 300 °C in 1-butyl-3-methylimidazolium tetrafluoroborate ([BMIM]BF<sub>4</sub>) IL.<sup>13</sup> Though the surface area is higher than these materials, the pore volume of our system (0.69 cm<sup>3</sup>/g) is comparable to Liu's work (0.66 cm<sup>3</sup>/g). Moreover, the pore size shown here is significantly smaller (3.3 nm) than those seen by Liu (7.7 nm). To further confirm whether the final porosity was obtained due to the IL or PVP, a control titania sample was prepared in the [BMIM]PF<sub>6</sub> IL/methanol cosolvent without the presence of PVP. The as-synthesized titania samples had a BET surface area of 5 m<sup>2</sup>/g which is only slightly higher than the one synthesized in the presence of PVP (surface area of 2 m<sup>2</sup>/g). However, upon calcination at 350 °C, a similar BET surface area 6 m<sup>2</sup>/g was obtained. Thus, it can be confirmed that the higher surface area and pore volume obtained after calcination was mostly due to PVP which acts as a template towards the final porosity of the calcined sample. This suggests the IL play a very minor role templating role in these materials using this synthetic method.

**Table 6.2.** Porosity properties of materials prepared by hydrolysis of titanium isopropoxide in [BMIM]PF<sub>6</sub>/methanol mixture.

Oxide	Porosity (cc/g)	Pore size (Å <sup>0</sup> )	BET Surface area (m <sup>2</sup> /g)
Au-TiO <sub>2</sub> at 350 °C	0.69	34	200
Au-TiO <sub>2</sub> at 550 °C	0.63	33	107

(A)



(B)

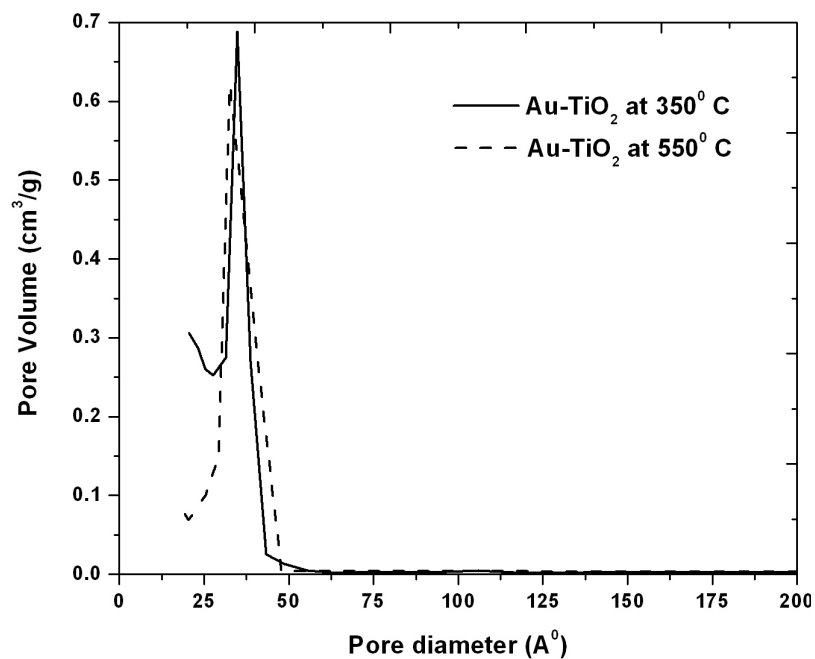


**Figure 6.5.** (A) Nitrogen adsorption-desorption isotherms and (B) BJH pore-size distributions for calcined Au-TiO<sub>2</sub> samples.

To further check the thermal stability of the Au-TiO<sub>2</sub> system, the sample was calcined at 550 °C for 5 h, followed by reduction under H<sub>2</sub> at 300 °C for 1 h. Upon calcination to 550 °C, the BET surface area dropped from 200 m<sup>2</sup>/g to 107 m<sup>2</sup>/g while there was little to no change in pore volume and pore size (Table 6.2). The decrease in surface area can be attributed to the loss of porosity arising from the crystallization of titania matrix during high temperature calcination.<sup>41</sup> Indeed, XRD results support the increase in crystallinity of the titania sample after calcination at 550 °C (see below).

The x-ray powder diffraction (XRD) peaks of the supported nanoparticle catalysts are shown below in Figure 6.6. The XRD pattern of the as-synthesized xerogel-supported nanoparticles has broad peaks which can be attributed to the presence of nanoparticulate and/or amorphous titania framework. The broad peaks at 2 theta values of 24° and 45° came from the glass substrate. Upon calcination at 350 °C, the crystallinity of the titania increased; the diffraction peaks were assigned to anatase TiO<sub>2</sub> without any indication of other crystalline products, including the rutile phase. Crystalline anatase form of titania are important in many applications photocatalysis, liquid solar cells, and electroluminescent hybrid devices due to its higher surface area compared with other titania phases like rutile and brookite.<sup>11</sup> The average crystal size of the titania sample calcined at 350 °C was around 4.4 nm calculated using Scherrer formula.<sup>42</sup> No XRD peaks due to the polycrystalline gold were observed, which is expected given the low Au loading (1 wt%) and the presence of very small gold nanoparticles dispersed on the titania matrix.<sup>43</sup> Further calcination to 550 °C aimed at improving the crystallinity of the final porous materials showed that the materials have moderate thermal stability. As mentioned above, the BJH pore size and pore volume changed very little after the second

thermal treatment (Table 6.2), while the XRD pattern indicated the presence of highly crystalline anatase with an average crystallite size of 8.5 nm as calculated by the Scherrer equation. This increase in crystallite size can be attributed to the sintering of particles upon calcination.

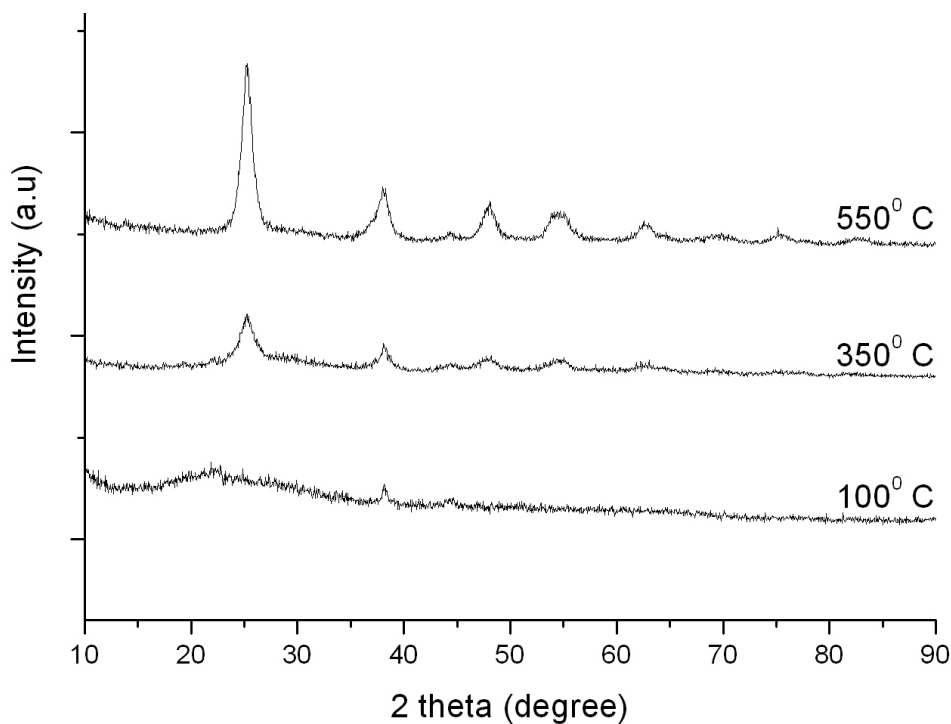


**Figure 6.6.** X-ray powder diffraction patterns of Au-TiO<sub>2</sub> systems before and after calcination.

## 6.5 Conclusions

We have developed a one pot method for the synthesis of highly porous supported nanoparticle catalysts in IL. The encapsulation of PVP-stabilized Au nanoparticles inside the porous titania matrix using a methanol/IL co-solvent was the most successful strategy. Highly mesoporous catalysts (BET surface area of 200 m<sup>2</sup>/g, pore size of 3-5

nm, and pore volume of 0.69 cm<sup>3</sup>/g) with anatase crystalline phase was obtained at low temperature calcination, with homogeneous dispersion of the Au nanoparticles throughout the titania. The PVP template plays a dual role as a template for both nanoparticle formation and as a porogen for the final sol-gel materials. We are currently investigating the use of this methodology for the synthesis of supported catalysts involving other metal oxides like silica and alumina.

### **Acknowledgements**

The authors would like to acknowledge financial assistance from the National Sciences and Engineering Research Council of Canada (NSERC), and thank J. H. Kwon for assistance with gas adsorption measurements.

### **6.6 References**

- (1) Astruc, D.; Lu, F.; Aranzaes, J. R. *Angew. Chem., Int. Ed.* **2005**, *44*, 7852-7872.
- (2) Migowski, P.; Dupont, J. *Chem. -Eur. J.* **2007**, *13*, 32-39.
- (3) Ma, Z.; Yu, J. H.; Dai, S. *Adv. Mater.* **2010**, *22*, 261-285.
- (4) Cooper, E. R.; Andrews, C. D.; Wheatley, P. S.; Webb, P. B.; Wormald, P.; Morris, R. E. *Nature* **2004**, *430*, 1012-1016.
- (5) Parnham, E. R.; Morris, R. E. *Chem. Mater.* **2006**, *18*, 4882-4887.
- (6) Zhou, Y.; Antonietti, M. *Adv. Mater.* **2003**, *15*, 1452-1455.
- (7) Zhou, Y.; Antonietti, M. *Chem. Mater.* **2004**, *16*, 544-550.
- (8) Zhou, Y.; Schattka, J. H.; Antonietti, M. *Nano Lett.* **2004**, *4*, 477-481.



- (9) Ding, K. L.; Miao, Z. J.; Liu, Z. M.; Zhang, Z. F.; Han, B. X.; An, G. M.; Miao, S. D.; Xie, Y. *J. Am. Chem. Soc.* **2007**, *129*, 6362-6363.
- (10) Zhou, Y.; Antonietti, M. *J. Am. Chem. Soc.* **2003**, *125*, 14960-14961.
- (11) Yoo, K.; Choi, H.; Dionysiou, D. D. *Chem. Commun.* **2004**, 2000-2001.
- (12) Nakashima, T.; Kimizuka, N. *J. Am. Chem. Soc.* **2003**, *125*, 6386-6387.
- (13) Liu, Y.; Li, J.; Wang, M.; Li, Z.; Liu, H.; He, P.; Yang, X.; Li, J. *Cryst. Growth Des.* **2005**, *5*, 1643-1649.
- (14) Yoo, K. S.; Lee, T. G.; Kim, J. *Micropor. Mesopor. Mater.* **2005**, *84*, 211-217.
- (15) Zheng, W.; Liu, X.; Yan, Z.; Zhu, L. *ACS Nano*, **2009**, *3*, 115-122.
- (16) Scott, R. W. J.; Sivadinarayana, C.; Wilson, O. M.; Yan, Z.; Goodman, D. W.; Crooks, R. M. *J. Am. Chem. Soc.* **2005**, *127*, 1380-1381.
- (17) Parvulescu, V. I.; Parvulescu, V.; Eudruschat, U.; Filoti, G.; Wagner, F. E.; Kubel, C.; Richards, R. *Chem. -Eur. J.* **2006**, *12*, 2343-2357.
- (18) Dai, S.; Ju, Y. H.; Gao, H. J.; Lin, J. S.; Pennycook, S. J.; Barnes, C. E. *Chem. Commun.* **2000**, 243-244.
- (19) Dupont, J.; Fonseca, G. S.; Umpierre, A. P.; Fichtner, P. F. P.; Teixeira, S. R. *J. Am. Chem. Soc.* **2002**, *124*, 4228-4229.
- (20) Fonseca, G. S.; Umpierre, A. P.; Fichtner, P. F. P.; Teixeira, S. R.; Dupont, J. *Chem. -Eur. J.* **2003**, *9*, 3263-3269.
- (21) Bruss, A. J.; Gelesky, M. A.; Machado, G.; Dupont, J. *J. Mol. Catal. A: Chem.* **2006**, *252*, 212-218.
- (22) Scheeren, C. W.; Machado, G.; Dupont, J.; Fichtner, P. F. P.; Texeira, S. R. *Inorg. Chem.* **2003**, *42*, 4738-4742.

- (23) Silveira, E. T.; Umpierre, A. P.; Rossi, L. M.; Machado, G.; Morais, J.; Soares, G. V.; Baumvol, I. L. R.; Teixeira, S. R.; Fichtner, P. F. P.; Dupont, J. *Chem. -Eur. J.* **2004**, *10*, 3734-3740.
- (24) Umpierre, A. P.; Machado, G.; Fecher, G. H.; Morais, J.; Dupont, J. *Adv. Synth. Catal.* **2005**, *347*, 1404-1412.
- (25) Migowski, P.; Machado, G.; Texeira, S. R.; Alves, M. C. M.; Morais, J.; Traverse, A.; Dupont, J. *Phys. Chem. Chem. Phys.* **2007**, *9*, 4814-4821.
- (26) Singh, P.; Katyal, A.; Kalra, R.; Chandra, R. *Tetrahedron Lett.* **2008**, *49*, 727-730.
- (27) An, J.; Wang, D. S.; Luo, Q. Z.; Yuan, X. Y. *Mater. Sci. Eng. C* **2009**, *29*, 1984-1989.
- (28) Wei, G. T.; Yang, Z. S.; Lee, C. Y.; Yang, H. Y.; Wang, C. R. C. *J. Am. Chem. Soc.* **2004**, *126*, 5036-5037.
- (29) Wang, Y.; Yang, H. *Chem. Commun.* **2006**, 2545-2547.
- (30) Dash, P.; Dehm, N. A.; Scott, R. W. J. *J. Mol. Catal. A: Chem.* **2008**, *286*, 114-119.
- (31) Anderson, K.; Fernandez, S. C.; Hardacre, C.; Marr, P. C. *Inorg. Chem. Commun.* **2004**, *7*, 73-76.
- (32) Gelesky, M. A.; Chiaro, S. S. X.; Pavan, F. A.; dos Santos J. H. Z.; Dupont, J. *Dalton Trans.* **2007**, 5549-5553.
- (33) Zhang, H.; Li, X.; Chen, G. *J. Mater. Chem.* **2009**, *19*, 8223-8231.
- (34) Zhang, H.; Chen, G. *Environ. Sci. Technol.* **2009**, *43*, 2905-2910.
- (35) Brunauer, S.; Emmett, P. H.; Teller, E. *J. Am. Chem. Soc.* **1938**, *60*, 309-319.
- (36) Barrett, E. P.; Joyner, L. G.; Halenda, P. P. *J. Am. Chem. Soc.* **1951**, *73*, 373-380.

- (37) Pietron, J. J.; Stroud, R. M.; Rolison, D. R. *Nano Lett.* **2002**, *2*, 545-549.
- (38) Zheng, M. -P.; Gu, M. -Y.; Jin, Y. -P.; Wang, H. -H.; Zu, P. -F.; Tao, P.; He, J. -B. *Mater. Sci. Eng., B*, **2001**, *87*, 197-201.
- (39) Wang, W.; Jin, Y.; *Mater. Lett.* **2003**, *57*, 3276-3281.
- (40) Dash, P.; Bond, T.; Fowler, C.; Hou, W.; Coombs, N.; Scott, R. W. J.; *J. Phys. Chem. C* **2009**, *113*, 12719-12730.
- (41) Scott, R. W. J.; Wilson, O. M.; Crooks, R. M. *Chem. Mater.* **2004**, *16*, 5682-5688.
- (42) Klug, H.; Alexander, L. *X-ray Diffraction Procedures*; Wiley: New York, **1962**.
- (43) Centeno, M. A.; Hidalgo, M. C.; Dominguez, M. I.; Navio, J. A.; Odriozola, J. A. *Catal. Lett.* **2008**, *123*, 198-206.

## CHAPTER 7

### 7.1 Summary and Conclusions

The first major objective of this thesis was to use imidazolium-based ILs as greener media for the synthesis of quasi-homogeneous nanoparticle catalysts. In particular, the recyclability, reuse, mode-of-stability, and long-term stability of ionic-liquid supported Au, Pd, and bimetallic Pd-Au nanoparticle catalysts was studied; all of which can be important factors in determining the overall “greenness” of such synthetic routes. In Chapter 2-4, all these parameters were studied in [BMIM]PF<sub>6</sub> IL.

As presented in Chapter 2, the objective was to find routes to synthesize stable, active, and reusable nanoparticle catalysts in [BMIM]PF<sub>6</sub> IL. In this work, PVP-stabilized Pd, Au, and bimetallic PdAu nanoparticles were solubilized in imidazolium-based IL by a simple phase-transfer method from methanol to [BMIM]PF<sub>6</sub> IL. It was found that there was no significant change in particle size observed after the phase transfer. For the first time, the catalytic behavior of IL-phase bimetallic nanoparticles was explored. Bimetallic Pd-Au nanoparticles in the IL were shown to have excellent activities for the hydrogenation of a range of substrates (allyl alcohol, 1,3- cyclooctadiene, *trans*-cinnamaldehyde, and 3-hexyn-1-ol), with the highest catalytic activities seen for bimetallic nanoparticles with high Pd loadings. For the hydrogenation of 1,3-cyclooctadiene, 3:1 Pd:Au nanoparticles showed 100% selectivity for the formation of cyclooctene and also showed nearly 100% selectivity for the hydrogenation of 3-hexyn-1-ol to hexenol (> 94 % *cis*-hexenol). Thus, these catalysts were also found to be highly selective catalysts for a number of hydrogenation reactions. To compare the catalytic

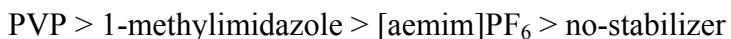
activity in IL to that of conventional solvents like water, the same reaction was studied in water under exactly same conditions and it was found that the catalytic activity was similar to that in IL. However, it is important to note that the negligible volatility and high thermal stability of [BMIM]PF<sub>6</sub> IL can allow experimental conditions not accessible by conventional solvents. For example, this medium can easily be recycled by removing unreacted substrates and products from the IL-phase under reduced pressure. The catalyst solution could be reused with very little change in catalytic activity (< 4% after 2 cycles).

Extreme care was taken to synthesize nanoparticle catalysts in very clean and pure [BMIM]PF<sub>6</sub> IL. This was needed to minimize the amounts of possible halide and other impurities which could affect nanoparticle stability, as well as maximize the transparency of the IL in the visible regions such that nanoparticle formation and transfer could be followed by UV–Vis spectroscopy. It was found that several recrystallizations (at least 3 times) of the [BMIM]Cl precursor were necessary to yield colourless IL (with minimal absorption above 290 nm). In dried IL, the water level was found to be 27 ppm by Karl-Fisher titrations and chloride levels below 1.8 mgL<sup>-1</sup> by AgNO<sub>3</sub> tests. The synthesis of clean ILs gave us a platform to study the effect of impurities on nanoparticle stability. In particular, 1-methylimidazole was found to be one of most common impurities present after the synthesis of [BMIM]PF<sub>6</sub> IL, often at or below the detection levels of <sup>1</sup>H NMR spectroscopy. Others had previously shown the formation of imidazole and 1-methylimidazole monolayers on gold and silver surfaces, thus the effect of 1-methylimidazole on nanoparticle stability was investigated. Initially, efforts were carried out to minimize the level of 1-methylimidazole in [BMIM]PF<sub>6</sub> IL. 1-methylimidazole levels in the final [BMIM]PF<sub>6</sub> IL were found to be below 0.5 mM via careful <sup>1</sup>H NMR

detection limit studies and colorimetric titrations with  $\text{Cu}^{2+}$  salts. Then, Au and PdAu nanoparticles were synthesized in the  $[\text{BMIM}]\text{PF}_6$  IL in the presence of a 1.0 mM 1-methylimidazole additive. For comparisons, the same nanoparticles were synthesized in IL in the absence of 1-methylimidazole additives. It was found that Au nanoparticles were stable for a much longer period of time (no clear signs of aggregation after 2 weeks) in solutions containing low concentrations of 1-methylimidazole additives, while Au nanoparticles prepared in IL without 1-methylimidazole additives precipitated out in less than a week. To compare the effect of nanoparticle stability on catalytic activity, the hydrogenation of allyl alcohol was carried out by 3:1 Pd:Au nanoparticles in these two media. It was found that the activity of the nanoparticles synthesized directly in the pure IL began to drop dramatically within 10 min upon addition of the substrate, while PdAu nanoparticles synthesized in the presence of 1.0 mM 1-methylimidazole show dramatically improved retentions of catalytic activity over time. Finally, the generality of this new mode of stabilization was tested by carrying out similar studies in  $[\text{BMIM}]\text{OTf}$  IL. Similar trends in stability and activity were found in this IL, though higher amounts (10-100 mM) of 1-methylimidazole were needed to stabilize the nanoparticles over long time periods.

In Chapter 4, a comparative study documenting the relative stability of nanoparticles using stabilizers in IL on the effective relative catalytic activities and lifetimes of such nanoparticle/IL mixtures was presented. Four different stabilization methods in  $[\text{BMIM}]\text{PF}_6$  were used, including the synthesis of nanoparticles in pure IL, and the addition of secondary PVP, 1-methylimidazole, and  $[\text{aemim}]\text{PF}_6$  (an amine-

containing task-specific ionic liquid) stabilizers. Initially, the stability of pure Au nanoparticles was studied in those media. The trend for the stability was as follows:



The activity and lifetimes of 3:1 PdAu nanoparticle catalysts synthesized by these four methods were measured by hydrogenation of a 1,3-cyclooctadiene and 3-buten-1-ol substrates, and while short-term catalytic results suggested that PVP stabilized particles had lower surface activities than other particles, they retained their catalytic activity over long periods of time due to their high stability. PVP-stabilized nanoparticles were found to be the most stable, and had the highest catalytic activity and longer lifetimes than catalysts prepared by the other stabilization routes.

The field of heterogeneous catalysis has long recognized the advantages of using nanostructured materials in order to take advantage of their large surface area and resulting high catalytic activities. This field has also greatly been improved by the development of nanoparticle synthesis and characterization methods over the past twenty years. In Chapter 5, we sought to investigate the synthesis of rationally designed catalysts from pre-synthesized solution-phase nanoparticles. In particular, the synthesis and characterization of supported-PdAu nanoparticles with controlled nanoparticle size, composition, and structures via the trapping of nanoparticle precursors into metal oxide supports prepared by sol-gel chemistry was explored. The structural, chemical, and electronic properties of the supported nanoparticle catalysts were characterized by HRTEM and energy dispersive spectroscopy (EDS), TGA, and x-ray absorption spectroscopy (XANES, EXAFS). The nanoparticles were uniformly distributed on the

porous alumina frameworks as observed from HRTEM images. Large-area energy-dispersive spectroscopy (EDS) analysis confirmed the high compositional uniformity of the bimetallic supported catalysts. Low temperature calcinations (at  $\sim 300^{\circ}\text{C}$ ) were employed for the removal of PVP polymer. From HRTEM, EDS, and EXAFS measurements it was found that the structural integrity of the particles was maintained in the calcined samples with minor changes in particle sizes and co-ordination environments. The Au  $L_{III}$  XANES spectra revealed an increase in the occupancy of d-electron in the Au 5d valence band as Au content rises in the co-reduced PdAu bimetallic nanoparticle catalysts which can be attributed to the charge transfer from the Pd s-band (and perhaps p-band) to the Au d-band. Further, this rational methodology can be applied in the design of supported-core-shell nanoparticles; Pd core-Au shell nanoparticles could be incorporated into alumina frameworks and that the structural integrity of the particles was maintained after the calcination step. Finally, these catalysts were found to active catalysts for the hydrogenation of allyl alcohol.

Finally, the rational design of supported catalysts in imidazolium-based ILs was described. Two different techniques were employed for the synthesis of Au nanoparticle-decorated titania materials. It was found that the combination of the polymer stabilizer and IL can act as template towards the final porosity of materials, though the major contribution to porosity comes from the polymer stabilizer. The method of trapping the pre-synthesized PVP-stabilized Au nanoparticles into a titania matrix within an IL/methanol mixture was found to be the most suitable method in which all the Au nanoparticles were trapped in a titania matrix. Low temperature calcinations at  $350^{\circ}\text{C}$



resulted in highly mesoporous materials with BET surface areas of *ca.* 200 m<sup>2</sup>/g and average BJH pore-sizes of ~ 3.3 nm.

## **7.2 Outlook and Future Work**

### **7.2.1 Ionic Liquid Project**

Compared with traditional solvents, ILs have shown to provide many advantages, such as negligible vapor pressure, good thermal stability, a wide electrochemical potential windows, and tunable solubility. Therefore, the amount of research interest in ILs over the last few years has been overwhelming. In this thesis the focus has been on catalytic applications of metallic and bimetallic nanoparticles in ILs. Towards this objective, we investigated the usefulness of IL media for the synthesis and stabilization of nanoparticle catalysts. The big question we wanted to answer was how “green” are IL-stabilized nanoparticles as an alternative to conventional solvents (including water) and heterogeneous oxide-supported nanoparticle catalysts?

Some of the findings of this Ph.D. project are quite interesting. These are outlined below:

- (1) The negligible volatility of ILs is advantageous, as it can greatly facilitate the separation of products from catalysts. Due to this property, recyclability of IL-stabilized nanoparticles looks attractive. At the end of the reaction, substrate/product can be removed under vacuum (or extracted) and catalysts can be reused several times with negligible change in activity.

- (2) Presence of low amounts (1 mM) of 1-methylimidazole impurity in [BMIM]PF<sub>6</sub> IL can enhance the stability and activity of metal nanoparticles.
- (3) Long-term catalytic activity is excellent for PVP-stabilized PdAu nanoparticles in [BMIM]PF<sub>6</sub> IL. The PVP-stabilized nanoparticles are quite stable for many months (more than 2 months).

Though the use of ILs as a novel medium for nanoparticle synthesis has some advantages, it has some major disadvantages also. For example, H<sub>2</sub> has moderate to low solubility in ILs, thus hydrogenation reactions in ILs can often be mass-transfer limited. Another major disadvantage is the lengthy and costly process involved in the synthesis of these ILs, in particular to the level of purity needed to get reproducible results with regards to nanoparticle stability.

So the answer the bigger question as to whether quasi-homogeneous catalysis in ionic liquids is an alternative “greener” process is a difficult task. However, it has shown the potential to provide greener processes as understood by the twelve principles of green chemistry; for example, point 1 and 3 in the above findings. As Prof. T. Welton documented, *“ionic liquids has the potential to provide greener chemical processes. However, it does not mean that it will always provide the greenest process for all products”*.<sup>1</sup>

### **7.2.2 Future Work**

As described in Chapter 4, task-specific ionic liquids can be used for the stabilization of nanoparticles. They offer much flexibility for the synthesis and

stabilization of metal nanoparticles due to the fact that they can be functionalized with various chemical groups. Further studies in the group will investigate the synthesis of several task-specific ILs for use as stabilizers for nanoparticle synthesis and catalysis. Specifically, the synthesis of alkyl-methylimidazolium analogues such as 1-methyl-3-(2-aminoethyl) imidazolium hexafluorophosphate as well as thiolate and phosphine analogues will be ideal ILs given the fact that thiols and phosphines strongly bind to the nanoparticle surfaces.<sup>2-5</sup> Once the syntheses of several different task-specific ionic liquids are achieved, routes for the successful synthesis of highly stable and active nanoparticles can be explored. In addition, catalytic studies will be carried out to determine which route(s) are the most attractive method for the synthesis of nanoparticle/IL mixtures which can provide both longevity and recyclability. Several major pitfalls of using these thiol and nitrile functionalized ILs are as follows; labour intensiveness, multiple step synthesis and the possibility that such functional groups may passivate the nanoparticle surfaces completely and thus make them catalytically inactive. One possible research direction would be to probe the synthesis of functionalized ILs with fewer synthetic steps.

Sequestration of CO<sub>2</sub> from gaseous mixtures and conversion of CO<sub>2</sub> into value added chemicals is a subject of major research interest due to the fact that CO<sub>2</sub> is a major greenhouse gas. The high solubility of CO<sub>2</sub> in many ILs (which is typically much higher than the solubility of H<sub>2</sub> and O<sub>2</sub> in ILs) has opened up many possibilities of using ILs in this direction.<sup>6</sup> Davis and co-workers designed an amine-functionalized task-specific imidazolium IL for capturing CO<sub>2</sub> from sour gases (natural gas, CH<sub>4</sub>, which is contaminated with CO<sub>2</sub> and hydrogen disulfide, H<sub>2</sub>S).<sup>7</sup> The task specific ILs sequesters CO<sub>2</sub> from the gas forming an ammonium carbamate salt. The IL was recovered from the

CO<sub>2</sub>-capturing process by heating under process and was recycled for CO<sub>2</sub> uptake with a high degree of efficiency.<sup>7</sup> Jessop *et al.* have examined homogeneous hydrogenation catalysts for CO<sub>2</sub> to form formic acid (and formate salts), alkyl formates, and formamides.<sup>8,9</sup> Several groups have indicated the use of heterogeneous catalysts containing Raney nickel,<sup>10</sup> Pd,<sup>11</sup> and Ru<sup>12</sup> metals for the hydrogenation of carbon dioxide. Recently, Han and co-workers showed that hydrogenation of CO<sub>2</sub> to formic acid can be obtained with satisfactory activity and selectivity by using task specific ionic liquids containing amine groups (such as 2-[aemim]PF<sub>6</sub>) as the solvent.<sup>13</sup> More importantly, formic acid could be recovered easily, and the IL and catalyst can be reused by a separation process with no change in activity after five cycles.<sup>13</sup> All these examples indicate that ILs can provide potential media for the CO<sub>2</sub> sequestration and reduction processes.

During this PhD research, as described in Chapter 2-4, the usefulness of imidazolium-based IL ([BMIM]PF<sub>6</sub>) as a medium for quasi-homogeneous catalysis with high activity and selectivity has been shown. Also, highly porous heterogeneous supported nanoparticle catalysts can be synthesized in ILs as described in Chapter 6. As both quasi-homogeneous and heterogeneous catalysts can be synthesized in imidazolium-based ILs, one research direction would be to examine metal nanoparticle-IL mixtures (both quasi-homogeneous and heterogeneous) as potential catalysts for CO<sub>2</sub> hydrogenation using H<sub>2</sub> gas. Initial studies will focus the CO<sub>2</sub> hydrogenation to methanol and methane using H<sub>2</sub> gas; however, more selective routes to CO<sub>2</sub> hydrogenation towards formic acid salts and formamides can also be pursued, as they may be more economically desirable. However, there will be some potential hindrances in achieving this goal. H<sub>2</sub> has

limited solubility in imidazolium-based ILs, thus potential mass-transfer limitations can arise. Also, the moderate to high viscosity of imidazolium-based ILs may limit the potential use for large scale applications.

### **7.2.3 Supported Nanoparticle Catalysts Project**

In this work, a rational methodology was developed to synthesize supported-nanoparticle catalysts in which the structural integrity of the nanoparticles was maintained after the removal of organic stabilizers used to synthesize the nanoparticles in solution. This project is significant as it describes the design of heterogeneous catalysts from the presynthesized nanoparticles; it allows for facile tuning of the activity and selectivity of bimetallic nanoparticles for catalytic applications. This methodology can be applied to both alloy and core-shell nanoparticles. Thus, the rational design of supported nanoparticle catalysts is possible. Ideally, core-shell particles can be used that maximize the atom economy of expensive noble metal catalysts and could allow for tailored electronic interactions between core and shell metals. Some unpublished and future works related to this methodology are highlighted below.

#### **7.2.3.1 Room-temperature Plasma Cleaning**

As described in Chapter 5 and 6, low temperature calcinations (at 300-350 °C) in air, followed by reduction in H<sub>2</sub> was found to be a good method to remove the organic stabilizer with minimal changes in particle size, structure, and composition. However, small changes in average particle size were observed upon calcination which could not be avoided. Another possible way to potentially remove the PVP stabilizer with no

nanoparticle growth is by using low temperature plasma cleaning. Others have shown that plasma treatments of nanoparticles (either oxygen or hydrogen plasmas) can be done under relatively moderate thermal conditions ( $< 100\text{ }^{\circ}\text{C}$ ) which results in the retention of nanoparticle size, structure, and composition after the treatment.<sup>14-16</sup> Towards this objective, room temperature oxygen plasmas were used to remove the PVP polymer in 1 wt % Au-TiO<sub>2</sub> system. As seen in Figure 7.1, the C-H stretching regions around  $2900\text{ cm}^{-1}$  were completely removed upon the plasma treatment for 20 h indicating all the alkyl groups were removed. Also, the amide band at around  $1650\text{ cm}^{-1}$  was also significantly lowered,<sup>17</sup> and new bands were developed around  $1800\text{ cm}^{-1}$  which can be attributed to the formation of surface oxygenates such as carbonates. This initial result suggested that room temperature oxygen plasma treatments can be used to partially remove the organic polymer stabilizers at low temperatures. However, carbonate groups are still present on the surface of the oxide which may potentially hinder catalytic access. Future studies will involve examining the change in nanoparticle size and structure by HRTEM, EDS mapping, and EXAFS techniques.

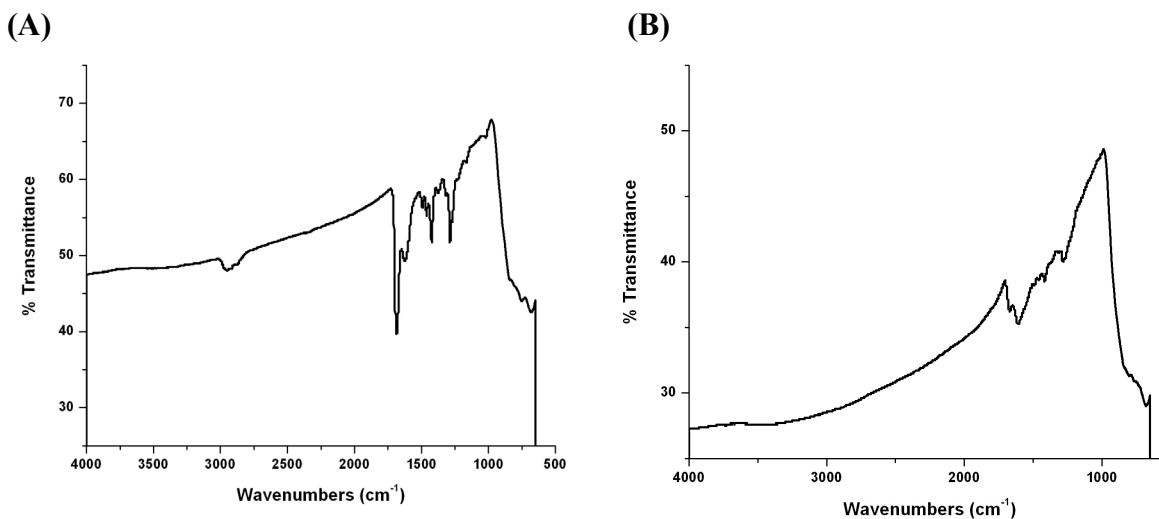


**Figure 7.1.** Surface-FTIR spectra of PVP-stabilized Au nanoparticles trapped in a titania xerogel (A) before room temperature plasma treatment and (B) after room temperature plasma treatment for 20 h. The sample was subjected to oxygen plasma at 100 W within a Harrick plasma cleaner (PDC-32 G).

### 7.2.3.2 Synthesis of Porous Materials using Non-aqueous Routes

For the synthesis of porous metal oxides, most of the methods are based on sol-gel methods which involve the hydrolysis of a metal alkoxide or halide precursor, followed by the condensation of the inorganic network. While porous silica has been synthesized in aqueous systems, similar syntheses of semiconducting metal oxides such as titania are much more difficult in aqueous systems due to the rapid hydrolysis and condensation of their alkoxide precursors. To overcome this, non-aqueous methods can be suitable alternative.<sup>18</sup> Thus, the synthesis of porous titania in [BMIM]PF<sub>6</sub> IL using a non-aqueous hydrolysis route was investigated.

In the non-aqueous route, oxygen donor molecules like alcohol or ether are used to hydrolyze and condense metal chloride precursors.<sup>18</sup> Benzyl alcohol was chosen as the oxygen donor molecule and titanium tetrachloride as the titanium source. In a typical synthesis, 3 ml of [BMIM]PF<sub>6</sub> was added to a 50 ml round bottomed-flask, followed by purging the system with N<sub>2</sub> for 30 min. Then, 0.25 ml of TiCl<sub>4</sub> (2.28 mmol) was added to the IL and stirred for 15 min, followed by addition of 11.8 ml (0.11 mol) of benzyl alcohol. A white precipitate formed after the addition which was kept overnight for gelation. The precipitate was washed with hot methanol (two times with 25 ml methanol). After washing, the material was collected by centrifugation and dried in oven at 100 °C (yield ~ 80 %). The white powder was then calcined in air at 500 °C. Adsorption-desorption isotherms of the final porous materials were obtained using a Micrometrics ASAP 2010 volumetric adsorption analyzer. The BET surface area of the calcined sample was found to be 88 m<sup>2</sup>/g with average pore diameter of 29 nm. These results suggest the formation of highly porous titania in IL using a non-aqueous route.

As ILs have negligible vapor pressure and high thermal stability, another promising avenue for future work is to explore high temperature ageing of sol-gel frameworks in ILs. By employing this method, a higher degree of structural integrity can be obtained. For example, Park *et al.* fabricated crystalline mesoporous  $\gamma$ -alumina by high temperature (120 °C) thermal processing/ageing in hexadecyl-3-methylimidazolium chloride IL.<sup>19</sup>



### 7.2.3.3 Structured Bimetallic Nanoparticles

After the successful realization of the rational design methodology in Chapters 5 and 6, work is continuing on the synthesis of core-shell nanoparticles which have thin layers of the shell metal, as shown in Figure 7.2. By maximizing the surface area of the precious metal, in principle more economical nanoparticle catalysts can be generated. Several groups have already documented this methodology using Ni-Pd,<sup>20</sup> Ni-Pt<sup>21</sup> and Cu-Pt<sup>22</sup> core-shell systems. One good example towards this direction that is being explored is the synthesis of Ag-Pd core-shell nanoparticles in which Pd shells are carefully grown on Ag cores via galvanic metal exchange reactions. This is important because Ag-Pd alloys have previously attracted a great deal of attention for the partial hydrogenation of ethylene and other unsaturated substrates.<sup>23,24</sup>

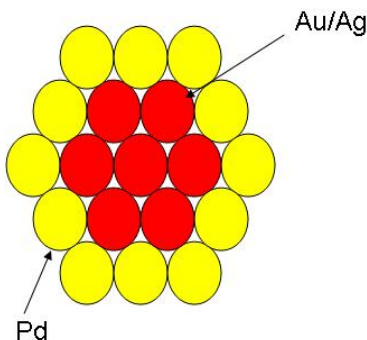


**Figure 7.2.** Schematic diagram of core-shell nanoparticles with a very thin shell.

Initial results have suggested that extremely high activities and selectivities are obtained for the hydrogenation of unsaturated substrates which can be attributed to the formation of thin Pd shells on Ag seeds, such that the core can electronically influence the Pd shell and thus modify its catalytic activity. The electronic interactions between

these metals will be thoroughly probed using x-ray absorption measurements (EXAFS and XANES) on the Ag and Pd K and L edges.

Besides Ag-Pd core-shell nanoparticles, design of core-shell nanoparticles with other precious shell metals such as Pt and Rh as well as other core-metals such as Cu and Fe can be envisioned. Such systems should be highly desirable for hydrogenation catalysts as well as fuel cells catalysts (particularly Fe-Pt core-shell systems).<sup>25</sup> Though the design of these bimetallic architectures looks attractive, some major problems could be encountered. The design of Ag-Pd core-shell nanoparticles by galvanic reactions with Pd salts may not lead to the formation of desired structure; surface tension effects may lead to ripening of thin core-shell particles towards a different bimetallic structure, *i.e.*; alloy or cluster-in-cluster structure. This will make it very challenging for the rational design of heterogeneous catalysts while employing such bimetallic nanoparticle precursors. During the removal of polymer by thermal activation step, nanoparticle sintering, alloying/segregation, and metal oxidation can happen which may lead to different structures.<sup>27</sup> Another important problem which might be encountered will be the *in-situ* particle structure changes in different reactive conditions. For example, Somorjai and co-workers have showed that bimetallic Rh-Pd core-shell nanoparticles undergo profound structural and compositional changes during catalytic reactions in different gaseous environments (O<sub>2</sub>, NO, CO, H<sub>2</sub>).<sup>28</sup> Interestingly, it was found that surface segregation of Rh and Pd atoms from core to shell (or shell to core) happens by changing from oxidizing (O<sub>2</sub> and NO) to reducing (H<sub>2</sub> and CO) environments, respectively. This suggests that *in-situ* studies of catalytic structures may be imperative to completely understand structure-property relationships in such catalysts.

### 7.3 References

- (1) Welton, T. *Green Chem.* **2008**, *10*, 483-483.
- (2) Harjani, J. R.; Friscic, T.; MacGillivray, L. R.; Singer, R. D. *Dalton Trans.* **2008**, 4595-4601.
- (3) Kim, K. S.; Demberehnyamba, D.; Lee, H. *Langmuir* **2004**, *20*, 556-560.
- (4) Chiappe, C.; Pieraccini, D.; Zhao, D. B.; Fei, Z. F.; Dyson, P. J. *Adv. Synth. Catal.* **2006**, *348*, 68-74.
- (5) Wang, Z. J.; Zhang, Q. X.; Kuehner, D.; Ivaska, A.; Niu, L. *Green Chem.* **2008**, *10*, 907-909.
- (6) Anthony, J. L.; Maginn, E. J.; Brennecke, J. F. *J. Phys. Chem. B* **2002**, *106*, 7315-7320.
- (7) Bates, E. D.; Mayton, R. D.; Ntai, I.; Davis, J. H. *J. Am. Chem. Soc.* **2002**, *124*, 926-927.
- (8) Jessop, P. G.; Ikariya, T.; Noyori, R. *Nature* **1994**, *368*, 231-233.
- (9) Jessop, P. G.; Hsiao, Y.; Ikariya, T.; Noyori, R. *J. Am. Chem. Soc.* **1996**, *118*, 344-355.
- (10) Farlow, M. W.; Adkins, H. *J. Am. Chem. Soc.* **1935**, *57*, 2222-2223.
- (11) Kudo, K.; Phala, H.; Sugita, N.; Takezaki, Y. *Chem. Lett.* **1977**, 1495-1496.
- (12) Zhang, Y. P.; Fei, J. H.; Yu, Y. M.; Zheng, X. M. *Catal. Commun.* **2004**, *5*, 643-646.
- (13) Zhang, Z. F.; Xie, E.; Li, W. J.; Hu, S. Q.; Song, J. L.; Jiang, T.; Han, B. X. *Angew. Chem., Int. Ed.* **2008**, *47*, 1127-1129.
- (14) Boyen, H. G.; Kastle, G.; Weigl, F.; Koslowski, B.; Dietrich, C.; Ziemann, P.; Spatz, J. P.; Riethmuller, S.; Hartmann, C.; Moller, M.; Schmid, G.; Garnier, M. G.; Oelhafen, P. *Science* **2002**, *297*, 1533-1536.
- (15) Jaramillo, T. F.; Baeck, S. H.; Cuenya, B. R.; McFarland, E. W. *J. Am. Chem. Soc.* **2003**, *125*, 7148-7149.
- (16) Spatz, J. P.; Mossmer, S.; Hartmann, C.; Moller, M.; Herzog, T.; Krieger, M.; Boyen, H. G.; Ziemann, P.; Kabius, B. *Langmuir* **2000**, *16*, 407-415.

- (17) Korkosz, R. J.; Gilbertson, J. D.; Prasifka, K. S.; Chandler, B. D. *Catal. Today* **2007**, *122*, 370-377.
- (18) Niederberger, M.; Bartl, M. H.; Stucky, G. D. *Chem. Mater.* **2002**, *14*, 4364-4370.
- (19) Park, H.; Yang, S. H.; Jun, Y. S.; Hong, W. H.; Kang, J. K. *Chem. Mater.* **2007**, *19*, 535-542.
- (20) Son, S. U.; Jang, Y.; Park, J.; Na, H. B.; Park, H. M.; Yun, H. J.; Lee, J.; Hyeon, T. *J. Am. Chem. Soc.* **2004**, *126*, 5026-5027.
- (21) Chen, Y. M.; Yang, F.; Dai, Y.; Wang, W. Q.; Chen, S. L. *J. Phys. Chem. C* **2008**, *112*, 1645-1649.
- (22) Muraviev, D. N.; Macanas, J.; Ruiz, P.; Munoz, M. *Phys. Status Solidi B* **2008**, *205*, 1460-1464.
- (23) Studt, F.; Abild-Pedersen, F.; Bligaard, T.; Sorensen, R. Z.; Christensen, C. H.; Norskov, J. K. *Science* **2008**, *320*, 1320-1322.
- (24) Khan, N. A.; Shaikhutdinov, S.; Freund, H. J. *Catal. Lett.* **2006**, *108*, 159-164.
- (25) Toda, T.; Igarashi, H.; Uchida, H.; Watanabe, M. *J. Electrochem. Soc.* **1999**, *146*, 3750-3756.
- (26) Cobley, C. M.; Campbell, D. J.; Xia, Y. N. *Adv. Mater.* **2008**, *20*, 748-752.
- (27) Mayrhofer, K. J. J.; Hartl, K.; Juhart, V.; Arenz, M. *J. Am. Chem. Soc.* **2009**, *131*, 16348-16349.
- (28) Tao, F.; Grass, M. E.; Zhang, Y. W.; Butcher, D. R.; Renzas, J. R.; Liu, Z.; Chung, J. Y.; Mun, B. S.; Salmeron, M.; Somorjai, G. A. *Science* **2008**, *322*, 932-934.